Climate change in mountainous river basins

Understanding climate change impacts and challenges across different spatial scales

Klimaatverandering in bergachtige stroomgebieden

De effecten en uitdagingen van klimaatverandering op verschillende ruimtelijke schalen
(met een samenvatting in het Nederlands)

PROEFSCHRIFT

ter verkrijging van de graad van doctor aan de Universiteit Utrecht
op gezag van de rector magnificus, prof. dr. H.R.B.M. Kummeling,
ingevolge het besluit van het college voor promoties in het openbaar
te verdedigen op woensdag 11 september 2019 des middags te 12.45 uur

door

René Reijer Wijngaard

geboren op 6 maart 1990 te Heemskerk

Promotoren:

Prof. dr. W.W. Immerzeel
Prof. dr. ir. M.F.P. Bierkens

Copromotor:

Dr. A.F. Lutz

Utrecht Studies in Earth Sciences 193

Climate change in mountainous river basins

Understanding climate change impacts and challenges across different spatial scales

René R. Wijngaard

Utrecht 2019

Promotoren:
Prof. dr. W.W. Immerzeel
Prof. dr. ir. M.F.P. Bierkens

Copromotor:
Dr. A.F. Lutz

Examination committee:
Prof. dr. Yao Tandong
Institute of Tibetan Plateau Research, Chinese Academy of Sciences, China

Prof. dr. M. Stoffel
University of Geneva, Switzerland

Prof. dr. ir. E.J. Moors
IHE Delft Institute for Water Education, the Netherlands

Prof. dr. R.S.W. van de Wal
Utrecht University, the Netherlands

Prof. dr. Y. Wada
International Institute for Applied Systems Analysis, Austria

ISBN 978-90-6266-551-8
Published by Faculty of Geosciences of Utrecht University, the Netherlands in:
Utrecht Studies in Earth Sciences (ISSN 2211-4335)
Printed by ProefschriftMaken || proefschriftmaken.nl

Correspondence to René Wijngaard, r.r.wijngaard.uu@gmail.com.

Cover photo: the Schlatenkees and -bach in Hohe Tauern National Park, Austria (R.R. Wijngaard).

The mountains are silent - over a loud world
The mountains rest - over a bustling world
The mountains demand - in a softened world
The mountains warm - in a cold world
The mountains shine - over a dark world
- Reinhold Stecher

Contents

<< Ama Dablam (6814 m) seen from the mountain village Pangboche (4252 m) in Sagarmatha National Park, Nepal (R.R.Wijngaard).

Summary

Freshwater resources are essential for human life. Significant portions of freshwater are provided by mountains, which are largely determined by meltwater originating from glaciers and snow reserves, and orography-induced precipitation that is generally higher in mountain ranges than in surrounding lowlands. Mountain ranges can, due to their large storage potential, act as water towers, sustain seasonal water availability, and provide important water resources for agriculture, drinking water supply, energy production, shipping, tourism, industry, and ecosystems. For this reason, mountain water resources can be considered as important freshwater resources for billions of people living in mountain regions and surrounding lowlands, and it does illustrate the high vulnerability of mountain regions to climate change. Climate change is expected to impact the hydrology and cryosphere of mountainous river basins. Surface and groundwater availability will likely be affected and the frequency and intensity of natural hazards are expected to change. It can therefore be expected that climate change will have a large impact on the society and the environment; impacts that will be amplified with the anticipated socio-economic developments and associated changes in water demand. Understanding climate change impacts in mountainous river basins is challenging due to the complexity of the mountain environment and the wide range of scales on which mountain-hydrological processes can occur. This makes it necessary to examine these effects at different spatial scales. The research described in this thesis aims therefore at understanding the cryospheric and hydrological impacts and challenges of climate change across different spatial scales in mountainous river basins. To this end, novel modelling approaches have been developed and applied to assess the effects of climate change at catchment- and regional/basin-scale.

Ongoing global warming has resulted in a widespread retreat of glaciers since the end of the Little Ice Age. To attribute the response of glaciers to natural and anthropogenic historical climate change over time a spatially-distributed coupled glacier mass balance and ice-flow model is developed and applied that does not require a priori information about the flowline geometry of glaciers. The model is applied for the debris-covered Langtang Glacier in the Central Himalayas and the clean-ice Hintereisferner in the European Alps from the end of the Little Ice Age (1850) to the present-day (2016). The model is forced with four bias-corrected climate models that represent region-specific cold-dry, cold-wet, warm-dry, and warm-wet climate conditions. To isolate the effects of human-induced climate change on glacier mass balance and dynamics, runs are selected from the climate models with and without further anthropogenic forcing after 1970 until 2016. The model outcomes reveal that both glaciers experience the largest reduction in area and volume under warm climate conditions and that simultaneously with changes in glacier area and volume, surface velocities generally decrease over time. Without further anthropogenic forcing the analysis reveals that the decline in glacier area and volume is smaller, indicating that the response of the two glaciers can mainly be attributed to anthropogenic climate change. Here, a debris-covered glacier shows a limited retreat and tends to lose less mass due to insulation of the glacier surface by a layer of supraglacial debris, where a clean-ice glacier responds faster to climate change and shows a larger retreat.

<< View on the Cholatse (6440 m), the debris-covered tongue of the Chola Glacier, and the Cholatse Tso (lake) (R.R. Wijngaard).

It is expected that glaciers will continue to lose mass in the future and that snow cover and volumes will decline. The diminishing glaciers and snow reserves will likely affect the hydrology of river basins, especially in glacierized headwater catchments where the contributions of meltwater from ice and snow reserves can be large. To investigate the hydrological response of glacierized headwater catchments to future climate change until 2100 a multi-model assessment is conducted for three (nested) glacierized catchments in the Ötztal Alps, Austria. Two conceptual hydrological models are applied and forced with downscaled climate change projections and outputs from an empirical glacier change model. The model projections show in the short term increasing river flows without changes in the seasonality of the river flow regime. In the long term summer river flows are expected to decrease and winter/spring river flows are expected to increase in all catchments. These changes are accompanied by intra-annual shifts in the river flow regime, where ice-melt dominated regimes tend to shift to more snowmelt-dominated regimes. Further the changes might be accompanied by changes in the seasonality of annual flood peaks with an earlier appearance of flood peaks, and an increased frequency of summer low flows. As a result risks for local floods and droughts might increase.

Future changes in the precipitation climatology of large-scale atmospheric systems, such as the Indian and East Asian monsoon circulations are likely. The changes might have implications for the regional hydrology and the occurrence of hydrological extremes in mountainous domains, which may pose serious threats for the livelihoods of people. For this reason, the impacts of climate change on future hydrological extremes need to be investigated in these domains. A fully-distributed cryospheric-hydrological model is used to simulate current and future hydrological fluxes until 2100 in the upstream domains of the Indus, Ganges, and Brahmaputra (IGB) river basins. The model is forced with an ensemble of downscaled climate models and is calibrated on observed daily discharge and geodetic glacier mass balances. The climate forcing and the outputs of the hydrological model are used to analyze future changes in climatic extremes, and hydrological extremes by focusing on high and low river flows. The analysis reveals that the magnitude of climatic means and extremes will increase towards the end of the 21st century where climatic extremes tend to increase stronger than climatic means. Future mean discharge and high river flow conditions will very likely increase, which can mostly be attributed to increasing precipitation extremes. To some extent temperature extremes that trigger rapid ice and snowmelt might contribute to increasing discharge extremes as well. Low river flow conditions may occur less frequently, but are partly accompanied by large uncertainties. These uncertainties can mainly be attributed to the large spread among the different climate models.

Diminishing ice and snow reserves and changes in the precipitation climatology will likely affect the regional availability of water that is provided for people living in (densely-populated) downstream river basins, such as the IGB. These river basins provide about 900 million people with water resources used for agricultural, domestic, and industrial purposes and are marked as "climate change hotspots", where climate change is expected to affect the regional water availability. Simultaneously, rapid and continuous population growth as well as strong economic development will likely result in a strong increase in water demand and withdrawals in the region. These developments will most likely lead to an increased pressure on water resources and the development of a potential water gap. Since quantification of these future trends is missing, it is rather uncertain how the future South Asian water gap will develop. For this reason, an impact assessment is conducted on the combined impacts of climate change and socio-economic development on the

future “blue” water gap in the IGB until the end of the 21st century. A novel coupled modelling approach consisting of a fully-distributed cryospheric-hydrological model and a fully-distributed hydrology and crop production model is used to simulate current and future up- and downstream water supply and downstream water demand. The coupled models are forced with an ensemble of representative downscaled climate models and a set of land use and socio-economic scenarios. The simulation outputs are used to analyze changes in the water availability, supply, demand, and gap. The analysis reveals that surface water availability will increase towards the end of the 21st century, which can mainly be attributed to increases in monsoon precipitation. Despite the increase in surface water availability, the strong socio-economic development and associated increase in water demand will likely lead to an increase in the water gap during the 21st century. This indicates that socio-economic development is the key driver in the evolution of the future South Asian water gap.

The research described in this thesis stands out in comparison with previous research conducted in the European and South Asian catchments and river basins. Novel modelling approaches have been developed and applied, and new and valuable insights have been gained on the future cryospheric and hydrological impacts of climate change in mountainous river basins. The outcomes generated throughout this thesis might contribute to the formulation of (transboundary) adaptation policies, which are highly needed to reduce the adverse impacts of climatic and socio-economic changes in mountain regions and surrounding lowlands. Further, the thesis describes challenges that need to be faced and provides recommendations for future research to improve understanding of the essential processes of the high-altitude water cycle and the cryospheric and hydrological impacts of climate change in mountain environments.

Samenvatting

Zoetwatervoorraden zijn essentieel voor het menselijke leven. Een aanzienlijke hoeveelheid zoet water is afkomstig uit gebergten, welke grotendeels bepaald wordt door smeltwater afkomstig van gletsjers en sneeuw, en door de orografie-geïnduceerde neerslag die over het algemeen hoger is in gebergten dan in de omringende laaglanden. Door hun grote opslagpotentieel kunnen bergketens fungeren als watertorens, de seizoensgebonden waterbeschikbaarheid ondersteunen, en belangrijke watervoorraden bieden voor landbouw, drinkwatervoorziening, energieproductie, scheepvaart, toerisme, industrie, en ecosystemen. Daarom kunnen bergwatervoorraden beschouwd worden als belangrijke zoetwaterbronnen voor miljarden mensen in berggebieden en omringende laaglanden, en illustreert het de grote kwetsbaarheid van berggebieden voor klimaatverandering. Verwacht wordt dat klimaatverandering een effect zal hebben op de hydrologie en cryosfeer van bergachtige stroomgebieden. De oppervlakte- en grondwaterbeschikbaarheid zal waarschijnlijk beïnvloed worden en de intensiteit en frequentie van natuurrampen zal naar verwachting veranderen. Het is daarom te verwachten dat klimaatverandering grote gevolgen zal hebben voor de samenleving en het milieu; effecten die versterkt zullen worden met de geanticipeerde sociaaleconomische ontwikkelingen en de daarmee samenhangende veranderingen in de vraag naar water. Het begrijpen van de effecten van klimaatverandering in bergachtige stroomgebieden is een uitdaging door de complexiteit van het bergmilieu en het brede scala aan schalen waarop berg-hydrologische processen kunnen plaatsvinden. Dit maakt het noodzakelijk om deze effecten op verschillende ruimtelijke schalen te onderzoeken. Het onderzoek beschreven in dit proefschrift is daarom gericht op het begrijpen van de cryosferische en hydrologische effecten en uitdagingen van klimaatverandering op verschillende ruimtelijke schalen in bergachtige stroomgebieden. Hiertoe zijn nieuwe modelleringsmethoden ontwikkeld en toegepast om de effecten van klimaatverandering op stroomgebieds- en regionaal/bekkenniveau te beoordelen.

De aanhoudende opwarming van de aarde heeft geresulteerd in een wijdverbreide terugtrekking van gletsjers sinds het einde van de kleine ijstijd. Om de respons van gletsjers op natuurlijke en antropogene historische klimaatverandering door de tijd heen toe te kunnen schrijven, wordt een ruimtelijk verdeelde gekoppelde gletsjermassabalans en ijsstroommodel ontwikkeld en toegepast die geen a priori informatie over de stroomlijngeometrie van gletsjers vereist. Het model wordt toegepast voor de met puin bedekte Langtanggletsjer in de centrale Himalaya en de Hintereisferner in de Europese Alpen vanaf het einde van de kleine ijstijd (1850) tot het heden (2016). Het model wordt aangestuurd met vier bias gecorrigeerde klimaatmodellen die regio-specifieke koude-droge, koude-natte, warme-droge, en warme-natte klimaatomstandigheden representeren. Om de effecten van door de mens veroorzaakte klimaatverandering op de massabalans en dynamiek van gletsjers te isoleren, worden runs geselecteerd uit de klimaatmodellen met en zonder verdere antropogene aansturing na 1970 tot 2016. Uit de modeluitkomsten blijkt dat beide gletsjers de grootste reductie in oppervlakte en volume ervaren onder warme klimaatomstandigheden en dat gelijktijdig met veranderingen in het gletsjeroppervlak en -volume, de stroomsnelheden over het algemeen in de loop van de tijd afnemen. Zonder verdere antropogene aansturing suggereert de analyse dat de afname in gletsjeroppervlak en -volume kleiner is, wat aangeeft dat de respons van de twee gletsjers

<< Terrace agriculture in the Bajhang District, Nepal (USAID Biodiversity and Forestry)

voornamelijk kan worden toegeschreven aan antropogene klimaatverandering. Hier toont een puingletsjer een beperkte terugtrekking en heeft deze de neiging minder massa te verliezen door de isolerende werking van het puin op het gletsjerijs, waar een gletsjer met schoon ijs sneller reageert op klimaatverandering en een grotere terugtrekking vertoont.

De verwachting is dat gletsjers in de toekomst massa zullen blijven verliezen en dat de sneeuwbedekking en -volume zal afnemen. De afname in gletsjers en sneeuw zullen waarschijnlijk een invloed hebben op de hydrologie van rivierbekkens, vooral in de vergletsjerde bovenloopgebieden waar het aandeel van smeltwater uit ijs en sneeuw groot kan zijn. Om de hydrologische veranderingen in vergletsjerde stroomgebieden als gevolg van de toekomstige klimaatverandering tot 2100 te onderzoeken, wordt een multi-modelanalyse uitgevoerd voor drie (geneste) vergletsjerde stroomgebieden in de Ötztaler Alpen, Oostenrijk. Twee conceptuele hydrologische modellen worden toegepast en aangestuurd met neergeschaalde klimaatprojecties en uitkomsten van een empirisch gletsjermodel. De modelprojecties laten op korte termijn toenemende rivierafvoeren zien zonder veranderingen in de seizoensgebondenheid van het stroomregime van rivieren. Op de lange termijn zullen naar verwachting de zomerafvoeren afnemen en de winter-/lenteafvoeren toenemen in alle stroomgebieden. Deze veranderingen gaan gepaard met intra-jaarlijkse verschuivingen in het stroomregime van de rivier, waar regimes die door ijssmelt gedomineerd worden de neiging hebben te veranderen in regimes die meer door sneeuwsmelt gedomineerd worden. Verder kunnen de veranderingen vergezeld gaan met veranderingen in de seizoensgebondenheid van jaarlijkse hoogwaterpieken met een eerdere verschijning van hoogwaterpieken en een verhoogde frequentie van lage zomerafvoeren. Als gevolg hiervan kunnen de risico's voor lokale overstromingen en droogtes toenemen.

Toekomstige veranderingen in de neerslagklimatologie van grootschalige atmosferische systemen, zoals de Indiase en Oost-Aziatische moessoncirculaties zijn waarschijnlijk. De veranderingen kunnen gevolgen hebben voor de regionale hydrologie en het voorkomen van hydrologische extremen in bergachtige gebieden die een ernstige bedreiging kunnen vormen voor het bestaan van mensen. Om deze reden is het nodig dat de effecten van klimaatverandering op toekomstige hydrologische extremen in deze gebieden worden onderzocht. Een ruimtelijk gedistribueerd cryosferisch-hydrologisch model wordt gebruikt om huidige en toekomstige hydrologische fluxen te simuleren tot 2100 in de bovenstroomse stroomgebieden van de Indus, Ganges en Brahmaputra (IGB). Het model wordt aangestuurd met een reeks neergeschaalde klimaatmodellen en wordt gekalibreerd op dagelijks gemeten rivierafvoeren en geodetische gletsjermassabalansen. De klimaatprojecties en de uitkomsten van het hydrologische model worden gebruikt om toekomstige veranderingen in klimatologische extremen en hydrologische extremen te analyseren waarbij de focus van de analyse op hoge en lage rivierafvoeren ligt. De analyse laat zien dat de omvang van de klimatologische gemiddelden en extremen zal toenemen tegen het einde van de 21^{e} eeuw, waarbij de klimatologische extremen de neiging hebben om sterker toe te nemen dan de klimatologische gemiddelden. Toekomstige gemiddelde en hoge rivierafvoeren zullen zeer waarschijnlijk toenemen, wat vooral kan worden toegeschreven aan de toenemende neerslagextremen. Tot op zekere hoogte kunnen extreme temperaturen, die een snelle ijs- en sneeuwsmelt teweegbrengen, een bijdrage leveren aan de toename in afvoerextremen. Lage rivierafvoeren kunnen minder vaak voorkomen, maar gaan gedeeltelijk gepaard met grote onzekerheden. Deze onzekerheden kunnen vooral worden toegeschreven aan de grote spreiding in de uitkomsten van de verschillende klimaatmodellen.

De afname in ijs en sneeuw en veranderingen de neerslagklimatologie zullen waarschijnlijk van invloed zijn op de regionale beschikbaarheid van water voor mensen die wonen in (dichtbevolkte) benedenstroomse riviergebieden, zoals de IGB. Deze rivierbekkens voorzien ongeveer 900 miljoen mensen van waterbronnen die worden gebruikt voor agrarische, huishoudelijke en industriële doeleinden en zijn gemarkeerd als "hotspots voor klimaatverandering", waarbij wordt verwacht dat klimaatverandering de regionale beschikbaarheid van water zal beïnvloeden. Tegelijkertijd zullen een snelle en voortdurende bevolkingsgroei en een sterke economische ontwikkeling waarschijnlijk leiden tot een sterke toename in de vraag en onttrekking van water in de regio. Deze ontwikkelingen zullen hoogstwaarschijnlijk leiden tot een verhoogde druk op watervoorraden en de ontwikkeling van een mogelijke water gap. Omdat de kwantificering van deze toekomstige trends ontbreekt, is het onzeker hoe de toekomstige Zuid-Aziatische water gap zich zal ontwikkelen. Om deze reden wordt er een beoordeling uitgevoerd naar de gecombineerde effecten van klimaatverandering en sociaaleconomische ontwikkeling op de toekomstige "blauwe" water gap in de IGB tot het einde van de 21^{e} eeuw. Een nieuwe gekoppelde modelleringsaanpak bestaande uit een ruimtelijk gedistribueerde cryosferisch-hydrologisch model en een ruimtelijk gedistribueerde hydrologie- en gewasproductiemodel wordt gebruikt om de huidige en toekomstige boven- en benedenstroomse watertoevoer en benedenstroomse watervraag te simuleren. De gekoppelde modellen worden aangestuurd met een reeks representatieve neergeschaalde klimaatmodellen en een reeks landgebruiks- en sociaaleconomische scenario's. De simulatie uitkomsten worden gebruikt om veranderingen in de waterbeschikbaarheid, toevoer, vraag en gap te analyseren. Uit de analyse blijkt dat de beschikbaarheid van oppervlaktewater aan het einde van de 21^{e} eeuw zal toenemen, wat voornamelijk kan worden toegeschreven aan de toename van de moessonneerslag. Ondanks de toename van de beschikbaarheid van oppervlaktewater, zal de sterke sociaaleconomische ontwikkeling en de daarmee gepaard gaande toename in de vraag naar water waarschijnlijk leiden tot een toename van de water gap in de 21e eeuw. Dit geeft aan dat sociaaleconomische ontwikkeling de belangrijkste drijfveer is voor de ontwikkeling van de toekomstige water gap in Zuid-Azië.

Het onderzoek beschreven in dit proefschrift blinkt uit in vergelijking met eerder verricht onderzoek in de Europese en Zuid-Aziatische stroomgebieden en rivierbekkens. Nieuwe modelleermethoden zijn ontwikkeld en toegepast, en nieuwe en waardevolle inzichten zijn verkregen over de toekomstige cryosferische en hydrologische effecten van klimaatverandering in bergachtige stroomgebieden. De resultaten die in dit proefschrift worden gegenereerd, kunnen bijdragen aan de formulering van (grensoverschrijdende) aanpassingsbeleidslijnen, die zeer nodig zijn om de negatieve gevolgen van klimatologische en sociaaleconomische veranderingen in berggebieden en omliggende laaglanden te verminderen. Verder beschrijft het proefschrift uitdagingen die moeten worden aangepakt en biedt het aanbevelingen voor toekomstig onderzoek om het inzicht in de essentiële processen van de watercyclus op grote hoogte en de cryosferische en hydrologische effecten van klimaatverandering in bergachtige omgevingen te verbeteren.

1 Introduction

1.1 Background: climate change in mountainous river basins

Freshwater resources are essential for human life. Significant portions of freshwater are provided by mountains, which function as natural barriers in the landscape. The natural barriers induce orographic lifting of moving air masses, which consequently result in precipitation of rain or snow (i.e. depending on the prevailing air temperatures) at the windward side and dry climate conditions at the leeward side. As a result precipitation amounts are higher in mountain ranges than in surrounding lower areas. For example, in the European Alps, annual precipitation amounts to about 1450 mm yr^{-1}, whereas the average annual precipitation in Europe is about 650 mm yr^{-1} (Weingartner et al., 2009). Once the water reaches the surface it is transported in the downstream direction by surface runoff, lateral flow, or baseflow when water is in a liquid state. In a solid state, water can be transported downstream by glacier flow, wind-driven transport of snow, or avalanching. During transport, water can be stored temporarily for shorter periods in soils and snow reserves and for longer periods in glaciers, firn, permafrost, or groundwater reserves. In addition, water can return to the atmosphere by evapotranspiration or sublimation. Mountain ranges, often referred to as water towers, can, due to their large storage potential, sustain seasonal water availability and provide important water resources for agriculture (e.g. irrigation), drinking water supply, energy production (e.g. hydropower), shipping, tourism, industry, and ecosystems. For this reason, mountain water resources (i.e. meltwater and orographic-induced precipitation) can be considered as important freshwater resources for billions of people living in mountain areas and adjacent lowlands. This also results in a high vulnerability of mountain regions to climate change (Biemans et al., 2019; Huss et al., 2017; Immerzeel et al., 2010; Kaser et al., 2010; Kohler et al., 2014; Viviroli et al., 2007, 2011). Figure 1.1 sheds light on the level of hydrological importance mountain ranges have as water towers of the world. The figure shows that particularly large parts of HMA (High Mountain Asia), the Andes, Eastern and Southern Africa, and Mexico heavily rely on mountain water resources.

Climate change is expected to affect mountain ranges and adjacent lowlands, which eventually will have an impact on freshwater supplies from mountainous areas to downstream-located lowlands. For instance, in HMA, temperature increases between 1.7 °C and 6.3 °C are projected for the end of the 21st century (Lutz et al., 2016b) while in the European Alps temperatures are projected to increase with 3.3 °C by the end of the 21st century (Gobiet et al., 2014). Moreover, future temperature increases are expected to be stronger at higher altitudes due to elevation-dependent warming (Gobiet et al., 2014; Kotlarski et al., 2012; Liu and Chen, 2000; MRI, 2015; Palazzi et al., 2016; Pepin et al., 2015). Warming will have a large impact on human society. Snow cover and snow volumes will most likely reduce due to higher fractions of liquid to total precipitation. This will cause an upward shift of the snowline of approximately 150 m per 1 °C increase in temperature, and a shorter duration of the snow season (Beniston et al., 2018; Frei et al., 2018; Marty et al., 2017b; Viste and Sorteberg, 2015). The reduction in snow cover and volume will subsequently amplify warming due to rising albedos and might affect large-scale atmospheric circulations such as the monsoon circulations (Kohler and Maselli, 2009; Lau and Kim, 2018; Li et al., 2018). Additionally, the declining snow cover and snow volumes might threaten the local livelihoods in mountain valleys. For instance, in the European Alps, up to 90% of the local economy is dependent on winter tourism and is therefore highly dependent on the amount of snow and duration of snow cover

<< The Umbal Waterfalls, located in the upstream domain of the Isel catchment, East Tyrol, Austria (R.R. Wijngaard)

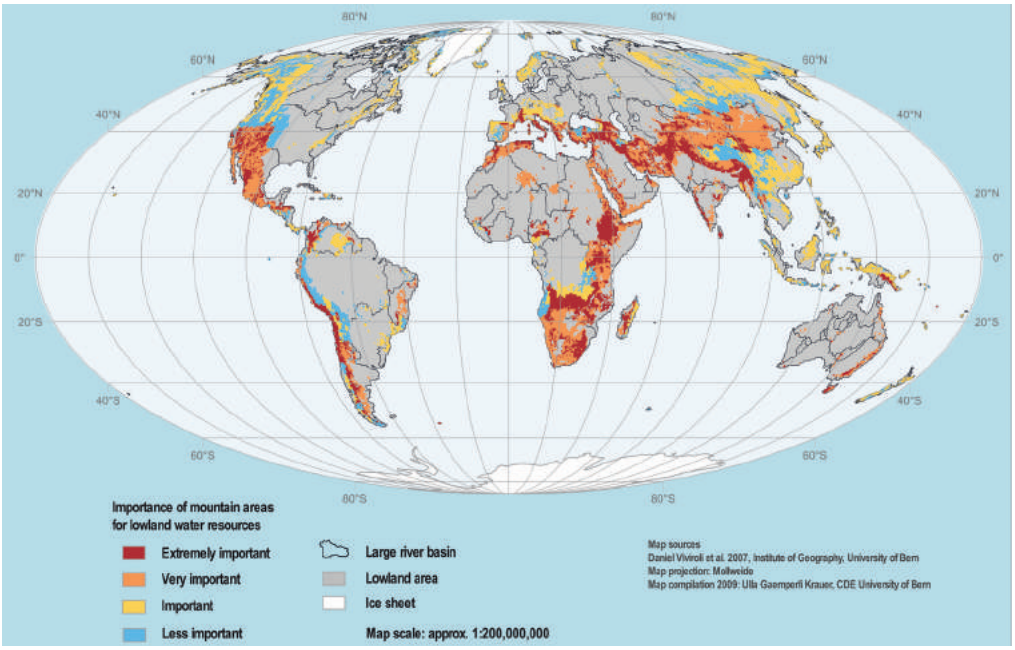

Figure 1.1. The hydrological importance of mountain ranges for surrounding lowlands (Viviroli et al., 2007)

(Abegg et al., 2007; Marty et al., 2017a). The warming is also expected to result in glacier retreat and permafrost thawing. This will affect the global sea-level, trigger natural hazards that follow from the destabilization of mountain slopes or the development of moraine-dammed lakes, and affect glacier dynamics (Frey et al., 2010; Gregory et al., 2013; Haeberli et al., 2017). Furthermore, this will have an impact on the seasonal water availability by altering discharge regimes and the timing of the annual peak discharge. In many mountain areas it is expected that in the coming decades water availability will increase due to enhanced melt, followed by a steady decline due to diminishing ice and snow reserves (Huss and Hock, 2018). In the floodplain regions, evapotranspiration rates will most likely increase as a response to rising temperatures (e.g. Lutz et al., 2018), and the associated increase in heat stress will affect crop yields, which eventually will affect food security (Porter et al., 2015).

Besides the temperature increase, the annual amount of precipitation, the intensity and frequency of extreme precipitation events, and the precipitation patterns are also expected to change. In many parts of HMA, it is projected that precipitation will increase accompanied by an increased frequency in heavy precipitation events during the monsoon period (Lutz et al., 2014, 2016b, 2018; Palazzi et al., 2015). Only in the westernmost region of HMA (i.e. the Indus river basin) precipitation decreases are more likely (Lutz et al., 2016b, 2018). In the European Alps, the precipitation will most likely decrease during the summer season accompanied by a decreasing number of wet days, in particular at the southern side of the Alps (Gobiet et al., 2014). During the winter season, precipitation will likely increase, where the largest increases are also projected along the southern periphery of the Alps. Furthermore, extreme precipitation events are expected to become more intense, particularly at the northern side of the Alps (Rajczak et al., 2013). The projected precipitation changes are, however, accompanied by large uncertainties, and the climate model confidence is low due to their limitation in simulating the complex climate of the mountain

environment (Gobiet et al., 2014; Lutz et al., 2016b; Seneviratne et al., 2012). It is likely that the precipitation changes will subsequently lead to a change in the frequency of flood hazards and droughts, affect the magnitude and timing of discharge, and affect the groundwater availability due to long-term changes in groundwater storage and recharge (Asoka et al., 2017). These projected changes show that climate change can have a large impact on human society. This impact might even become larger with the anticipated socio-economic developments, and the associated population growth and increase in water demands, which will likely result in potentially and even larger pressure on water resources. An improved understanding of the effects of climate change on mountain-hydrological processes is therefore urgently needed to reveal the past, present and future impacts of climate change in mountainous river basins.

1.2 Understanding and modelling climate change impacts at different spatial scales

Mountain river basins can roughly be subdivided into three zones as suggested by Miller and Spoolman (2012). Figure 1.2 shows the different zones and their upstream-downstream relationship, which are typical for many river basins around the world. The following zones can be distinguished:

- **Source zone**: this zone is also known as the headwater zone (Nepal et al., 2018). It is characterized by steep slopes, high mountain peaks, glaciers, snow, permafrost, and extreme climate conditions. This zone is a hotspot for climatic changes where global warming is expected to affect snow, glaciers, permafrost, and associated melt regimes. A source zone is typically located above the treeline. In regions, such as the Himalayas and the European Alps, the treeline is in general located above 3800-4200 m above sea level (a.s.l.) and 2000-2300 m a.s.l., respectively (Nepal et al., 2018; Pecher et al., 2011; Sigdel et al., 2018).

- **Transition zone**: this zone connects the upstream-located source zone with the downstream-located floodplain zone. In this zone anthropogenic activities become increasingly important. Forests and mountain agriculture are the dominant land uses. Water resources are mainly provided by groundwater from springs on the hill slopes. Via infrastructure such as irrigation canals, agriculture can be sustained (e.g. Ishaq et al., 2017). In this zone, also water infrastructure in the form of hydropower reservoirs and dams can be found. By means of hydropower, energy is produced that is utilized by local communities and in the downstream-located floodplains. Climate change, socio-economic changes and land use and cover changes are identified as the main drivers for environmental change in this zone (Nepal et al., 2018). Typical regions that fall within this zone are the Siwaliks (i.e. hilly regions in the forelands of the Himalayas) and the Alpine valleys and forelands.

- **Floodplain zone**: this zone is also mentioned as the depositional zone since sediments transported from upstream-located source and transition zones are deposited in the floodplains of this zone. A classic example of a region that falls in the floodplain zone is the Indo-Gangetic plain. This region is home to millions of people living in rural areas and large cities, like New Delhi, Lahore, Jaipur, and Islamabad. The region is also known as a hotspot for socio-economic changes (De Souza et al., 2015) that is characterized by rapid population growth and urbanization, strong economic developments, and an increase in water demand. The Indo-Gangetic plain is also home to the world's largest irrigation system: the Indus Basin Irrigation

System (IBIS). The water resources are mainly driven by groundwater and upstream meltwater and rainfall-runoff.

In this thesis, I make the distinction between the source and transition zones, i.e. upstream domain, and the floodplain zone, i.e. downstream domain.

Understanding the implications of climate change in the different zones of mountainous river basins is challenging, especially in the upstream domains where mountain-hydrological processes prevail. The quantification of mountain-hydrological processes is hampered by (1) the complexity of the mountain topography where the variability in climatic, cryospheric, and hydrological processes is large over a short horizontal distance, (2) the difficulties in the theoretical understanding of mountain-hydrological processes, (3) the limited data availability, especially at higher altitudes and in remote areas, and (4) the accuracy of data that is available (Klemeš, 1990). To overcome many of these issues, advanced models that have a good representation of mountain-hydrological processes can be very useful. These models need to be calibrated and validated on satellite-derived imagery or field data from regions where data is available, and need to be forced with downscaled climate change projections and/or socio-economic scenarios. Eventually the models can be useful for studying the effects of climate change on variables and processes, such as ice and snowmelt, runoff variability, the magnitude and frequency of hydrological extremes, and water supply.

Mountain-hydrological processes occur at a wide range of temporal and spatial scales. Temporally, this can vary from avalanching with a typical timescale of several minutes to groundwater flow in aquifers with a typical timescale of hundreds of years. Spatially, this can vary from the unsaturated flow at a scale of less than 1 m to the monsoon circulation that reaches over 1000 km or more (Blöschl and Sivapalan, 1995). The combination of the complexity of the mountain environment and especially the wide range of spatial scales on which mountain-hydrological processes can occur make it inevitable to apply models at a wider range of scales to understand the impacts of climate change in different domains of a river basin. This can either be done by high resolution modelling that can reduce the spatial process variability, or by larger scale model applications that include simplified model assumptions and subgrid parameterizations accounting for the spatial process variability (Hrachowitz and Clark, 2017; Sivapalan, 2018). According to Dooge (1986) and Blöschl and Sivapalan (1995) spatial hydrological modelling scales can typically be subdivided into four different domains:

- The local-scale has typically a scale of 1 m. On this scale, processes such as unsaturated flow are investigated.
- The hillslope-scale can be used to study processes such as avalanching, and is typically 100 m in scale.
- The catchment-scale falls between 1 km for small subcatchments and 100 km for large catchments (Gleeson and Paszkowski, 2014). On this scale catchment-scale modelling applications can be used to study processes such as the river runoff variability.
- The regional/basin-scale has typically a scale of 1000 km or more and is, for instance, used to study the impacts of climate change on a regional level or in a large river basin.

In this thesis my main focus will be on catchment-scale applications in upstream domains and regional/basin-scale applications in both upstream and downstream domains of large mountainous

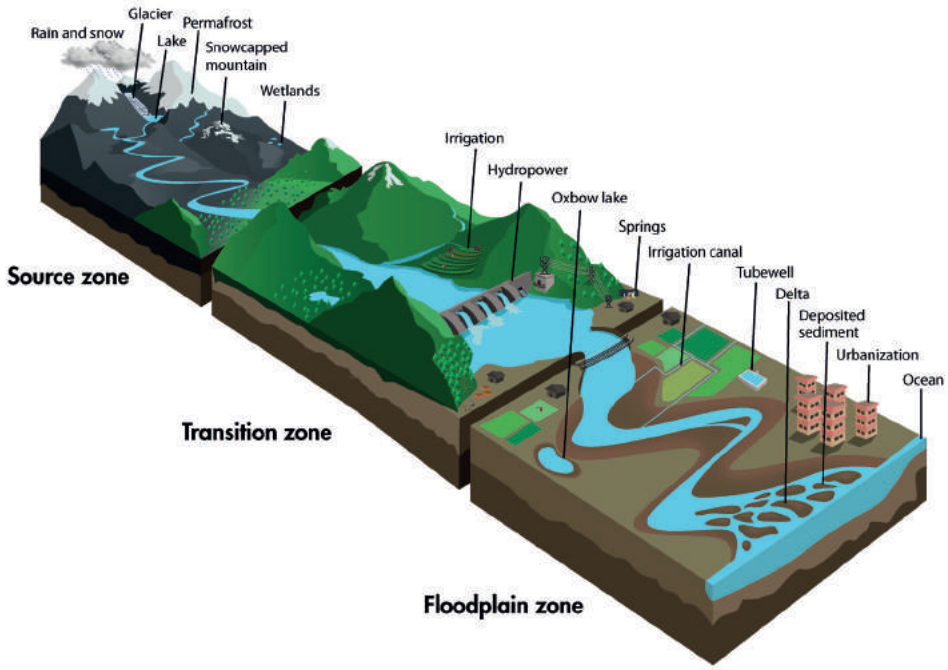

Figure 1.2. Schematic diagram of a river including its three zones and their upstream-downstream linkages. The schematized basin structure is typical for river basins, such as the Indus, Ganges, and Brahmaputra rivers (Nepal et al., 2018).

river basins. In the following subsections I will focus more on the understanding and modelling of climate change impacts at the different scales and some challenges that need to be faced in the specific spatial domains.

1.2.1 Understanding and modelling glaciological impacts of climate change at the catchment scale

1.2.1.1 Glaciers

Mountain glaciers are typical features that can be found in high-mountain environments. These features, which are also mentioned as 'rivers of ice', flow from high-altitude areas to the valleys due to gravitational forces. Glaciers are typically formed when accumulated snow at higher altitude is transformed into ice and flows down under the force of gravity. The mass balance of a glacier is thereby determined by the sum of all processes that add mass to a glacier (accumulation) and removes mass from a glacier (ablation), and can be considered as in equilibrium when accumulation equals ablation (Haeberli, 2011). When accumulation is higher than ablation, due to increased snowfall or decreased melt, a glacier advances/thickens, and when ablation is higher than accumulation, due to decreased snowfall or increased melt, a glacier retreats/thins. Besides precipitation and temperature, variables such as sublimation, wind-blown transport of snow, and avalanching also influence the rate of ablation and accumulation on the glacier.

Ablation characteristics are different on debris-covered glaciers than on clean-ice glaciers (i.e. visual examples of a representative debris-covered and clean-ice glacier are given in Figure 1.3). On this type of glaciers, the amount of ablation depends on several factors, e.g. debris thickness and the presence of ice cliffs and supraglacial ponds (Pellicciotti et al., 2015; Ragettli et al., 2016a; Reid and Brock, 2010; Steiner et al., 2015). The ablation zone of a debris-covered glacier is (partly) covered with a layer of supraglacial debris and can mainly be found in the tectonic-active orogenic belts, such as the Southern Alps in New Zealand, the European Alps, the Andes, and HMA (Gibson et al., 2017; Kirkbride, 2011). The magnitude of ablation depends on the thickness of debris on the glacier. Very thin layers of debris (<2 cm) enhance melt rates due to the lower albedos, whereas thicker layers of debris reduce melt rates due to the insulation of the surface (Kraaijenbrink et al., 2017; Nicholson and Benn, 2006; Østrem, 1959; Reid and Brock, 2010; Rowan et al., 2015). The debris thickness of a glacier generally increases in downward direction and reaches its maximum at the termini (Anderson, 2000; Gibson et al., 2017). The thickness distribution of debris is highly heterogeneous and variable in space and time, which depends on debris input from the hillslopes by rock/snow avalanches, rockfalls, rock slides, and the supra- and englacial transport of debris (Rowan et al., 2015; van Woerkom et al., 2019). The spatial and temporal variability of debris thickness leads to spatially and temporally variable melt rates, which eventually result in the development of ice cliffs, supra-glacial ponds, and topographic highs and lows that makes the glacier surface hummocky. The ice cliffs and supra-glacial ponds locally enhance ice melt rates, which increases the thinning rate on debris-covered glaciers, lowers the surface gradient, and stagnates the terminus (Miles et al., 2018; Pellicciotti et al., 2015; Ragettli et al., 2016a; Steiner et al., 2015). Thinning rates on debris-covered glaciers might also increase due to declining emergence velocities that determine the ice flux from the upper part to the lower part of glaciers (Banerjee, 2017; Brun et al., 2018; Nuimura et al., 2017).

Glaciers typically flow with velocities ranging from a few meters to a few kilometers per year (Cuffey and Paterson, 2010). Glacier flow is driven by the gravitational driving stress, which depends on ice thickness and surface slope. Thereby, glaciers generally flow faster when the ice thickness is larger or the surface slope is steeper. Further glacier flow is opposed by several resistant forces, namely (1) the basal drag, which is an indicator for the resistance induced by the glacier bed, (2) the resistance associated with the longitudinal stress gradient, which is an indicator for the rate of stretching or compression along the direction of the flow, and (3) the lateral drag, which is an indicator for

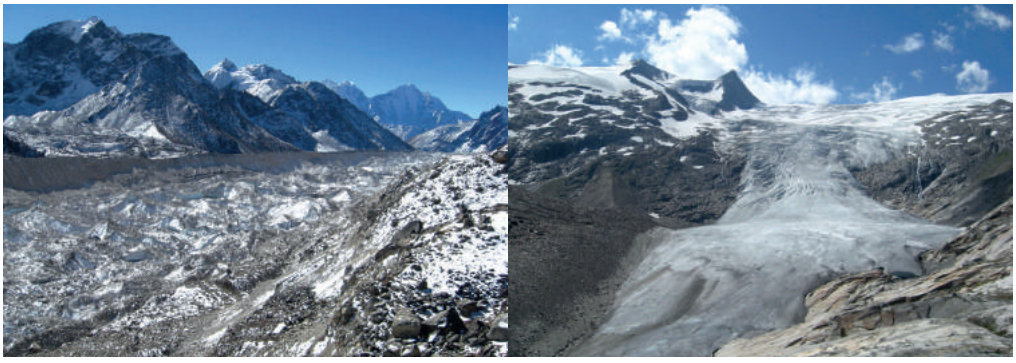

Figure 1.3. The debris-covered Khumbu Glacier, Nepal (a) and the clean-ice Schlatenkees, Austria (b). (Photos were taken by R.R. Wijngaard in 2010 and 2013, respectively).

the resistance induced by the side walls (Adhikari and Marshall, 2013; Cuffey and Paterson, 2010; van der Veen, 1999). The ratios between the gravitational driving stress and the resistant forces determine how fast a glacier flows. For instance, a grounded glacier that has a high gravitational driving stress and a low basal resistance due to a slippery bed (i.e. caused by a very thin layer of water between the glacier bed and the base of the glacier) flows faster than a glacier with a high basal resistance. The speed of glacier flow is an indicator for the ability of the glacier to evacuate supra- and englacial debris. In general, when a glacier stagnates and debris input fluxes are high, the glacier loses the ability to evacuate the debris, which results in a development/thickening of a supra-glacial debris layer (Jouvet et al., 2011).

1.2.1.2 Modelling of glaciers

To understand the response of glaciers to climate change numerical models are required that can simulate the interactions between climate change, mass balance, and ice flow dynamics. To this end, glacier mass balance models are used in combination with statistical models such as volume-area scaling, or dynamical ice-flow models. Glacier mass balance models calculate the sum of accumulation and ablation on a glacier, which can be simulated in different ways. The most common method for the simulation of ablation is the temperature-index approach or the degree-day approach (Hock, 2003; Konz and Seibert, 2010; Radić et al., 2014). This approach simulates glacier and snow melt using air temperature and calibrated degree day factors as input, where degree day factors stand for the daily amount of melt produced per positive degree of air temperature. More advanced approaches also include the effects of aspect (Immerzeel et al., 2012b) and important energy-balance components, such as albedo and radiation (Pellicciotti et al., 2005). The degree-day models that include energy-balance components can be conceived as transitional models between the simplified degree-day models and the more complex energy-balance models. Energy-balance models (e.g. Mölg et al., 2008; Paul, 2010; Reid and Brock, 2010; Strasser et al., 2008; Weber et al., 2010) are less common in use due to the model complexity, computational feasibility, and the larger requirements for data (e.g. wind speed and humidity) which are often not available. However, these models can be useful for the quantification of sublimation, which can be an important component in the mass balance of glaciers. Also, this type of model can be coupled with atmospheric models. An example of such a coupled modelling system is the high-resolution WRF-CMB modelling system that is developed by Collier et al. (2013). This modelling system consists of the Weather Research and Forecasting (WRF) mesoscale atmospheric model (Skamarock and Klemp, 2008) and a surface energy- and climate mass balance (CMB) model (Mölg et al., 2008, 2009). The modelling systems have been applied to simulate glacier-atmosphere interactions at several glaciers in HMA and have the advantage that it is able to include feedbacks between changing glacier surface conditions and atmospheric forcings. Besides the degree-day and the energy-balance models, there are also other methodologies to simulate ice ablation. For instance, Marzeion et al. (2012) estimated ice ablation based on the temperature sensitivities of glaciers, and Racoviteanu et al. (2013) estimated ice ablation by applying an ice ablation gradient model that increases melt with lowering altitude, thereby assuming zero melt at the equilibrium line altitude (ELA).

Glacier accumulation is mainly influenced by the amount of snowfall. However, avalanches may also contribute significantly to glacier accumulation, especially in steep mountain terrain (Laha et al., 2017; Ragettli et al., 2015; Scherler et al., 2011; Shea et al., 2015). Modelling approaches to simulate avalanching are, however, limited. One example of an approach that has been developed is the mass-conserving algorithm of Gruber (2007). This algorithm is an extension of flow-routing and terrain

parameterization techniques, which is able to simulate the gravitational redistribution of snow and other types of movements, such as debris flows, ice avalanches and lahars. Another similar approach is a snow transport algorithm, called SnowSlide (Bernhardt and Schulz, 2010). The algorithm is based on an exponential regression function that enables snow to be transported downslope or down-valley when a maximum snow-holding depth and threshold slope is exceeded. This means that when areas are flat the maximum snow-holding depth is large and that the maximum snow-holding depth will decrease exponentially with increasing slope angle. Also, a commonly used approach is the numerical RAMMS model (Christen et al., 2010). This model consists of a simplified model that is able to simulate avalanche runout and a random kinetic energy model that is able to simulate velocity changes over the length of an avalanche. With the RAMMS model, more realistic simulations can be achieved on the runout distance of snow avalanches and the entrainment and deposition of snow. A more recently developed approach is based on a simplified flowline model that uses observed glaciological mass balances, surface velocities, and surface-elevation profiles to estimate avalanche contributions (Laha et al., 2017). Although the method is able to indicate the importance of avalanching on glaciers well, it is difficult to apply in data scarce areas due to its dependency on the availability of field observations on glaciers.

To simulate glacier-climate interactions, glacier mass balance models are commonly used in combination with statistical models or dynamical ice-flow models. Statistical models are mostly used for regional/global model applications, where the use of dynamical flow models becomes infeasible due to the computational cost. The most commonly used statistical modelling approach is glacier volume-area scaling (Bahr et al., 1997, 2015; Marzeion et al., 2012; Radić and Hock, 2011). This approach estimates glacier volumes based on observed glacier areal extents and an empirical relationship between glacier area and volume. Other statistical approaches are, for instance, implemented by Seibert et al. (2018) using the Δh parameterization method of Huss et al. (2010) that is a single-valued relation between glacier mass and area, and by Farinotti et al. (2009) who developed a method to estimate glacier volumes based on glacier mass turnover and glacier flow dynamics that are described by Glen's flow law (Glen, 1955).

There is a variety of dynamical ice-flow models that can be used. The simplest models are flowline models that simulate ice flow along one or multiple flowlines of a glacier (Banerjee and Shankar, 2013; Huss et al., 2007; Oerlemans et al., 2017). These models often follow the (zeroth-order) Shallow Ice Approximation (SIA; Hutter, 1983; van der Veen, 1999), which drives glacier flow by ice thickness and local gradients in the surface elevation (Egholm et al., 2011). The (zeroth-order) SIA approach has the main advantage that it is computationally efficient, but has also the shortcoming that it lacks important physics that account for the effects of lateral and basal drags, which makes this approach less feasible for steep/narrow and fast-flowing glaciers (Le Meur et al., 2004). To account for these effects often correction factors are used (Adhikari and Marshall, 2011, 2012b; Nye, 1965; Oerlemans et al., 1998). Models with a higher complexity are the spatially-distributed two- and three-dimensional ice flow models that often follow higher-order or Stokes approaches. An example of a higher-order ice flow model is the iSOSIA model (Egholm et al., 2011), which includes longitudinal and transverse stress gradients. The model has been used, for instance, to simulate the feedbacks between debris accumulation, mass balance, and ice flow at debris-covered glaciers in the Khumbu region, Nepal (Rowan et al., 2015). The Stokes approach includes the full force balance of a glacier and has been used, for instance, to simulate the future evolution of the Greater Aletsch Glacier, Switzerland (Jouvet et al., 2011) or even to reconstruct the space-time trajectories of the

corpses of disappeared mountaineers (Jouvet and Funk, 2014). Drawbacks of the higher-order approaches and the Stokes approach is that the computational requirements are high and that the approaches require input data (e.g. bed topography, ice thickness) that are often not available. These drawbacks eventually hamper the application of higher-order or Stokes models in a regional setting. For this reason, spatially-distributed models with simple physics have been developed that can simulate the glaciological variables, such as ice flow velocities and thickness, reasonably. An example of such a model is the glacier mass balance and redistribution model developed by (Immerzeel et al., 2012b, 2013), which describes glacial movement by means of the Weertman sliding law (Weertman, 1957) and assumes basal sliding to be the main driver of glacial movement. The disadvantage of the model is that the glacier flow velocities simulated by the model do not represent surface flow velocities and can thus not be verified by satellite-derived or measured surface flow velocities.

1.2.1.3 Challenges

Major challenges exist in the simulation of the interactions between climate change, mass balance, and glacier dynamics. Based on the shortcomings mentioned in the previous paragraphs there is a need to develop coupled glacier mass balance and ice-flow models that are based on less complex approaches than the higher-order or Stokes approaches, with lower input data requirements and computational resources. Further, it would be advantageous when model outcomes can be verified with satellite-derived or measured glacier surface velocities. The most obvious approach would be the application of a (zeroth-order) Shallow Ice Approximation. This approach is, however, mainly used in combination with flowline models, which require knowledge of the number of flowlines. The method is thus limited in use at larger scales where multiple converging and diverging glacier flows are involved, which eventually reduces the compatibility of flowline models with gridded regional-scale hydrological models. A major challenge is therefore to develop a spatially-distributed coupled glacier mass balance and ice-flow model that is based on a gridded formulation of the Shallow Ice Approximation and does not need a priori knowledge of flowlines. Such an approach can help to overcome the drawbacks that are related to the computational expense, the data requirements, the verification of model outcomes, and the spatial scale of application.

A spatially-distributed glacier mass balance and ice-flow model has the advantage that the interactions between climate change, mass balance and glacier dynamics can be simulated. There are many studies that used a wide range of ice-flow models to assess the impacts of climate change on glacier dynamics, both from historical and future perspectives (Banerjee and Shankar, 2013; Berthier and Vincent, 2012; Jouvet et al., 2011; Oerlemans et al., 1998; Zekollari et al., 2014). Although there is knowledge of how glaciers respond to climate change, the understanding of the attribution of observed glacier changes to anthropogenic or natural climate change is limited, which can be testified by the limited number of studies on the subject (e.g. Hirabayashi et al., 2016; Marzeion et al., 2014). These studies have mainly assessed the anthropogenic and natural influences on glaciers by focussing on glacier mass balances without taking glacier dynamics into consideration. Several studies have, however, found a relation between glacier dynamics and thinning rates on glaciers (Banerjee, 2017; Berthier and Vincent, 2012; Brun et al., 2018; Dehecq et al., 2019; Huss et al., 2007; Nuimura et al., 2017). In addition it has been found that clean-ice glaciers show a different response to climate change than debris-covered glaciers due to debris that insulates the glacier (Jouvet et al., 2011; Østrem, 1959; Reid and Brock, 2010; Rowan et al., 2015). Therefore another challenge is to understand the response of clean-ice and debris-covered glaciers to anthropogenic and natural climate change.

1.2.2 Understanding and modelling hydrological impacts of climate change at the catchment scale

1.2.2.1 Hydrological modelling in mountainous catchments

Mountainous (headwater) catchments are the domains where cryospheric and hydrological processes interact and influence the local natural water balance, which is determined by the amount of water that enters or leaves a catchment and the changes in storage over time (Dingman, 2008). Water enters a catchment by precipitation that falls in the form of rain, snow, or a rain-snow mixture, depending on the prevailing air temperature, and leaves a catchment by evapotranspiration (i.e. transpiration from vegetation and evaporation from soils and open water), sublimation, or stream outflow. Between the moment water enters a catchment and leaves a catchment, water can be transported or stored by means of several pathways or storages, respectively. Transportation can occur via fast pathways, such as avalanching or surface runoff, or via slower pathways, such as lateral flow through soils, groundwater flow through aquifers, or glacier flow. Storage of water can occur in a solid state by glaciers or snow reserves where water can reside for time scales varying from several months (snow) to hundred years (mountain glaciers) until its release by melting during spring and summer seasons (Marshak, 2008). In a liquid state, storage of water occurs in streams, lakes, soils, and groundwater aquifers over scales varying from several months (streams and soils) up to thousands of years (deep groundwater aquifers) (Marshak, 2008).

Understanding the response of cryospheric-hydrological processes to climate change is important since many people living in mountain catchments heavily rely on mountain water resources. Especially during very dry summer seasons or in (semi-)arid catchments the meltwater originating from glaciers might be the only substantial water resource. Glacier retreat as a response to climate change is expected to result in vanishing meltwater resources, which will eventually have a devastating impact on the local societies in mountain catchments. For example, currently more than 50% of the total electricity production in countries like Austria, Nepal, and Switzerland is generated by hydropower plants (IRENA, 2018). Although the hydropower potential is often higher (Gernaat et al., 2017; Gurung et al., 2016; Vaidya, 2012), it is questionable whether these potentials can be reached considering the prospects on climate-induced decreases in meltwater. Besides changes in water availability, local hydrological extremes can also change that might result in increased risks of floods or droughts. These natural hazards might affect, for instance, local agricultural production by the loss of agricultural land due to landslides, river floods, or land degradation (Abbasi et al., 2017). To deal with the potential impacts of climate change, we need to improve our knowledge of the hydrological response of mountain environments to climate change. Therefore, it is necessary to develop and apply hydrological models that have an accurate representation of cryospheric-hydrological processes (state, pathways, and residence times).

Hydrological models are commonly categorized in terms of model structure or spatial discretization. In terms of model structure, hydrological models can be classified as empirical, conceptual and physically-based. Empirical models are based on empirical relationships between precipitation and runoff, physically-based models have a detailed representation of biophysical processes, and conceptual models are in between empirical and physically-based models. In terms of spatial discretization, models can be classified as lumped, semi-distributed, or distributed, where semi-distributed models enable the subdivision of catchments in several subbasins, elevation zones, or zones with a similar hydrological response (i.e. hydrological response units, HRUs). In

mountainous catchments, semi-distributed conceptual and distributed physically-based models are the most frequently used hydrological models, especially because these models can cover the high spatial variability in mountain-hydrological processes better compared to lumped empirical models. A key characteristic of semi-distributed conceptual and distributed physically-based models is that the models contain routines that can simulate snow/glacier melt and accumulation, which are important processes in high-mountain hydrology.

Semi-distributed conceptual models that are frequently applied in mountainous catchments are the Snowmelt Runoff Model (SRM) (Martinec and Rango, 1986) and the Hydrologiska Byråns Vattenbalansavdelning (HBV) model (Bergström, 1992). These models have been applied, for instance, in catchments located in HMA and the European Alps (Akhtar et al., 2008; Immerzeel et al., 2010; Junghans et al., 2011; Li et al., 2015). The models have a similar structure, subdivide catchments into several elevation zones, and simulate snow and glacier melt by means of degree-day approaches. In addition, the HBV model enables a subdivision of elevation zones in several vegetation/land cover zones (e.g. glacier, bare rock, and grasslands). Further, the HBV model considers also the effects of the aspect on snow and glacier melt (Konz and Seibert, 2010). Examples of spatially-distributed physically-based models that have been applied are the Topographic Kinematic Wave Approximation and Integration (TOPKAPI) model (Ragettli and Pellicciotti, 2012) and the Water Flow and Balance Simulation Model (WASIM-ETH) (Schulla, 2017). These models have mainly been applied in catchments located in HMA, the European Alps, and the Andes (Ayala et al., 2016; Kormann et al., 2016; Ragettli et al., 2016b; Strasser et al., 2018), and contain modules that simulate glacier and snowmelt by simple energy-balance approaches or temperature-index approaches that either include the effects of shortwave radiation and albedo or the effects of wind on melt (Pellicciotti et al., 2005; Schulla, 2017). An advantage of using physically-based models above conceptual models is that the parameters of physically-based models can be assessed directly by using measurements (e.g. Graham and Bergström, 2001). The disadvantage is that physically-based models require more input data, which is often not or limited available in data-scarce areas. Also, the computational cost of physically-based models is higher, which makes conceptual models more favourable in use. Lastly, the spatial variability in cryospheric-hydrological processes in a (headwater) catchment is relatively small compared to the spatial process variability in river basins. Therefore, the application of conceptual hydrological models can be considered as more favourable.

1.2.2.2 Challenges

Forthcoming from the previous paragraphs, one of the main challenges that can be identified is the improvement of our understanding of the hydrological response of glacierized (headwater) catchments to future climate change. This knowledge might be used for the development of future adaptation strategies that can reduce the hydrological impacts in mountain valleys. To study the impacts of climate change on the hydrology of glacierized catchments, conceptual hydrological models can be considered as favourable tools. The use of single conceptual hydrological models is, however, questionable since large differences may exist between the outcomes of different hydrological models under the same climate change scenarios (Eregno et al., 2013; Jiang et al., 2007). Therefore, another main challenge is to increase the reliability of model outcomes by using multiple conceptual hydrological models with different degrees of complexity.

1.2.3 Understanding and modelling regional/basin-scale climate change impacts

1.2.3.1 Modelling of hydrological extremes

Climatic changes that occur in mountainous headwater catchments not only affect the local hydrology and cryosphere but also affect the hydrology of catchments that are located downstream since catchments are spatially connected within a basin. According to Sivapalan (2018), catchments are connected to each other in three ways: 1) downwind movement of water via the atmosphere, 2) downstream movement of water via surface runoff (e.g. streams and rivers), and 3) downstream movement of water via subsurface runoff (e.g. lateral flow through soils and baseflow through groundwater aquifers) from recharge areas (i.e. in the mountains) to discharge areas (i.e. in the streams, lakes, deltas, and estuaries of the floodplains). The downwind movement via the atmosphere is coherent with the large-scale atmospheric circulations driven by pressure gradients, such as the monsoon systems in South and East Asia and the Atlantic low-pressure systems in Central Europe (Khanal et al., 2019; Lau and Kim, 2018; Li et al., 2018; Ridder et al., 2018). These large-scale atmospheric circulations dominate the regional climate and produce large amounts of precipitation over the continents and its mountain ranges. To understand the changes in the regional climate, its patterns, and its impacts on future hydrological extremes it is therefore inevitable to apply hydrological models on a regional/basin scale.

In recent years, many studies have outlined the impacts of future climate change on hydrological extremes in river basins. Global studies on river basins were performed, for example, by Hirabayashi et al. (2013) and Pechlivanidis et al. (2016). Hirabayashi et al. (2013) used a global river routing model (including an inundation scheme) forced with runoff outputs of eleven atmospheric-ocean general circulation models (AO-GCMs) to analyse future changes in flood frequencies for four Representative Concentration Pathways (RCPs). The projections of this study show a large increase in flood frequency in a large part of Asia, eastern Africa, and the northern half of the Andes. Pechlivanidis et al. (2016) applied five different (semi-)distributed physically-based hydrological models to five different river basins (i.e. Lena, Rhine, Ganges, Niger, and Tagus) by forcing the models with five different general circulation models (GCMs) that represent four RCPs. The outcomes of this study show a varied distribution of changes in hydrological extremes with both increases and decreases in extremes. This variation in response mainly depends on the hydro-climatic gradient, the climate projections and the used impacts models. Examples of regional basin-scale studies that have been performed in recent years are the studies by Gu et al. (2015) in the Yangtze river basin and Lutz et al. (2016a) in the upper Indus basin. Gu et al. (2015) investigated hydrological extremes by forcing a semi-distributed physically-based surface water and energy balance model with outputs of a regional climate model (RCM) for the SRES A1B scenario. The outputs show a projected increase in the frequency of extreme floods towards the future. Lutz et al. (2016a) used the fully-distributed physically-based Spatial Processes in Hydrology (SPHY) model (Terink et al., 2015) to simulate future changes in the hydrological means and extremes by forcing the model with downscaled GCM model outputs for RCP4.5 and RCP8.5. This study shows projected increases in the frequency and intensity of extreme river discharge conditions. Most of the studies mentioned above have in common that there is no emphasis on the effects of climate change on mountain-hydrological processes, such as snow and ice melt, which is an important component in the hydrology of mountainous river basins. The absence of this emphasis hampers the understanding of how climate change will impact mountain-hydrological processes and subsequently which implications changes in these processes have on the occurrence of hydrological

extremes. For example, temperature increases will most likely result in increased ice and snowmelt, which subsequently might contribute to the occurrence of high flows, especially in basins where ice and snowmelt are large contributors to the total runoff (e.g. Rao et al., 2018).

1.2.3.2 Modelling of water supply and demand

Another reason to apply hydrological models on a regional/basin scale is to improve understanding of the water resources management of river basins. Over the last decades, the global population has grown rapidly, which is expected to continue in the future. It is projected that the global population will increase from about 6 billion people nowadays up to about 12 billion people in 2100 (Riahi et al., 2017). The rapid global population growth will most likely be accompanied by strong economic developments and a growing demand for food and energy. This requires an increase in food production and thus an expansion of agricultural land, which will be a challenge due to the rising competition among land users (van der Esch et al., 2017). Not only agricultural land will expand. It is also likely that more human interventions, such as the construction of irrigation canal systems hydropower dams, and reservoirs, will take place. These interventions can, for instance, cause a lowering of river discharge rates (Biemans et al., 2011). The rapid population growth and associated strong socio-economic developments are expected to result in a strong increase in water demand and withdrawals, which eventually will lead to an increased pressure on surface water and groundwater resources (e.g. Liu et al., 2017; Wada et al., 2016a). The pressure on water resources is already large in regions where high water demands coincide with a limited (seasonal) water availability (e.g. Pakistan, India, Middle East, and the USA) (e.g. Wada et al., 2016a). These regions already face groundwater depletion and severe water scarcity during several months a year (e.g. Wada, 2016). The complexity of interactions between water demand and water availability necessitates the application of hydrological models on a regional/basin scale instead of applying models for a few isolated catchments (Liu et al., 2014; Sivapalan, 2018).

The interactions between water availability and water demand have been investigated extensively on a global scale and regional scale as well over the past decades (Liu et al., 2017). To this end, several high-resolution global modelling applications, such as PCR-GLOBWB (Sutanudjaja et al., 2018; van Beek et al., 2011), LPJmL (Bondeau et al., 2007; Schaphoff et al., 2018), H08 (Hanasaki et al., 2008a), and WaterGAP (Alcamo et al., 2003) have been developed. These models have been applied for global and regional assessments on the past, present, and future impacts of climate change and socio-economic developments on water resources availability (Arnell and Lloyd-Hughes, 2014), water use (Wada et al., 2014, 2016b), water scarcity (Gain and Wada, 2014; Hanasaki et al., 2013; Hoekstra et al., 2012; Veldkamp et al., 2017; Wada et al., 2011a), environmental flows (Jägermeyr et al., 2017), groundwater depletion (de Graaf et al., 2017; Wada, 2016), amongst others. The main advantage of the models is that feedbacks between water availability and the major types of water uses (agricultural, domestic, and industrial) are represented and that human interventions, such as land use change, man-made reservoirs, and irrigation canal systems, can be included as well (Biemans et al., 2011; Veldkamp et al., 2017). However, a drawback is that often no explicit distinction is made between upstream and downstream domains and their roles in supply and demand. To consider the upstream-downstream linkages is important to understand, for example, what impacts climate change can have on upstream water supply and its subsequent implications for downstream water availability (e.g. Nepal et al., 2018). To some extent, upstream-downstream linkages have been applied in global water stress assessments by Munia et al. (2016). The authors did not, however, subdivide upstream and downstream domains based on its topographic location

(i.e. mountain areas vs. floodplains) but based on its location in relation to other countries. In this manner, it is difficult to make a distinction in the role of processes that are dominant the different domains. For instance, in the upstream domains (i.e. mountain ranges), mountain-hydrological processes are most dominant and the spatial process variability is large over a short horizontal distance. To simulate the evolution of mountain water resources properly, higher resolution models are thus required that have a sufficient representation of the mountain-hydrological processes. In the downstream domains (i.e. the floodplains), other processes are dominant, such as irrigation and other human interventions. To consider the effects of these interventions on the hydrological cycle a high-resolution model is therefore required that has an explicit representation of human interventions.

1.2.3.3 Challenges

In the previous paragraphs, the modelling of hydrological extremes and water resources have been introduced. From this introduction, it can be concluded that mountain-hydrological processes are often not represented sufficiently in models, which eventually either impose uncertainties in the simulation of hydrological extremes or the simulation of upstream water supplies. One major challenge is therefore to improve our understanding of the impacts of climate change on mountain-hydrological processes and its implications for the occurrence of hydrological extremes in mountainous domains. In addition, a challenge is to understand how climatic extremes (i.e. precipitation and temperature extremes) can be related to the occurrence of hydrological extremes. Another major challenge that can be identified is to understand to which extent water availability can fulfill the current water demand and future water demand under combinations of future climate change and socio-economic developments that occur in mountainous river basins. Here, the challenge is to make an explicit distinction between upstream and downstream domains by using models that have a sufficient representation of mountain-hydrological processes in the upstream mountainous domains and the effects of human interventions on the hydrological cycle in the downstream-located floodplains.

1.3 Research aim and outline

In the preceding sections, several major challenges were identified that need to be faced to improve our knowledge of the cryospheric and hydrological impacts of climate change on different spatial scales in mountainous river basins. In summary, the challenges that have been identified, are:

- Developing a spatially-distributed coupled glacier mass balance and ice-flow model that includes a gridded formulation of the shallow ice approximation and can be used to separately assess the effects of human-induced climate change on glacier mass balance and dynamics.
- Reliable simulation of the hydrological response of glacierized (headwater) catchments to future climate change by using multiple conceptual hydrological models.
- Improving our understanding of the impacts of climate change on hydrological extremes in regional mountainous domains.
- Developing a basin-scale coupled modelling approach, consisting of a cryospheric-hydrological model and a hydrology and crop production model, that can simulate the interactions between water availability and demand, and the related potential development of a water gap under present and future climatic changes and socio-economic developments.

The main objective of this Ph.D. thesis is

Understanding the (cryospheric-)hydrological impacts and challenges of climate change across different spatial scales in mountainous river basins

Forthcoming from the main objective and the identified challenges, the following research questions (RQs) are formulated:

RQ1 What are the attributions of natural and anthropogenic climate change in the response of single glaciers to climate change?

RQ2 Is it possible to make reliable projections of climate change impacts on the hydrology of glacierized headwater catchments by using multiple conceptual hydrological models?

RQ3 What is the impact of climate change on hydrological extremes in regional mountainous domains?

RQ4 What are the key drivers in the potential development of a water gap in large mountainous river basins?

In the following chapters I will address the research questions. In Chapter 2 a spatially-distributed coupled glacier mass balance and ice-flow model is presented that is developed and applied to investigate the response of the debris-covered Langtang Glacier in the Himalayas and the clean-ice Hintereisferner in the European Alps under changing climate conditions since the end of the Little Ice Age. The effects of human-induced climate change on glacier mass balance and dynamics will be assessed separately by the following two scenarios: a scenario with further anthropogenic forcing and one scenario without further anthropogenic forcing from 1971 onwards. In Chapter 3 two semi-distributed conceptual hydrological models with different degrees of complexity are applied to investigate the hydrological response of an Austrian glacierized headwater catchment to future climate change. The outputs of the model are used to analyse changes in the seasonality of high runoff conditions and annual flood peaks, absolute and relative runoff changes, and the low flow characteristics. In Chapter 4 a fully-distributed cryospheric-hydrological model is applied to assess the impacts of climate change on the occurrence of future hydrological extremes in the upstream mountainous domains of the Indus, Ganges and Brahmaputra river basins for two RCPs. The outputs are used to analyse future changes in hydro-climatic extremes with a focus on high and low flows. In Chapter 5 a coupled modelling approach is applied that consists of a fully-distributed cryospheric-hydrological model, simulating the current and future upstream water supplies, and a fully-distributed hydrology and crop production model that simulates the current and future downstream water supplies and demands. The modelling approach is applied to investigate the combined impacts of climate change and socio-economic developments on the development of the future water gap in South Asia. In Chapter 6 the main findings of the Ph.D. research are synthesized and discussed, and an outlook is provided on possible future research directions.

Chapter 2 to 5 are based on published peer-reviewed scientific journal publications.

2 Modelling the response of glaciers to historical climate change

This study aims at developing and applying a spatially-distributed coupled glacier mass balance and ice-flow model to attribute the response of glaciers to natural and anthropogenic climate change. We focus on two glaciers with contrasting surface characteristics: a debris-covered glacier (Langtang Glacier in Nepal) and a clean-ice glacier (Hintereisferner in Austria). The model is applied from the end of the Little Ice Age (1850) to the present-day (2016) and is forced with four bias-corrected General Circulation Models (GCMs) from the historical experiment of the CMIP5 archive. The selected GCMs represent region-specific warm-dry, warm-wet, cold-dry, and cold-wet climate conditions. To isolate the effects of anthropogenic climate change on glacier mass balance and flow runs from these GCMs with and without further anthropogenic forcing after 1970 until 2016 are selected. The outcomes indicate that both glaciers experience the largest reduction in area and volume under warm climate conditions, whereas area and volume reductions are smaller under cold climate conditions. Simultaneously with changes in glacier area and volume, surface velocities generally decrease over time. Without further anthropogenic forcing the results reveal a 3% (9%) smaller decline in glacier area (volume) for the debris-covered glacier and an 18% (39%) smaller decline in glacier area (volume) for the clean-ice glacier. The difference in the magnitude between the two glaciers can mainly be attributed to differences in the response time of the glaciers, where the clean-ice glacier shows a much faster response to climate change. We conclude that the response of the two glaciers can mainly be attributed to anthropogenic climate change and that the impact is larger on the clean-ice glacier. The outcomes show that the model performs well under different climate conditions and that the developed approach can be used for regional-scale glacio-hydrological modelling.

Based on: *Wijngaard, R.R., Steiner, J.F., Kraaijenbrink, P.D.A., Klug, C., Adhikari, S., Banerjee, A., Pellicciotti, F., van Beek, L.P.H., Bierkens, M.F.P., Lutz, A.F., and Immerzeel, W.W. Modelling the response of the Langtang Glacier and the Hintereisferner to a changing climate since the Little Ice Age. Frontiers in Earth Science 7 (143). DOI: 10.3389/feart.2019.00143.*

2.1 Introduction

Ongoing global warming has resulted in the retreat of glaciers over the last decades with important consequences for society and environment. Glacier mass loss has contributed to global sea-level rise (Gregory et al., 2013; Radić and Hock, 2011) and seasonal changes in river discharge (Beniston et al., 2018; Hanzer et al., 2018; Huss and Hock, 2018; Immerzeel et al., 2012b; Kaser et al., 2010; Lutz et al., 2014). In addition, glacier retreat will most likely lead to natural hazards as a result of the destabilization of mountain slopes and hanging glaciers or the development of moraine-dammed lakes (Faillettaz et al., 2015; Frey et al., 2010; Haeberli et al., 2017).

<< The debris-covered Khumbu Glacier seen from the Kala Patthar (5545 m), Nepal (R.R. Wijngaard)

Global glacier retreat started at the end of the Little Ice Age (LIA), which terminated globally around 1850 (Leclercq et al., 2011) and coincided with the Industrial Revolution that led to an increase in the emission of greenhouse gasses. Since the glacier area/length response to climate change has a lag of several decades (Adhikari et al., 2011; Banerjee, 2017; Banerjee and Shankar, 2013; Johannesson et al., 1989) it is difficult to unambiguously attribute glacier retreat to anthropogenic causes (Marzeion et al., 2014). In the 19th century, the anthropogenic influence on the climate system was limited, which therefore could not be the main cause of glacier mass losses (Myhre et al., 2013). Over the 20th century, however, the anthropogenic influence increased rapidly as a result of the ongoing industrialization, in particular after the 1970s (Myhre et al., 2013). These increases have resulted in the anthropogenic climate signal becoming a prevailing explanation for the observed decrease in glacier mass since the 1980s (Hirabayashi et al., 2016; Marzeion et al., 2014).

Until now, the anthropogenic and natural influences on historical glacier changes have mainly been investigated in studies with a focus on changes in glacier mass balance (Hirabayashi et al., 2016; Marzeion et al., 2014). Several studies have, however, found a relation between glacier dynamics and thinning rates on glaciers (Banerjee, 2017; Berthier and Vincent, 2012; Dehecq et al., 2019; Huss et al., 2007). For example, Berthier and Vincent (2012) found that accelerated thinning rates during the last decades on the Mer de Glace Glacier, a partially debris-covered glacier in France, could partly be attributed to reduced ice fluxes. A more recently published study on glacier slowdown in High Mountain Asia (Dehecq et al., 2019) revealed that glaciers in most parts of the region show a sustained slowdown that is associated with ice thinning. Also, the authors found stable or increased ice flow in the regions around the Tibetan Plateau and the Tarim river basin where stable or positive mass balances are observed. Banerjee (2017) found that thinning rates on both debris-covered and clean-ice glaciers were dependent on the relation between mass balance changes and ice flux changes. Clean-ice glaciers show a different response to climate change than debris-covered glaciers because the supraglacial debris generally insulates the ice (Jouvet et al., 2011; Nicholson and Benn, 2006; Østrem, 1959; Reid and Brock, 2010; Rowan et al., 2015). On clean-ice glaciers, larger thinning rates are caused by a combination of reduced ice flow and a negative surface mass balance, which correspond to receding termini. On debris-covered glaciers, on the other hand, the negative mass balance is rather small due to insulation of the surface, which in combination with a reduced ice flow result in surface lowering, but without an considerable retreat of the glacier terminus (Banerjee, 2017; Banerjee and Shankar, 2013; Hambrey et al., 2009; Naito et al., 2000; Rowan et al., 2015). To understand the response of both types of glaciers to climate change, it is therefore necessary to make a proper coupling between mass balance models and ice flow models that have a sufficient representation of glacier dynamics (Adhikari and Marshall, 2013; Clarke et al., 2015; Huss et al., 2007; Shea et al., 2015).

Existing ice flow models vary between simple flowline models (Aðalgeirsdóttir et al., 2011; Adhikari and Huybrechts, 2009; Banerjee and Shankar, 2013; Greuell, 1992; Huss et al., 2007; Oerlemans et al., 1998; Span et al., 1997; van de Wal and Oerlemans, 1995) and spatially-distributed three-dimensional higher-order or Stokes models (Adhikari and Marshall, 2012a, 2013; Jouvet et al., 2011; Jouvet and Funk, 2014; Leysinger Vieli and Gudmundsson, 2004; Seroussi et al., 2011; Zekollari et al., 2014). A simple description of glacial ice deformation is provided by the so-called Shallow Ice Approximation (SIA) of Stokes equations (Hutter, 1983), where ice flow can be obtained from a local gradient in glacier surface elevation and ice thickness (Egholm et al., 2011). This approach has the main advantage that the computational cost and data demand are low in comparison with the

more complex higher-order or Stokes models, and is therefore useful in large-scale studies of glacier dynamics in data-scarce regions, such as High Mountain Asia. In addition, the approach enables the calibration against observed surface velocities (e.g. those derived from satellite-based imagery) more readily. For large-scale applications, glacier flow is also represented using a simpler approach that assumes basal sliding, such as the one described by Weertman's sliding law (Weertman, 1957), to be the main driver of glacial movement. Many glaciers, however, are driven by a combination of internal deformation and basal sliding, which therefore hampers the calibration and validation of modelling approaches that solely rely on basal sliding laws (Adhikari and Marshall, 2013; Cuffey and Paterson, 2010; Nye, 1965). SIA models, by design, assume the dominance of vertical shear stress at the ice/bed interface and ignore higher-order stresses that describe lateral and longitudinal drags, which might limit its use on fast-flowing or steep/narrow valley glaciers (Adhikari and Marshall, 2013; Le Meur et al., 2004). To overcome this drawback, higher-order perturbative corrections to shallow ice models may be considered (Egholm et al., 2011; Rowan et al., 2015). However, the implementation of such corrections increases numerical complexity. Therefore, to account for the higher-order physics, correction factors are used that can sustain the simplicity of SIA models and yet obtain more realistic results at the same time (Adhikari and Marshall, 2011, 2012b; Nye, 1965).

Many models based on the SIA have been applied as flowline models (Adhikari and Huybrechts, 2009; Banerjee and Shankar, 2013). Although these types of models are easy to apply, they still require a priori knowledge of the number and orientation of flowlines on glaciers. This can be a disadvantage when applied over longer timescales (i.e. due to the varying orientation of flowlines over time) or at a larger spatial scale (i.e. when a larger number of flowlines is required to represent realistic dynamics of glaciers), which eventually reduces the compatibility of flowline models with gridded regional-scale hydrological models. In this context, spatially-distributed SIA models can be useful. As these models simulate the two-dimensional flow of ice, a priori information about flowline geometry is not required. These spatially-distributed SIA models are useful in simulating the evolution of the boundary and hypsometry of glaciers that naturally allows the feedbacks between glacier dynamics and mass balance forcing to be taken into account. Spatially-distributed SIA models should be invaluable for the accurate and efficient representation of glaciers in gridded regional-scale hydrological models (e.g. Immerzeel et al., 2012, 2013; Shea et al., 2015).

The main aim of this study is to develop and apply a spatially-distributed coupled glacier mass balance and dynamical ice-flow model towards understanding the response of glaciers to natural and anthropogenic climate change. We focus on two glaciers with contrasting surface characteristics: the Hintereisferner, which is a clean-ice glacier located in the European Alps, and the Langtang Glacier, which is a debris-covered glacier located in the Central Himalayas. We apply the model from the end of the LIA (1850) to the present-day (2016) and force the model with the outputs of four bias-corrected General Circulation Models (GCMs) that were pre-selected from the historical experiment of the Coupled Model Intercomparison Project Phase 5 (CMIP5). For the selected GCMs we selected runs with and without further anthropogenic forcing from 1971 onwards to separately assess the effects of anthropogenic climate change on glacier mass balance and flow. The novelty of this study in comparison with previous works in the two regions is its attribution of the response of two contrasting glaciers (i.e. in terms of surface characteristics) to natural and anthropogenic historical climate change using a coupled glacier mass balance and dynamical ice-flow model.

2.2 Study area

We have selected two glaciers: the Langtang Glacier (Central Himalayas, Nepal), and the Hintereisferner (Central Eastern Alps, Austria) (Figure 2.1).

Langtang Glacier (28.296972 °N 85.709775°E) is a debris-covered valley glacier, which is located approximately 70 km north of Kathmandu. The glacier has a length of approximately 18 km and covers an area of 46.5 km^2 (2006; Ragettli et al., 2016). The elevation ranges from 4370 m a.s.l. at the terminus to 7119 m a.s.l. in the northernmost part of the catchment. The glacier surface slope varies from 4% to 88% with a mean of 32%. About 35% of Langtang Glacier is covered with debris, where most of the debris can be found in the ablation areas below 5200 m. a.s.l. The transition from debris-covered to clean-ice surfaces is very short and the heterogeneous surface of the Langtang Glacier is characterized by scattered ice cliffs and supraglacial ponds throughout all seasons (Ragettli et al., 2016; Steiner et al., 2019). The climate in the Langtang Valley is dominated by the Indian monsoon with predominant easterly winds during the monsoon period and westerly winds from October to May (Immerzeel et al., 2012b). During the monsoon period, more than 70% of the annual precipitation falls, whereas winters are relatively dry (Collier and Immerzeel, 2015; Immerzeel et al., 2012b). In general, precipitation decreases with altitude during the monsoon season, whereas during the winter season precipitation increases with altitude (Collier and Immerzeel, 2015). The mean daily temperature at Kyangjin meteorological station (3930 m a.s.l.; located ~12 km from Langtang Glacier) is 4.0 °C, and the mean annual precipitation sum 665 mm (over 1988-2016).

Hintereisferner (46.798814°N 10.770068°E) is a clean-ice valley glacier located in the upper part of the Rofental, Ötztal Alps, Austria. The glacier has a long record of investigations with the first measurements dating from 1894 and is classified as a 'reference glacier' by the World Glacier Monitoring Service. This means that glacier changes are mainly driven by climate inputs and are not subject to other major influences, such as heavy debris cover, avalanching, surging, ice calving, or artificial snow (WGMS, 2018). The glacier has a length of approximately 7 km and an area of 7.4 km^2 (2006; Charalampidis et al., 2018). The total area of glaciers (including the adjacent Kesselwandferner and Hochjochferner) amounts to 19.5 km^2. During the LIA, the length of the Hintereisferner reached up to about 10 km. Further, the Kesselwandferner used to be linked with the Hintereisferner, but has been detached since the 1920s (Kuhn et al., 1985). The elevation ranges from 2238 m a.s.l. at the LIA terminus of the Hintereisferner to 3661 m a.s.l. The glacier surface slope varies from less than 1% to 78% with a mean of 25%. The climate in the Rofental can be characterized as a dry inner alpine climate with the lowest precipitation sums during winter (~125 mm) and the highest precipitation sums during summer (~265 mm) at the meteorological station in Vent (1900 m a.s.l.; located ~10 km from the Hintereisferner) (over 1987-2016). The mean annual precipitation sum amounts to 750 mm and the higher annual precipitation sums (>1500 mm) are mainly measured at the higher altitudes around 3000 m a.s.l. (Strasser et al., 2018). The annual average temperature at the meteorological station in Vent is 3 °C (over 1988-2016).

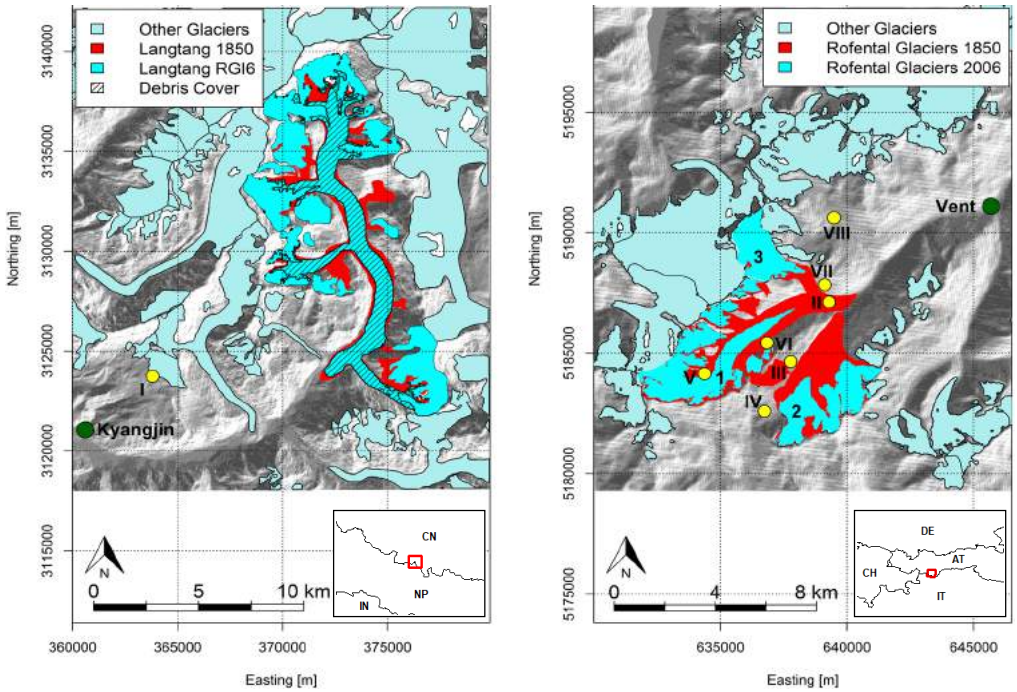

Figure 2.1. The Langtang Glacier (left) and Hintereisferner (right) with the glacier outlines of 1850 (turquoise), the current glacier outlines (red), and the current debris extents (black stripes; Langtang Glacier). The other glaciers (light blue) and the locations of the primary and secondary meteorological stations (green and yellow dots, respectively) in the region are also shown. The numbers 1, 2, and 3 denote the locations of the Hintereisferner, Hochjochferner, and Kesselwandferner, respectively. The numbers I-VIII denote the locations of the Yala base camp (I), Hochjochhospiz (II), Latschbloder (III), Bella Vista (IV), Hintereis (V), Rofenberg (VI), Proviantdepot (VII), and Vernagtbrücke (VIII) stations. Source of the glacier outlines are the Randolph Glacier Inventory v6 (Pfeffer et al., 2014) and the Austrian glacier inventories (Abermann et al., 2009; Fischer et al., 2015). The debris extents are obtained from Kraaijenbrink et al. (2017).

2.3 Data and methods

2.3.1 Historical & reference daily climate forcing

The glacier mass balance and ice-flow model is forced with climate data for the period 1851-2016. The forcing consists of two datasets: observed climate data derived from local meteorological stations and modelled climate data derived from GCM outputs.

The observed climate data consists of daily precipitation and mean air temperature data extracted from the Vent and Kyangjin stations for a 30-year period (1987-2016) and a 29-year period (1988-2016), respectively. The meteorological data of Vent station were complete, whereas the data of Kyangjin station required some gap filling. About 13% of the data is missing and gaps mainly occur randomly with the majority of the missing values occurring in the periods 1989-1994 and 2012-2016. These gaps were filled with bias-corrected ERA-Interim data (Dee et al., 2011). The temperature data are spatially interpolated by lapsing temperature from the station elevation to

the grid cell elevation, using a 30 m DEM and vertical monthly temperature lapse rates. We use the SRTM DEM (Farr et al., 2007) and the EU-DEM (EEA, 2017) for the Langtang Glacier and Hintereisferner, respectively. The monthly temperature lapse rates for the Langtang Glacier are derived from daily mean air temperature data for the period 2013-2014, which are measured at Kyangjin station and Yala base camp station (28.23252°N 85.61208°E; 5090 m a.s.l.). For the Hintereisferner, the monthly temperature lapse rates are derived from daily mean air temperature records for the period 2013-2016, which are measured at the Vent, Latschbloder (46.80118°N 10.80561°E; 2910 m a.s.l.), and Bella Vista (46.78284°N 10.79138°E; 2805 m a.s.l.) stations (Strasser et al., 2018;). The derived temperature lapse rates are subsequently corrected by correction factors to account for the long-term uncertainty in the derived lapse rates. To this end, the mean elevation of the 0 °C isotherm derived by Heynen et al. (2016) and the long-term mean elevation of the 0 °C isotherm (3220 m a.s.l.) derived by Fischer (2010) are used as reference for Langtang Glacier and Hintereisferner, respectively. The corrected averaged annual temperature lapse rates are 0.0064 °C m^{-1} and 0.0073 °C m^{-1} at Langtang Glacier and Hintereisferner, respectively. The corrected lapse rates are 0.001 °C m^{-1} and 0.0015 °C m^{-1} higher than the original rates derived from the meteorological stations. On monthly basis the corrected maximum (minimum) lapse rates are 0.0076 (0.0052) °C m^{-1} in March-April (July) at Langtang Glacier and 0.0086 (0.0049) °C m^{-1} in March (December) at Hintereisferner. The monthly lapse rates are subsequently used to distribute the daily mean air temperature data from the Kyangjin and Vent stations over the Langtang Glacier and Hintereisferner areas, respectively.

The precipitation data are spatially distributed using a 30 m DEM, vertical monthly precipitation lapse rates for the Hintereisferner, and normalized monsoon and winter precipitation fields for Langtang Glacier. The monthly precipitation lapse rates are derived from monthly precipitation sums measured at the Vent, Latschbloder, Hochjochhospiz (46.82310°N 10.82616°E; 2360 m a.s.l.), Vernagtbrücke (46.85461°N 10.82979°E; 2600 m a.s.l.), Proviantdepot (46.82951°N 10.82407°E; 2737 m a.s.l.), Rofenberg (46.80847°N 10.79344°E; 2827 m a.s.l.), and Hintereis (46.79727°N 10.76096°E; 2964 m a.s.l.) stations (over the period 1987-2016) (Strasser et al., 2018). The precipitation lapse rates vary between 1.3 % km^{-1} and 4.7 % km^{-1}, with the highest and lowest lapse rates in the summer and winter seasons, respectively. The monthly precipitation lapse rates are subsequently used to distribute the daily precipitation data from Vent station over the Hintereisferner area. For Langtang Glacier, tabulated gradients of accumulated precipitation reported by Collier and Immerzeel (2015) for the monsoon and winter seasons are used in combination with a 30 m DEM to derive spatial precipitation distributions for Langtang Valley. The monsoon gradients are in general negative above 3000 m a.s.l.., whereas during the winter season the situation is reversed, with in general positive gradients (Collier and Immerzeel, 2015). The spatial distributions are normalized and used to distribute precipitation from Kyangjin station over upper Langtang Valley. Normalized winter distributions are used for the winter, pre-monsoon, and post-monsoon seasons, and normalized monsoon distributions are used for the monsoon season.

For the representation of historical climate change, we force the glacier mass balance and flow model with an ensemble of downscaled general circulation models (GCMs) that are realizations from the historical experiment (1851-2005), i.e. forced with combined anthropogenic and natural forcings (e.g. solar and volcanic). For each region of interest, four GCM runs are selected from the CMIP5 multi-model ensemble (Taylor et al., 2012) for the historical experiment. The GCMs runs are selected by using an advanced envelope-based approach (Lutz et al., 2016b), and are selected

to represent the full CMIP5 ensemble in terms of simulated ranges in the means of historical air temperature and precipitation, and have sufficient skill in the simulation of the present-day climate over our region of interest. The selected GCM runs and their simulated changes in air temperature and precipitation are listed in Table 2.1.

The selected models are statistically downscaled using the meteorological data of the Kyangjin and Vent stations by applying a Quantile Mapping methodology that performs well for mountainous terrains (Themeßl et al., 2011). This method is applied by constructing monthly empirical cumulative distribution functions that are calculated for the meteorological data and the historical GCM runs. This encompasses the period 1988-2005 for the Kyangjin station and 1987-2005 for the Vent station. The empirical cumulative distribution functions of the meteorological data and the historical GCM runs are used to calculate correction factors that are subsequently used to bias-correct the historical GCM runs spanning 1851-2005 at a daily time step. The bias-corrected GCM runs are subsequently spatially distributed by using the same temperature and precipitation lapse rates and normalized precipitation fields that are used for the spatial distribution of the meteorological data.

To separately assess the effects of anthropogenic climate change on glacier mass balance and dynamics, we follow two different scenarios: FULL (i.e. combined anthropogenic and natural climate change) and NATURAL (i.e. natural climate change only). The FULL scenario follows climate change simulations according to the outputs of the selected GCMs. To follow the NATURAL scenario, an approach is used that deviates from the CMIP5 approach, which uses climate models that are realizations of the historicalNat experiment, i.e. forced with natural climate forcings only. A different approach is used due to uncertainties that might be introduced by the downscaling of climate change simulations of the historicalNat experiment and by the inconsistencies in the simulated temperature trends that may rise between climate models from the historical experiment and historicalNat experiment. In this study, the NATURAL scenario follows climate change simulations that consist of two parts. The first covers the period 1851-1980 and is identical to the historical GCM runs. The second covers the period 1971-2016 and repeats the historical GCM runs

Table 2.1. Selected ensemble of historical GCM runs for the Hintereisferner and Langtang glaciers with simulated basin-averaged changes in mean temperature and precipitation in 1861-1890 relative to 1971-2000.

Location	Projection	GCM run	Period	ΔT (°C)[1]	ΔP (%)[2]
Hintereis	Cold,wet	CSIRO-MK3-6-0_r8i1p1	1851-2005	-0.1	+3.7
	Cold,dry	IPSL-CM5A-MR_r3i1p1	1851-2005	-0.7	-2.6
	Warm,dry	CSIRO-MK3-6-0_r1i1p1	1851-2005	+0.1	+1.3
	Warm,wet	GFDL-CM3_r5i1p1	1861-2005	+0.3	+7.9
Langtang	Cold,wet	CSIRO-MK3-6-0_r3i1p1	1851-2005	-0.8	+11.8
	Cold,dry	bcc-csm1-1_r1i1p1	1851-2005	-0.8	-8.3
	Warm,dry	CSIRO-MK3-6-0_r10i1p1	1851-2005	-0.2	-3.3
	Warm,wet	ACCESS1-3_r2i1p1	1851-2005	+0.1	+15.6

1 $\Delta T = \bar{T}_{1861-1890} - \bar{T}_{1971-2000}$

2 $\Delta P = \left(\left(\frac{\bar{P}_{1861-1890}}{\bar{P}_{1971-2000}} \right) * 100 \right) - 100$

that span the period 1925-1970. By means of this approach we remove the trend in historical climate change simulations after 1970. There is evidence that the anthropogenic climate signal has become a prevailing explanation for the observed decrease in glacier mass since the 1980s (Hirabayashi et al., 2016; Marzeion et al., 2014). Furthermore, the temperature shows stronger increases since the late 1970s and early 1980s (Hartmann et al. (2013); Figure 2.3). For this reason, we choose to remove the trend in historical climate change simulations after 1970 and to retain the statistics of 1925-1970 in order to cover the second part of the climate change simulations that represent the NATURAL scenario.

2.3.2 Glacier mass balance and flow model

We use a spatially-distributed coupled glacier mass balance and ice-flow model to simulate the glacier response under historical climate change. The mass balance model is based on a glacier model developed by (Immerzeel et al., 2012b) and further refined by (Immerzeel et al., 2013) and (Shea et al., 2015). The model is set up at a spatial resolution of approximately 30 x 30 m and runs on a daily time step.

Daily accumulation is assumed to be equal to the total precipitation when the daily air temperature is below a critical threshold temperature. Daily melt (ablation) is simulated by a degree-day approach that distinguishes the effects of aspect and occurs when the daily air temperature is above a critical threshold temperature (Immerzeel et al., 2012b; Konz and Seibert, 2010):

$$\boldsymbol{M = DDF_M * (T - T_c) \ : for \ T > T_c} \tag{2.1}$$

where M (mm d^{-1}) is the amount of melt, T (°C) is the daily air temperature, T_c (°C) is the critical threshold temperature, and DDF_M is the modified degree-day factor. The modified degree-day factor is calculated as (Immerzeel et al., 2012b):

$$\boldsymbol{DDF_M = DDF(1 - R_{exp} \cos \theta)} \tag{2.2}$$

where DDF is the degree-day factor (mm $°C^{-1}$ d^{-1}) and R_{exp} is a factor that quantifies the aspect (θ) dependence of the degree-day factor. For debris-covered glaciers, an elevation-dependent melt factor, R_{debris}, is applied to account for the effect of the debris thickness on melt rates, where the magnitude of melt rates generally decreases with increasing debris thickness. The debris melt factors are derived for 50 m elevation bands by using a relative relation between the mean debris thickness in each elevation band and ablation rates (Østrem, 1959). The debris thickness is estimated by an exponential relation between debris thickness and surface temperature, using surface temperature grids that are derived from the TIR band 10 of the Landsat 8 composite and are corrected for emissivity using the ASTER global emissivity product (Kraaijenbrink et al., 2017). It is assumed that the debris thickness and debris melt factors remain constant over time. The effects of supraglacial ponds and ice-cliffs on melt rates are not considered explicitly.

In addition to precipitation, avalanches also contribute significantly to glacier accumulation in steep mountain terrain (Laha et al., 2017; Ragettli et al., 2015; Scherler et al., 2011; Shea et al., 2015). To simulate avalanching, the gravitational snow transport module SnowSlide (Bernhardt and Schulz, 2010) is used, which assumes snow to be transported downslope when a maximum snow-holding depth and a threshold slope of 25° are exceeded (Bernhardt and Schulz, 2010). The maximum snow-

holding depth is deep for flat areas, decreases exponentially with increasing slope angle, and is calculated by an exponential regression function (Bernhardt and Schulz, 2010; Ragettli et al., 2015; Stigter et al., 2017):

$$\boldsymbol{SWE_{max} = SS_1 * e^{-SS_2 * S}} \tag{2.3}$$

where SWE_{max} (m w.e.) is the maximum snow water equivalent, SS_1 (m) and SS_2 (-) are calibrated empirical coefficients, and S (°) is the slope angle. We assume that avalanching does not occur on pixels classified as glaciers. Hence, on slopes steeper than the threshold slope for avalanching (i.e. 25°), all snow water equivalent values of more than 0.5 m are identified as glaciers and the avalanching of this material is disabled.

In the original model of Immerzeel et al. (2012) glacier movement is simulated by Weertman's sliding law. This approach assumes that glaciers flow as ice slides over the bedrock. Although this simplistic approach may be reasonable to represent glacier flow in a regional-scale gridded hydrological model, it certainly does not capture the essence of glacier flow: a combination of basal sliding and internal deformation (Cuffey and Paterson, 2010). Here, we model glacier flow based on SIA in which the ice surface velocity is governed by the local ice thickness and surface slopes. Unlike existing flow-line models (Adhikari and Huybrechts, 2009; Banerjee and Shankar, 2013; Huss et al., 2007), we allow ice to flow on a regular gridded mesh in its preferred direction. This requires us to define the depth-averaged velocity in x and y direction independently as follows (Le Meur et al., 2004):

$$\left(\boldsymbol{u_x(s), u_y(s)}\right) = \boldsymbol{\frac{2A(C\rho g)^n}{n+1}} \left|\boldsymbol{\nabla_{xy} s}\right|^{\boldsymbol{n-1}} \left(\boldsymbol{\frac{\partial s}{\partial x}, \frac{\partial s}{\partial y}}\right) \boldsymbol{h^{n+1}} \tag{2.4}$$

Note that $\left|\boldsymbol{\nabla_{xy} s}\right|^{\boldsymbol{n-1}}$ assumes that viscosity is isotropic. In the above equation, $u_x(s)$ and $u_y(s)$ (m d^{-1}) are horizontal depth-averaged velocity components in two dimensions as a function of the surface elevation s (m), A (Pa^{-3} s^{-1}) is the temperature-dependent Glen's flow-law rate constant (Glen, 1955), $n = 3$ is Glen's flow-law exponent, ρ (kg m^{-3}) is the ice density (916.7 kg m^{-3}), g (m s^{-2}) is the gravitational acceleration, and h (m) is the ice thickness. Equation 2.4 has been modified by the implementation of a correction factor C. This correction factor modifies the gravitational driving stress by accounting for higher-order physics that are not captured in the SIA model, such as resistances to ice flow due to longitudinal and lateral stress gradients, and basal sliding (Adhikari and Marshall, 2011, 2012b; Farinotti et al., 2009; Nye, 1965). The gravitational driving stress in two horizontal dimensions is described by (Le Meur et al., 2004):

$$\left(\boldsymbol{\tau_{xz}, \tau_{yz}}\right) = \boldsymbol{\rho g (z - s)} \left(\boldsymbol{\frac{\partial s}{\partial x}, \frac{\partial s}{\partial y}}\right) \tag{2.5}$$

where z (m) represents the depth of a glacier. By modifying the gravitational driving stress with the correction factor C the equation becomes:

$$\left(\boldsymbol{\tau_{xz}, \tau_{yz}}\right) = \boldsymbol{C\rho g (z - s)} \left(\boldsymbol{\frac{\partial s}{\partial x}, \frac{\partial s}{\partial y}}\right) \tag{2.6}$$

According to Le Meur et al. (2004) equation 2.5 is eventually used to derive an equation that describes the change in velocity over depth *z:*

$$\frac{\partial u_x, \partial u_y}{\partial z} = -2A(\rho g)^n (s - z)^n |\nabla s|^{n-1} \left(\frac{\partial s}{\partial x}, \frac{\partial s}{\partial y}\right) \tag{2.7}$$

Implementing the correction factor *C* it results in:

$$\frac{\partial u_x, \partial u_y}{\partial z} = -2A(C\rho g)^n (s - z)^n |\nabla s|^{n-1} \left(\frac{\partial s}{\partial x}, \frac{\partial s}{\partial y}\right) \tag{2.8}$$

Eventually the integration of equation 2.8 from $z = B$ (bedrock elevation) to $z = s$ (surface elevation) leads to the formulation of equation 2.4, where $h = s - B$.

Mass conservation is ensured by a mass transport equation that relates ice thickness changes to the horizontal flux divergence and changes in the net surface mass balance (e.g. Adhikari and Huybrechts, 2009; Cuffey and Paterson, 2010; Oerlemans et al., 1998):

$$\frac{\partial h}{\partial t} = M - \nabla_{xy} q \tag{2.9}$$

where M is the net surface mass balance (m w.e.) and $(q_x, q_y) = (u_x(s)h, u_y(s)h)$ are the horizontal ice fluxes ($m^2\ d^{-1}$). Equation 2.4 and 2.9 are implemented for each grid cell in the model by means of a (centred) finite difference scheme. The finite difference scheme is applied to a regular gridded mesh with an horizontal grid spacing of approximately 30 m. Furthermore, a forward explicit time stepping scheme with a daily step is used, which is found to be stable.

2.3.3 Model initialization

To initialize the model, the ice thickness for the Hintereisferner and Langtang Glacier in 1850 is reconstructed.

2.3.3.1 Hintereisferner

The initial ice thickness for the Hintereisferner is reconstructed using glacier outlines obtained from the Austrian glacier inventories of 1850 and 2006 (Abermann et al., 2009; Fischer et al., 2015), recent (EU-DEM) and reconstructed (1850) DEMs of the glacier surface, and observed ice thickness profiles over the period 1855-2006 that are extracted from Schlosser (1997) and Kuhn (2008). The reconstruction of the initial ice thickness consists of four steps. First, the ice thickness of 2006 and the bed elevation is estimated by the GlabTop2 approach (Frey et al., 2014) using the 2006 outline and the recent surface DEM. Second, average mass balance changes between 1850 and 2006 are derived from the observed ice thickness profiles for 100 m elevation zones. Combined with the recent surface DEM and the 1850 outline, the average mass balance changes are used to derive a first temporary ice thickness map. Third, a surface DEM for 1850 is constructed by inverse distanced weighted interpolation of the 1850 outline elevation. The 1850 surface DEM and the bed elevations are used to derive a second temporary ice thickness map. The final 1850 ice thickness map is the maximum thickness of both temporary maps.

2.3.3.2 Langtang Glacier

For the Langtang Glacier, observations of ice thickness profiles are not available. For this reason, a different approach is followed to reconstruct the initial ice thickness for 1850. The initial ice

thickness is reconstructed by using recent glacier outlines obtained from the Randolph Glacier Inventory (RGI) v6 (Pfeffer et al., 2014), reconstructed glacier outlines (1850), and recent (SRTM) and reconstructed (1850) DEMs of the glacier surface. The reconstruction of the initial ice thickness consists of four steps as well. First, the present ice thickness and bed elevation are estimated by the GlabTop2 approach (Frey et al., 2014) using recent glacier outlines and a recent surface DEM. Second, a first temporary ice thickness map is derived by using the GlabTop2 approach (Frey et al., 2014) in combination with glacier outlines and a surface DEM for 1850. The glacier outlines for 1850 are reconstructed based on the LIA moraines that are derived from Landsat 8 imagery (Roy et al., 2014). Subsequently, the 1850 surface DEM is constructed by inverse distance weighted interpolation of the 1850 lateral moraine elevation. Finally, the 1850 surface DEM and the bed elevations are used to calculate a second temporary ice thickness map. The final 1850 ice thickness map is the maximum thickness of both temporary maps. Due to the lack of knowledge of the 1850 debris extent on Langtang Glacier, we assumed the initial debris extent to be similar to the present-day debris extent (Kraaijenbrink et al., 2017), but extended it laterally (and longitudinal at the terminus) to cover the larger footprint of the glacier in 1850.

2.3.4 Model calibration and validation

We use the Parameter ESTimation (PEST) algorithm (Doherty, 2018) to calibrate the model. The model is calibrated in a three-step approach. First, we run the model manually from 1851 to 2005 for each GCM that follows the FULL scenario by applying several iterations. The simulated ice thickness and glacier extents at the end of each run are compared to the current glacier extents and ice thickness, i.e. the outlines and ice thickness of the RGI and 2006 for the Langtang Glacier and Hintereisferner, respectively. The model results from the single GCM runs that, eventually, correspond best to the current outlines and ice thickness are used as initialization for the model calibration runs. These are the cold-wet (Langtang Glacier) and cold-dry (Hintereisferner) GCM-glacier model combinations. Secondly, the model is calibrated on zonal-averaged observed glacier surface velocities and mean glacier surface elevation changes that are estimated over 50-m elevation zones (see below for details). The model is run from 2006 to 2016 and seven parameters are calibrated that influence glacier dynamics and mass balance: the degree day factors for clean-ice (DDF_C) and snow (DDF_S), the critical threshold temperature (T_c), the Glen's flow rate factor (A), the correction factor that accounts for resistances to ice flow due to lateral and longitudinal stress gradients, and basal sliding (C), and the empirical coefficients SS_1 and SS_2. The model is calibrated on the main trunks of Langtang Glacier and Hintereisferner. Finally, several model parameters (see Table 2.2) and debris melt factors (i.e. R_{debris}) are manually optimized to improve the long-term model performance. The manual optimization is necessary since the PEST algorithm is not able to optimize the debris melt factors and some of the model parameters (Table 2.2). To evaluate the model performance, the coefficient of determination (R^2) and correlation (R) are used as main efficiency criteria, where the coefficients represent the overall standardized performance of the model in simulating both surface velocities and elevation changes. Additionally, the performance is evaluated on the simulation of surface velocities and elevation changes separately by using the Mean Absolute Error (MAE) as criterium.

The zonal-averaged observed glacier velocities are calculated using COSI-Corr (Co-registration of Optically Sensed Images and Correlation) (Leprince et al., 2007). For Hintereisferner, we derived velocities over the period 2016-2018 using PLANET VNIR bands with an initial window of 128 x 128 pixels (px), a final window of 8 x 8 px, and a step size of 4 px. For Langtang Glacier, velocities

are derived over the period 2010-2012, using ASTER VNIR band 2 with an initial window of 64 x 64 px, a final window of 16 x 16 px, and a step size of 4 px. The calculated glacier velocities are subsequently averaged over 50 m elevation zones, which are then used for the calibration of glacier surface velocities. The calibration on zonal-averaged glacier surface elevation changes on Langtang Glacier (over 2006-2014) and Hintereisferner (over 2006-2011) is conducted by using mean annual surface elevation change grids of Langtang Glacier and Hintereisferner that are calculated by means of DEM differencing. We refer to Ragettli et al. (2016) and Klug et al. (2018) for more detailed descriptions on the DEM differencing and the calculation of mean surface elevation changes on Langtang Glacier and Hintereisferner, respectively. The mean surface elevation changes are subsequently averaged over 50m elevation zones, which are then used for model calibration.

The best performing parameter sets are used to run the model from 1851 till 2016 by using the modelled (1851-2005) and observed (2006-2016) climate data, and to validate the calibrated model on glacier area changes and ice thickness. To reveal the anthropogenic influence on the response of glaciers the model results for the FULL and NATURAL scenarios are compared with each other. The comparison is done for the period 1971-2016 and is conducted by using the outcomes of GCM-glacier model combinations that generate outcomes in close agreement with the observed changes in the glacier mass balance and flow.

2.3.5 Sensitivity analysis

To gain an improved insight on the sensitivity of surface velocities and elevation changes to model parameter changes, a local One-At-A-Time (OAT) sensitivity analysis (Pianosi et al., 2016) is performed using the SENSAN sensitivity analyser of the PEST algorithm (Doherty, 2018). The analysis is done by varying values of calibration parameters (DDF_C, DDF_S, T_c, A, C, SS_1, and SS_2) independently within ranges that are listed in Table 2.2 but does not account for parameter interactions. To conduct the analysis, surface velocities and elevation changes are averaged over the calibration period (2006-2016) and the main trunks of Langtang Glacier and Hintereisferner. The sensitivity of these variables are measured by the average linear sensitivity index (ALS) of Nearing et al. (1989):

$$\boldsymbol{ALS} = \frac{\left[\frac{y_2 - y_1}{\bar{y}}\right]}{\left[\frac{x_2 - x_1}{\bar{x}}\right]} \tag{2.10}$$

where y_2 and y_1 represent the output values (y) obtained for the maximum (x_2) and minimum (x_1) of the input parameter ranges (x) (Table 2.2). $\bar{x}$ and $\bar{y}$ represent the means of the parameter values (x_1 and x_2) and respective output values (y_1 and y_2).

2.4 Results

2.4.1 Model calibration and validation

The best performing parameter sets that result from the calibration approach are listed in Table 2.2. The parameters associated with melt and accumulation (DDF_C, DDF_S, and T_c) agree well with those observed/modelled in other studies (Hock, 2003; Immerzeel et al., 2013; Konz and Seibert, 2010; Lambrecht et al., 2011). However, the calibrated degree-day factor for snow at the Hintereisferner (i.e. 9 mm $°C^{-1}$ d^{-1}) is higher than the snow degree-day factors observed/modelled in most studies (i.e. 3-6 mm $°C^{-1}$ d^{-1}) (Braithwaite and Zhang, 2000; Hock, 2003; Singh et al., 2000). A potential explanation is the absence of sublimation in the model that can amount to 150 mm yr^{-1}

at Hintereisferner (Kaser, 1983). This might cause mass balance changes to be corrected by a higher snow degree-day factor. The Glen's flow rate constant (*A*) calibrated for Langtang Glacier is in range of values typical for temperate glaciers (Cuffey and Paterson, 2010). Also, the correction factor (*C*) of 0.8 falls within the expected range (i.e. 0.45-0.85, based on the study of Farinotti et al. (2009)). The same applies for the *C* factor of 0.65 calibrated for Hintereisferner. However, the calibrated Glen's flow rate constant for the Hintereisferner is high and falls outside the expected range. There are several factors that may contribute to the high Glen's flow rate constant as it is affected by factors that are related to the ice rheology of the glacier, such as temperature, density, and water content (Cuffey and Paterson, 2010), and vary widely in space and time. The parameters associated with snow avalanching (SS_1 and SS_2) in the Langtang area are adopted from former studies conducted in the region (Ragettli et al., 2015). The parameters for the Hintereisferner are difficult to compare since no studies have been conducted before in the region using the SnowSlide algorithm. However, the parameters are similar with those in the study of Shea et al. (2015). The debris melt factors are lowest at the lower reaches of the Langtang Glacier due to the presence of thick debris, and highest in the central and upper reaches of the debris-covered part of Langtang Glacier. The high debris melt factors can most likely be explained by thinner debris layers, which cause a smaller reduction

Table 2.2. Calibrated model parameters, their calibration ranges, and their calibrated values. In the lower part model performance ratings are given in terms of the overall coefficient of determination (R^2) and coefficient of correlation (R), and the mean absolute error (MAE) for the calibrated surface velocities (VE) and mean elevation changes (EC).

Parameter	Description	Unit	Range	Hintereis	Langtang
Melt and Accumulation					
DDF_C	Clean-ice melt factor	mm °C^{-1} d^{-1}	3-9	9.0	5.1[1]
DDF_S	Snow melt factor	mm °C^{-1} d^{-1}	3-9	9.0	3.0[2]
T_c	Critical temperature threshold	°C	-6-2	0.8	0.0
Glacial Movement					
A	Temperature-dependent Glen's flow rate constant	(x 10^{-25}) Pa^{-3} s^{-1}	1-300	200[2]	55
C	Correction factor stress/drag components	-	0.1-1	0.65[2]	0.8
Snow Avalanching					
SS_1	Empirical parameter for snow holding depth dependence on slope angle	m	50-300	93	250[3]
SS_2	Empirical parameter for snow holding depth dependence on slope angle	-	0.15-0.2	0.15	0.172[3]
Efficiency Criterium		**Units**		**Hintereis**	**Langtang**
R^2 *All*		-		0.87	0.81
R All		-		0.93	0.90
MAE VE		m a^{-1}		6.5	0.3
MAE EC		m w.e. a^{-1}		-0.25	-0.17[4]

[1] For the debris-covered parts elevation-dependent melt factors are used that are in the range 0.2-0.3 in the lower zone (<4750 m. a.s.l.), 0.3-1.0 in the mid zone (4750-5050 m a.s.l.), and 0.7-1.0 in the upper zone (>5050 m a.s.l.) of the debris-covered part of the glacier.
[2] These parameters are manually optimized to increase the long-term model performance.
[3] adopted from Ragettli et al. (2015).
[4] Unit = m a^{-1}

of melt rates, and the higher number of supraglacial ponds and ice cliffs in the central domain of the glacier that locally enhance melt (Ragettli et al., 2016; Steiner et al., 2019). An alternative explanation for the high debris melt factors are reduced emergence velocities, which also have been found to contribute to increased thinning on debris-covered glaciers (Brun et al., 2018).

Figure 2.2 shows the simulated and observed surface velocities and elevation changes for Langtang Glacier and Hintereisferner. The best overall model performance is achieved for Hintereisferner (R^2 = 0.87; Table 2.2). The mean (minimum/maximum) elevation change is -1.53 (-6.36/+3.73) m w.e. a^{-1}, which is larger than the mean (minimum/maximum) observed elevation change of -1.32 (-6.50/+1.87) m w.e. a^{-1} (Table 2.3). The differences between simulated and observed elevation changes can most likely be attributed to local avalanches; at the western margin of the main trunk the maximum and mean simulated positive elevation changes are higher than the observed elevation changes. The largest differences can be found between the observed and simulated velocities with a zonal MAE of 6.5 m a^{-1} (Table 2.2), where the mean (minimum/maximum) simulated velocity is 6 (0/26) m a^{-1} and the mean (minimum/maximum) observed velocity is 12 (0/27) m a^{-1}. The large differences can mainly be explained by the presence of large distortions in the upper part of the glacier that are found in the satellite-derived velocities and reduces the reliability of the observed values. Nevertheless, the modelled velocities are comparable with observed velocities at stone line 6 (i.e. at this location ice flow velocities are measured in situ by using the annual motion of stones placed on the ice surface as a proxy) (Figure 2.2; Span et al., 1997). The model simulates velocities of 3.2 m a^{-1} in 2016, which is close to the observed velocities of about 4 m a^{-1} (Stocker-Waldhuber et al., 2019). The maximum ice thickness of 215 m simulated at the end of 2006 is comparable with the ice thickness estimated with GlabTop2 (220 m). Furthermore, the model can simulate glacier area changes that are in reasonable agreement with the observed ones. The model simulates a glacier area reduction of about 0.5 km^2 over the period 2006-2011, whereas the observations indicate a reduction of about 0.6 km^2 (Charalampidis et al., 2018; Klug et al., 2018).

The overall fit between the observations and calibrated outcomes (R^2 = 0.81) is satisfactory for Langtang Glacier as well. The mean (minimum/maximum) elevation change is -0.48 (-2.74/+6.64) m a^{-1}, which is lower than the mean (minimum/maximum) observed elevation change of -0.67 (-7.49/+7.38) m a^{-1}. The largest elevation changes are simulated in the central reaches of the main trunk (4800-5100 m a.s.l.). The high elevation changes can primarily be explained by the higher debris melt factors in this part of the glacier that are due to the presence of melt-enhancing ice cliffs and supraglacial ponds. The model is, however, not able to represent the spatial distribution of ice cliffs and supraglacial ponds sufficiently, which can explain the underestimation of the modelled mean elevation change. The simulated positive elevation changes are largest at the glacier head, i.e. in the accumulation zone, and along the margins of the tongue. The positive elevation changes along the margins can mainly be attributed to avalanching, which is especially large at the eastern side of the main trunk due to the steep side walls generating more avalanches. The observed and modelled velocities are comparable with each other with mean (minimum/maximum) values of 7 (0/82) m a^{-1} and 6 (0/64) m a^{-1}, respectively. The maximum ice thickness of about 280 m simulated at the end of 2001 (i.e. year of RGI glacier outline) is comparable with the ice thickness estimated with GlabTop2 (290 m), where the maximum ice thickness is simulated in the upper reaches of the main trunk. Further, the modelled glacier area changes between 2006-2015 are with 0.55 km^2 in reasonable agreement with the observed glacier area decline of 0.45 km^2 (Ragettli et al., 2016a).

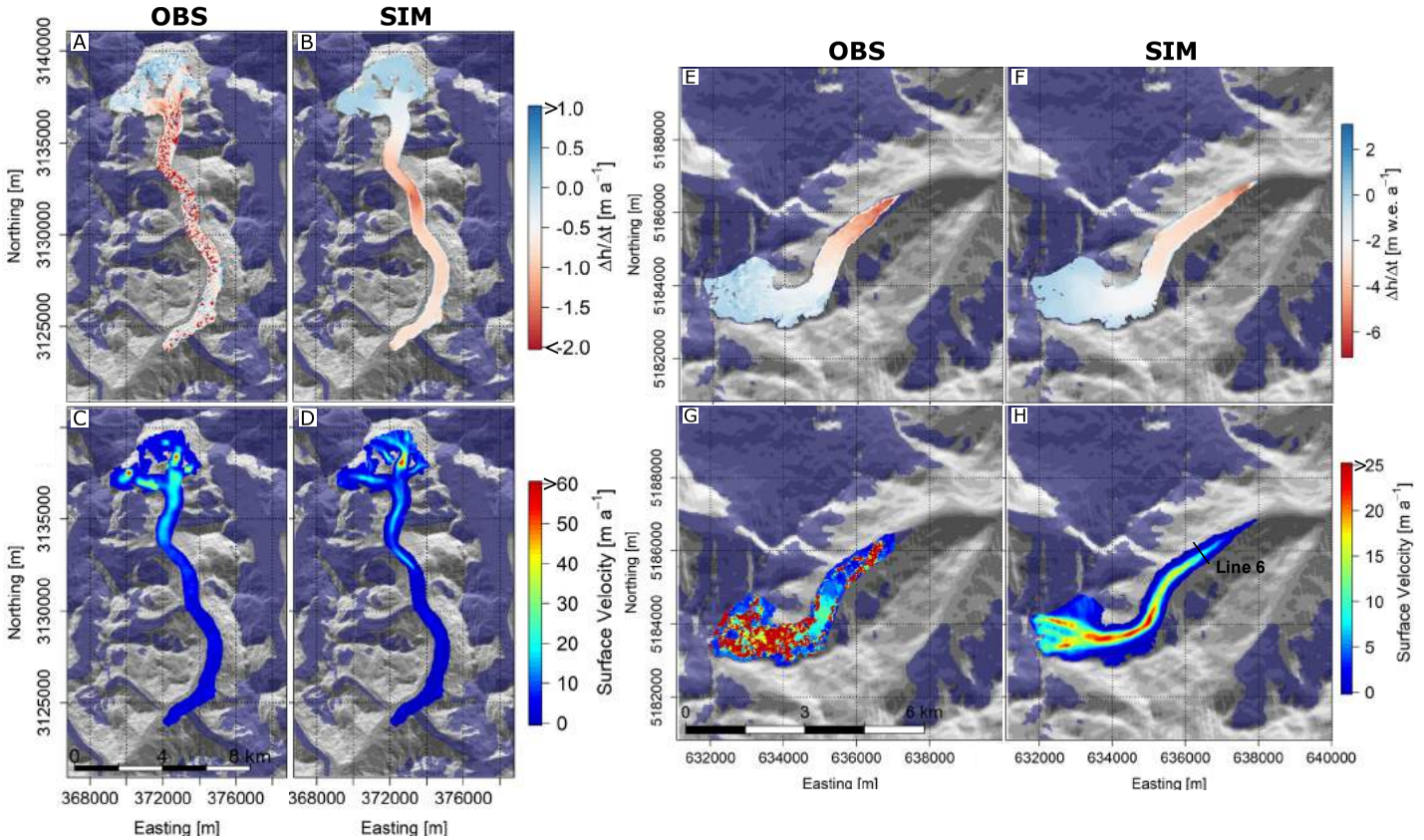

Figure 2.2. Observed (OBS) and simulated (SIM) mean surface elevation change (A, B, E, F) and velocities (C, D, G, H) for the Langtang (A-D) and Hintereisferner (E-H) glaciers. Line 6 indicates the location of stone line 6 (Span et al., 1997). Source of the observed mean surface elevation change grids are Ragettli et al. (2016) for the Langtang Glacier and Klug et al. (2018) for the Hintereisferner.

Table 2.3. Simulated and observed mean surface velocities and elevation changes per glacier tongue. The values between the parentheses represent the minimum and maximum of the calibrated surface velocities and elevation changes.

Location	Variable	Unit	OBS	SIM
Hintereis	Surface velocity	m a^{-1}	12 (0/27)	6 (0/26)
	Elevation change	m w.e. a^{-1}	-1.32 (-6.50/+1.87)	-1.53 (-6.36/+3.73)
Langtang	Surface velocity	m a^{-1}	7 (0/82)	6 (0/64)
	Elevation change	m a^{-1}	-0.67 (-7.49/+7.38)	-0.48 (-2.74/+6.64)

2.4.2 Model sensitivity

Table 2.4 lists the sensitivity of surface velocities and elevation changes to model parameter changes. The modelled velocities are most sensitive to changes in the correction factor *C* followed by Glen's flow rate constant *A*. Modelled elevation changes are most sensitive to changes in DDF_C, where Langtang Glacier tends to be less sensitive to changes in DDF_C than the Hintereisferner. The lower sensitivity can most likely be explained by the presence of a thick debris layer at Langtang Glacier that reduces ice melt. Further, modelled velocities and elevation changes are more sensitive for changes in the snow avalanching parameters SS_1 and SS_2 than on the Hintereisferner. The higher sensitivity can most likely be explained by the larger contributions of snow avalanching to accumulation at Langtang Glacier.

Table 2.4. Model parameters and parameter ranges used for the sensitivity analysis. The values in the table denote the average linear sensitivity of surface velocities (VE) and mean surface elevation changes (EC).

		Hintereis		Langtang	
Parameter	Range	VE	EC	VE	EC
DDF_C	3-9	0.251	2.318	0.116	1.753
DDF_S	3-9	0.006	0.015	0.005	0.082
T_c	-6-2	0.343	0.394	0.223	0.550
A	1-300	0.999	0.009	0.998	0.193
C	0.1-1	1.219	0.012	1.219	0.031
SS_1	50-300	0.001	0.007	0.006	0.020
SS_2	0.15-0.2	0.007	0.053	0.042	0.143

2.4.3 Past climate forcing

Since the end of the LIA, both precipitation and temperature have changed in magnitude and distribution. Figure 2.3 shows the 10-years moving average of daily air temperature and precipitation at the Kyangjin and Vent stations for the FULL and NATURAL scenarios over the past 166 years, i.e. 1851-2016. The precipitation has decreased by 5% (range: -7 to -1%) for FULL and 2% (-3 to -1%) for NATURAL between 1861-1890 and 1981-2010 at Vent station. At Kyangjin station the decreases are a bit larger with relative changes of 6% and 5% for FULL and NATURAL (-18 to +3% for FULL and -11 to +3% for NATURAL), respectively. At the same station the temperature has increased with 0.8 °C (range: -0.1 to +1.3 °C) for FULL and 0.3 °C (-0.3 to +0.6 °C) for NATURAL between 1861-1890 and 1981-2010. At Vent station the temperature has increased with 0.6 °C (-0.1 to +1.3 °C) for FULL and 0.2 °C for NATURAL (-0.1 to +0.7 °C). The NATURAL scenario shows a decline in temperature after 2000 at the Kyangjin and Vent stations, which is equivalent to the

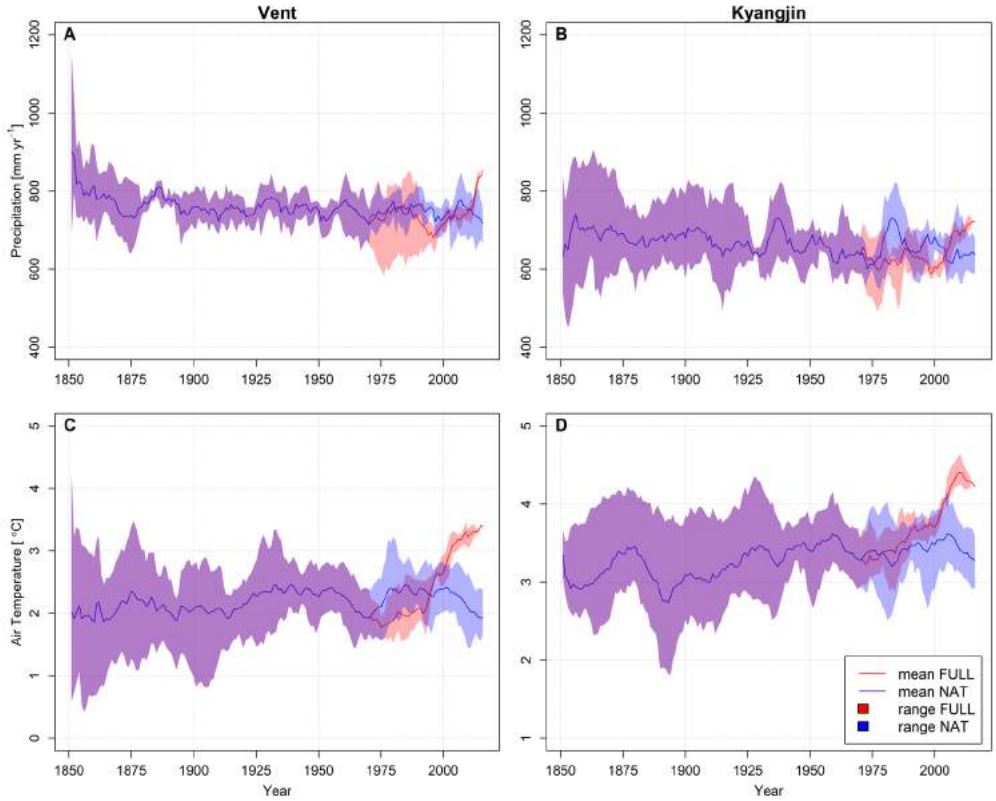

Figure 2.3. 10-yrs moving averages of simulated precipitation (A, B) and temperature (C, D) changes for the period 1971-2016 for FULL (red) and NATURAL (blue). The moving averages are given for the Vent (A, C) and Kyangjin (B, D) stations. The coloured bands denote the range of the simulations.

decline in temperature that is simulated by the climate models between the mid 1950s and 1970. This equivalence can be explained by the preservation of the statistics for the period 1925-1970 after 1970. The spread in model hindcasts for precipitation is highly variable in time at both stations, whereas the model spread for temperature shows a clear diverging pattern with the largest spread at the end of the LIA and the smallest at present. For the NATURAL scenario, the model spread after 1970 is equal to the model spread prior to 1970, since the statistics for the period 1925-1970 have been retained.

2.4.4 Glacier evolution & dynamics

Figure 2.4 shows the change in the glacier areas, volumes, and specific mass balance of the Langtang Glacier and Hintereisferner between 1850 and 2016 for the different climate models. At Langtang Glacier, the largest area and volume reductions are simulated under warm climate conditions with an area (volume) reduction from about 60 km^2 (5.5 km^3) in 1850 to about 39 km^2 (2.0 km^3) in 2016. For cold climate conditions the model shows a smaller decline in area (volume) from 60 km^2 (5.5 km^3) to about 50 km^2 (3 km^3). Under both cold/dry and cold/wet climate conditions the modelled extent is in close agreement with the observed extent in 1974 (53.5 km^2; (Pellicciotti et al., 2015). The modelled extent under cold/dry conditions is in closest

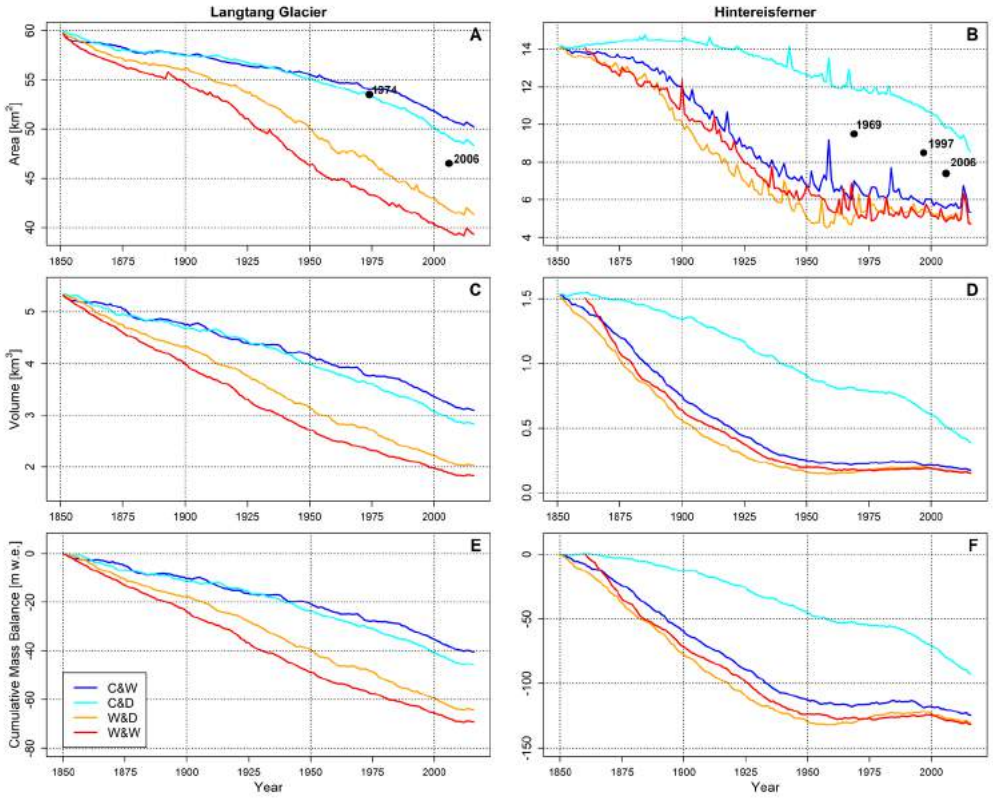

Figure 2.4. Modeled changes in glacier area (A,B), volume (C,D), and specific mass balance (E,F) of the Langtang Glacier (A,C,E) and Hintereisferner (B,D,F) for four different historical climate change simulations (CW: cold and wet; CD: cold and dry; WW: warm and wet; WD: warm and dry). The black points denote the observed glacier extents at Langtang Glacier (1974, 2016; Pellicciotti et al., 2015; Ragettli et al., 2016) and Hintereisferner (1969, 1997, 2006; Abermann et al., 2009; Charalampidis et al., 2018; Patzelt, 2013).

agreement with the observed extent in 2006 (46.5 km^2; (Ragettli et al., 2016a) compared to the modelled extents under other climate conditions. Under cold climate conditions, the model following a wet climate scenario shows a slightly smaller loss in ice mass than the model following a dry climate scenario, which is explained by the differences in precipitation since both models simulate the same temperature trends (Table 2.1). With a cumulative mass loss of about 40 m w.e. since the end of the LIA, the models following cold climate scenarios show a smaller mass loss than those following warm climate scenarios, which simulate a mass loss up to about 70 m w.e.

At Hintereisferner, the largest area (volume) reductions are simulated under warm and cold/wet climate conditions with a decline in area/volume from 14 km^2 (1.5 km^3) up to about 5 km^2 (0.15 km^3), and are accompanied by cumulative mass losses up to about 135 m w.e. Under cold/dry climate conditions, area (volume) reductions are smaller with a decline in area/volume up to about 8 km^2 (0.4 km^3) and a cumulative mass loss up to about 90 m w.e. Under these conditions, extents are simulated that are in closest agreement with the observed extents in 1969 (9.5 km^2), 1997 (8.5 km^2), and 2006 (7.4 km^2) (Abermann et al., 2009; Charalampidis et al., 2018; Patzelt, 2013). All

model simulations on the extents show strong inter-annual variability. Since the model reports the ice thickness used for the estimation of extents at the end of the year (i.e. during the winter season), the temporal peaks might be explained by extensive snowfall. This would subsequently cause the threshold value used for the identification of glaciers (0.5 m w.e.) to be exceeded, which explains the short temporal increases in extent. The cumulative mass balance shows a period of reduced mass loss or even a slight mass gain between the 1960s and 1990s, which is commonly known as a period with close-to-balanced climate conditions in the European Alps (Huss, 2012).

Along with changes in the glacier area and volume, surface velocities also change over time. Figure 2.5 shows transient time series of surface velocity for three different transects along the glaciers. In general, velocity decreases over time at most transects, especially at the main trunks. In the uppermost reaches of Langtang Glacier, velocities are relatively constant after 1875. In the central and lower reaches of the glacier, velocities increase during the late 19th and early 20th century, which can most likely be explained by a redistribution of ice mass from the side branches into the main

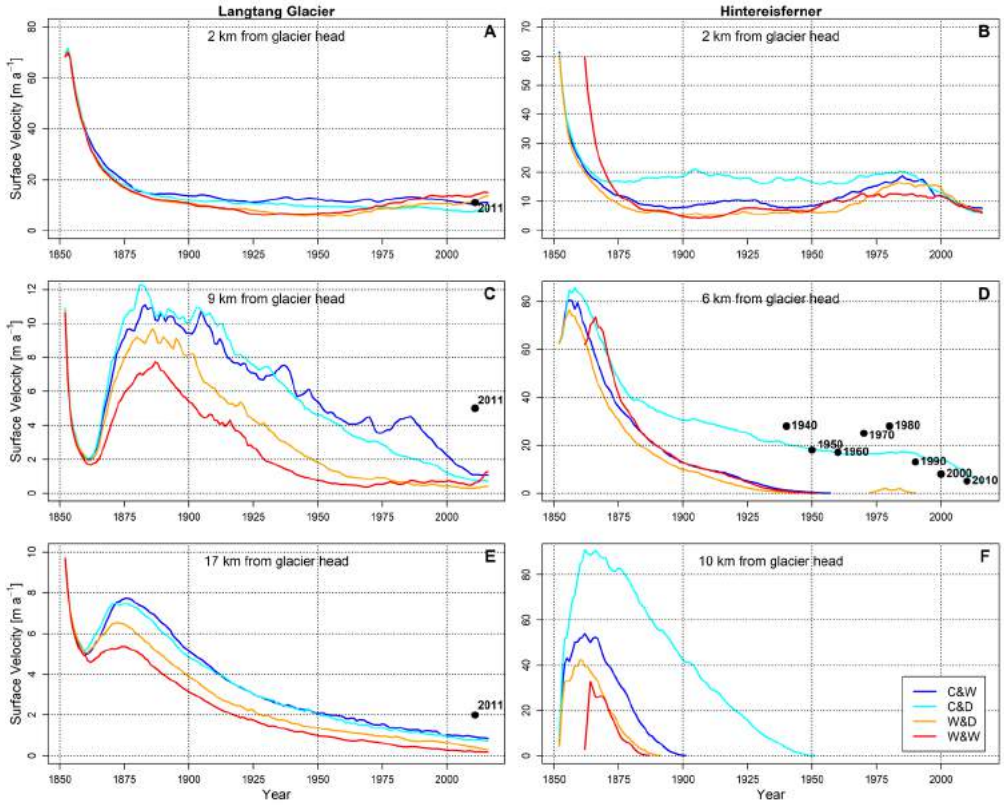

Figure 2.5. Modeled changes in surface velocity at three different transects along the Langtang Glacier (A,C,E) and Hintereisferner (B,D,F) for four different historical climate change simulations (CW: cold and wet; CD: cold and dry; WW: warm and wet; WD: warm and dry). The locations of the three transects are given in Figure 2.6. The black points denote the observed velocities at Langtang Glacier (2011) and Hintereisferner (1940, 1950, 1960, 1970, 1980, 1990, 2000; Stocker-Waldhuber et al. (2019)).

trunk itself. The simulated velocities under cold/wet and warm/dry conditions are with a velocity of about 10 m a^{-1} in closest agreement with the observed satellite-derived velocities (10 m a^{-1} for 2010-2012) in the upper domain of the glacier. In central and lower reaches, the simulations deviate from the observations, which can most likely be explained by higher ablation rates that result from neglecting varying surface conditions by the model, e.g. no temporal variation of debris thickness and supraglacial features. Models forced with cold climate models simulate velocities that are in a closer agreement with the observed velocities than the models forced with warmer climate models. In the uppermost reaches of the Hintereisferner, velocities are also relatively constant with exception of the period between the 1960s and 1990s where the velocity time series show a slight increase under warm and cold/wet climate conditions. The slight increases can most likely be explained by the positive mass balance during this period. In the central and lower reaches of the glacier, most simulations show the velocity to become zero due the disappearing glacier in these domains. In the central reaches, the model forced by cold/dry climate change simulations simulates velocities that are comparable with the observed velocities at stone line 6 (Span et al., 1997; Stocker-Waldhuber et al., 2019). The model is however not able to simulate the higher velocities in the 1940s, 1970s, and 1980s, which can most likely be explained by neglecting changing surface or englacial conditions.

Figure 2.6 shows the simulated spatial ice thickness and surface velocity fields for 1850, 1860 (i.e. only for surface velocity) and 2016 under cold/dry and cold/wet conditions, which are selected as conditions that are in closest agreement with the observed changes at Hintereisferner and Langtang Glacier, respectively. At Langtang Glacier the model shows a very limited decrease in length up to about 50 m between 1850 and 2016 (Figure 2.7), which can mainly be explained by the strong reduction of melt rates due to the presence of thick debris at the lower reaches of the glacier. The limited decrease in length is accompanied by a thinning of the glacier from about 200-300 m (maximum: 355 m) to 100-150 m (maximum: 273 m) under current conditions. An average thinning rate (over 1850-2016) of -0.32 m a^{-1} and -0.27 m a^{-1} is estimated for the debris-covered tongue of the glacier and the entire glacier, respectively. These changes are accompanied by decreases in the velocities from up to about 275 m a^{-1} to 66 m a^{-1} in the higher parts of the glacier and from about 10-15 m a^{-1} to about 1-2 m a^{-1} at the terminus of the glacier. The very low velocities at the terminus of the glacier are typical for the debris-covered Langtang Glacier. Due to enhanced melt in the central reaches of the main trunks (which can be attributed to supraglacial features or reduced emergence velocities) the thinning rate increases, which eventually result in a shallower slope and a stagnation of the terminus. Similar observations have been made in other studies at the Langtang Glacier, and at other debris-covered glaciers in the Central Himalayas as well (Brun et al., 2018; Ragettli et al., 2016; Steiner et al., 2019).

The Hintereisferner shows a different trend with a significant decrease in length and reduction of ice thickness. The model simulates a decrease in length of about 3 km, which is close to the observed changes in glacier length (e.g. Leclercq and Oerlemans, 2012), and a reduction in ice thickness from about 340 m to about 180 m. Thereby, an average thinning rate (over 1850-2016) of -0.47 m a^{-1} is estimated for the main trunk of the glacier. Initially the Kesselwandferner and Hintereisferner (Figure 2.1) were attached to each other, whereas the Hochjochferner was detached. However, the distance between the terminal point of the Hochjochferner and the tongue of the Hintereisferner was with only 50-100 m very short (Blümcke and Hess, 1895). Under cold/dry conditions the model simulates an advance of the Hintereisferner and Hochjochferner in the late 19th and early 20th century, which eventually results in a re-connection of the two glaciers

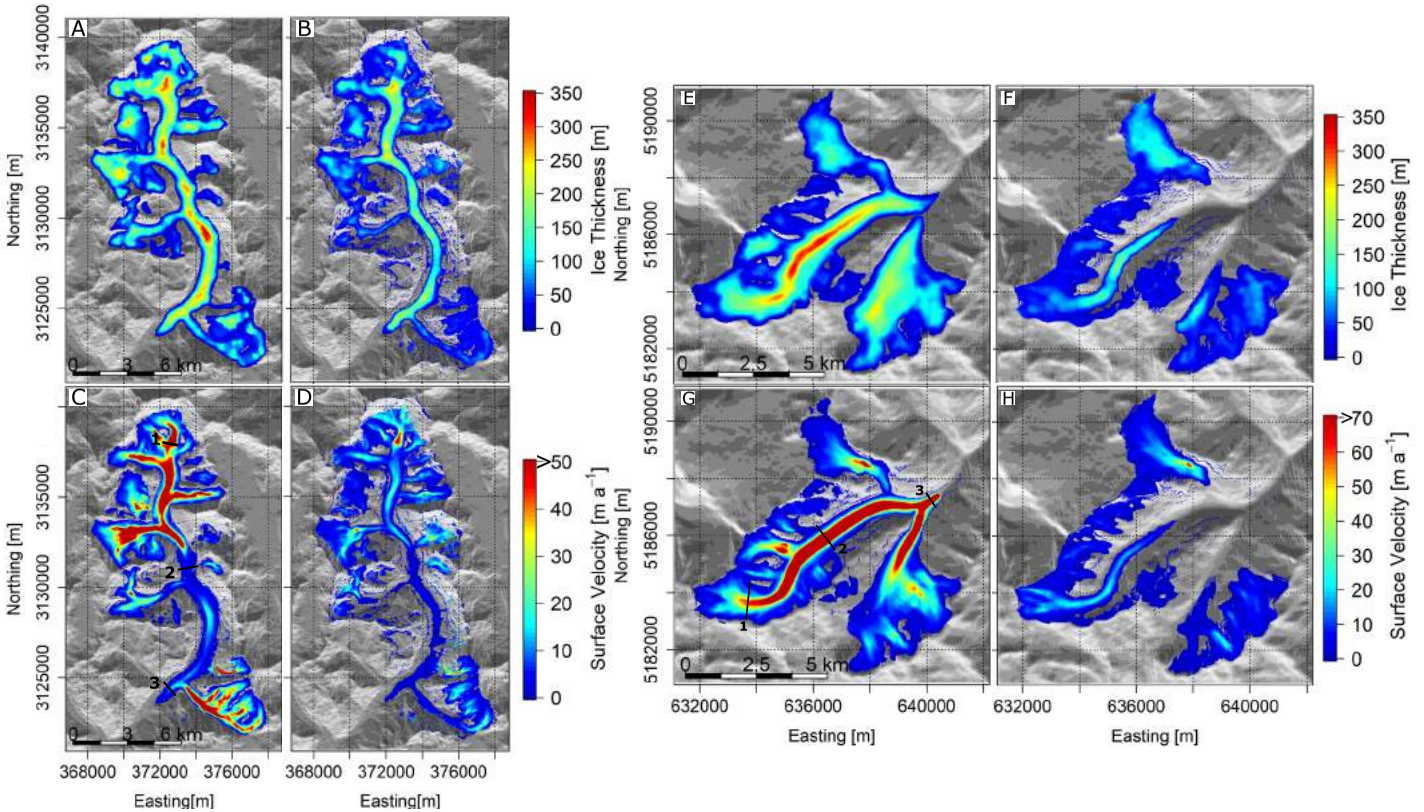

Figure 2.6. Ice thickness and surface velocity fields of Langtang Glacier (A-D) and Hintereisferner (E-H), showing modelled ice thickness/velocity in 1850/1860 (A, C, E, G) and 2016 (B, D, F, H) for cold/wet (Langtang Glacier) and cold/dry climate conditions (Hintereisferner). The coloured filled outlines denote the modelled glacier extents of 1850 (black), 1900 (red), 1950 (yellow), and 2000 (green). The transects denote locations used for the modelled velocities given in Figure 2.5 and 2.9.

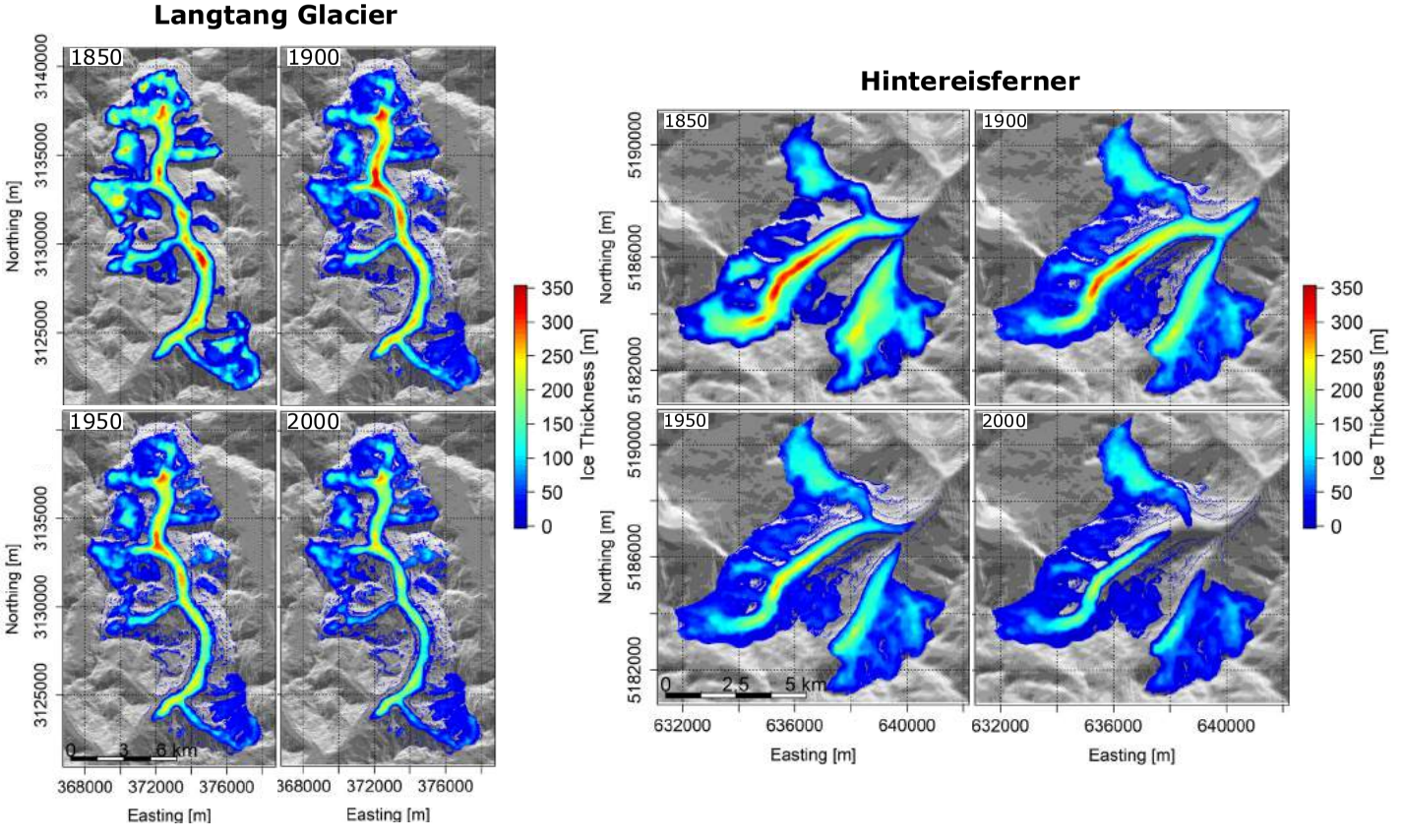

Figure 2.7. The modelled glacier extents and ice thickness fields of Langtang Glacier (left panels) and Hintereisferner (right panels) in 1850, 1900, 1950, and 2000 for cold/wet (Langtang Glacier) and cold/dry climate conditions (Hintereisferner).

(Figure 2.7). The modelled connection lasts till the 1940s followed by the detachment of the Hintereisferner and Kesselwandferner in the 1980s, which is about six decades later than the observed detachment (Kuhn et al., 1985). This modelled re-connection between the Hochjochferner and Hintereisferner has however never been observed, which can most likely be explained by biases between the climate inputs and the observed climate change, or the limitation of the ice-flow model to simulate changes in the flow characteristics of the glacier. The changes in ice thickness are accompanied by a decline in surface velocities from about 310 m a^{-1} to about 25 m a^{-1} at the Hintereisferner. Initially, the highest velocities are simulated at the Hintereisferner. Under current conditions, the model simulates the highest velocities of about 77 m a^{-1} at the terminus of the Kesselwandferner, which can mainly be attributed to the relatively steep slope (40-45 °).

2.4.5 Anthropogenic vs. natural influences

Figure 2.8 shows the changes in glacier area, volume and cumulative mass balance for Langtang Glacier and Hintereisferner under the FULL and NATURAL scenarios between 1971 and 2016. The differences in outcomes between the FULL and NATURAL scenarios are less pronounced for Langtang Glacier. Here, the changes remain negative also under a colder scenario (NATURAL), although the changes are smaller. Only in the late 1980s and early 2010s the glacier mass balance is close to equilibrium. The relative difference in area, volume, and cumulative mass balance between the FULL and NATURAL scenarios is 3%, 9%, and 40%, respectively, in 2016. At Hintereisferner, glacier area, volume and mass balance decrease initially and are almost balanced after 2000. In 1989, 2005 and 2013, the extent of Hintereisferner shows short temporal increases, which can mainly be explained by extensive snowfall that causes the snow-ice threshold to be exceeded. This phenomenon can also be observed in Figure 2.4. The relative difference in area, volume, and cumulative mass balance is more pronounced at Hintereisferner with relative differences of 18%, 39%, and 64%, respectively.

The differences in response between Langtang Glacier and Hintereisferner under the FULL and NATURAL scenarios can mainly be explained by differences in the response time. First, the response time of Langtang Glacier is significantly longer than the response time of Hintereisferner. Based on the method of Johannesson et al. (1989), which calculates the response time at the glacier terminus by a ratio between the ice thickness and the mass balance rate, a response time of about 300 years is estimated for Langtang Glacier, whereas Hintereisferner has an estimated response time of about 20 years. These estimates are an indicator for the time a glacier requires to respond to climatic changes. The estimated response times are in the range of those that are found for other debris-covered and clean-ice glaciers (e.g. Shea et al., 2015). The longer response time at Langtang Glacier can most likely be explained by the debris cover that results in a relatively stable terminus position. For this reason, the differences in area, volume, and mass balance are less pronounced between the FULL and NATURAL scenarios. Contrastingly, for Hintereisferner, the differences are pronounced.

The changes in glacier area, volume, and mass balance eventually also influence glacier dynamics. Figure 2.9 shows the surface velocity time series for two transects in the upper and central reaches of Langtang Glacier and Hintereisferner that are simulated for the FULL and NATURAL scenarios. In the upper reaches of Langtang Glacier, the velocity generally decreases between the late 1980s and late 2000s, and increases during the 1970s, early 1980s, early 1990s, and early 2010s. The increases are most likely due to higher accumulation in the upper reaches of the glacier

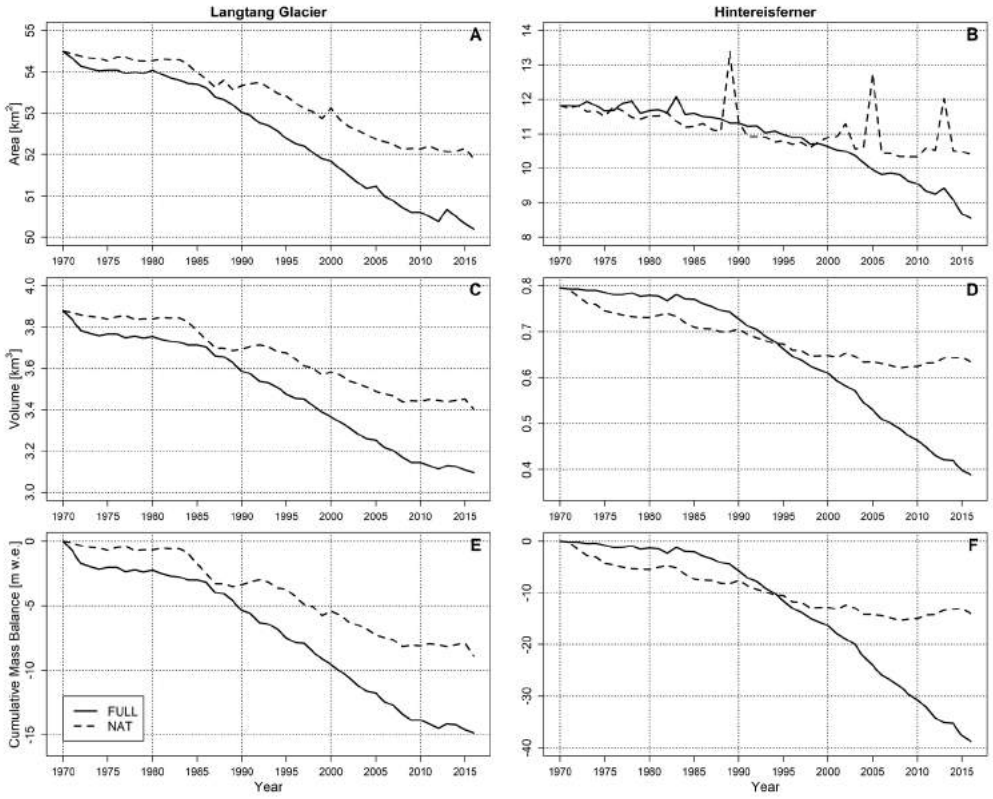

Figure 2.8. Modeled changes in glacier area (A,B), volume (C,D), and specific mass balance (E,F) of the Langtang Glacier (A,C,E) and Hintereisferner (B,D,F) for the cold/wet (Langtang Glacier) and cold/dry (Hintereisferner) FULL (solid) and NATURAL scenarios (dashed).

during these periods. Similar changes are simulated in the upper reaches of Hintereisferner after 1990. In the central reaches, velocity initially decreases, followed by velocities that do not change significantly or show a slight increase. These changes can most likely be explained by higher accumulations compared to the FULL scenario or close to equilibrium conditions that implies the ice thickness does not change and subsequently the velocity does not change either. The velocity changes for Langtang Glacier are smaller than the velocity changes at Hintereisferner. These differences can mainly be explained by the shorter response times at Hintereisferner. The shorter response time causes the glacier to react faster to climatic changes and thinning rates to be higher under a FULL scenario. At Hintereisferner a thinning rate of -0.59 m a^{-1} is estimated (over 1971-2016) for a FULL scenario relative to an estimated thinning rate of -0.16 m a^{-1} for a NATURAL scenario, whereas at the debris-covered tongue of Langtang Glacier thinning rates of -0.56 m a^{-1} and -0.43 m a^{-1} are estimated for the FULL and NATURAL scenarios, respectively. The higher thinning rates at Hintereisferner lead subsequently to a larger decline in velocity and thus explain the larger changes in velocity. The changing surface velocities and associated changes in thinning rates found at Hintereisferner and Langtang Glacier are in agreement with the recently observed link between glacier flow and thinning rates in High Mountain Asia (Dehecq et al., 2019).

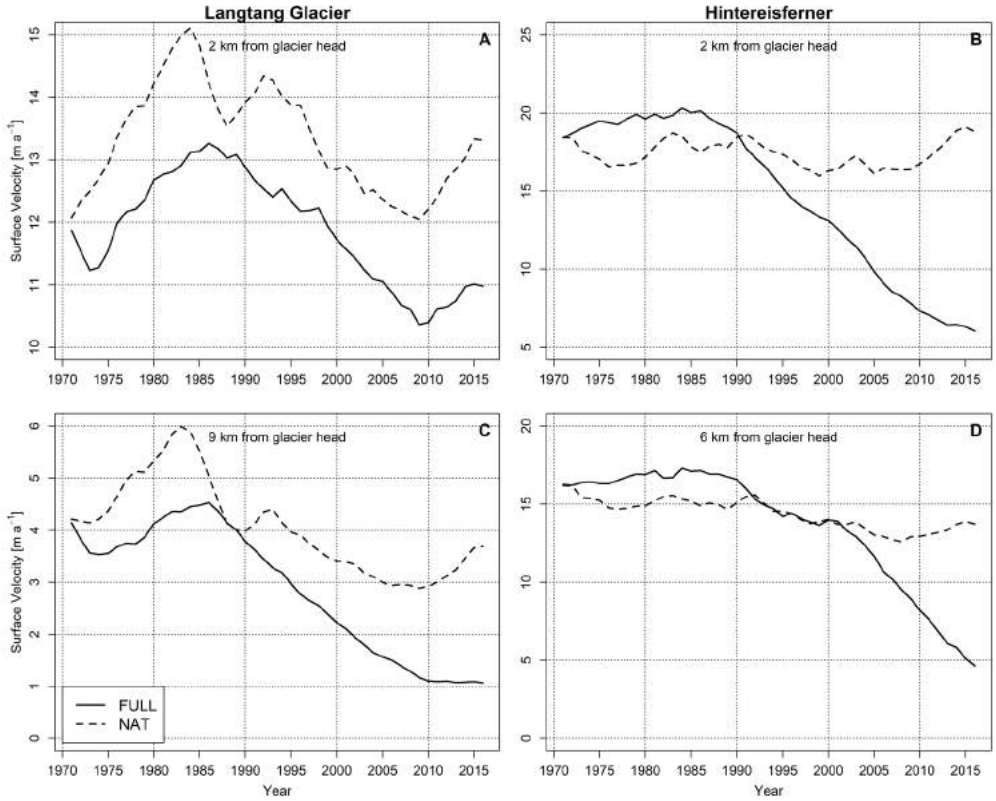

Figure 2.9. Modeled changes in surface velocity at two different transects along Langtang Glacier (A,C) and Hintereisferner (B,D) for the cold/wet (Langtang Glacier) and cold/dry (Hintereisferner) FULL (solid) and NATURAL scenarios (dashed). The locations of the two transects are given in Figure 2.6.

The less negative or even close to equilibrium glacier mass balance at Langtang Glacier and Hintereisferner eventually result in larger ice thickness at the end of a model run. Figure 2.10 shows the ice thickness and velocity fields at the end of a FULL-run and a NATURAL-run. At Langtang Glacier the difference between the maximum ice thickness of 283 m for NATURAL and 273 m for FULL is small. The higher ice thickness leads subsequently to higher flow velocities up to about 87 m a^{-1}. At Hintereisferner the differences in outcomes between the FULL and NATURAL scenarios are larger. Instead of a maximum ice thickness of about 180 m, ice thickness up to about 230 m is simulated for NATURAL. The associated velocities are higher with rates up to about 156 m a^{-1} at the terminus of the Kesselwandferner. There, the high velocities can mainly be attributed to the relatively steep slope in combination with a larger ice thickness than simulated for the FULL scenario. It can therefore be concluded that human-induced climate change has a significant impact on the mass balance and dynamics of glaciers. The magnitude of impact depends on the response time of the glacier, where a debris-covered glacier such as the Langtang Glacier shows a longer response time than a clean-ice glacier such as the Hintereisferner. It is therefore likely that that human-induced climate change has a larger impact on clean-ice glaciers than on debris-covered glaciers.

2.5 Discussion

2.5.1 Uncertainties and limitations

The outcomes of the glacier mass balance and ice-flow model are subject to several uncertainties and limitations that can be subdivided into three main groups: climate change simulations, the parameterization and representation of physical processes in the model, and the calibration procedure.

To assess the response of glaciers to historical climate change, an ensemble of four distributed and bias-corrected GCMs were used that cover a wide range of possible climate conditions. These models have been selected by means of an advanced envelope-based selection approach based on changes in climatic means and their skill in simulating the local climate. The outputs of the selected climate models are bias-corrected on meteorological data of the Kyangjin and Vent stations and are subsequently spatially distributed by using local monthly temperature lapse rates, normalized seasonal precipitation fields and high-resolution digital elevation models. The lapse rates are assumed to be constant in space and from year-to-year, whereas lapse rates are variable in space and time (Heynen et al., 2016; Immerzeel et al., 2014; Kirchner et al., 2013; Steiner and Pellicciotti, 2016). The lack of interannual and spatial variability might eventually introduce uncertainties in the climate fields, which propagates into the model results. The lack of spatiotemporal variability in lapse rates also introduce long-term uncertainties, especially since glaciers are sensitive to temperature changes that emerge from small changes in temperature lapse rates. Therefore, a correction of lapse rates might be needed to improve the long-term performance of the model. In our study temperature lapse rate corrections resulted in steeper lapse rates with monthly maximum (minimum) lapse rates that amount to 0.0076 (0.0052) °C m^{-1} in March-April (July) at Langtang Glacier and 0.0086 (0.0049) °C m^{-1} in March (December) at Hintereisferner. Thereby, the corrected lapse rates at Langtang Glacier fall in range with the lapse rates observed by Heynen et al. (2016). The corrected lapse rates at Hintereisferner are relatively steep compared to lapse rates that are mostly found in the European Alps (Rolland, 2003), but are still comparable with lapse rates found in other parts of the European Alps (Nigrelli et al., 2018). In addition, the limited data availability at higher altitudes hampers the validation of climate fields, especially in areas with difficult accessibility, such as upper Langtang Valley. Techniques, such as dynamical downscaling using high-resolution weather models, might contribute to an improvement of the accuracy and quality of climate fields in the complex mountainous environments of the upper Langtang and Rofental valleys (Bonekamp et al., 2018).

To separately assess the effects of human-induced climate change on the glacier response we followed two scenarios: FULL and NATURAL. The FULL scenario followed climate change simulations according to GCM outputs that follow the historical experiment of the CMIP5 archive, whereas the NATURAL scenario followed climate change simulations that are identical to the FULL scenario (until 1970) and retained the statistics of the climate change simulations prior to 1970 (i.e. 1925-1970). A limitation of retaining the statistics is that temperature trends such as the temperature decline simulated at the Kyangjin and Vent stations between the mid 1950s and 1970 are repeated after 1970, which subsequently introduces uncertainties in the model outcomes. An alternative approach would be to follow climate change simulations of the historicalNat experiment (i.e. GCM experiment forced with natural forcings only). However, the limitation of this approach is that simulations of the historicalNat experiment are difficult to bias-correct which might

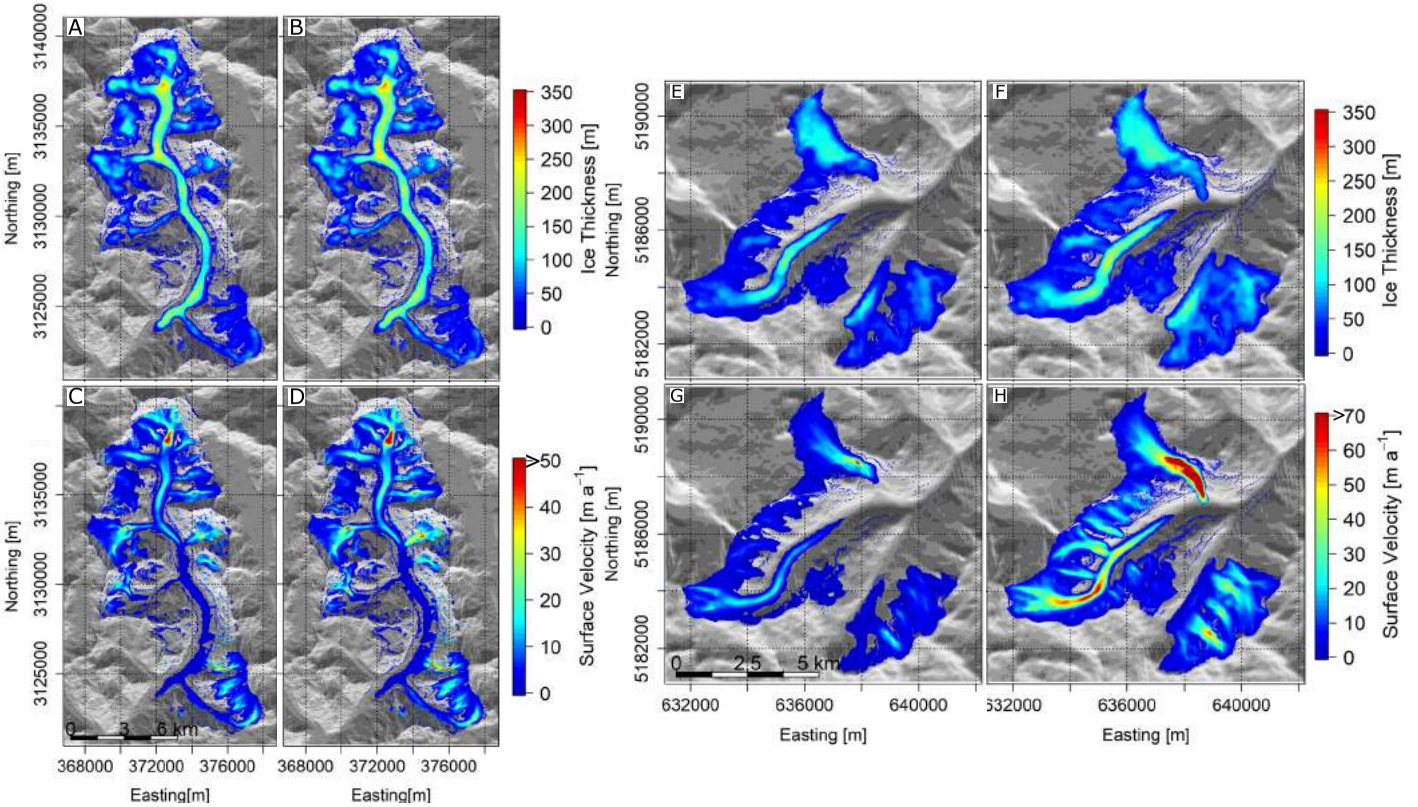

Figure 2.10. Ice thickness and surface velocity fields of the Langtang Glacier (A-D) and Hintereisferner (E-H), showing modelled ice thickness/velocity in 2016 for the cold/wet (Langtang Glacier) and cold/dry (Hintereisferner) FULL (A, C, E, G) and NAT scenarios (B, D, F, H).

introduce additional uncertainties. Additionally, the selection approach we followed would allow us to select the same ensemble models and members as the historical experiment. This might have a limitation since the forcing of a historicalNat experiment is different, which in combination with a different parameterization might lead to a trend opposite of what is expected under natural climate conditions, i.e. increasing temperatures relative to a historical experiment instead of constant or decreasing temperatures. Since our aim was to attribute the response of glaciers to anthropogenic and natural climate change, we chose to remove the trend in historical climate change simulations after 1970, which are clearly anthropogenic due to the strong observed human-induced increases in temperature, and to repeat the historical GCM runs spanning the period 1925-1970.

The glacier mass balance and dynamics were simulated by using a coupled glacier mass balance and ice-flow model that is based on a gridded formulation of the shallow ice approximation. One limitation is that sublimation processes are not included in the model, which is a considerable loss term in high mountain environments. For instance, at Hintereisferner sublimation losses of about 150 mm yr^{-1} have been reported by Kaser (1983). In the Langtang Valley, sublimation losses can amount up to 21% of the total snowfall, and can even be higher at wind-exposed locations (Stigter et al., 2018). The model might correct for these mass losses by adapting degree-day factors to increase the amount of loss by melt, which subsequently might result in overestimation of the calibrated glacier and snow degree-day factors. Another scenario is that snow storage and cover is overestimated, particularly at the high ridges that are prone to wind-blown transport of snow. To account for sublimation techniques are required that do not have a high data demand, but still can give reasonable sublimation estimates. Another limitation might be the use of a simple degree-day approach for the simulation of ice and snowmelt. Gabbi et al. (2014) found in a model comparison study that parameters of a simplified degree-day approaches are not robust in time and require recalibration for different climate conditions. The authors found that models including a separate term for shortwave radiation are able to produce robust simulations of ice and snowmelt. Therefore, these types of models can be seen as a suitable alternative to simplified degree-day approaches. Similar findings were also found by Litt et al. (2019) who tested the performance of (enhanced) temperature-index approaches in the Central Himalayas. The authors found however that these approaches can be underperforming where sublimation or other wind-driven processes contribute to ablation, such as in the accumulation zones. To improve the performance of the simplified degree-day approach applied in this study we distinguish the effect of aspect and include an elevation-dependent melt factor that accounts for the effect of debris thickness on melt rates.

A limitation that also might affect the model outcomes is the way how avalanching is simulated in the model. To simulate avalanching the gravitational snow transport module SnowSlide (Bernhardt and Schulz, 2010) is used. The drawback of this approach is that the module is solely restricted in use to snow avalanching, which disables the possibility to apply the algorithm for pixels that are classified as glacier. This means that on slopes steeper than the threshold slope (i.e. 25°) the avalanching of this material needs to be disabled, achieved in this study by assuming a threshold value that identifies a pixel as a glacier when the snow water equivalent is higher than 0.5 m. Although the model is able to simulate avalanches sufficiently at Langtang Glacier (i.e. especially at the eastern margins with steep side walls; Figure 2.2), the threshold value might also introduce uncertainties. For instance, the strong interannual variability in glacier area at Hintereisferner can mainly be attributed to the used threshold value. It is, however, difficult to validate the threshold value and the contribution of avalanching to the mass balance of the glaciers due to a lack of reliable

snowfall observations. Further improvements in the simulation of avalanching might be achieved by the combination of the SnowSlide module with existing modelling tools, such as the mass-conserving algorithm of Gruber (2007). This algorithm is an extension of flow-routing and terrain parameterization techniques and has the advantage that it can simulate the gravitational transport of other types of movements, such as ice avalanches or debris flows, as well. Further, the algorithm can easily be integrated in glacier mass balance and ice-flow models similar to the one presented here.

Flow velocities are largely dependent on ice rheology and dynamics as well as ice thickness and surface slope. Large unknowns, or processes not considered in the model, likely introduced uncertainties. Large unknowns are for instance the ice thickness changes since the end of the LIA, especially at Langtang Glacier where observations are lacking. Processes that have not been considered in the model are, for instance, the role of crevassing. Crevasses can play a crucial role in the mass balance and dynamics of glaciers by locally enhancing ablation and ice flow velocities (Colgan et al., 2016).

Another limitation is the assumed stationarity of model parameters in the model, which is also recognised as a major limitation in other type of models, such as hydrological models (e.g. Merz et al., 2011; Westra et al., 2014; Wijngaard et al., 2018). For instance, the spatial distribution of supraglacial debris, ponds and cliffs are highly variable over time. The spatio-temporal variability influences melt factors that in the model are assumed to be constant over time, which eventually might result in a local over- or underestimation of melt and subsequently also in an over- or underestimation of flow velocities. In addition, the debris and supraglacial characteristics of Langtang Glacier at the end of the LIA are a large unknown. Another example is the spatio-temporal variability in ice parameters, such as ice density or ice temperature, which influences ice viscosity and subsequently ice dynamics (e.g. Zhang et al. 2013). Since ice flow parameters, such as ice density, the temperature-dependent flow rate parameter A, and the correction factor C are assumed to be stationary, uncertainties might be introduced in the simulated flow velocities. For instance, the assumed stationarity of the correction factor C might be an explanation for the underestimated flow velocities at Hintereisferner during the 1940s, 1970s, and 1980s. To improve the representation of feedbacks between ice temperature and flow velocities, combined modelling approaches including models that simulate the thermodynamical behaviour of a glacier would be a future improvement. To improve the spatio-temporal variability of supraglacial debris and thus the amount of melt on the glacier, coupled mass balance and ice-flow models need to be combined with modelling approaches that can simulate the spatio-temporal evolution of supraglacial debris (Jouvet et al., 2011; Naito et al., 2000; Rowan et al., 2015).

The coupled glacier mass balance and ice-flow model is calibrated on observed mean surface elevation changes and surface velocities that are both derived from spaceborne imagery. This can be major advantage in remote areas where mass balance or surface velocity data are limited or not available at all. The limitation, however, is that the use of satellite images is restricted in use to several conditions, such as the absence of clouds and snow. When satellite images are available, the images might be prone to noise or distortions, which, in turn, hampers calibration of the model. Further, uncertainties might have been introduced through the calibration approach. The model parameters have been calibrated using an automatic optimization algorithm followed by a manual optimization. No distinctions have been made in the performance of the model in

simulating separate components of the high-mountain cryosphere, such as snow cover. Because of that equifinality problems might have been introduced that affect the amount of melt simulated by the model. To minimize equifinality problems in the future, systematic approaches (Lutz et al., 2016a; Pellicciotti et al., 2012; Wijngaard et al., 2017) are recommended that can calibrate the model in multiple consecutive steps by using the combination of snow cover, mass balance and surface velocity data.

2.5.2 Shallow ice approximation

To assess the response of glaciers under changing climate conditions we apply a coupled glacier mass balance and ice-flow model that is based on a spatially-distributed formulation of the SIA. The main advantage of this approach is that the model does not require a priori information on the flowline geometry, but also has other advantages which are mainly related to the low computational expense and complexity. There is a concern that the SIA becomes deficient for fast-flowing glaciers and steep/narrow glacier since the approach does not account for higher-order physics, such as longitudinal and lateral stress gradients (Adhikari and Marshall, 2013; Le Meur et al., 2004). According to Le Meur et al. (2004) the slope is the most important criterion for the applicability of the SIA, where SIA models can still be considered as acceptable for bedrock slopes smaller than 20%. The mean (minimum/maximum) bedrock slope of Langtang Glacier and Hintereisferner are 44% (0%/93%) and 44% (0%/81%), respectively, which means from this point of view the SIA approach would be deficient. However, Le Meur et al. (2004) did not include correction factors that account for higher-order physics, which are normally neglected by the SIA approach. Also, the authors did not calibrate the Glen's flow rate constant. In our model correction factors that account for longitudinal and lateral stress gradients are included (Adhikari and Marshall, 2011, 2012b; Nye, 1965). Furthermore, Glen's flow rate constant is calibrated on observed surface velocities. This combination results in valid outcomes, which shows that the SIA approach is even reliably on steeper slopes. For example, at the Kesselwandferner velocities up to 77 m a^{-1} are simulated where the bedrock slope is approximately 44%. Although these velocities do not agree with the present-day observed velocities of approximately 20 m a^{-1} (i.e. ablation stakes L8, L9 and L10) due to an overestimation of ice thickness, velocities with the same order of magnitude (80-90 m a^{-1}) have been observed in the 1970s/1980s (Stocker-Waldhuber et al., 2019). It illustrates the ability of the model to simulate realistic velocities at steeper slopes. Additionally, the use of correction factors in combination with the SIA approach sustains the simplicity of ice flow models, which makes it suitable for potential application in catchment- or regional scale (cryospheric-)hydrological models.

2.6 Conclusions and outlook

The aim of this study is to develop and apply a spatially distributed coupled glacier mass balance and ice-flow model to attribute the response of two glaciers to anthropogenic and natural climate change. We focus on two glaciers with contrasting surface characteristics: the debris-covered Langtang Glacier in the Central Himalayas, and the clean-ice Hintereisferner in the European Alps. We apply the model from the end of the Little Ice Age (1850) to the present-day (2016) by forcing the model with bias-corrected and distributed GCM runs that represent a wide range of region-specific possible climate conditions. The model outputs are used to analyse the evolution and dynamics of the two glaciers, and subsequently to reveal the anthropogenic influence by comparing outputs of two scenarios: one scenario considering the human-induced rapid increases in temperature after 1970 and one scenario that retains the climate conditions prior to 1970.

The results indicate that the coupled glacier mass balance and ice-flow model, based on a gridded formulation of the shallow ice approximation, performs reasonably well for both clean-ice and debris-covered glaciers.

Both glaciers experience the largest area and volume reductions under warm climate conditions, whereas for cold climate conditions the model show a smaller reduction. In addition, the cold model (i.e. cold/dry for Hintereisferner and cold/wet for Langtang) simulates changes that are close to the observed trends. These models simulate area (volume) reductions of 16% (42%) for the Langtang Glacier and of 40% (75%) for the Hintereisferner between 1850 and 2016. Simultaneously with changes in the extents and volumes, surface velocities generally decrease over time from up to 275 m a^{-1} to 66 m a^{-1} at Langtang Glacier and from up to 310 m a^{-1} to 25 m a^{-1} at Hintereisferner. The simulated changes over time are smaller in magnitude for the Langtang Glacier, which can mainly be attributed to the debris cover that insulates the surface and thus reduces the amount of melt. Additionally, the debris cover maintains the position of the terminus. Instead the glacier thins, which eventually result in a shallower profile and a stagnation of velocities at the terminus of the glacier. At Hintereisferner melt rates are higher and the glacier retreats with about 3 km over length under cold/dry climate conditions.

Simulations show that anthropogenic climate change has been accompanied with a rapid increase in temperature after 1970. This has resulted in a larger decline in area/volume compared to a scenario where the anthropogenic influence is less significant (i.e. NATURAL scenario). At Langtang Glacier, the changes in area, volume, and ice thickness remain negative for the NATURAL scenario. Only in the late 1980s and early 2010s the glacier mass balance is close to equilibrium. The relative area, volume and cumulative mass balance difference between a cold/wet FULL and NATURAL scenario at the end of 1971-2016 is 3%, 9%, and 40%, respectively. At Hintereisferner the glacier area, volume, and ice thickness decrease initially followed by an almost balanced state after 2000. Here, the relative area, volume and cumulative mass balance difference between a cold/dry FULL and NATURAL scenario at the end of 1971-2016 is 18%, 39%, and 64%, respectively. The decline in area, volume, and ice thickness are accompanied by changing surface velocities that generally increase or do not change significantly. The difference in the response of glaciers between a FULL and a NATURAL scenario is larger for the Hintereisferner mainly due to shorter response times. The shorter response times cause the glacier to react faster to climatic changes and thinning rates to be larger. The larger thinning rates do subsequently lead to a larger decline in area, volume, cumulative balance, and velocity. The simulated velocity changes and associated changes in thinning rates are in agreement with the recently observed link between glacier flow and thinning rates in High Mountain Asia. For a debris-covered glacier the differences are less pronounced due to a longer response time, which can mainly be attributed to the debris cover that insulates the glacier surface and reduces melt.

The outcomes of this study show that the gridded formulation of the shallow ice approximation performs well and is a suitable alternative for higher order or Stokes approaches, especially while modelling a large-scale ensemble of glaciers. Although improvements are needed in future research, the combination of satellite-based imagery and the use of the gridded formulation of the shallow ice approximation should be explored towards investigating the dynamical response of glaciers and its implications for hydrology at a regional scale.

Acknowledgements

I would like to thank Silvan Ragettli for sharing the mean annual surface elevation change grids of Langtang Glacier. I would like to thank Maxime Litt and Sonu Khanal for the helpful discussions.

3 Hydrological response of glacierized catchments to future climate change

This paper investigates the hydrological response of glacierized headwater catchments to future climate change in the Ötztal Alps, Austria. In this study, two conceptual hydrological models, HBV (Hydrologiska Byråns Vattenbalansavdelning) and HQsim, are applied for the simulation of future daily discharge in three (nested) catchments with varying degrees of glaciation. The models are forced with downscaled climate change projections, and outputs from an empirical glacier model, which is able to simulate future glacial evolution. Under the future conditions, the outcomes initially show that runoff increases for all catchments without changes in the runoff regimes. In the long term, summer runoff is expected to decrease and winter/spring runoff is expected to increase in all catchments. These runoff changes are accompanied by regime shifts from glacial/glacio-nival runoff regimes to runoff regimes with a higher nival component. Changing runoff conditions might also lead to changes in the seasonality of annual flood peaks with an earlier appearance of flood peaks, and an increasing appearance of low flow conditions during summer months. The outcomes of the two hydrological models show minor differences. The results of this study provide improved understanding of the future impact of climate change on the water cycle of glacierized Alpine catchments.

Based on: *Wijngaard, R.R., Helfricht, K., Schneeberger, K., Huttenlau, M., Schneider, K., and Bierkens, M.F.P. 2016. Hydrological response of the Ötztal glacierized catchments to climate change. Hydrology Research 47(5), 979-995. DOI: 10.2166/nh.2015.093.*

3.1 Introduction

Millions of citizens living in large river basins are dependent on the water supply from mountain ranges, such as the Himalayas and the European Alps (EEA, 2009; Immerzeel et al., 2010). The water supply is thereby largely determined by the contribution of meltwater originating from glaciers and snow storage. Water supply is generally lowest during winter as water is stored in the form of snow and ice, and highest during the summer season, i.e. when the water demand is high (Casassa et al., 2009). The timing and the magnitude of water supply underlines therewith the hydrological importance of mountain ranges for river basins and therefore mountain ranges can be defined as the 'water towers' of these areas (Viviroli et al., 2007). Viviroli and Weingartner (2004) show for instance that the European Alps have a mean contribution varying from 26% to 53% to the total discharge at the outlets of the Danube and Po Rivers, respectively. In summer, the mean contributions are even higher with proportions varying from 36% to 80% for the same respective rivers, which is caused by a combination of high amounts of meltwater originating from glaciers and snow storages located in the Alps and an evapotranspiration surplus in lowland regions.

Future climate change is expected to have an impact on the runoff characteristics of river basins (IPCC, 2013), especially in glacierized headwater catchments that are characterized by high runoff contributions from ice and snow storages. The expectation is that due to climate change glaciers will retreat or even disappear (Huss et al., 2008) and seasonal snow cover will decline, which eventually will affect runoff characteristics (Huss et al., 2014; Salzmann et al., 2014). These changes are considered to have consequences for the water availability of, for instance, drinking water supply, agricultural purposes (e.g. irrigation), and energy production (e.g. hydropower)(Immerzeel et al., 2010; Viviroli et al., 2011), especially for water originating from glacierized headwater catchments. For this reason, it is important to understand and to assess the impact of climate change on the hydrology of these catchments and to use this knowledge for developing adaptation strategies that aim at reducing the possible adverse impacts in light of integrated water resources management (IWRM).

There have been quite a number of studies dedicated to assessing the impact of climate change on runoff characteristics in glacierized headwater catchments. To assess these impacts, mostly conceptual hydrological models (e.g. Bergström et al., 1992; Huss et al., 2008) and in lesser extent physically based hydrological models (Ragettli and Pellicciotti, 2012; Weber et al., 2010) were used. These models were often forced by climate projections derived from General Circulation Models (GCMs) or Regional Climate Models (RCMs) (Farinotti et al., 2012; Lutz et al., 2014; Weber et al., 2010). Depending on the modelling approach, glacial melt was simulated by a combination of assuming a hypothetical reduction of glacier area and temperature-index approaches (Hagg et al., 2007), by the combination of temperature-index approaches and parameterizations of future glacier change (Farinotti et al., 2012; Li et al., 2015; Lutz et al., 2014), by the use of temperature-index approaches alone (e.g. Einarsson and Jónsson, 2010), or by the use of energy-balance models (e.g. Weber et al., 2010), among others. In most of these studies, runoff increases were generally projected until 2050 for catchments located in areas such as Iceland (e.g. Einarsson and Jónsson, 2010), the European Alps (e.g. Farinotti et al., 2012), and the Himalayas (e.g. Lutz et al., 2014). After 2050, annual runoff decreases, summer runoff decreases, and winter/spring runoff increases were generally projected for catchments located in areas such as the European Alps (e.g. Farinotti et al., 2012; Weber et al., 2010), Central Asia (e.g. Hagg et al., 2007), and the Canadian Coast Range (e.g. Stahl et al., 2008). Thus, projected changes particularly affect the seasonal distribution of runoff.

The aim of this study is to investigate how glacierized catchments in the Ötztal Alps (Austria) will respond hydrologically to future climate change. In this study, two conceptual semi-distributed hydrological models with different degrees of complexity, HBV (Light) and HQsim, are applied to three different catchments in the Ötztal Alps. These models are forced with downscaled climate change projections and outputs from an empirical glacier model, able to simulate future glacial evolution as a result of climate change. Subsequently, the outcomes of the hydrological models are used to analyse changes in the seasonality of high runoff conditions, absolute changes, relative changes, the seasonality of annual flood peaks, and low flow characteristics. This study distinguishes from previous studies in the region (e.g. Tecklenburg et al., 2012) in that this is the first study using a combination of multiple hydrological models, multiple downscaled climate models, and a glacier model. It is expected that the changes estimated from these catchments are exemplary for changes in the drier parts of the European Alpine regions.

The remainder of the chapter is set up as follows. First, the study area is described, followed by a description of data and methods used, i.e. the field data, the hydrological modelling, the future climate forcing, and modelling change of glacial extent. Next, results are presented and discussed, followed by the main conclusions.

3.2 Study area

This study focuses on catchments in the Ötztal Alps, which are the catchments of the Ötztaler Ache and its headwaters, the Venter Ache and the Gurgler Ache. The reason for choosing the Ötztal Alps as study area is the high research activity and data availability in this area.

The Ötztaler Ache, located in the Austrian Federal Province of Tyrol (Figure 3.1), is with a total length of 67 km the largest tributary of the river Inn (Achleitner et al., 2012). In the Ötztaler Ache catchment (catchment area of 891 km^2) elevation ranges from 710 to 3766 m above sea level (a.s.l.). The degree of glaciation is 11.7% (based on the Austrian glacier inventory of 2006; Abermann et al., 2012). In the headwaters of the Venter Ache (catchment area of 165 km^2) and Gurgler Ache (catchment area of 72 km^2) the degree of glaciation is 32.2% and 29.4%, respectively. The higher parts of the Ötztaler Ache catchment are dominated by glacial cover and bare vegetated rock surfaces where coniferous woodlands and alpine meadows are the main land cover types in the lower parts (CORINE land cover; Bossard et al., 2000). The Ötztaler Ache catchment experiences a dry inner-alpine climate with annual precipitation sums varying from 650 mm (Umhausen; 1041 m a.s.l.) to 850 mm (Obergurgl; 1938 m a.s.l.) (ZAMG, 2013) with the highest precipitation sums in the summer period, mainly due to convective events (Hagg, 2003), and the lowest precipitation sums in the winter period. The explanation for the comparatively dry climate is that the Ötztal is shielded from precipitation deriving from the north (Northern Calcareous Alps) and the south (Alpine Main Range) (Kuhn et al., 1982). The mean annual temperature varies between 2.2 °C (Obergurgl) and 6.3 °C (Umhausen) (ZAMG, 2013). The runoff regimes can be classified as glacio-nival (gauging station Brunau) and glacial (gauging stations Obergurgl and Vent) with highest runoff conditions in the period June-August and low runoff conditions in the winter period.

3.3 Data and methods

3.3.1 Field data

In this study, the following field data were used as input for HBV and HQsim:

- Daily air temperature and precipitation,
- Daily-observed discharge,
- Digital terrain model (DTM), with 10 m x 10 m resolution,
- Land cover data,
- Soil maps (only for HQsim), and
- Glacier cover data.

Daily air temperature and precipitation were extracted from the meteorological stations of the Zentralanstalt für Meteorologie und Geodynamik (ZAMG), Tirol Wasserkraft AG (TIWAG AG), Hydrographical Service Tyrol and the Commission of Glaciology, Bavarian Academy of Sciences for the period 1986-2012. Time series of observed daily discharge were obtained from the gauging

stations Brunau (Ötztaler Ache), Vent (Venter Ache) and Obergurgl (Gurgler Ache) for the period 1983-2012. The DTM, land cover data, soil maps and glacial cover data were derived from the Airborne Laserscan (ALS) recordings of 2006 (Land Tirol, 2006), the Coordination of Information on the Environment (CORINE) land cover dataset (Bossard et al., 2000), the Hydrological Atlas of Austria (BMLFUW, 2007), and the Austrian glacier inventories of 1997 (Lambrecht and Kuhn, 2007) and 2006 (Abermann et al., 2012), respectively.

Figure 3.1. Map of the study area showing the catchment of the Ötztaler Ache (upstream of gauging station Brunau), and its headwaters, the Venter Ache (upstream of gauging station Vent) and the Gurgler Ache (upstream of gauging station Obergurgl).

3.3.2 Hydrological modelling

Two hydrological models were used to simulate current and future daily discharge for the Ötztaler, Venter and Gurgler Ache: HBV (Light) (Seibert and Vis, 2012) and HQsim (Kleindienst, 1996). HBV (Light) is a user-friendly version of the semi-distributed conceptual HBV-96 model of Bergström et al. (1992), which uses the concept of elevation vegetation units (EVUs). HQsim is a semi-distributed conceptual model based on the concept of hydrological response units (HRUs) and uses the BROOK model of Federer and Lash (1978) as foundation. More detailed information of the key characteristics and the contrasts between both models is given in Table 3.1.

HBV and HQsim were applied by using 250m elevation zones and HRUs, respectively. The HRUs were delineated using elevation, aspect (derived from the DTM), land cover, and glacial extent (derived from the glacial inventories of 2006). Subsequently, daily temperature and precipitation values were calculated for each HRU. For the calculation of daily temperature, single time series of daily temperature data (considering a reference elevation of 0 m a.s.l.) and daily temperature gradients were composed for the entire catchment of the Ötztaler Ache. These series were composed by a simple linear regression analysis using the daily temperature data of meteorological stations as input, and were subsequently used to calculate daily temperature for the mean elevation of each HRU. To calculate daily precipitation for each HRU, daily precipitation data were projected on a 5 km x 5 km grid, using inverse distance weighting (IDW) as a methodological approach to interpolate precipitation data from meteorological stations to the grid points. Finally, the gridded precipitation data were weighted for each HRU, based on the areal weight of each HRU inside a grid cell. The type of precipitation depends on the temperature. Precipitation may occur as rain, snow or as a rain-snow mixture.

In HBV, elevation was used in combination with land cover and glacial extent to determine aspect-elevation area distributions for the different vegetation zones used in HBV (for this study the maximum number of 3 vegetation zones was applied, representing glacial cover, bare vegetated rock

Table 3.1. Key characteristics of HBV and HQsim.

Hydrological Model	HBV (Light)	HQsim
Model structure	Snow, glacier, soil, groundwater, and routing routine	Snow, glacier, vegetation, soil, groundwater, and routing modules
Spatial representation	Elevation Vegetation Units (EVUs)	Hydrologic Response Units (HRUs)
Input variables	Temperature, Precipitation, Observed Discharge, Potential Evapotranspiration	Temperature, Precipitation, Observed Discharge, Potential Evapotranspiration
Potential evapotranspiration	Temperature-based approach (Hamon, 1961)	Temperature-based approach (Hamon, 1961)
Glacier melt, snow melt and accumulation	Degree-day approach with aspect and albedo correction (Konz and Seibert, 2010)	Degree-day approach, distinguishing the effects of aspect, slope, and inclination of the sun (Hock, 1999)
Glacier outflow	Glacier storage-outflow relationship (Stahl et al., 2008)	Integrated glacier module, consisting of three internal reservoirs representing, snow, firn and ice
Overland flow	Linear groundwater reservoir	Simulated for each HRU. Depending on fraction of area contributing area, which is a function of soil water content (Achleitner et al., 2012)
Subsurface flow	Linear groundwater reservoir	Simulated with Mualem van Genuchten approach (van Genuchten, 1980)
Baseflow	Linear groundwater reservoir	Linear groundwater reservoir
Routing	Triangular Weighting Function	Approach of Rickenmann (1996)

surfaces and vegetated areas (woodlands and meadows)). For the application of daily temperature in HBV, the former composed time series of daily temperature data (considering a reference elevation of 0 m a.s.l.) were used as input. The series of daily temperature gradients were, however, not applied in HBV, since only one value is required as temperature gradient in HBV. For the application of daily precipitation in HBV, single time series of daily precipitation data were composed from the gridded precipitation data for the catchments of the Ötztaler Ache and the headwaters of the Venter and Gurgler Ache separately. Dependent on temperature, precipitation may occur as rain or as snow.

HBV and HQsim were calibrated and validated using manual calibration under a split-sample approach (Klemeš, 1986). The models were both calibrated and validated for the same periods (Table 3.2), although it has to be mentioned that for the calibration and validation of HBV a warming-up period (of one year) was needed to fill the reservoirs in the model. We chose to start the calibration in the late 1990s, because of the low data quality and availability in the 1980s and the beginning of the 1990s, making this period less feasible for calibration. For the Venter Ache however, it was not possible to start the calibration in the late 1990s since observed discharge time series were not available for the period 2003-2006. Therefore this period was deemed as unsuitable for the calibration of HBV and HQsim. Furthermore, we chose to have two validation periods to identify differences between the model performances that are accompanied by the validation periods.

3.3.3 Future climate forcing

To estimate the effects of climate change, time series of future climate variables were used as developed by the University of Natural Resources and Life Sciences, Vienna, Austria in cooperation with alpS Centre for Climate Change Adaptation, Innsbruck, Austria. To simulate future climate variables the output of three combinations of GCMs and RCMs were realised, used under CO2 forcing following the SRES A1B scenario of the 4th IPCC assessment report:

- ARPEGE-ALADIN (Déqué et al., 1994; Farda et al., 2010),
- ECHAM5-RegCM3 (Giorgi et al., 1993; Roeckner et al., 2003),
- ECHAM5-REMO (Jacob and Podzun, 1997; Roeckner et al., 2003).

Table 3.2. Calibration (Cal. P.) and validation periods (Val. P. I and II) Abbreviations: ÖA = Ötztaler Ache, Ob = Gurgler Ache, and VA = Venter Ache.

		HBV	HQsim
ÖA	Cal. P.	1998-2007	1998-2007
	Val. P. I	1987-1997	1987-1997
	Val. P. II	2008-2012	2008-2012
GA	Cal. P.	1998-2007	1998-2007
	Val. P. I	1987-1997	1987-1997
	Val. P. II	2008-2012	2008-2012
VA	Cal. P.	1993-2002	1993-2002
	Val. P. I	1987-1992	1987-1992
	Val. P. II	2008-2012	2008-2012

These climate change simulations provided daily temperature and daily precipitation for the period 1985-2100. Error correction was applied by a per-month quantile mapping approach (Déqué, 2007; Formayer and Haas, 2010), thereby adjusting RCM output according to daily observed values of temperature and precipitation, and retaining the statistics of these observations for each month separately (12 quantile mappings). The observed values of temperature and precipitation were obtained from the E-OBS 1981-2010 dataset (Haylock et al., 2008) and the gridded precipitation dataset of Frei and Schär (1998), respectively. The error-corrected 25 km x 25 km RCM output was subsequently scaled down to the 1 km x 1 km grid of the Integrated Nowcasting through Comprehensive Analysis (INCA) system (Haiden et al., 2011) using the localisation method of Pospichal et al. (2010), accounting for the complex topography of the European Alps.

These projections were subsequently analysed in a so-called 'delta change approach' on daily basis (Bosshard et al., 2011). The mean annual cycle of precipitation and temperature was calculated for the 30-year reference period 1985-2014 and the scenario periods 2010-2039 (near future), 2040-2069 (mid-future), and 2070-2099 (far future). The mean annual cycle was smoothed, eliminating the high frequency part of the daily signal by using a low-pass filter according to Bosshard et al. (2011). The standard deviation (σ) of the extracted high frequency part of the climate signal was calculated in a moving window of 31 days to estimate the natural variability of temperature and precipitation in the 30-year periods (Figure 3.2).

Absolute temperature and relative precipitation changes between the reference period and the scenario periods were calculated on a daily basis. This climate signal was used to alter the original input of meteorological data series of 1983-2012. Note that a shift of 2 years exists between the period of meteorological input and the reference period due to data unavailability. However, this small difference is neglected with respect to the overall variability in climate data.

The hydrological models HQsim and HBV were forced by delta change-modified time series related to projections that were resulting from each GCM-RCM combination. The mean of the outcomes, resulting from the three different simulations, was used for the analysis of changes in runoff characteristics. Highest temperature changes were observed from the ALADIN simulation for all three periods (Figure 3.2). The realisations based on REMO and RegCM3 showed similar changes, most likely as they were forced by the same GCMs. The precipitation changes were rather small compared to the natural variability. The peak increase of precipitation in October is seen in all three realisations, but is also accompanied by a high variability.

3.3.4 Modelling change in glacier extent

In HBV and HQsim, glacier melt is simulated by using different approaches. In HBV, glacier melt is simulated using a degree-day approach with aspect and albedo correction (Konz and Seibert, 2010), while in HQsim glacier melt is simulated by using a degree-day approach, which distinguishes the effect of aspect, slope and inclination of the sun (Hock, 1999) based on the HRUs. Despite the ability to simulate glacier melt, none of these models is capable of simulating changes in glacial extent over time. Therefore future glacial extent was simulated separately with a glacier change model, able to simulate future ice thickness, glacier area and volume on a 50 m x 50 m grid as a result of changing climate conditions. To simulate future glacial extent, the following steps were conducted:

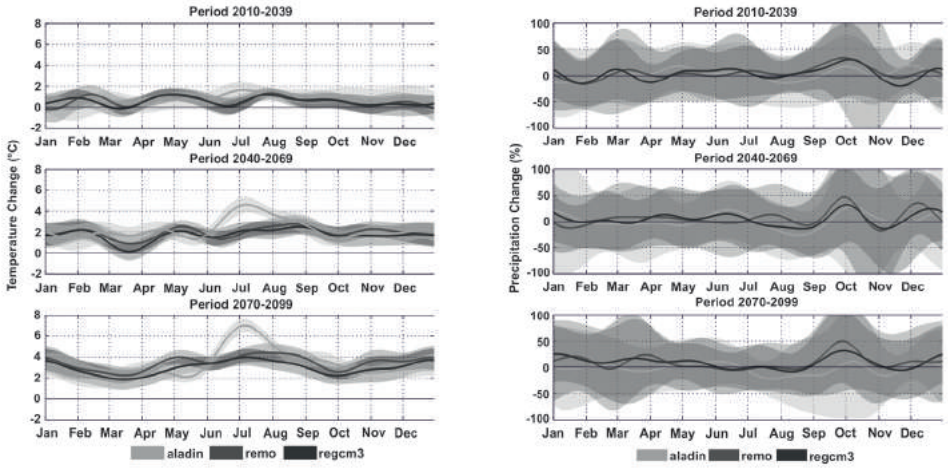

Figure 3.2. Low-pass filtered signals and natural variabilities (±) of absolute temperature and relative precipitation changes for the near, mid, and far future.

1. Spatially distributed elevation changes over a 9-year period (1997-2006) were obtained from the glacier inventories of 1997 (Lambrecht and Kuhn, 2007) and 2006 (Abermann et al., 2012) and scaled to a mean annual surface elevation change.
2. Initial ice thickness distributions were inverted from the glacier surface topography following the ice thickness estimation method (ITEM) of Huss and Farinotti (2012), which is a method, based on glacier mass turnover and ice flow mechanisms. The 2006 DTM of Tyrol (Land Tirol, 2006) and glacier outlines of the Austrian glacier inventory of 2006 were used as input. Subsequently, the glacier bed elevations were derived, subtracting the ice thicknesses from the 2006 glacier surface elevations.
3. Mean surface elevations were obtained for the period 2005-2105 with an interval period of 10 years (i.e. 2005, 2015, 2025, etc.), using the observed annual surface elevation change. Additionally a climate sensitivity of -0.89 m annual surface elevation change (i.e. specific mass balance of -0.8 m we converted by an assumed density of 900 kg m^{-3}; Braithwaite and Zhang, 2000; Kuhn and Batlogg, 1998) was added for each grid cell per 1 °C of temperature increase given in the climate scenarios.
4. New ice thickness distributions were calculated, using the estimated mean surface elevations and the former estimated glacier bed elevations. In case of lower surface elevations than the glacier bed elevations, ice thickness was set to zero. The remaining grid cells with a positive ice thickness constituted the future glacier area.

With respect to the uncertainties of the used ice thickness estimation method (ITEM), initial ice thickness was changed by ±20% to assess the resulting uncertainty in glacier area (Figure 3.3). Whereas glacier volume is expected to change first, caused by a strong reduction in mean ice thickness, glacier area is set to decrease by a temporal delay of 15 to 20 years. The temporal uncertainty range of total glacierized area will increase with time, whereas the uncertainty in area relative to the 2006 reference is highest between 2050 and 2060 and will decrease afterwards. The glacier area relative to the 2006 reference is shown in Figure 3.3. Depending on the applied GCM-

RCM combination, about 10 to 20% of the present glacierized area is expected to exist at the end of the 21st century.

From the outcomes of the glacier change model, projections of glacial extent were obtained for 2025, 2055, and 2085 and assumed to be constant throughout the scenario periods (i.e. 2010-2039, 2040-2069, and 2070-2099). Finally, HBV and HQsim were run for these periods with the glacial extent projections as input.

3.4 Results

3.4.1 Calibration and validation

In Table 3.3, the calibration and validation periods are given for Brunau, Obergurgl, and Vent with respective model efficiency criteria according to Nash and Sutcliffe (1970). For the calibration period, both models perform 'very good' (Moriasi et al., 2007) with NSE values of 0.86 or higher. In the validation periods, both models perform 'very good' as well. Nevertheless, there is a slight difference in performance between the two validation periods. In the second validation period both models perform slightly better than in the first validation period with NSE values of 0.84 or higher.

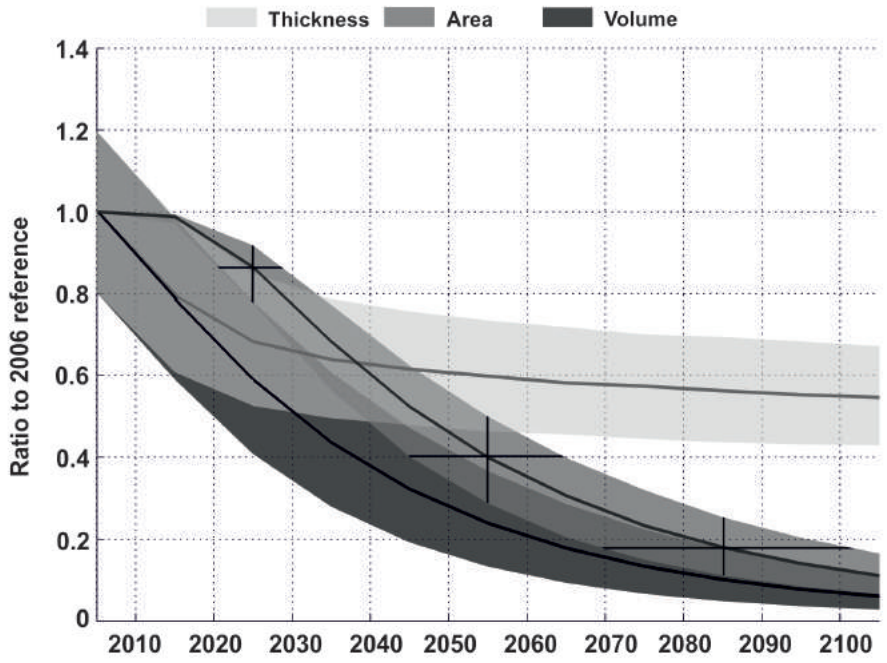

Figure 3.3. Calculated changes of ice thickness, glacierized area, and glacier volume in relation to the 2006 extent of all glaciers in the Ötztal catchment. Shaded areas show the range of results based on an initial ice thickness variation of ±20%. Black crosses show the resulting uncertainty of glacier area in time and relative to the 2006 reference area at the central years of the climate periods used in this study.

Table 3.3. Calibration (Cal. P.), validation periods (Val. P. I and II), and respective Nash-Sutcliffe efficiency (NSE) values.

			HBV	HQsim
Brunau	Cal. P.	1998-2007	0.87	0.89
	Val. P. I	1987-1997	0.85	0.85
	Val. P. II	2008-2012	0.90	0.89
Obergurgl	Cal. P.	1998-2007	0.86	0.87
	Val. P. I	1987-1997	0.80	0.83
	Val. P. II	2008-2012	0.86	0.84
Vent	Cal. P.	1993-2002	0.87	0.87
	Val. P. I	1987-1992	0.85	0.86
	Val. P. II	2008-2012	0.90	0.87

The level of performance differs from season to season, but also among the different models and locations. These differences in performance are observable in the percent bias (PBIAS) between observed and simulated discharge of the period 1987-2012 (Figure 3.4). Based on the assumption that a model performs well if the PBIAS is less than 15% (Moriasi et al., 2007), HBV performs well for the simulated spring, summer, and autumn runoff in Brunau, the simulated winter, summer, and autumn runoff in Obergurgl, and the simulated spring, summer, and autumn runoff in Vent, with the best performance for the simulated spring runoff in Brunau and the worst performance for the simulated spring runoff in Obergurgl. HQsim performs well for the simulated winter, summer, and autumn runoff in Brunau, the simulated summer runoff in Obergurgl, and the simulated winter, spring, and summer runoff in Vent, with the best performance for the simulated summer runoff in Vent and the worst performance for the simulated autumn runoff in Vent either.

3.4.2 Change in future runoff

In Figure 3.5, runoff regime changes are projected for the near (2010-2039), mid (2040-2069), and far future (2070-2099). For Brunau, a glacial/glacio-nival regime is projected for the reference period with highest mean runoff values in July. The near future projections indicate that no significant changes will appear. Changes express themselves mainly in small absolute and relative changes that generally occur in April/May (see Table A.1 and A.2 in Appendix A). For the mid and far future larger runoff changes are projected, with relative increases up to 132% in April and relative decreases up to 51% in August. The combination of a runoff increase during spring and a runoff decrease during summer is expected to evolve the glacial/glacio-nival regime into a moderate nival regime with highest runoff conditions in May/June.

For Obergurgl and Vent, glacial runoff regimes are simulated for the reference period with highest mean monthly runoff values in July-August. These regimes are expected to persist in the near future, although annual and mean monthly runoff are projected to increase. For the mid and far future, the flow regimes will shift from a glacial regime to a nivo-glacial/nival regime in Obergurgl with highest runoff conditions in June-July, and from a glacial regime to a nivo-glacial regime in Vent with highest runoff conditions in June. The relative changes accompanied by the regime shift in Obergurgl vary from relative increases up to 249% in April to relative decreases up to 46% in August, whereas annual runoff is projected to decrease up to 29%. In Vent, runoff changes are projected, with relative increases up to 186% in May and relative decreases up 53% in August.

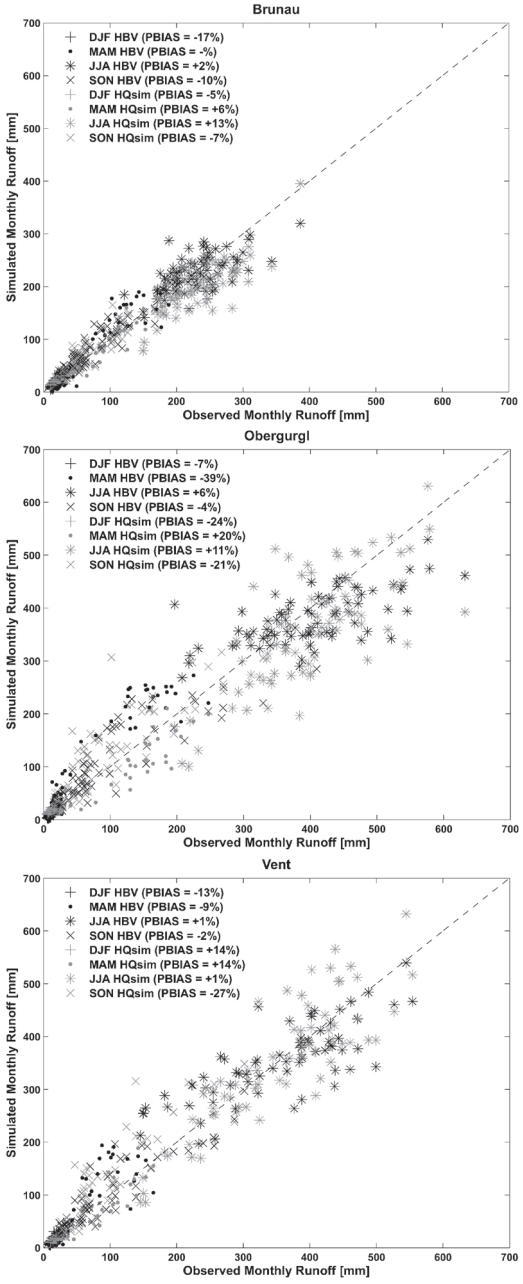

Figure 3.4. Simulated vs. observed monthly discharge volumes for the period 1987-2012, including the PBIAS calculated over the seasons. Positive PBIAS values indicate an underestimation of simulated runoff and negative PBIAS values indicate an overestimation of simulated runoff. Abbreviations: DJF = December, January, February, MAM = March, April, May, JJA = June, July, August, and SON = September, October, November.

The simulated changes in runoff can be explained by several factors. In near future the main factor responsible for runoff increases during summer and early autumn is likely to be an increase in glacial melt as a result from an increase in temperature. For the runoff increases during winter/spring other factors may be responsible either. Temperature increases result in a) an earlier onset of snowmelt, leading to shorter snowpack durations, b) a lower fraction of solid to total precipitation, and c) a rise of the snowline by about 150 m for every 1 °C increase in temperature (Beniston, 2003). The combination of lower fractions of solid precipitation and a rise in the snowline will lead to a decline in snow-covered area and to higher fractions of direct runoff. With a decline in snow-covered area, snow storage reduces, meaning that large volumes of precipitation cannot be stored any more. Normally, high fractions of snow-covered area ensure low runoff conditions during winter, but with a decreasing amount of snow storage, low runoff conditions cannot be sustained any more. Eventually the combination of shorter snowpack durations, higher direct runoff fractions, and declining snow-covered areas will result in runoff increases during winter/spring period.

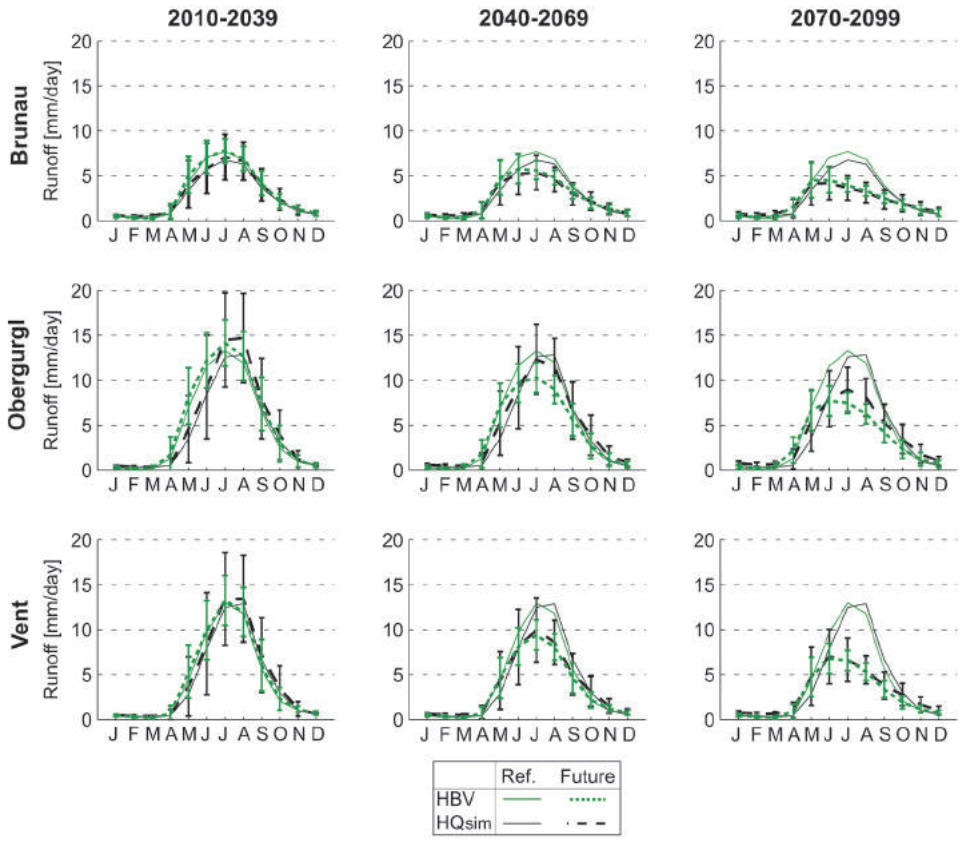

Figure 3.5. Mean monthly runoff (mm d^{-1}) for reference and future periods. The error bars, which have been plotted for the future periods represent the variability (±σ) of the mean monthly runoff that has been projected by the hydrological models.

In the mid and far future, the earlier onset of snowmelt, lower fractions of solid precipitation, and a rise of the snowline are also likely to be the main drivers of runoff increases during winter/spring. For the summer runoff, reduction of glacial areas, a decrease in precipitation, and an increase in evapotranspiration are supposed to be the main drivers of decreases in runoff. The reason for the shift from summer runoff increases in the near future to summer runoff decreases in the mid and far future is likely to be that in the near future glacial thinning is the dominant melting process above glacial area reduction (Figure 3.3), which means runoff regimes do not change and no decreases in runoff appear (Casassa et al., 2009). In the mid and far future, glacial area reduction is projected to be more dominant, which means runoff regimes will shift and summer runoff will decrease.

3.4.3 Seasonality of annual flood peaks

The changes of the seasonality under future climate scenarios were investigated by analysing the occurrence date of annual maximum series (AMS). For this purpose, rose diagrams were used, where the monthly frequency of annual maximum flood peaks was depicted for reference simulations and future scenarios. Figure 3.6 shows that the annual peaks of the reference simulations (i.e. HBV, HQsim) occur in the same months. Under reference conditions annual flood peaks occur from May to August for river gauging station Brunau and from June to September for gauges Obergurgl and Vent. For the near future (2010-2039) the peak occurrence is similar to the reference simulation for the three investigated time series (Figure 3.6, 1st column). In the mid-future (2040-2069) flood peaks occur more often in early summer/late spring. The most pronounced changes are observed for the far future (2070-2099); under this scenario the modal month of flood (MMF) (i.e. the month with the largest number of events) shifts from July/August (i.e. reference simulation HBV and HQsim) to May for the station Brunau. For gauging station Obergurgl the variability of the occurrence date of annual flood peaks increases. For the station Vent the MMF shifts form July/August to June. Two general trends can be observed regarding the seasonality: (1) a shift of the MMF from July/August to May/June and (2) an increased variability of the occurrence date of the annual flood peaks.

3.4.4 Low flow

Since summer runoff is expected to decrease in all catchments in the mid and far future, it is likely that future low-flow frequency will increase at the same time. To investigate whether future low-flow frequencies will increase or not, Flow Duration Curves (FDCs) (Figure 3.7) were estimated from observed summer runoff and the simulated summer runoff of the mid and far future simulations of HBV and HQsim. For the FDCs, the 70- (Q_{70}) and 95-percentile (Q_{95}) thresholds were used to analyse future low-flow frequencies. These thresholds represent low-flow indices, which have a common use in investigations to the low flow characteristics of perennial streams (WMO, 2008). For the catchments in this study the Q_{70} (Q_{95}) thresholds were approximately estimated as 5.9 (3.5) mm d^{-1} for Brunau, 9.8 (4.4) mm d^{-1} for Obergurgl, and 8.0 (3.2) mm d^{-1} for Vent.

The Q_{70} and Q_{95} thresholds FDCs at Brunau show that low flow conditions will become more frequent in the mid and far future. An exception is, however, the mid-future simulation of HBV with Q_{95} as reference. The FDC of this simulation indicates that low flow conditions will become less frequent. For the more glacierized catchments of Obergurgl and Vent, the same trend of less frequent low flow conditions is projected for the mid and far future simulations of HBV and HQsim, using Q_{95} as reference. However, the mid-future HQsim simulation for Obergurgl shows

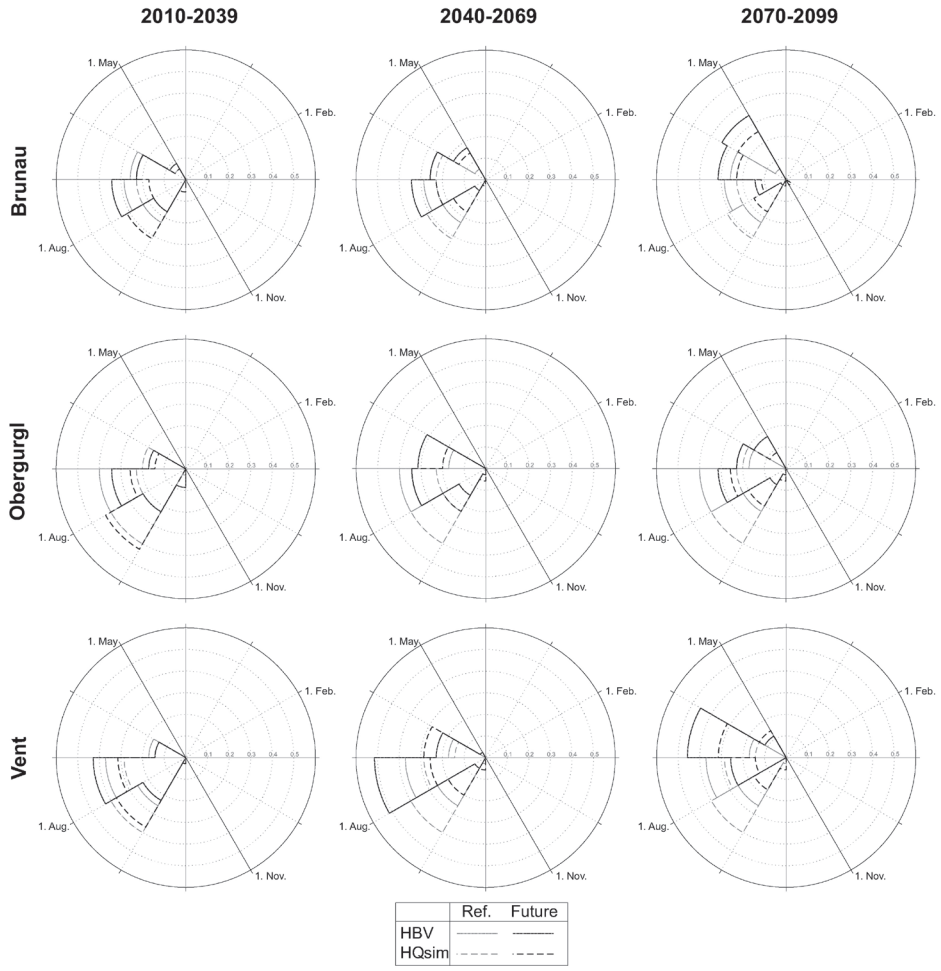

Figure 3.6. Rose diagram of AMS considering the reference simulations (grey lines) and climate change scenarios (black lines) simulated with two different hydrological models. The rows represent three gauging stations and the column represents the future climate change.

no change in the low-flow regime. Likewise, using Q_{70} as reference, there will be no change either. All other mid and far future simulations indicate an increase in low-flow frequency. The increase and decrease in low-flow frequencies for Q_{70} and Q_{95}, respectively, is likely to be caused by the influence of the remaining part of glaciers in the catchments of Obergurgl and Vent. Although the expectation is that glacier retreat will lead to an increase in low-flow frequency, the remaining part of glaciers still might function as a buffer for the low flow extremes (i.e. Q_{95}). Since the influence of glaciers is higher in the catchments of Obergurgl and Vent, it may explain why, for the Q_{95} threshold, low-flow frequency decreases in Obergurgl and Vent and increases in Brunau.

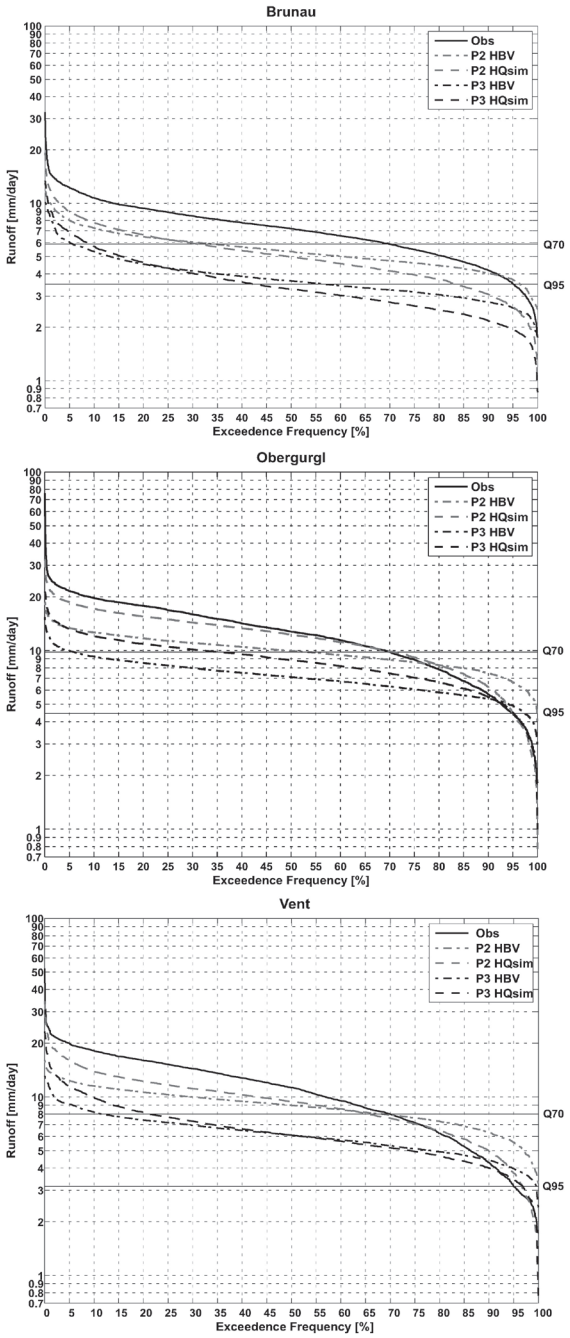

Figure 3.7. FDCs of the period June-August for Brunau, Obergurgl, and Vent. Abbreviations: P2 = 2040-2069, and P3 = 2070-2099.

3.5 Discussion

Two conceptual semi-distributed hydrological models, HBV and HQsim, were used to investigate the hydrologic response to future climate change. According to several studies (e.g. Eregno et al., 2013; Jiang et al., 2007) it is desirable to use more than one hydrological model to investigate the hydrological impact of future climate change since large differences may exist between the outcomes of different hydrological models. In this study, small differences between the outcomes of HBV and HQsim are found. Future runoff changes and changes in low flow conditions are predicted similarly, although some small differences exist in the runoff and low flow projections (i.e. flow duration curves) of Obergurgl (Figure 3.5 and 3.7). Likewise, HQsim projects greater runoff variability for Brunau, Obergurgl, and Vent than HBV. Finally, differences between the HBV- and HQsim-projected changes of the seasonality of annual flood peaks (Figure 3.6) are found. Whereas the shift of the MMF and the variability in the occurrence date of annual flood peaks are predicted similarly, differences exist in the occurrence of the MMF and the monthly frequency of annual flood peaks. Since both models have been forced by the same input data (with exception of the soil maps), climate change projections, and glacier change projections, it is likely that the structural differences between HBV and HQsim are one of the main factors responsible for the variation between the outcomes of these models.

The outcomes of this study are generally in agreement with the outcomes of similar studies conducted in the Ötztal and European Alps. For instance, Tecklenburg et al. (2012) showed a similar trend for the Ötztaler Ache catchment with runoff increases in winter and spring, and runoff decreases in summer until 2099. It should be, however, mentioned that these outcomes were obtained under the assumption of complete loss of glaciers where in this study a loss of about 80 to 90% is projected for the end of the 21st century. In the same region, similar but slightly different results were obtained by Weber et al. (2010). They projected annual runoff increases for the period 2011-2020 and annual runoff decreases for the periods 2031-2040 and 2051-2060, while in this study annual runoff increases and decreases were generally projected for the periods 2010-2039 and 2040-2069, respectively. The main explanation for the differences between the outcomes is probably that in the study of Weber et al. (2010) a higher loss of glaciers has been projected for the first decades, resulting in an earlier appearance of annual runoff decreases towards the future.

Similar outcomes were also reported in other parts of the European Alps. For instance, Huss et al. (2014) projected for a catchment in the Swiss Alps annual runoff changes between -53% and +50% and August runoff changes between -89 and +22% for 2075. The outcomes of this study show comparable results with a projected 10-34% annual runoff decrease and a projected 36-53% runoff decrease in August for the period 2070-2099. Similar results were also obtained from another study implemented in the Swiss Alps (Addor et al., 2014) with lower summer flows, higher winter flows, and an earlier spring-summer peak discharge. The main difference is that in this study additional processes have been identified to drive these changes: lower summer flows are driven by both glacial area reduction and a decrease in summer precipitation, instead of a decrease in summer precipitation alone. Also, in this study higher winter flows are driven by a combination of decreases in glacial and snow storage, lower fractions of solid to total precipitation, and shorter snowpack durations. Previous studies attributed this mainly to lower fractions of solid to total precipitation. The projected changes in seasonality of annual flood peaks are comparable with outcomes of several

other studies (Farinotti et al., 2012; Schneeberger et al., 2015), whereas outcomes related to low flow characteristics are deemed to be less reliable (see hereafter).

Despite the overall agreements with outcomes of other studies, still outcomes should be treated with care since the outcomes of this study are subject to several uncertainties that are accompanied by input data, climate projections, glacier change projections, and hydrological modelling. These uncertainties can be subdivided into two classes: aleatory and epistemic uncertainties. Aleatory uncertainties are the result of inherent variability related to variables such as temperature and precipitation (NRC, 2000). Epistemic uncertainties are the result of incomplete knowledge due to model uncertainties and parameter uncertainties (Apel et al., 2004; Neuhold, 2010).

Input data, such as daily precipitation and potential evapotranspiration, are mainly dominated by parameter uncertainties resulting from scarcity of data, measurement errors and parameter estimation methods. For instance, potential evapotranspiration has been estimated according to the temperature-based 'Hamon' approach, meaning that only variables such as daily temperature were used to estimate potential evapotranspiration. Since potential evapotranspiration highly depend on wind speed, global radiation, and relative humidity either it would mean that potential evapotranspiration is overestimated on cloudy and humid days, and is underestimated on windy days (Allen et al., 1998). Parameter uncertainties dominate also the parameterizations of the hydrological models HBV and HQsim. Since both models have been calibrated manually, parameters can be over-parameterized or inter-correlation can appear between parameters (Seibert, 1997). Likewise, more than one parameter set can result in a good model performance, which complicates finding a unique parameter set.

Climate projections, glacier change projections and the hydrological modelling approaches are mainly associated with model uncertainties. For climate projections, these uncertainties emerge from downscaling, accuracy and the resolution of GCM and RCM outputs (Immerzeel et al., 2012b). In addition, the delta change approach lacks in the representation of future changes to hydrological extreme events since the climate variability of the future climate scenarios rests on the climate variability of the present climate (Graham et al., 2007). This implies that for instance the number of wet and dry days does not change for the future climate scenarios, which produces an uncertainty in the outcomes related to the seasonality of annual flood peaks, and especially low flow characteristics. Since the outcomes related to low flow characteristics are more difficult to compare due to limited amount of studies investigating this topic, the conjecture is that these outcomes are deemed to be less reliable.

Glacier change projections are mainly associated with model uncertainties that emerge from the simplified model assumptions used to model glacier changes. The modelling approach used for simulating glacier changes lacks for instance the possibility to assimilate simulated accumulation and ablation. Simplified model assumptions are also the main factor with regards to model uncertainties related to hydrological modelling approaches as well. For instance, both HBV and HQsim use simplified temperature-index approaches in which degree-day factors are assumed to remain constant over time. Nevertheless, degree-day factors vary in space and time (Hock, 2005), which means uncertainties exist in relation with the ice- and snowmelt simulated by both models. To account for the temporal variability in degree-day factors one may consider the use of physically based approaches including energy balance components to get a more sophisticated view on melt

processes. Disadvantage is, however, that physically based approaches require more meteorological input variables (i.e., temperature, precipitation, incoming solar radiation, wind speed, and humidity, among others) than simplified temperature-index models (Jost et al., 2012). In addition, it is also found that simplified temperature-index models often outperform physically based energy-balance approaches on catchment scale (Hock, 2003), which is another reason one may use simplified temperature-index approaches.

3.6 Conclusions and outlook

The aim of this study was to investigate how glacierized catchments in the Ötztal Alps (Austria) will respond hydrologically to future climate change. Two conceptual semi-distributed hydrological models with different degrees of complexity were applied and forced using a combination of future climate simulations and outputs from a glacier change model. The outcomes of the models were analysed in terms of absolute and relative changes in mean runoff and runoff seasonality. Furthermore, the change of occurrence time of annual flood peaks was analysed as well as the change in low-flow frequency.

The outcomes indicate that in all catchments, the prevailing glacial melt dominated runoff regimes will shift to (more) snowmelt dominated runoff regimes towards the far future with the highest runoff occurring in May/June. These shifts are accompanied by relative spring runoff increases up to 132% in Brunau, up to 249% in Obergurgl, and up to 186% in Vent, and relative summer runoff decreases up to 51% in Brunau, up to 46% in Obergurgl, and up to 53% in Vent. Relative winter/spring runoff increases are likely to be caused by a combination of an earlier onset of snowmelt, a lower fraction of solid to total precipitation, and a rise of the snowline. Relative summer runoff decreases are likely to be caused by a combination of glacial area and volume reduction, a decrease in precipitation, and an increase in evapotranspiration.

Accompanied by future runoff changes, annual flood peaks are expected to become less frequent in July-August and to become more frequent in May (Brunau/Obergurgl) and June (Obergurgl/Vent). Low flow conditions are generally expected to become more frequent in Brunau in the mid and far future. In the glacierized catchments of Obergurgl and Vent low flow conditions are generally expected to become less frequent with regards to the Q_{95} threshold and to become more frequent with regards to the Q_{70} threshold.

Minor differences between the outcomes of the two hydrological models are found, which are mainly attributed to the structural differences between the two models.

The outcomes of this study aimed to contribute to a better understanding of how glacierized catchments respond hydrologically to future climate change. The outcomes might contribute to the development of adaptation strategies with respect to CCA and IWRM. Although the outcomes are sufficiently reliable to extract main trends, the outcomes are still subject to a lot of uncertainties. Therefore improvements are needed in future research to the impact of climate change on the hydrology of glacierized catchments.

Acknowledgements

Parts of this study were funded by the project StartClim2013.C (StartClim2013, BOKU). I would like to thank the Leonardo da Vinci programme (EU Lifelong Learning Programme) for funding my research fellowship at alpS Centre for Climate Change Adaptation. The provision of meteorological and discharge data by the Zentralanstalt für Meteorologie und Geodynamik (ZAMG), the Tiroler Wasserkraft AG (TIWAG AG), the Hydrographical Service Tyrol, and the Commission of Glaciology, Bavarian Academy of Sciences are greatfully acknowledged. I acknowledge Matthias Huss, University of Fribourg, Switzerland for his cooperation in developing initial ice thickness distributions for glaciers in the Ötztal. I also acknowledge Herbert Formayer, University of Natural Resources and Life Sciences, Vienna, Austria for his cooperation in the computation of climate data. Kristian Förster, Christian Georges (both alpS GmbH), and Walter Immerzeel (Utrecht University) are gratefully acknowledged for the helpful discussions and comments.

4 The impacts of climate change on hydrological extremes in upstream mountainous domains

Future hydrological extremes, such as floods and droughts, may pose serious threats for the livelihoods in the upstream domains of the Indus, Ganges, Brahmaputra. For this reason, the impacts of climate change on future hydrological extremes is investigated in these river basins. We use a fully-distributed cryospheric-hydrological model to simulate current and future hydrological fluxes, and force the model with an ensemble of eight downscaled general circulation models (GCMs) that are selected from the RCP4.5 and RCP8.5 scenarios. The model is calibrated on observed daily discharge and geodetic mass balances. The climate forcing and the outputs of the hydrological model are used to evaluate future changes in climatic extremes, and hydrological extremes by focusing on high and low flows. The outcomes show an increase in the magnitude of climatic means and extremes towards the end of the 21st century where climatic extremes tend to increase stronger than climatic means. Future mean discharge and high flow conditions will very likely increase. These increases might mainly be the result of increasing precipitation extremes. To some extent temperature extremes might also contribute to increasing discharge extremes, although this is highly dependent on magnitude of change in temperature extremes. Low flow conditions may occur less frequently, although the uncertainties in low flow projections can be high. The results of this study may contribute to improved understanding of the implications of climate change for the occurrence of future hydrological extremes in the Hindu Kush-Himalayan region.

Based on: *Wijngaard, R.R., Lutz, A.F., Nepal, S., Khanal, S., Pradhananga, S., Shrestha, A.B., and Immerzeel, W.W. 2017. Future changes in hydro-climatic extremes in the Upper Indus, Ganges, and Brahmaputra River basins. PLoS ONE 12(12). DOI: 10.1371/journal.pone.0190224*

4.1 Introduction

The Hindu Kush-Himalayan (HKH) region plays a crucial role in the South Asian hydrology (Nepal, 2016; World Bank, 2013). It encompasses the headwaters of the Indus, Ganges and Brahmaputra (IGB), and supports the livelihoods of about 700 million people living in these basins (Eriksson et al., 2009; Shrestha et al., 2015). It sustains the seasonal water availability by means of meltwater originating from upstream ice and snow reserves and it supplies water that is utilized for agriculture (e.g. irrigation), energy production (e.g. hydropower), industry, shipping, and drinking water supply (Immerzeel et al., 2010; Mirza et al., 2003; Nepal and Shrestha, 2015; Viviroli et al., 2011). There is a growing concern that the hydrology in the IGB might be affected by future climate change. In the last few decades, several studies (Nepal, 2016; Nepal and Shrestha, 2015; Viviroli et al., 2011) have outlined that future climate change will affect the hydrological regimes in the IGB.

<< A house destroyed by flash floods that occured in Uttarakhand, India in 2012 (European Commision ECHO).

It is likely that rising temperatures and precipitation changes will affect glacier volumes, seasonal snow cover, and runoff characteristics, and thus the water availability in both up- and downstream parts of the IGB (Bolch et al., 2012; Lutz et al., 2014; Viste and Sorteberg, 2015). Likewise, it is expected that the frequency and magnitude of extreme hydrological events (i.e. the occurrence of floods and droughts) will rise, posing serious threats for the livelihoods of people living in the IGB (Hirabayashi et al., 2013; Lutz et al., 2016a; Mirza, 2011).

Many studies have documented evidences of historic climate change in the IGB. Among the observed trends in climatic variables, the increasing temperature trend is most consistent over the region. For instance, in parts of the upper Ganges Basin (Nepal) temperature have increased at a rate of 0.06 °C yr^{-1} between 1978 and 1994, with higher rates at higher elevations (Shrestha et al., 2000). In the upper Brahmaputra Basin, the average annual temperature has increased at a rate of 0.03 °C yr^{-1} between 1961 and 2005 (Flügel et al., 2008), whereas in the upper Indus Basin, both, increasing and decreasing temperature trends have been observed since the 1960s. Thereby, the decreasing temperature trends were attributed to the decline in mean summer temperature (Fowler and Archer, 2006). Precipitation trends that have been reported in the HKH region show mixed signals with increasing precipitation trends in the western part of the HKH (Archer and Fowler, 2004; Eriksson et al., 2009), and no distinct trends in other parts of the HKH (Immerzeel, 2008; Nepal, 2016; Shrestha et al., 2000).

Future climate change will likely be associated with a continued warming over the 21st century. Temperature increases between 1.7 °C and 6.3 °C are projected towards the end of the 21st century in the IGB, where elevation-dependent warming will likely result in stronger temperature increases in the mountainous regions of the HKH than in the adjacent lowland regions (Lutz et al., 2016b; MRI, 2015; Palazzi et al., 2016) as observed in the historical temperature trends (Shrestha et al., 2000). Based on the projected increases, accelerated melt rates can be expected until the mid of the 21st century, thereby affecting stream flow. In the second half of the 21st century melt water rates are projected to decline in the HKH. Stream flow is, however, still projected to increase by then, which can mostly be attributed to increases in precipitation (Immerzeel et al., 2013).

In general, future precipitation is projected to increase in the upstream basins of the IGB (Akhtar et al., 2008; Forsythe et al., 2014; Immerzeel, 2008; Lutz et al., 2014; Palazzi et al., 2015; Rajbhandari et al., 2014). In addition, there are also parts of the HKH region (e.g. the north-western part of the upstream Indus basin) where precipitation is projected to decrease (Lutz et al., 2016a). The confidence in future precipitation projections is, however, low due to the large spread in future projections and the model's limitations to simulate complex mountainous climates of South and Central Asia (Lutz et al., 2016b; Seneviratne et al., 2012). Based on the projected precipitation changes, it is likely that both droughts and floods will occur more frequently into the future. According to a previously published report (World Bank, 2013) it is likely that droughts will occur more often in the Indus basin, thereby having consequences for the food production. The projected precipitation increases are likely to result in higher peak flows and associated risks for flood hazards. The Pakistan floods of July-September 2010, caused by intense monsoonal rainstorms that penetrated unusually far in the Himalaya and the Karakoram (Houze et al., 2011), illustrate the devastating impact floods can have on a society. The floods resulted in about 1950 fatalities, an estimated overall loss of 9.5 billion US dollars, and affected about 20 million people (Munich RE, 2011; Webster et al., 2011; World Bank, 2013). Considering economic and population growth in the

flood-prone areas of the IGB (e.g. Bangladesh), losses and the number of fatalities could be even larger in the future (Mirza, 2011; Winsemius et al., 2015). The (potential) impacts of droughts and floods on the livelihoods in the IGB illustrate the vulnerability to hydrological extremes.

In recent years, many climate impact studies have so far mainly focussed on the impacts of climate change on hydrological regimes in, both, large and small river basins (Akhtar et al., 2008; Immerzeel et al., 2010, 2012b; Lutz et al., 2014; Masood et al., 2015; Nepal, 2016; Nepal et al., 2014). These studies have shown that future water availability will likely be sustained over the 21st century. Some studies have also indicated that hydrological extremes pose a larger threat. The problem is, however, that knowledge about future changes in hydrological extremes resulting from climate change is lacking in the IGB. Few studies have been conducted on the explicit effects of climate change on hydrological extremes in the IGB. For instance, a recent study, assessing the impacts of climate change on hydrological regimes and extremes in the upper Indus Basin, showed that, in general, summer peak flow will likely shift to other seasons, and projected an increase in the frequency and intensity of extreme discharge conditions (Lutz et al., 2016a). Another study projected increases in heavy precipitation indices during monsoon period, accompanied by extended periods of no precipitation during the winter months, in the Ganges basin (Mittal et al., 2014). Hence, the cited study (Mittal et al., 2014) indicated an increase in the incidence of extreme weather events over the first half of the 21st century. Studies performed on global flood risk show similar patterns (Hirabayashi et al., 2008, 2013; Pechlivanidis et al., 2016). Significant increasing trends in high flows (i.e. 10-percentile exceedance discharge) were found in the Ganges basin with relative increases up to about 100% (Pechlivanidis et al., 2016). Thereby, the changes in high flows were projected to be more significant than the changes in low flows (i.e. 90 percentile exceedance discharge). Assessments on future flood and drought frequencies in a number of basins spread across the world, including the IGB basins, found that, in the Ganges and Brahmaputra river basins, a future 100-year flood (i.e. equivalent to discharges with a 100-year return period in the 20th century (1901-2000)) will occur once in 26.1 years and 3.8 years, respectively, at the end of the 21st century (Hirabayashi et al., 2008). Furthermore, the average number of drought days were found to increase by a factor 1.17 and 4.05 in the Ganges, and Indus basins, respectively (Hirabayashi et al., 2008). Most of the studies regarding hydrological extremes have focussed on both up- and downstream parts of the IGB without considering the effects of climate change on hydrological processes that are relevant in mountainous basins, such as snow and ice melt. For this reason, an improved understanding is needed on the impact of climate change on these processes and their implications for the occurrence of hydrological extremes in mountainous basins.

The representation of future hydrological extremes is highly depending on the representation of climatic extremes in general circulation models (GCMs) that force the hydrological models. Previous studies (Sillmann et al., 2013b, 2013a) investigated the performance of GCMs from the Coupled Model Intercomparison Project 5 (CMIP5) in simulating climatic extremes. These studies show that the climate models are generally able to simulate climatic extremes and their trend patterns, and that the spread among different climate models for several temperature indices has reduced in comparison with CMIP3 models, despite the larger number of CMIP5 models. In addition, the representation of precipitation extremes has also improved. Nevertheless, there is still some discrepancy in the simulation of some precipitation indices. Further it is shown that the analysed CMIP5 models generally agree on the projected trends in temperature extremes. However, in some regions, such as South Asia, there is no consensus between GCMs on projected trends in

a few precipitation indices, such as consecutive dry days (CDD). Some of the models project an increase in CDD, whereas others project a decrease in CDD. Similar contradictive projections were also found for the Indus, Ganges, and Brahmaputra, whereas other indices were in line with projected trends in climate extremes, though the spread between the models can be large (Lutz et al., 2016b). The presence of discrepancies between GCMs emphasizes the importance of selecting climate models, based on the model's skill to simulate climatic extremes in regions of interest, for the assessment of hydrological extremes.

The main aim of this study is to investigate the impacts of climate change on future hydrological extremes in the upstream domains of the Indus, Ganges, and Brahmaputra basins. To this end, we apply a fully-distributed cryospheric-hydrological model. The model is forced with the outputs of eight GCMs (i.e. representing RCP4.5 and RCP8.5) that were pre-selected by using an advanced envelope-based selection approach (Lutz et al., 2016b). Subsequently, the outputs of the hydrological model are analysed on hydrological extremes by focusing on high and low flows. The novelty of this study in comparison with previous work in the region (e.g. Lutz et al., 2016a) is that it is first to investigate the full range of possible impacts of climate change (i.e. in terms of climate extremes) on the occurrence of both high and low flows in the upstream mountainous domains of the entire IGB. Most studies that have been conducted in the IGB only focused on the downstream parts of the IGB or in the entire IGB (Gain et al., 2011; Hirabayashi et al., 2013) and did not take processes into account that are relevant in mountainous basins (e.g. ice and snowmelt). In the upstream domains of the IGB, where mountain-hydrological processes are important, the number of studies on extremes is very limited. To our knowledge, a previous study conducted in the upstream Indus basin (Lutz et al., 2016a) is so far the only study on hydrological extremes at this scale, and taking mountain-hydrological processes into account. Nevertheless, the cited study (Lutz et al., 2016a) is only about high flows and does not take the effects of climate change on low flows into consideration. For this reason, our study contributes to an improved understanding of the effects of climate change on both high and low flows in the mountainous domains of the Indus, Ganges, and Brahmaputra.

4.2 Study area

Future changes in hydrological extremes are assessed for the upstream parts of three major river basins with origins in the Hindu Kush-Himalaya (HKH): the upper Indus Basin (UIB), the upper Ganges Basin (UGB), and the upper Brahmaputra Basin (UBB) (Figure 4.1). The upper basins are defined as the areas that extend from the sources of the Indus, Ganges and Brahmaputra to the northern margins of the Indo-Gangetic plains. The UIB, UGB, and UBB cover a surface area of about 399,000 km^2, 168,000 km^2, and 370,000 km^2, respectively, in the HKH mountain ranges. The altitude ranges from 8850 m above sea level (a.s.l.) in the UGB to about 100 m a.s.l. at the southern margins of the UBB. Glaciers cover a total surface area of about 21,000 km^2, 9,000 km^2, and 14,000 km^2 in the UIB, UGB, and UBB, respectively (Bajracharya and Shrestha, 2011).

The climate of the upstream domains of the IGB is dominated by the East Asian and Indian monsoon systems, and the Westerlies. The influence of the East Asian and Indian monsoon systems is generally largest in the eastern part of the Himalayas. In these regions most precipitation occurs during the period June-September (Figure 4.2d), and orographic effects result in a strong north-south gradient in precipitation intensities (Galewsky, 2009). More to the west, the westerlies become

increasingly important. In the Hindu Kush and Karakoram, precipitation is more equally divided over the year due to the influence of both the westerlies in the winter and the monsoon systems in the summer (Bookhagen and Burbank, 2010). In the Karakoram and at the western margins of the UIB most precipitation occurs during the winter period (Figure 4.2c). Annual precipitation sums in the entire IGB ranges from ~100 mm at the Tibetan Plateau to ~5500 mm at the southern margins of the UBB (Figure 4.2a). In the latter area, the precipitation extremes (i.e. 95th (P95) and 99th (P99) percentiles of daily precipitation sums) are also largest (Figure 4.2e and 4.2f). The annual average temperature is highest at the southern margins of the UGB with ~24 °C and lowest in the high-altitude regions of the Karakoram with ~-19 °C (Figure 4.2b).

The hydrological regimes that dominate in the IGB differs per region. In the UIB, a glacial melt dominated regime prevails with a glacier melt contribution of 40.6% to the total runoff (Lutz et al., 2014). In the UGB and UBB, rainfall dominated regimes prevail with a slightly higher contribution of snow- and glacier melt in the UBB (Lutz et al., 2014).

4.3 Data and methods

4.3.1 Cryospheric-hydrological modelling

We use the physically-based fully-distributed Spatial Processes in Hydrology (SPHY) cryospheric-hydrologic model (Terink et al., 2015) to simulate current and future daily discharge in the upstream

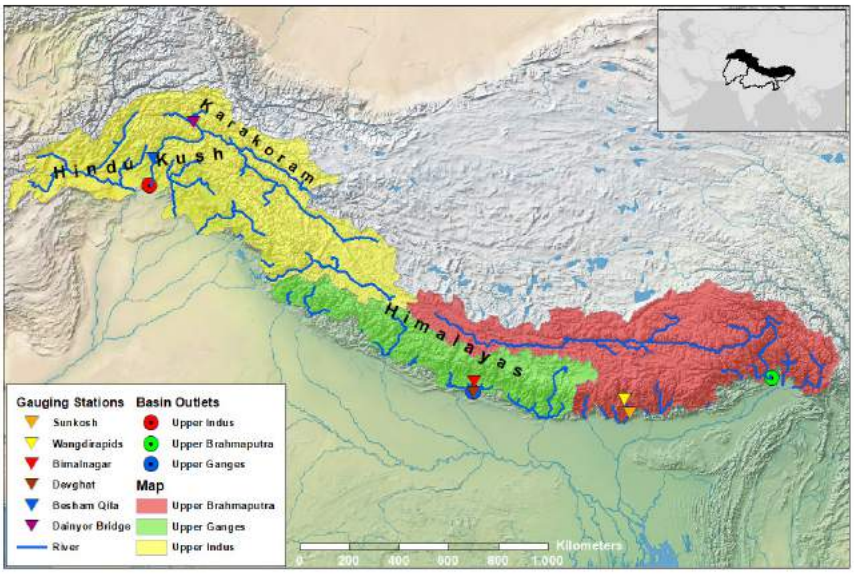

Figure 4.1. Map of the study area showing the outlets of the basins and the gauging stations used for calibration and validation of the model. Source of the background basemap imagery and the political borders displayed in the inlet of the figure is www.naturalearthdata.com.

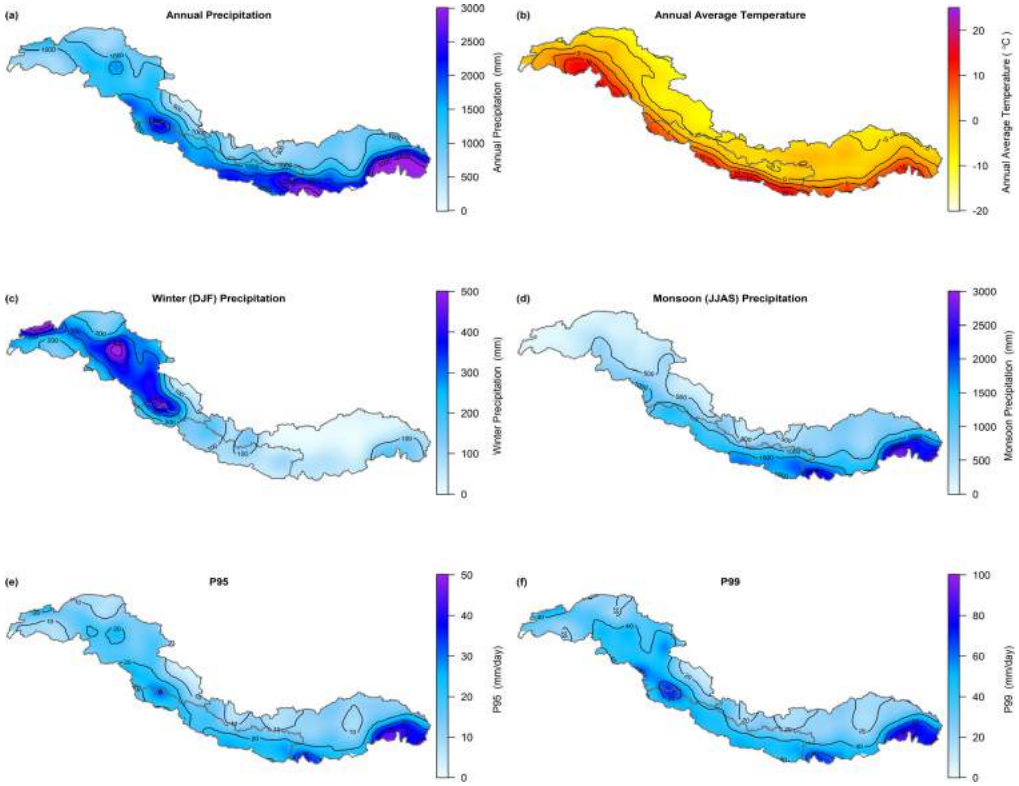

Figure 4.2. Maps of the upstream domains of the Indus, Ganges, and Brahmaputra showing the annual precipitation (a), the average air temperature (b), the winter precipitation (c), the monsoon precipitation (d), and the precipitation extremes (P95 (e) and P99 (f)) for the reference period. Abbreviations: DJF = December, January, February, JJAS = June, July, August, September, P95 = 95th percentile of daily precipitation sums, P99 = 99th percentile of daily precipitation sums. Source of the maps is a reference climate dataset (Lutz and Immerzeel, 2015).

domains of the Indus, Ganges, and Brahmaputra. The model is set up at a spatial resolution of 5 km x 5 km and reports on a daily time step.

Daily discharge is simulated by a) calculating total runoff for each grid cell, consisting of four different runoff components: glacier runoff, snow runoff, rainfall runoff (i.e. the sum of surface runoff and lateral flow), and baseflow, and b) routing the total runoff and its components downstream, using a simplified routing scheme that requires a digital elevation model (DEM) and a recession coefficient. The total runoff (Q_{TOT}) is calculated for each time step by:

$$\boldsymbol{Q_{TOT} = Q_{GM} + Q_{SM} + Q_{RR} + Q_{BF}} \quad \textbf{(4.1)}$$

where Q_{GM} (mm) is glacier runoff, Q_{SM} (mm) is snow runoff, Q_{RR} (mm) is rainfall runoff, and Q_{BF} (mm) is baseflow. For the estimation of the contribution of glacier runoff, sub-grid variability (i.e. on 1 km x 1 km resolution) is taken into account. The sub-grid variability is determined by

fractional ice cover where fractional ice cover ranges between 0 (no ice cover) and 1 (complete ice cover). In addition, a unique identifier is created for each glacier, or a part thereof, within a model cell. This unique identifier is used for the attribution of information, such as glacier mean elevation, initial ice-thickness, and the type of glacier (i.e. debris-free or debris-covered). Hence, the type of glacier is determined by the differentiation between debris-covered and debris-free glaciers, which is based on thresholds for slope and elevation (Paul et al., 2004). Initial ice thicknesses are estimated according to a methodology that has been described in previous studies (Immerzeel et al., 2012b, 2013). Glacier melt is calculated according to a degree-day approach (Hock, 2003), where different factors are applied to debris-free and debris-covered glaciers. The produced melt is subsequently subdivided over the surface runoff and baseflow pathways by a calibrated glacier runoff fraction.

To model future changes in the fractional glacier cover, the SPHY model is modified by improving the existing glacier module. In the former glacier module, glaciers were implemented as fixed masses, which could change over time using a parameterization for glacier changes at the large river basin scale (Lutz et al., 2013). This approach has no consideration of mass conservation and ice redistribution. In the improved glacier module, these processes are included. A more detailed description regarding the improved glacier module of the SPHY model has been published before (Terink et al., 2016).

For those parts of the cells that are not covered by glaciers, a dynamic snow storage is simulated according to a degree-day snow model (Kokkonen et al., 2006). The snow accumulation and-melt is simulated by a degree-day approach similar to the approach that is used to simulate glacier melt. Snow sublimation is estimated by a simple elevation-dependent potential sublimation function (Lutz et al., 2016a). This function assumes potential sublimation to increase linearly with elevation above 3000 m a.s.l. by a calibrated sublimation factor and presumes the majority of sublimation to originate from snowblown sublimation, thereby assuming that the highest wind speeds and driest air conditions prevail at the higher altitudes. The actual sublimation is limited by total snow storage within the grid cell. In addition to snow melt, accumulation, and sublimation, refreezing of snowmelt and rain are included as well. When snow cover is absent, rainfall runoff processes are simulated where a part of the rain is transported directly into the river network by surface runoff, and another part is transported to the network via lateral flow from the soil water storage or baseflow from the groundwater storage. For the simulation of soil water processes, processes as evapotranspiration, infiltration, and percolation are included. These processes are simulated for a topsoil and subsoil layer. A more detailed description of the SPHY model has been published before (Terink et al., 2015).

4.3.2 Datasets

As meteorological forcing, we use a dataset of daily air temperature and precipitation fields at 5 km x 5 km resolution developed for the Indus, Ganges and Brahmaputra river basins (Lutz and Immerzeel, 2015). This dataset is based on the Watch Forcing ERA-Interim (WFDEI) dataset (Weedon et al., 2014). The raw temperature data are spatially interpolated (i.e. by using a cubic spline interpolation) from a resolution of 0.5° x 0.5° to a resolution of 1 km x 1 km, and subsequently downscaled using a 1 x 1 km digital elevation model (DEM) and vertical monthly temperature lapse rates. The downscaled temperature data are bias-corrected to the observations of 40 meteorological stations located in the study area. The downscaled temperature data are bias-corrected to the observations of 40 meteorological stations located in the study area. To correct for

elevation differences, temperature values were lapsed from station elevation to grid cell elevation using a constant temperature lapse rate of -0.0065 °C m^{-1}. Long-term mean biases between the gridded product and station data at the station's locations were interpolated spatially to generate a spatial correction grid, which was applied to the uncorrected temperature fields. In addition, a temperature bias-correction is conducted, by capping the average annual glacier ablation to a maximum plausible value (Immerzeel et al., 2012b; Ragettli et al., 2015), to avoid unrealistic high temperatures at high altitudes. The raw precipitation data are spatially interpolated by means of a cubic spline interpolation too, and are subsequently corrected by using geodetic mass balances as a proxy to reconstruct precipitation amounts (Immerzeel et al., 2015). Finally, the corrected 1 km x 1 km temperature and precipitation datasets are resampled to a resolution of 5 km x 5 km (i.e. the model resolution).

High-altitude precipitation is often highly uncertain, due to lacking high-altitude observations and the insufficiency of gridded precipitation products, such as ERA-Interim (Dee et al., 2011) and APHRODITE (Yatagai et al., 2012), in capturing the spatial variation and magnitude of high-mountain precipitation (Immerzeel et al., 2015). This is mainly caused by the poor coverage of precipitation gauging stations and limited detection of snow, which eventually results in significant underestimation of precipitation (Palazzi et al., 2013, 2015). For example, previous work (Immerzeel et al., 2015) showed by reconstructing required precipitation amounts to sustain observed glacier mass balance and observed discharge that precipitation in the upper Indus Basin is underestimated by ~200% in regularly used precipitation products, and that locally even ten times the amount of precipitation reported in gridded products would be more realistic. For this reason, spatial precipitation fields usually need correction for the simulation of reliable water balance components. Earlier validation of precipitation fields to observed discharge and estimates of actual evapotranspiration at several gauging stations (Lutz and Immerzeel, 2015) indicates that precipitation corrections are necessary due to the underestimation of precipitation at most gauging stations. To this end, a precipitation correction factor (i.e. 1.3 in the upstream domains of the IGB, with exception of the Tarbela basin (upstream of Besham Qila) where a factor of 0.85 is used) is applied, which is estimated as the relative difference between observed discharge and simulated discharge resulting from initial model runs with SPHY. The precipitation corrections are applied to the elevation zone between 4500 m a.s.l. and 5500 m a.s.l., which covers the steepest part of the hypsometry in the upstream domains of the IGB, and where the precipitation bias is largest (Immerzeel et al., 2012a, 2015). Below 2000 m a.s.l. and above 7000 m a.s.l. no correction is applied. In other elevation zones, linear relations between elevation and correction factors are used to estimate the magnitude of the correction factor.

The meteorological data required for the bias-correction of the temperature datasets are obtained from 40 meteorological stations that are acquired through Nepal Department of Hydrology and Meteorology (DHM), the Pakistan Meteorological Department (PMD), and the Pakistan Water and Power Development Authority (WAPDA). Time series of observed daily discharge from 6 gauging stations are provided by the Bhutan Department of Hydro Met Services (BDHMS), WAPDA, and DHM.

As DEM, we use the 15 arcsec HydroSHEDS DEM (Lehner et al., 2008), which is a void-filled and hydrologically conditioned DEM based on the SRTM DEM (Farr et al., 2007). The digital elevation model is resampled to 5 km x 5 km resolution. Land use information is extracted from the MERIS

Globcover product (Defourny et al., 2007) and soil information is derived from HiHydroSoil (de Boer, 2016), which is a high-resolution soil map of hydraulic properties. This map has been derived from the Harmonized World Soil Database (FAO/IIASA/ISRIC/ISSCAS/JRC, 2012) using pedotransfer functions. Glacier outlines are derived from the Randolph Glacier Inventory v5.0 (Pfeffer et al., 2014) and are recalculated to a fractional ice cover on a 1 km x 1 km grid. MODIS snow cover data (Hall et al., 2002; Hall and Riggs, 2015), IceSat-derived zonal glacier mass balances (Kääb et al., 2012), and discharge time series are used for the model calibration.

4.3.3 Calibration and validation

The calibration and validation of the SPHY model is performed by using a two-step systematic approach to minimize equifinality problems (e.g. Pellicciotti et al., 2012), which are a common problem in the simulation of high-mountain hydrology. Because of the common underestimate of high-mountain precipitation in meteorological forcing products, the water deficit is often compensated by unrealistic high ice melt rates to compensate for this, when calibrated to observed discharge. We followed two steps by first calibrating the snow and glacier parameters to observed snow cover and glacier mass balances, to ensure realistic parameter values for the model parameters related to cryospheric processes. Secondly, we calibrated the rainfall-runoff parameters to observed discharge. After the calibration of all parameters the model is validated to observed discharge. Plausible parameters ranges, used for the calibration of the parameters, are based on a previous report (Lutz et al., 2014) and a local One-At-A-Time (OAT) sensitivity analysis (Pianosi et al., 2016) that is conducted prior to the calibration. The parameter ranges are summarized in Table 4.1.

The parameters related to glacier melt, snow accumulation, and-melt (*DDFG, DDFDG, Tcrit, SnowSc, DDFS*, and *Subl3Rate*, Table 4.1) are calibrated manually on catchment-averaged glacier mass balances derived from the IceSat dataset (Kääb et al., 2012) for three upstream catchments: Hunza (Dainyor Bridge, UIB), Marshyangdi (Bimalnagar, UGB), and Sunkosh River (Wangdirapids, UBB). The IceSat dataset covers a 5-year period with an observation at the start of the period (i.e. October 2003) and an observation at the end of the period (i.e. September 2008). For the optimization of glacier and snow parameters, the model is run from October 2003 till September 2008, which is coinciding with the period that IceSat mass balances are available. The glacier mass balances resulting from the model runs are obtained by dividing the change in reported ice volumes over the entire run period 2003-2008 by the reported initial glacier area. Subsequently, a zonal average of the glacier mass balance is calculated for each upstream catchment, which is then used for calibration on the observed glacier mass balances. In addition to the calibration on glacier mass balances, simulated snow cover is compared with observed MODIS snow cover, which is derived from the MOD10CM dataset (Hall et al., 2002; Hall and Riggs, 2015). This comparison is performed on a monthly time step for the period March 2000-December 2010, which is based on MODIS data availability. For each month, zonal averages are calculated of the MODIS snow cover imagery and the SPHY model snow cover output for each upstream catchment. Subsequently, the SPHY simulated snow cover is compared with the MODIS observed snow cover, and differences between the observed and simulated snow cover are minimized. The comparison between observed and simulated snow cover is needed for the optimization of the parameters related to snow accumulation and-melt. By obtaining the most optimal agreement between observed and simulated values for IceSat-derived glacier mass balances and MODIS-derived snow cover, snow parameters can be optimized.

After calibration of snow and glacier parameters, the parameters related to baseflow, lateral flow, and routing (*alphaGw, deltaGw, kx, GlacF, Rootdepth*, and *Subdepth*, Table 4.1) are calibrated. Per basin, the simulated discharge is calibrated on time series of observed daily discharge from an up- and downstream gauging station. The following stations are used: Dainyor Bridge (Hunza, upstream UIB), Besham Qila (downstream UIB), Bimalnagar (Marshyangdi, upstream UGB), Devghat (downstream UGB), Wangdirapids (Sunkosh River, upstream UBB), and Sunkosh (downstream UBB) (Figure 4.1). These gauging stations are selected based on data availability, and to have a representation of each of the upstream and downstream locations in each of the three river basins. The model is calibrated for the periods 2000-2005 (UIB and UGB), and 1998-2003 (UBB). The calibration and validation periods are selected based on the data availability in both the up- and downstream gauging stations. To optimize the performance of the model, the calibrated snow and glacier parameters are used to simulate snow storage over a 10-year period. The reported snow storage at the end of the 10-year period is subsequently used as initial snow storage in the calibration runs. In addition, a spin-up period of 3 years is used to initialize model states, such as soil moisture, snow storage, and groundwater. The model is calibrated using a random sampling technique with 50 different parameter combinations. From these combinations, the set is selected with the best performance, and corrected manually afterwards to optimize the model's performance. After calibrating the model for the three upstream domains, the model is validated independently on different periods: 2008-2010 (UIB, Dainyor Bridge), 2006-2008 (UIB, Besham Qila), 2007-2009 (UGB), 2004-2008 (UBB).

4.3.4 Future climate forcing

To account for the uncertainty in future climate change, an ensemble of downscaled General Circulation Model (GCM) runs is used to force the cryospheric-hydrological model. We select model runs from the medium stabilization scenario RCP4.5 and the very high baseline emission scenario RCP8.5 (van Vuuren et al., 2011) to represent a wide range of possible futures. We did not include the mitigation scenario leading to a very low radiative forcing level (RCP2.6) as it is unlikely

Table 4.1. Parameters and their ranges used for the calibration.

Parameters	Description	Units	Range
Glacier			
DDFG	Degree-day factor debris-free glaciers	mm $°C^{-1}$ d^{-1}	3-9
DDFDG	Degree-day factor debris-covered glaciers	mm $°C^{-1}$ d^{-1}	1-7
Snow			
Tcrit	Critical temperature	°C	-3-3
SnowSc	Water storage capacity of snow pack	mm mm^{-1}	0-1
DDFS	Degree-day factor snow	mm $°C^{-1}$ day^{-1}	3-9
Subl3Rate	Sublimation rate	mm d^{-1}	0-10
Rainfall-Runoff			
alphaGw	Baseflow recession coefficient	-	0.001- 0.2
deltaGw	Groundwater recharge delay time	d	1-180
kx	Routing recession constant	-	0.01-0.99
GlacF	Glacier melt runoff factor	-	0-1
Rootdepth	Thickness of root zone	mm	50-1000
Subdepth	Thickness of subsoil	mm	300-3000

that this RCP can be met (Arora et al., 2011; Raftery et al., 2017; Rosenberg et al., 2015). To meet RCP2.6 a drastic decline in carbon emissions is required, followed by ongoing carbon sequestration in the second half of the 21st century (Arora et al., 2011). It is, however, expected that the median of future cumulative carbon emissions will lie between RCP4.5 and RCP6.0 under current emission mitigation policies (Raftery et al., 2017). Moreover, future emissions from existing carbon-intensive industrial and energy capital are expected to remain large, limiting transformations to new capital that emits less carbon (Rosenberg et al., 2015). To aim for realistic projections, we therefore choose not to include RCP2.6 in the climate model ensemble. From the CMIP5 multi-model ensemble (Taylor et al., 2012), we select four GCM runs for RCP4.5 and four GCM runs for RCP8.5 (Lutz et al., 2016b) (Table 4.5). The GCM runs are selected in such way that they represent the full CMIP5 ensembles in terms of the projected ranges in means of future air temperature and precipitation, extremes of temperature and precipitation, and have sufficient skill over our region of interest (Lutz et al., 2016b).

The selected climate models (Table 4.5) are downscaled using the reference climate dataset, by applying the robust and well established quantile mapping methodology (Piani et al., 2010; Themeßl et al., 2011), which has been proven to perform well over mountainous regions (Immerzeel et al., 2013; Themeßl et al., 2011). We construct empirical cumulative density distributions (ecdfs) for each month of the year, at 5 km x 5 km grid cells, from the daily values of the reference climate dataset and historical GCM runs for 1981-2010. These ecdfs are used to downscale and bias-correct future GCM runs spanning 2011-2100 at daily time step. We include frequency adaptation and the construction of new extremes. A detailed description of this approach has been published before (Themeßl et al., 2011). In this way, transient hydrological model forcing series from 2011 until 2100 at 5 km x 5 km spatial resolution and daily time step are constructed for each of the selected GCM runs.

4.3.5 Analysis of climatic and hydrological extremes

We use the climate forcing and the outcomes of current and future model runs to analyze future changes in climatic and hydrological extremes. Changes in climatic extremes are evaluated for air temperature and precipitation by considering changes in several climatic indices. To characterize changes in air temperature (extremes) we analyze changes in the mean temperature and the warm spell days index (WSFI, hereafter HWFI) as defined by the European Climate Assessment Project (ECA)(van Engelen et al., 2008), which is the number of days in intervals of at least 6 days that the daily mean temperature is higher than the 90th percentile of daily mean temperatures over a defined period. To characterize changes in precipitation (extremes) we analyze changes in the mean (annual) precipitation sum, the 95th (P95) and 99th (P99) percentiles of daily precipitation sums over a defined period, and the absolute maximum 5-day precipitation amount (RX5day) (van Engelen et al., 2008).

Changes in hydrological extremes are evaluated by focusing on high and low-flow indices. For high flow, we analyze future changes in 99th percentile of daily discharge levels, and the discharge levels of high flow events with a return period of 5, 25, and 50 years. The 5, 25, and 50-year return levels are calculated by determining the annual maximum flows, plotting the annual maximum flows by means of Gumbel plots (Gumbel, 1941), and calculating the discharge levels corresponding with events that occur once in 5, 25, and 50 years. In addition, we investigate future changes in annual maximum series (AMS) for the outlets of a rainfall-dominated basin (Brahmaputra) and a glacier/

snowmelt dominated upstream basin (Hunza). Changes in the occurrence of low flows are analyzed by using flow duration curves (FDCs). To analyze these changes, we focus on the area between the 70 and 95 percentile exceedance discharge levels, which have a common use in the analysis of low-flow frequencies (Wijngaard et al., 2016; WMO, 2008).

4.4 Results and discussion

4.4.1 Calibration and validation

The calibration and validation of the SPHY model is performed by using a two-step systematic approach. The simulated mean snow cover and glacier mass balances resulting from the first calibration step are summarized in Table 4.2. The simulated glacier mass balances match well with the observed glacier mass balances in all basins. Nevertheless, the mean snow cover is overestimated with 19-28%, where the largest overestimations occur in the Sunkosh basin. The overestimations in the snow cover may be attributed to the presence of cold biases in the temperature forcing, and to the fact that processes such as avalanching and snow re-distribution by wind were not considered in the model. This eventually may result in excessive accumulations of snow, and thus in the systematic overestimation of snow cover.

The best performing parameter sets resulting from the entire calibration approach are given in Table 4.3. Most calibrated snow and glacier parameters fall well within the range of those derived in other studies (Lutz et al., 2014, 2016a; Shea et al., 2015; Zhang et al., 2006). The calibrated snow parameter set in the UGB differs, however, from most calibrated values. For instance, the snow degree-day factor of 7.5 mm $°C^{-1}$ d^{-1} is slightly higher than the range of 3-6 mm $°C^{-1}$ d^{-1} that was found in other studies (e.g. Hock, 2003). Furthermore, the water storage capacity of the snow pack is lower than those that were found in previous work (Lutz et al., 2014, 2016a). Only using these values, it was feasible to simulate a glacier mass balance similar to the IceSat observations. Lower snow degree-day factors would have resulted in positive glacier mass balances, which can likely be attributed to cold biases in the temperature forcing. Besides snow and glacier parameters, the calibrated rainfall-runoff parameters fall also in range of those reported in other studies (Immerzeel et al., 2012b; Lutz et al., 2014, 2016a).

The best performing calibration parameter datasets are used to simulate current and future discharge. Table 4.4 lists the results of the calibration and validation at six gauging stations. For the calibration period, the model shows a 'satisfactory' to 'very good' performance (Moriasi et al., 2007) with Nash-Sutcliffe efficiency (NSE) values between 0.60 at Dainyor Bridge and 0.84 at Devghat. The biases between simulated and observed discharge are satisfactory at most gauging stations with biases up to 18% at Sunkosh station. At Dainyor Bridge the bias is large with a value of -31%.

Table 4.2. Simulated and Observed Mean Snow Cover and Glacier Mass Balance. Abbreviations: w.e. = water equivalent.

	Period	Hunza		Marshyangdi		Sunkosh	
		Obs	Sim	Obs	Sim	Obs	Sim
Mean Snow Cover (%)	2000-2010	56.6	81.0	26.7	46.1	19.2	47.6
Glacier Mass Balance (m w.e. yr^{-1})	2003-2008	-0.08	-0.08	-0.21	-0.21	-0.23	-0.23

For the validation period, the model shows similar performances with NSE values between 0.62 at Besham Qila and 0.82 at Devghat. The biases are smaller in comparison with those reported for the calibration period with biases up to 16% at Dainyor Bridge. The Q90 biases, indicating the model's performance under extreme flow conditions, show acceptable performances at the downstream located gauging stations with biases up to 12%, whereas at the upstream located gauging stations the biases are larger with values between -30% and -24%. The underestimation in the extreme flows and the flow at Dainyor Bridge (i.e. during the calibration period) as well are likely a consequence of the underestimate in high-mountain precipitation, and overestimated snow cover, which eventually may lead to an underestimation of the discharge due to lower fractions of direct runoff. Moreover, the spatial resolution of the model (i.e. 5 km x 5 km) might be a reason for the underestimations in the peak flows. Higher spatial resolutions would be more favorable for routing and could lead to better results, but is a large computational expense.

The annual water balances for 1998-2010 (i.e. coinciding the period between the first calibration year and the last validation year) show negligible gaps ranging 1-4 mm yr^{-1} (Figure 4.3). The gaps

Table 4.3. Calibrated model parameters and their values.

Parameters	Units	UIB	UGB	UBB
Glacier				
DDFG	mm $°C^{-1}$ d^{-1}	6.3	8.5	5
DDFDG	mm $°C^{-1}$ d^{-1}	3	6.5	3.5
Snow				
Tcrit	°C	0	0	0
SnowSc	mm mm^{-1}	0.5	0.2	0.5
DDFS	mm $°C^{-1}$ d^{-1}	6	7.5	4.1
Subl3Rate	mm d^{-1}	1.5	3.2	1.25
Rainfall-Runoff				
alphaGW	-	0.005	0.062	0.005
deltaGW	d	1	10	1
Kx	-	0.955	0.93	0.96
GlacF	-	0.6	0.9	0.9
RootDepth	mm	800	653	600
SubDepth	mm	2766	2679	2705

Table 4.4. Model performance ratings in terms of NSE and PBIAS that were calculated on daily basis for the calibration and validation periods, separately. PBIAS Q90 represents the percent bias for the 90-percentile discharge level for the calibration and validation periods. Abbreviations: C = Calibration, V = Validation.

	NSE C	NSE V	PBIAS C	PBIAS V	PBIAS Q90 C & V
Dainyor Bridge	0.60	0.74	-30.9	-16.0	-23.7[1]
Besham Qila	0.69	0.62	-9.2	2.6	8.8[2]
Bimalnagar	0.78	0.75	-10.0	-12.9	-29.7[3]
Devghat	0.84	0.82	1.8	3.1	-12.2[3]
Wangdirapids	0.76	0.75	-4.0	-8.7	-24.0[4]
Sunkosh	0.68	0.74	17.5	8.2	-0.6[4]

[1] 2000-2010, [2] 2000-2008, [3] 2000-2009, [4] 1998-2008

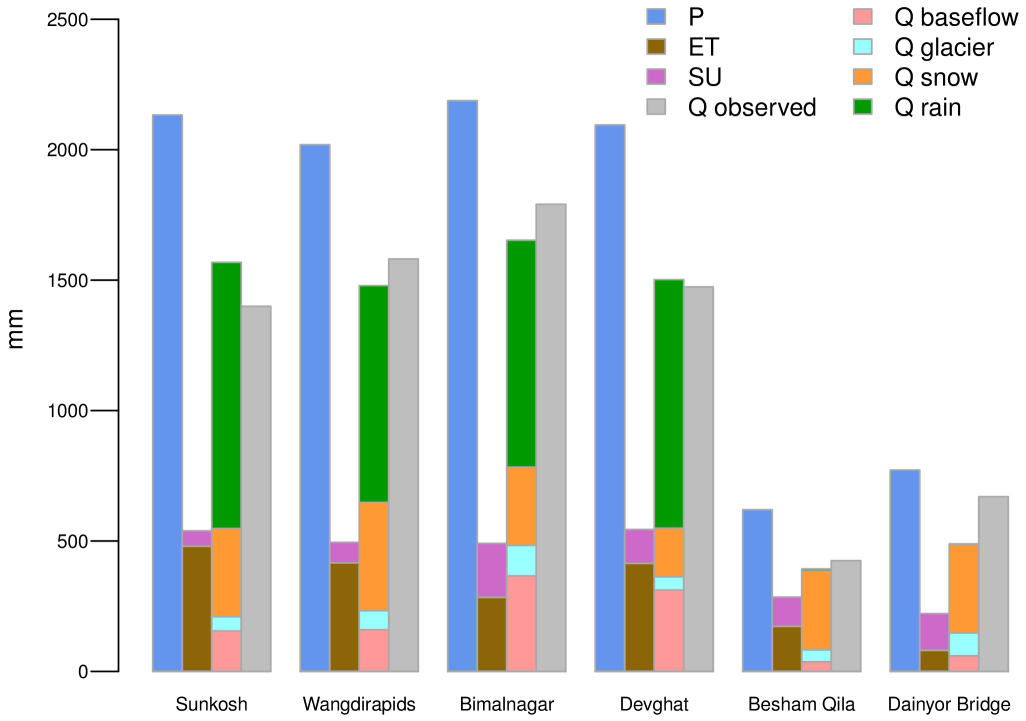

Figure 4.3. Annual catchment-averages of most important water balance components and observed discharge at 6 gauging stations used for calibration and validation. Abbreviations: P = precipitation, ET = actual evapotranspiration, SU = actual sublimation, Q observed = observed discharge, Q baseflow = baseflow, Q glacier = glacier melt, Q snow = snow melt, and Q rain = rainfall runoff.

can be attributed to changes in the storages of snow, soil, and groundwater reservoirs. Given the uncertainties in the meteorological forcing over high mountain terrain and the limitation in feasible model resolutions for simulating such large areas, we conclude that the model's performance is sufficient for the analysis of hydrological extremes.

4.4.2 Future climate change

Towards the end of the 21st century both selected RCP4.5 and RCP8.5 model runs indicate that both precipitation and temperature will increase in magnitude. Table 4.5 lists the basin-averaged values for several climate variables under reference climate conditions and their projected relative (precipitation) and absolute (temperature) changes under far future climate conditions (2071-2100). Under present climate conditions, both, the annual precipitation sums and the precipitation extremes are generally highest in the UGB. Only the present maximum 5-day precipitation amounts are highest in the UIB. All climate models indicate, in general, that future precipitation amounts and extremes will increase in all domains, where the relative changes in precipitation extremes are projected to be higher than the relative changes in annual precipitation sums. Climate models representing wet climate conditions project in general the largest relative increases in future annual precipitation sums, with increases up to 18% and 56% in the UIB and UBB, respectively, under RCP8.5. In the UGB, the largest increases are projected by cold/dry models under RCP8.5 (i.e.

inmcm4), with a relative increase of 41%. In terms of precipitation extremes, a consistent pattern can be observed with cold/wet climate models (i.e. bcc-csm) and warm/wet climate models (i.e. CanESM2) projecting the largest relative changes in the UIB and UBB, respectively, under RCP8.5. The same pattern can also be recognized for the projected relative changes in annual precipitation sums. In the UGB, the pattern is less consistent. Two precipitation extreme indices (P90 and RX5day) are projected to change most under warm/wet (RCP 4.5) climate conditions. P95 and P99 are projected to change most under cold/dry (RCP8.5) and warm/wet (RCP8.5) climate conditions, respectively. In addition to the projected increases in precipitation amounts and extremes, the mean air temperature is also projected to increase towards future, where the largest increases are projected under warm (RCP8.5) climate conditions, with temperature increases in the range 4.8-5.6 °C among the different basins. Significant increases in the HWFI are projected by models characterizing warm climate conditions, where the largest increases are projected by the CMCC-CMS model under

Table 4.5. Basin-averaged values for a range of climate variables for the reference period and the relative (precipitation) and absolute (temperature) changes at the end of the 21st century as projected by each of the downscaled GCM runs used in this study. Abbreviations: P = mean annual precipitation sum, P90, P95, and P99: 90th, 95th, 99th percentiles of daily precipitation sums, RX5 = maximum 5-day precipitation amount, T = annual mean temperature, and HWFI = warm spell days index.

		1981-2010	2071-2100							
			RCP4.5				RCP8.5			
Climate variable	Basin	Reference	BNU-ESM r1i1p1	inmcm4 r1i1p1	CMCC-CMS r1i1p1	CSIRO-Mk3-6-0 r4i1p1	inmcm4 r1i1p1	CMCC-CMS r1i1p1	bcc-csm1-1 r1i1p1	CanESM2 r3i1p1
P (mm yr^{-1})	UIB	1013	+21%	-1%	+4%	+18%	+17%	+3%	+18%	+14%
	UGB	1811	+21%	+2%	+1%	+20%	+41%	-5%	+28%	+34%
	UBB	1483	+15%	-2%	+6%	+7%	+29%	+12%	+23%	+56%
P_{90} (mm d^{-1})	UIB	15.1	+31%	+21%	+56%	+53%	+42%	+55%	+87%	+58%
	UGB	15.8	+17%	+10%	+30%	+68%	+66%	+23%	+62%	+54%
	UBB	12.8	+12%	-1%	+11%	+15%	+28%	+18%	+20%	+52%
P_{95} (mm d^{-1})	UIB	18.1	+25%	+14%	+39%	+40%	+29%	+40%	+66%	+43%
	UGB	23.2	+20%	+3%	+12%	+38%	+52%	+4%	+33%	+41%
	UBB	18.4	+16%	+1%	+9%	+12%	+30%	+18%	+29%	+61%
P_{99} (mm d^{-1})	UIB	36.8	+26%	+5%	+23%	+33%	+30%	+27%	+40%	+19%
	UGB	46.5	+34%	+10%	+11%	+43%	+62%	+11%	+47%	+68%
	UBB	35.2	+24%	+3%	+23%	+15%	+30%	+50%	+43%	+104%
RX5day (mm)	UIB	352	+55%	+26%	+52%	+72%	+51%	+59%	+108%	+39%
	UGB	325	+58%	+113%	+76%	+170%	+131%	+58%	+122%	+123%
	UBB	245	+61%	+40%	+71%	+32%	+107%	+87%	+70%	+115%
Mean air T (°C)	UIB	-1.9	+1,7	+0,6	+2,7	+3,1	+2,6	+5,3	+3,6	+5,6
	UGB	3.2	+1,5	+0,7	+2,5	+2,8	+2,5	+4,8	+3,0	+4,1
	UBB	-0.8	+1,5	+0,7	+2,7	+3,0	+2,6	+5,0	+3,3	+4,5
HWFI (d yr^{-1})	UIB	9	0	+104	+185	+28	+24	+103	+58	+107
	UGB	11	+2	+104	+182	+38	+69	+146	+83	+108
	UBB	12	0	+105	+178	+35	+65	+132	+70	+113

RCP4.5. Smaller increases are projected by models characterizing cold climate conditions, where the most limited change is predicted by the BNU-ESM model.

Figure 4.4 shows the mean magnitude of change in precipitation (i.e. P95) and temperature (i.e. HWFI) extremes that is expected to occur under RCP4.5 and RCP8.5. Relative changes in P95 are generally greatest in the UIB, with relative increases of more than 100% at the southern margins of the UIB under RCP4.5 and relative increases up to about 130% at the westernmost border of the UIB under RCP8.5. These relative increases can mainly be attributed to increases in P95 that are projected by all models characterizing warm and wet climate conditions. A pattern can be recognized with the largest increases in the western part of the IGB and smaller increases when moving eastward. This pattern can mainly be attributed to the projected changes that result from warm and wet climate models. The HWFI is projected to increase by a factor up to about 20 in parts of the UIB, the northern part of the UBB, and the southernmost margins of the UBB under RCP4.5, and with a factor of up to 40 at the southernmost margins of the UBB under RCP.8.5. These increases are mainly deriving from model runs characterizing warm climate conditions. Both, the relative changes in P95 and HWFI, are accompanied by large spreads in those regions where the greatest changes are projected, which indicates that these changes have a large uncertainty.

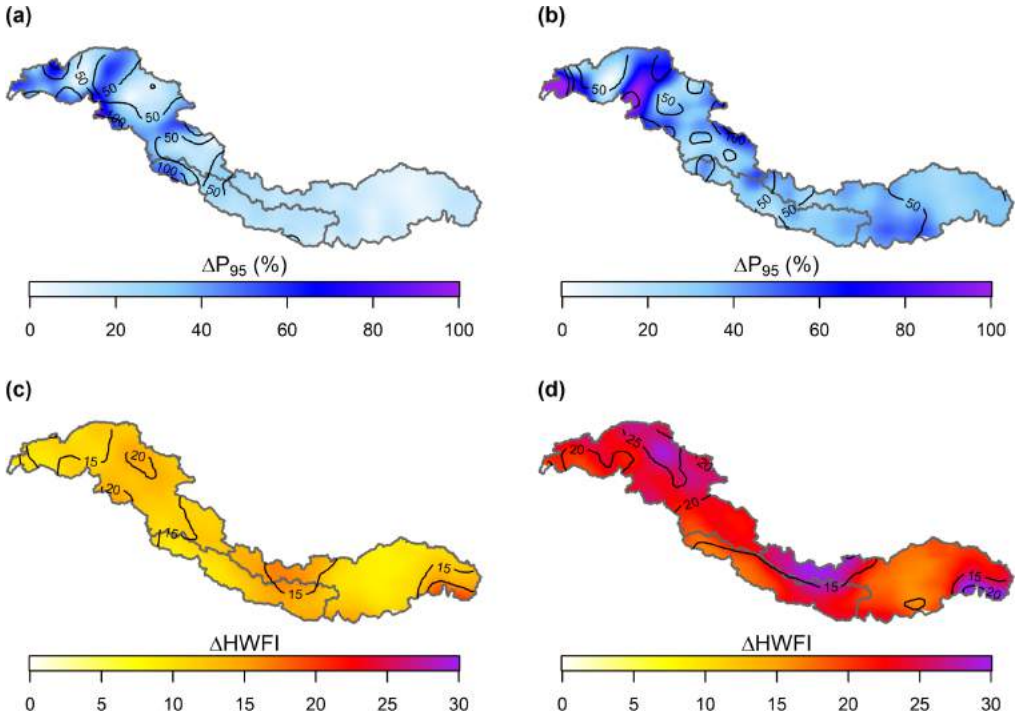

Figure 4.4. Changes in P95 and HWFI. Maps showing the changes in P95 and the HWFI index for RCP4.5 and RCP8.5. Contour lines denote the ensemble range of projections.

4.4.3 Future changes in hydrological extremes

4.4.3.1 High Flows

Based on the projected trends in precipitation amounts and extremes it can be expected that high flow conditions will occur more frequently in the IGB towards future. Figure 4.5a and 4.5b show the future projections in annual maximum series (AMS) for the outlets of the rainfall-dominated UBB and the glacier/snow-melt dominated Hunza basin (UIB) under RCP4.5 and RCP8.5 scenarios. Relative to the reference period (1981-2010) there is a significant increase in AMS in both basins and under both scenarios. In the Hunza basin the differences between RCP4.5 projections and RCP8.5 projections are relatively small, whereas in the UBB these differences are larger with a more significant increase in AMS under RCP8.5. The AMS increases in the Hunza basin can mainly be attributed to increases in snowmelt under RCP4.5 and a combination of increases in snowmelt and rainfall under RCP8.5. Since the increases in the HWFI and P95 are considerable in the UIB, especially under RCP8.5 (Figure 4.4), it is likely that increasing temperature and precipitation extremes under RCP4.5 and RCP8.5 may contribute to increasing AMS. In the UBB increasing precipitation extremes under RCP4.5 and RCP8.5 may contribute to increasing AMS. The P95 increases are not as large as in the UIB, and the HWFI increases are considerable (Figure 4.4), especially at the southernmost margins of the UBB where the Himalayas merge into the Indo-Gangetic plains. Nevertheless, HWFI increases are largest in those regions that are not or limited covered by snow and ice, which means precipitation extremes might be interpreted as the main responsible factor in AMS increases. Although the AMS increases are larger in the UBB, it can also be observed that the standard deviation becomes larger towards the end of the 21st century. A similar trend can be observed in the Hunza basin, which indicates a larger uncertainty in future AMS trends.

Increasing high flow trends have also been projected in other basins. In Table 4.6 the mean discharge, the 99th percentile of daily discharge values (Q1), and 5, 25, and 50-year return levels under present, near future (2035-2064), and far future (2071-2100) RCP4.5 and RCP8.5 climate conditions are listed for the outlets of the UIB, UGB, UBB, Hunza, Marshyangdi, and Sankosh

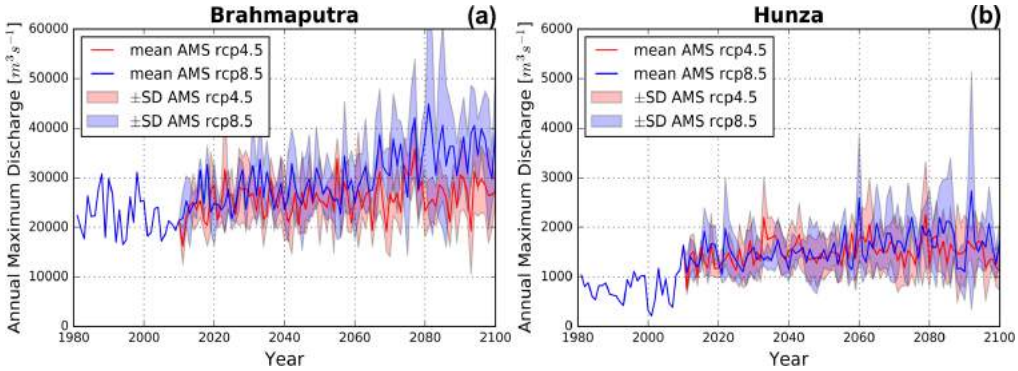

Figure 4.5. Present and future annual maximum series (AMS). The mean AMS for the period 1981-2100 under RCP4.5 (red) and RCP8.5 (blue). The AMS are given for the upper Brahmaputra and Hunza basins. The colored band represents the standard deviation resulting from forcing the hydrological model with the different climate models.

basins. The highest mean discharge values are simulated at the outlet of the UBB with a mean rate of 6120 m^3s^{-1} and is projected to change, with relative increases up to 49% at the end of the 21st century. The lowest mean discharge values are simulated at the outlet of the Hunza basin, with a mean rate of 160 m^3s^{-1}, and is projected to change, with relative increases up to 119% under RCP8.5, which will end up in a higher projected discharge rate than in another upstream catchment, the Marshyangdi basin (i.e. 350 m^3s^{-1} in the Hunza basin vs. 283 m^3s^{-1} in the Marshyangdi basin). The higher projected discharge rates can be explained by the increased snowmelt in the Hunza basin, whereas in the Marshyangdi basin snowmelt is projected to increase initially followed by a decline after 2040-2050. In addition to the mean discharge rates, flow extremes are also expected to increase

Table 4.6. Changes in the mean discharge, 99th percentile of daily discharge values (Q99), and the discharge levels of events with return periods of 5, 25 and 50 years at the outlets of the UIB, UGB, UBB, and the upstream catchments (Hunza, Marshyangdi, and Sankosh) under present (1981-2010), near future (2035-2064), and far future (2071-2100) RCP4.5 and RCP8.5 climate conditions. The values between the parentheses represent the standard deviation.

Basin	Period	Units	$\overline{Q}$	Q99	5-yr Q	25-yr Q	50-yr Q
Hunza	1981-2010	m^3s^{-1}	160	972	1045	1500	1689
	2035-2064 RCP4.5	%	+102 (39)	+93 (33)	+87 (34)	+76 (35)	+73 (35)
	2071-2100 RCP4.5	%	+88 (32)	+96 (51)	+89 (41)	+86 (44)	+85 (44)
	2035-2064 RCP8.5	%	+101 (30)	+86 (26)	+80 (34)	+70 (36)	+67 (37)
	2071-2100 RCP8.5	%	+119 (34)	+121 (27)	+118 (30)	+116 (31)	+116 (32)
Marshyangdi	1981-2010	m^3s^{-1}	199	884	1018	1275	1381
	2035-2064 RCP4.5	%	+16 (10)	+35(15)	+40 (17)	+53 (26)	+56 (29)
	2071-2100 RCP4.5	%	+28 (16)	+62 (23)	+63 (26)	+77 (30)	+81 (31)
	2035-2064 RCP8.5	%	+21 (11)	+54 (19)	+56 (15)	+74 (14)	+79 (14)
	2071-2100 RCP8.5	%	+42 (29)	+93 (53)	+96 (51)	+114 (59)	+120 (61)
Wangdirapids	1981-2010	m^3s^{-1}	288	1167	1176	1511	1650
	2035-2064 RCP4.5	%	+18 (14)	+28 (17)	+31 (18)	+36 (20)	+37 (21)
	2071-2100 RCP4.5	%	+29 (12)	+45 (17)	+46 (21)	+52 (22)	+54 (22)
	2035-2064 RCP8.5	%	+28 (15)	+40 (16)	+41 (20)	+46 (21)	+47 (22)
	2071-2100 RCP8.5	%	+66 (40)	+107 (73)	+121 (76)	+141 (92)	+147 (97)
Upper Indus	1981-2010	m^3s^{-1}	2177	13063	15281	21659	24301
	2035-2064 RCP4.5	%	+59 (25)	+54 (28)	+42 (18)	+39 (16)	+39 (16)
	2071-2100 RCP4.5	%	+49 (17)	+55 (32)	+48 (29)	+51 (32)	+52 (33)
	2035-2064 RCP8.5	%	+50 (11)	+46 (24)	+28 (28)	+24 (28)	+23 (28)
	2071-2100 RCP8.5	%	+51 (11)	+59 (29)	+47 (19)	+50 (21)	+51 (21)
Upper Ganges	1981-2010	m^3s^{-1}	1536	6639	7373	9015	9695
	2035-2064 RCP4.5	%	+16 (11)	+36 (15)	+38 (16)	+53 (24)	+57 (27)
	2071-2100 RCP4.5	%	+29 (17)	+60 (22)	+60 (29)	+75 (34)	+80 (35)
	2035-2064 RCP8.5	%	+20 (11)	+52 (18)	+49 (14)	+68 (14)	+74 (14)
	2071-2100 RCP8.5	%	+41 (31)	+83 (47)	+84 (53)	+102 (64)	+108 (68)
Upper Brahmaputra	1981-2010	m^3s^{-1}	6120	25495	25949	32242	34847
	2035-2064 RCP4.5	%	+16 (16)	+15 (10)	+21 (10)	+26 (8)	+28 (7)
	2071-2100 RCP4.5	%	+24 (11)	+21 (5)	+32 (6)	+39 (8)	+41 (10)
	2035-2064 RCP8.5	%	+24 (14)	+26 (17)	+29 (18)	+33 (20)	+34 (20)
	2071-2100 RCP8.5	%	+49 (33)	+57 (35)	+68 (36)	+77 (39)	+80 (39)

in magnitude towards future. The largest increases are projected in the Sunkosh basin, where the 50-year return level is expected to increase by 147% after 2071 under RCP8.5. In the UIB basin, the smallest increases are projected. In this basin, the 50-year return level is projected to increase by 51% under RCP8.5. Accompanied by higher discharge levels, standard deviations and thus uncertainties also increase.

Figure 4.6 shows the mean and the standard deviation of the relative change in the 50-year return period over the river network under RCP4.5 and RCP8.5 scenarios. In the most parts of the IGB the 50-year return level is projected to increase by relative increases up to about 305% under RCP8.5 climate conditions. The largest increases are projected for the easternmost upstream headwaters of the Brahmaputra. These increases can mainly be attributed to increases in rainfall resulting from increases in precipitation, and partly also to increases in ice melt. Besides increases, there are also river branches where the 50-year return level is projected to decrease. These decreases (i.e. up to about 25%) mainly occur in the westernmost part of the UIB (i.e. Kabul basin) and can mainly be attributed to decreases in ice and snowmelt, and precipitation as well. Similar trends were also projected by a previous study (Lutz et al., 2016a) in the UIB. The standard deviation of 50-year return levels is generally larger under RCP8.5 (Figure 4.6d), with the largest deviations at the southern margins of the UBB. In this region, relatively large changes are also projected, with relative increases up to about 200%

The projected changes in high flow characteristics are in line with the reported trends in other studies that were conducted in the Indus, Ganges and/or Brahmaputra basins (Gain et al., 2011; Hirabayashi et al., 2013; Lutz et al., 2016a; Pechlivanidis et al., 2016). Although the trends are similar, it is difficult to compare the magnitude of absolute and relative changes in discharge levels with those projected in other studies. The underlying reason is that other studies have used different climate forcing and approaches to investigate impacts of climate change on hydrological extremes. Furthermore, different locations hamper comparisons between our study and other studies. For instance, most studies have focused on the entire Indus, Ganges or Brahmaputra basins, whereas in our study the focus is on the upstream mountainous domains. Finally, different time periods may hamper the comparisons. Although there is a high degree of similarity between the periods used for comparing far future changes (e.g. Hirabayashi et al., 2013), the periods used for near future changes can differ. For example, one of the referred studies (Lutz et al., 2016a) defined 2021-2050 as a near future period, whereas we defined 2035-2064 as a near future period.

4.4.3.2 Low Flows

Low flows are in general projected to occur less frequently. In Figure 4.7 the flow duration curves (FDCs) are given for the outlets of the Hunza basin and the UBB under reference climate conditions, and RCP4.5 and RCP8.5 scenarios. Focusing on the area between the 70 and 95 percentile exceedance discharge levels, it can be observed that low flow conditions are in general projected to occur less frequently in the UBB under both RCP4.5 and RCP8.5. Previous work (Gain et al., 2011; Hirabayashi et al., 2008) projected similar trends for the Brahmaputra. In the Hunza Basin, a similar trend can be observed, although the uncertainty is quite large. These uncertainties can likely be attributed to the large spread among the different climate models. Both in the UBB and the Hunza basin there are a few climate models (i.e. mainly cold/dry climate models (inmcm4)) that project a slightly higher frequency in low flow conditions, especially for RCP4.5 in the Hunza basin. This may explain why the increase in the far future mean discharge in the Hunza basin is projected

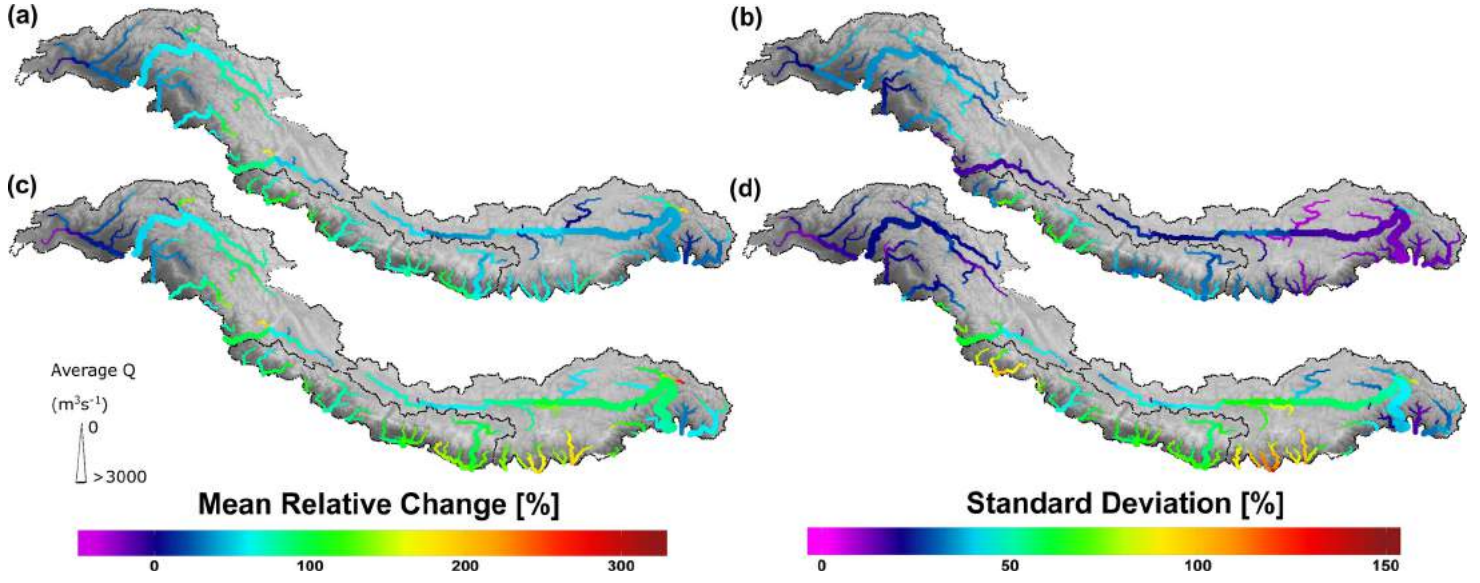

Figure 4.6. Relative changes in 50-year return period discharge level. Maps showing the mean relative changes (left) in 50-year return period discharge levels and their standard deviations (right) at the end of 21st century (2071-2100) under RCP4.5 (upper row) and RCP8.5 (lower row) scenarios.

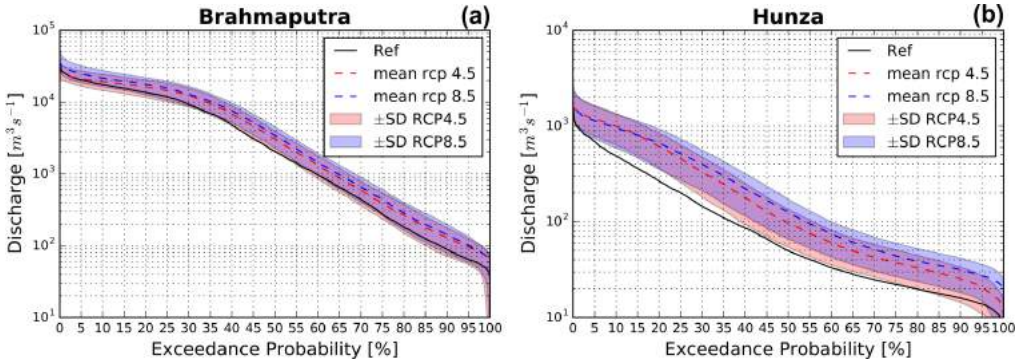

Figure 4.7. Reference and future flow duration curves (FDCs). The FDCs of the reference (black lines) and far future period (dashed lines) at the outlets of the upper Brahmaputra and Hunza basins. The FDCs represent mean flow conditions under RCP4.5 (red) and RCP8.5 (blue). The colored band represents the standard deviation resulting from forcing the hydrological model with the different climate models.

to be lower than the increase in the near future mean discharge for RCP4.5 (Table 4.6), and can be attributed to a decline in glacier melt after 2050.

4.4.4 Uncertainties and limitations

The projections of future hydrological extremes are subject to several uncertainties and limitations that are briefly discussed below. Although significant trends for the future have been identified, the outcomes of this study should be treated with care. The uncertainties and limitations are mainly related to the input data, the climate projections, the representation of physical processes in the hydrological model, and the parameterization of the model, or are emerging from the natural variability of climate variables.

In this study, input data, such as meteorological observation data, was used to force the hydrological model or to conduct bias-corrections on the reference climate dataset. As mentioned before, there were 40 meteorological data records available that are unequally distributed over the study area, and are valley-oriented. This means in many regions, and especially in the high-altitude areas, there is a lack of measurement data. Consequently, uncertainties are introduced when conducting station-based bias-corrections on temperature fields. The uncertainties in the reference climate dataset are subsequently introduced in the future climate forcing since the reference climate dataset was used to downscale different GCM runs.

The future climate forcing does consist of eight climate models, each representing different climate conditions, under the RCP4.5 and RCP8.5 emission scenarios. The models that were used for this study were selected according to an advanced envelope-based selection procedure (Lutz et al., 2016b), comprising three steps focusing on changes in climatic means and extremes, and the skill to simulate present and/or historical climate. The selection approach is decisive for which models are selected. Another selection approach may result in the selection of different climate models and thus in different projections of future hydrological extremes. The climate models selected in this study were evaluated for their projected changes in climatic extremes in an earlier published study (Lutz et al., 2016b). In general, there is a consensus between the selected models on the projected trends

in temperature and precipitation extremes. Nevertheless, the spread among the different models can be large. For instance, in the UBB the projected increases in P99 under RCP8.5 can vary from +30% under cold/dry climate conditions (i.e. inmcm4, Table 4.5) to +104% under warm/wet climate conditions (i.e. CanESM2). In addition, the spatial spread differences can be large. For example, the spread in relative P95 changes in the UIB (Figure 4.4) can exceed 100%, whereas in the UBB the spread can be smaller than 50%, meaning that there is less consensus about the projected changes in the UIB than in the UBB. Furthermore, it may happen that different climate models project the largest changes in different precipitation indices among the different basins. In the UIB and UBB, the largest changes are projected by cold/wet and warm/wet climate (models, respectively (Table 4.5), whereas in the UGB the largest changes are projected by both warm/wet and cold/dry models. The missing consensus among the different climate models indicate that further improvement is needed in the representation of climate extremes in GCMs.

The SPHY model was used for the simulation of present and future daily discharge. Within the SPHY model the representation of physical processes, such as the simulation of snow processes, introduces additional uncertainties. The SPHY model can simulate snow melt, accumulation, refreezing, and sublimation processes, but does not take processes such as gravitational snow transport or snow re-distribution by wind into account. This may eventually result in an overestimation of snow storage and cover. To overcome these uncertainties, snow transport models, such as SnowSlide (Bernhardt and Schulz, 2010), can be integrated at higher spatial resolutions of modelling to simulate e.g. gravitational snow transport by avalanching. In addition, uncertainties can be introduced by simplified model assumptions. For instance, snow sublimation is modelled by a simple elevation-dependent potential sublimation function (Lutz et al., 2016a), thereby assuming that sublimation is constant over time and that most sublimation occurs at higher altitudes where the highest wind speeds prevail and air is driest. Nevertheless, sublimation varies in time, due to its dependency on wind speed and humidity, amongst others. To account for this temporal variability, it may be considered to use more sophisticated approaches including energy balance components. However, these approaches require more data, which is often limited available or even absent in the remote areas of the IGB. Furthermore, future glacier change and melt projections are associated with limitations in the improved glacier module. The module is less accurate for very large model resolutions. At large resolutions, the small glaciers fall within one grid cell, which disables the possibility for re-distributing ice over these glaciers. Another disadvantage is that glaciers cannot increase in area, which disables the possibility to simulate glacier surges. Another uncertainty emerges from the differentiation of debris-free and debris-covered glaciers. The differentiation is based on thresholds of elevation and slope without consideration of local geology and geomorphology. This may affect the differentiation of glaciers and subsequently the amount of ice melt that can be produced from the glaciers. The problem is, however, that the knowledge about local geology and geomorphology is limited in the HKH region, and no glacier inventory, making a distinction in debris-covered and debris-free glaciers for the entire HKH, is available.

The calibration of the SPHY model resulted in a uniform parameter set for each river basin specifically. Uncertainties are introduced since the values of most parameters vary in space and time. To reduce the uncertainties related to the spatial variability in parameter values one may consider subdividing each domain in smaller sub-catchments and to use regionalization approaches. One of the regionalization approaches includes a similarity approach in which parameter sets that are calibrated for gauged catchments are transposed to ungauged catchments with similar climatic

and physiographic characteristics (e.g. topography, land use, soils, geology, stream network, etc.). A study to different regionalization approaches in the Austrian Alps showed that similarity approaches and kriging approaches belong to the best performing regionalization methods (Parajka et al., 2005). Regionalization approaches have recently also been applied in the HKH region. In a recent study a similarity approach was conducted in two glacierized subcatchments in the Koshi catchment, Nepal (i.e. located in the eastern part of the IGB) (Nepal et al., 2017). The outcomes of the cited study indicated that the transfer of calibrated parameters from a gauged catchment to a neighboring ungauged catchment is viable and that the use of regionalization approaches has potential in other ungauged catchments in the Himalayan region. It is, however, difficult to implement regionalization approaches in the entire HKH region, since a lot of detailed information (e.g. on geology) required for the implementation of regionalization approaches is lacking. Our approach in assigning parameter sets can be considered as a regionalization because we transfer parameter sets from gauged catchments within a river basin to ungauged parts of the basin, for the UIB, UGB, and UBB separately. Other parameter uncertainties might emerge from the over-parameterization of parameters or the appearance of inter-correlation between parameters (Seibert, 1997). Since the calibrated snow degree-day factor in the Marshyangdi basin is higher than the range of 3-6 mm $°C^{-1}$ d^{-1} found in other studies (Table 4.3) it might be concluded that this parameter is over-parameterized.

This study focused on the propagation of uncertainties in future climate (i.e. the spread in climate projections) and future hydrological projections and did not focus on uncertainties, such as parameter uncertainties in detail, since this focus is beyond the scope of this work. To have a full impression of the uncertainties a full uncertainty analysis is recommended for future work.

4.5 Conclusions

The aim of this study is to investigate the impacts of climate change on hydrological extremes in the upstream domains of the Indus, Ganges, and Brahmaputra. To this end, a fully distributed cryospheric-hydrological SPHY model is used to simulate current and future daily discharge. The model is forced by bias-corrected and downscaled GCM runs that represent different future climate conditions under RCP4.5 and RCP8.5. The climate forcing and the outcomes of the models are used to analyze climatic and hydrological extremes (i.e. high and low flow extremes).

Climatic extremes are projected to increase in magnitude towards the end of the 21st century. Thereby, the increases in climatic extremes are projected to be stronger than the increases in climatic means. The magnitude of the absolute and relative changes in temperature and precipitation extremes and the regions where these changes occur depend highly on which climate conditions will prevail. In general, it can be concluded that precipitation extremes (i.e. P95) will increase mostly in the upper Indus Basin with relative increases up to 130%. Temperature extremes are expected to appear more frequently in the future, where the HWFI is projected to increase by a factor up to 40 at the southern margins of the upper Brahmaputra Basin.

The outcomes indicate further that mean discharge and high flow conditions will increase towards future. In rainfall-dominated basins as the UBB increases in precipitation extremes may contribute in discharge extremes. To which extent precipitation and temperature extremes might contribute to increases in discharge extremes in glacier/snowmelt-dominated basins depend on the magnitude

of changes in extremes. In case of the Hunza basin, both temperature and precipitation extremes might contribute to increasing discharge extremes due to increasing temperature (i.e. HWFI) and precipitation (P95) indices. In general, an increase in mean discharge, the 99th percentile, and the 5, 25, and 50-year return levels is expected in all basins. The 50-year return level is expected to increase up to 305% relative to the current level with the largest increases in the upstream headwaters of the upper Brahmaputra basin. In the westernmost part of the upper Indus basin, the 50-year return level is expected to decrease up to 25%. These changes can be attributed to changing contributions of rainfall, ice and snowmelt. In the upstream headwaters of the UBB rainfall increases are mainly responsible for the changes in the 50-year return level, which is mainly a consequence of increasing precipitation. In addition, increases in ice melt also contribute to these changes. In the westernmost part of the UIB precipitation, ice and snowmelt decreases are mainly responsible for changes in the 50-year return level. Low flows are in general projected to occur less frequently in the upper Brahmaputra and Hunza basins. Nevertheless, the uncertainty of low flow projections in the Hunza basin is high.

The outcomes of this study aim to contribute to a better understanding of the impacts of climate change on hydrological extremes in the HKH region. The outcomes may contribute to the development of adaptation strategies to reduce the adverse impacts of changes in climatic and hydrological extremes. The outcomes are sufficiently reliable to extract main trends, but are also subject to many uncertainties, which means the outcomes should be treated with care and improvements are needed in future research on hydrological extremes.

Acknowledgements

I would like to thank D. Treichler for sharing the IceSat derived glacier mass balance data for specific catchments.

5 Climate change vs. socio-economic development: Understanding the drivers of the future water gap in mountainous river basins

The Indus, Ganges, and Brahmaputra (IGB) river basins provide about 900 million people with water resources used for agricultural, domestic, and industrial purposes. These river basins are marked as "climate change hotspots", where climate change is expected to affect monsoon dynamics and the amount of meltwater from snow and ice, and thus the amount of water available. Simultaneously, rapid and continuous population growth as well as strong economic development will likely result in a rapid increase in water demand. Since quantification of these future trends is missing, it is rather uncertain how the future South Asian water gap will develop. To this end, we assess the combined impacts of climate change and socio-economic development on the future "blue" water gap in the IGB until the end of the 21st century. We apply a coupled modelling approach consisting of the distributed cryospheric-hydrological model SPHY, which simulates current and future upstream water supply, and the hydrology and crop production model LPJmL, which simulates current and future downstream water supply and demand. We force the coupled models with an ensemble of eight representative downscaled general circulation models (GCMs) that are selected from the RCP4.5 and RCP8.5 scenarios, and a set of land use and socio-economic scenarios that are consistent with the shared socio-economic pathway (SSP) marker scenarios 1 and 3. The simulation outputs are used to analyse changes in the water availability, supply, demand, and gap. The outcomes show an increase in surface water availability towards the end of the 21st century, which can mainly be attributed to increases in monsoon precipitation. However, despite the increase in surface water availability, the strong socio-economic development and associated increase in water demand will likely lead to an increase in the water gap during the 21st century. This indicates that socio-economic development is the key driver in the evolution of the future South Asian water gap. The transgression of future environmental flows will likely be limited with sustained environmental flow requirements during the monsoon season and unmet environmental flow requirements during the low-flow season in the Indus and Ganges river basins.

Based on: *Wijngaard, R.R., Biemans, H., Lutz, A.F., Shrestha, A.B., Wester, P., and Immerzeel, W.W. 2018. Climate change vs. socio-economic development: understanding the future South Asian water gap. Hydrology and Earth System Sciences 22, 6297-6321. DOI: 10.5194/hess-22-6297-2018.*

5.1 Introduction

Freshwater resources are essential for hundreds of millions of people living in South Asian river basins. The Indus, Ganges, and Brahmaputra (IGB) river systems provide about 900 million people and the world's largest irrigation scheme (i.e. that of the Indus Basin Irrigation System, IBIS) with water, which is mainly used for agricultural (e.g. irrigation), domestic (e.g. drinking water supply), and industrial purposes (FAO, 2012; Klein Goldewijk et al., 2010; Rasul, 2014; Shrestha et al., 2013).

The water supply in the IGB is mainly dominated by two different components: locally pumped groundwater and surface water supplied by irrigation canals. Groundwater is an important water supplier for the agricultural sector with contributions of about 64% and 33% to the total irrigation water supply in India and Pakistan, respectively (Biemans et al., 2016; Siebert et al., 2010). Surface water is supplied by irrigation canals that are diverted from rivers and reservoirs and consist of direct rainfall runoff, meltwater from upstream located ice melt and snow reserves, and baseflow. Meltwater is the largest constituent of the total annual surface flow in the western part of the IGB, where the amount of winter precipitation is substantial and the largest ice reserves are present (Bookhagen and Burbank, 2010; Immerzeel, 2008; Lutz et al., 2014; Rees and Collins, 2006). In the eastern part of the IGB, where monsoon systems are more dominant, the monsoon precipitation is the largest constituent of the total annual surface flow (Immerzeel, 2008). It is expected that due to projected rises in temperature and precipitation changes, glaciers and seasonal snow cover will be affected, eventually affecting the amount of meltwater and thus the amount of surface water supply from upstream mountainous basins, especially in the western part of the IGB (Kraaijenbrink et al., 2017; Viste and Sorteberg, 2015). Further, monsoon dynamics will likely change, resulting in a decreasing number of rainy days, increasing intensity of precipitation, and increasing mean monsoon precipitation (Kumar et al., 2011; Lutz et al., 2018; Sharmila et al., 2015; Turner and Annamalai, 2012). This might eventually affect the water supply patterns in the eastern part of the IGB. On top of that, long-term precipitation changes may lead to changes in groundwater recharge and storage, which in turn will affect groundwater availability (Asoka et al., 2017). There are, however, large uncertainties in the projected precipitation changes due to the large spread among the different climate model runs (Arnell and Lloyd-Hughes, 2014; Lutz et al., 2016b; Moors et al., 2011; Wijngaard et al., 2017), which hampers the projection of future water supply rates. In addition to climate-induced changes in surface and groundwater supply, groundwater depletion is expected to intensify over the next decades due to socio-economic development (Rodell et al., 2009; Wada, 2016; Wada et al., 2010).

Simultaneous with changes in water supply under climate change, rapid and continuous population growth and strong economic development are expected to result in a rapid increase in water demand over the coming decades (Biemans et al., 2011; Rasul, 2014, 2016; Wada et al., 2016b). The population in the IGB is expected to grow from 900 million inhabitants in 2010 to 1.1-1.4 billion inhabitants in 2050, which will likely be accompanied by rapid urbanization (Klein Goldewijk et al., 2010; Rasul, 2016). For instance, in countries like India and Pakistan, the expectation is that by 2050 more than 50% of the population will live in urban areas (Mukherji et al., 2018; UN-DESA, 2018). The population growth is also expected to be accompanied by continuing fast economic growth (i.e. currently between 2.5% and 7.3% per year (ADB, 2018)), rapid industrialization, and an intensification of water use in food production (e.g. due to expansion of irrigated areas) (Biemans et al., 2013; Rasul, 2016). This will likely result in a potential water gap and increasing pressure on

water resources, which in turn will affect food security, safe access to drinking water, public health, and environmental well-being (Liu et al., 2017; Taylor, 2009).

The development of the future blue water gap in the IGB is rather uncertain. Some (global) studies (e.g. Alcamo et al., 2007; Arnell, 2004; Lutz et al., 2014) found that water availability is projected to increase due to climate change, indicating that the future (seasonal) blue water gap might decline. Other studies (e.g. Barnett et al., 2005; Gain and Wada, 2014; Hanasaki et al., 2013; Vörösmarty et al., 2000) found that water demand is projected to increase due to socio-economic changes, mainly resulting from population growth, or that water availability is projected to decrease. Both the projected increases and decreases in water demand and availability, respectively, might eventually result in an increasing (seasonal) blue water gap. The opposing trends in how the future South Asian blue water gap will develop indicate that the uncertainty is large and that an improved understanding of the development of the regional blue water gap is needed. One of the drawbacks in some of the cited studies is, for example, that, in general, the selection of climate models, RCPs, and SSPs (RCP-Representative Concentration Pathway; SSP-Shared Socio-economic Pathway) was not tailored to the representation of a wide range of possible futures in terms of climate change and socio-economic development. Consequently, a full picture of how future water availability, supply or demand can change cannot be provided. Model selection approaches (e.g. Lutz et al., 2016b) with a focus on a wide range of possible futures in terms of climate change, and the selection of contrasting RCP-SSP combinations according to a RCP-SSP framework (van Vuuren et al., 2014), can for instance be used to eliminate this drawback. Another drawback is that no models were used with a sufficient representation of cryospheric-hydrological processes. Therefore, the lack of proper simulations of the evolution of mountain water resources (e.g. glacier evolution) may have imposed uncertainties in the outcomes of these studies. Models with a sufficient representation of cryospheric-hydrological processes can be used to eliminate this drawback.

(Blue) water availability, supply, and demand have been assessed by different methodologies over recent decades. One type of assessments relied on statistics of water use (e.g. FAO AQUASTAT) and observations of meteorological and hydrological variables (Bierkens, 2015). Others were conducted by using several model types, such as global hydrological models (e.g. H08 (Hanasaki et al., 2008a, 2008b), LPJmL (Schewe et al., 2014) and PCR-GLOBWB (van Beek et al., 2011; Wada et al., 2014)) (Veldkamp et al., 2017). There are several advantages of the use of hydrological models above the use of statistics. One advantage is that water availability or supply, the main types of water use (i.e. agricultural, domestic, and industrial), and their relationships and feedbacks can be considered on a high spatial and temporal resolution (e.g. 5 arc min and daily). Another advantage is that models such as the LPJmL model can be used to assess the impacts of human interventions (e.g. reservoirs) on water availability and irrigation water supply (Biemans et al., 2011; Haddeland et al., 2014).

Large-scale hydrological models that simulate water supply and demand have mostly been applied without making an explicit distinction between up- and downstream domains and their roles in water supply and demand. To make an explicit distinction between the dominant processes in the different domains, different tools are required to simulate the domain-specific processes properly. For instance, in the upstream domains of the IGB, water availability is highly dependent on natural factors, such as ice and snowmelt (e.g. Lutz et al., 2014)). Since cryospheric and hydrological processes vary strongly over short distances in the upstream mountainous areas, higher-resolution models with a robust representation of mountain-specific cryospheric and hydrological processes

are required to simulate water availability and supply in and from the upstream (mountainous) domains accurately. In the downstream domains of the IGB, the human influence on the hydrological cycle is large, with large irrigation canal systems and reservoirs (e.g. Tarbela Dam) (Biemans et al., 2013). In addition, agricultural water use is a very important topic in this region, which requires knowledge of related processes, such as crop growth, and relations between water availability and food production. In these domains, therefore, a high-resolution model is required that a) has an explicit representation of human interventions in the hydrological cycle, and b) can link hydrological processes with crop processes.

Environmental flow requirements (EFRs) have not been considered in most future assessments on climate change-induced or socio-economic development-induced changes in water supply and demand in the region. EFRs have so far only been applied by Hanasaki et al. (2013) by using an EFR module (i.e. part of the H08 model) that controls the consumptive amount of water that is withdrawn from river systems. This allows the prioritization of maintaining EFRs, but also has the consequence that agricultural production might be affected. According to Jägermeyr et al. (2017) up to ~30% of the agricultural production in South Asia can be lost when EFRs are considered. In the IGB, rapid and continuous population growth is expected, which will most likely be accompanied by an increase in food demand and thus requires a higher agricultural production (Biemans et al., 2013). Therefore, agricultural needs will probably be prioritized at the cost of environmental flows and water use will most likely intensify, which subsequently might alter flow regimes and the ecological health of a river system (Döll et al., 2009; Pastor et al., 2014). To understand the impact of blue water consumption on environmental flow transgressions, it is therefore needed to estimate EFRs and to assess whether (future) EFRs are met or not.

The main objective of this study is to assess the combined impacts of climate change and socio-economic development on the future "blue" water gap for the downstream floodplains of the IGB river basins until the end of the 21st century. For the upstream mountainous domains, we apply a distributed model with a strong representation of cryospheric-hydrological processes that explicitly simulates cryospheric changes (i.e. glacier and snow cover) under climate change. For the downstream domains, we apply a distributed hydrology and crop production model with an explicit representation of human interventions in the hydrological cycle to simulate downstream water supply and demand. We use the RCP-SSP framework to include a wide range of possible futures in terms of climate change and socio-economic development (van Vuuren et al., 2014). Both models are forced with outputs of eight downscaled general circulation models (GCMs) representing a region-specific wide range of possible climate conditions (i.e. representing RCP4.5 and RCP8.5) (Lutz et al., 2016b). In addition, we use a set of regional land use scenarios and socio-economic scenarios (derived from SSP1 and SSP3 (Riahi et al., 2017)) to force the hydrology and crop production model. Water demand and consumption are estimated in terms of the amount of water that is required for withdrawal and that is consumed, respectively, by the agricultural, domestic, and industrial sectors. The blue water gap is estimated as the amount of unsustainable groundwater that is withdrawn to fulfill the blue water demand. Finally, EFRs are estimated according to the variable monthly flow (VMF) method (Pastor et al., 2014) to assess the impact of (future) blue water consumption on environmental flow transgressions, assuming that meeting EFRs have the lowest priority.

This study stands out in comparison with previous work in the region by means of multiple novelties. First, the main novelty is in understanding and assessing the combined impacts of climate change and socio-economic development on the future "blue" water gap in the major South Asian river basins. Second, the novelty of this study lies in the application of a coupled modelling approach, including a high-resolution cryospheric-hydrological model (5 x 5 km) and a high-resolution hydrology and crop production model (5 x 5 arc min), that can simulate up- and downstream water availability, the downstream water supply, demand, and the gap in the entire IGB. This modelling approach takes upstream-downstream links and lateral transport into consideration, which enables the possibility to assess the effects of changes in upstream water supply on downstream water availability and to improve analyses on the regional "blue" water gap. Third, the hydrology and crop production model applied for downstream domains, has been specially developed for this region in that it is able to a) simulate water distribution through extensive irrigation canal systems of the Indus and Ganges river basins, b) make improved simulations of the timing of water demand for agriculture due to an explicit representation of a multiple cropping system (Biemans et al., 2016), and c) simulate groundwater withdrawal and depletion rates. Fourth, the high-resolution models are forced with an ensemble of downscaled and bias-corrected GCMs that were selected by using an advanced selection approach and represent a wide range of possible futures in terms of climate change for RCP4.5 and RCP8.5. Fifth, the hydrology and crop production model is forced with a set of gridded socio-economic and land use scenarios that are most likely linked with the RCPs (i.e. according to the RCP-SSP framework). Finally, the outcomes of the hydrology and crop production model are used to assess the impact of (future) blue water consumption on environmental flow transgressions.

5.2 Study area

The future blue water gap is examined for three major South Asian river basins, which are considered as "hotspot" of climate and socio-economic changes: the Indus, Ganges, and Brahmaputra (De Souza et al., 2015) (Figure 5.1). The Indus, Ganges, and Brahmaputra river basins are selected as study area because these South Asian river basins depend to varying degrees on water generated in the Hindu-Kush-Himalayan (HKH) mountain ranges and at the same time have contrasting differences in terms of hydro-climatic and socio-economic characteristics. In a geopolitically complex region, the Indus (I), Ganges (G), and Brahmaputra (B) drain surface areas of around 1,116,000 km^2, 1,001,000 km^2, and 528,000 km^2, respectively, and traverse Afghanistan (I), Pakistan (I), India (I, G, B), China (I, G, B), Nepal (G), Bhutan (B), and Bangladesh (G, B). In this study, the IGB river system is subdivided into several upstream and downstream domains: the upper Indus Basin (UIB), upper Ganges Basin (UGB), upper Brahmaputra Basin (UBB), Lower Indus Basin (LIB), Lower Ganges Basin (LGB), and Lower Brahmaputra Basin (LBB). Thereby, the upstream domains are dominated by the mountainous terrains of the Tibetan Plateau and Hindu Kush-Himalayan mountain ranges with elevations up to ~8850 m above sea level, and the downstream domains are dominated by hilly regions and floodplains that are part of the Indo-Gangetic plains. The boundary between upstream and downstream domains is located at the southern margins of the Himalayan foothills and directly upstream of large reservoirs, such as the Tarbela and Mangla Dam reservoirs.

The Ganges river basin is the most densely populated basin, with a population density of about 580 inhabitants km^{-2}, and the Brahmaputra river basin is the least populated basin, with 131 inhabitants

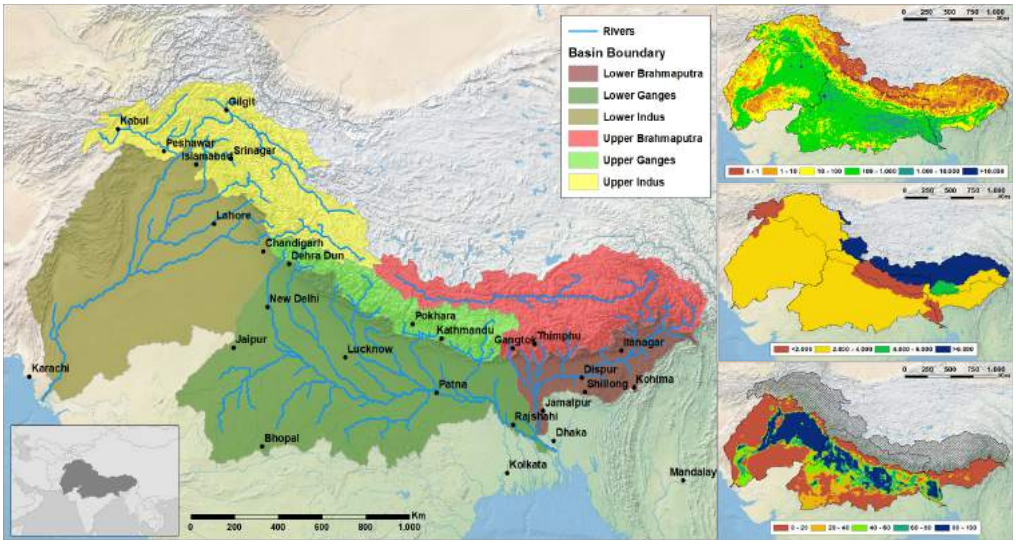

Figure 5.1. a) Map of study area showing the sub-basins and the largest cities in the region, b) the population density (inhabitants km^{-2}), c) the GDP (PPP) per capita per country (US$ inhabitant^{-1}), and d) the fraction of irrigated cropland (%). The source of the background imagery, the cities, and the political borders illustrated in the inlet is naturalearthdata.com. The source of the population density data is the HYDE v3.2 database (Klein Goldewijk et al., 2010). The GDP (PPP) per capita is derived from IIASA SSP database (IIASA, 2017). The fraction of the irrigated cropland is derived from the MIRCA2000 dataset (Biemans et al., 2016; Portmann et al., 2010).

km^{-2} (2016; Klein Goldewijk et al., 2010). India has the largest economy with a nominal GDP per capita of 1604 US$ yr^{-1}, whereas Nepal has the smallest economy with a nominal GDP per capita of 748 US$ yr^{-1} (International Monetary Fund, 2016). Water withdrawal (i.e. in South Asian countries) is highest in the agricultural sector (91%, corresponding with 913 km^3 yr^{-1}), followed by the domestic (7%, corresponding with 70 km^3 yr^{-1}) and industrial sectors (2%, corresponding with 20 km^3 yr^{-1}) (FAO, 2012). Much of the water withdrawn is used for the irrigated agricultural areas that are present in the IGB. Among the three river basins, the Ganges river basin has the largest irrigated area with 257,000 km^2 (i.e. situation in 2000), followed by the Indus river basin (213,000 km^2) and the Brahmaputra river basin (27,000 km^2) (Biemans et al., 2013). In the irrigated areas of the Indus and Ganges river basins, mainly cash crops, such as sugarcane, wheat, and rice are cultivated (FAO, 2012). Thereby, the annual production of sugarcane is highest with 431 Mt, followed by rice (233 Mt), and wheat (138 Mt) (2016; FAO, 2017).

The climate of the IGB river systems is mainly dominated by the East Asian and Indian monsoon systems, and the Westerlies. Westerlies are most dominant in the western part of the IGB with significant precipitation during the winter period. The East Asian and Indian monsoon systems become increasingly dominant when moving eastward causing most of the precipitation to occur during the monsoon season (June-September). In the Brahmaputra river basin, where the climate is mainly driven by the monsoon systems, 60-70% of the annual precipitation occurs during the monsoon season (Immerzeel, 2008). Annual precipitation amounts vary from less than 200 mm in the Thar desert (LIB) and the Tibetan Plateau (UIB) to more than 5000 mm in the floodplains of the

LBB (Lutz et al., 2018). The high-altitude regions of the HKH experience a cold climate with annual average temperatures down to -19 °C in the Karakoram (UIB), whereas the downstream domains experience mild winters and hot summers with annual average temperatures up to 28 °C at the southern margins of the LGB (Cheema and Bastiaanssen, 2010; Lutz et al., 2018; Wijngaard et al., 2017). Within the IGB two growing seasons are prevailing: the rabi season (November-April) and the kharif season (May-October) (Cheema et al., 2014; Portmann et al., 2010).

5.3 Data and methods

5.3.1 Definitions

Throughout this study, we use several terms, which we define as follows:

- **Blue water** is water that is withdrawn from surface water and groundwater bodies (surface water is defined as water withdrawn directly from rivers, lakes, and reservoirs, and groundwater is defined as water withdrawn from both shallow and deep aquifers, using (artificial) wells).
- **Green water** is water that is infiltrated into soils and that originated directly from precipitation.
- **Blue water availability** is the total amount of water available in rivers, reservoirs, and groundwater.
- **Blue water demand** is the total amount of blue water that is required for withdrawal by the agricultural, domestic, and industrial sectors.
- **Blue water consumption** is the total amount of blue water that is consumed (evapotranspiration in agriculture) by the agricultural (evapotranspiration), domestic, and industrial sectors (withdrawal minus return flows).
- **Blue water gap** is the amount of unsustainable groundwater that is withdrawn to fulfill the blue water demand. The blue water gap occurs when the mean annual groundwater withdrawal exceeds the mean annual groundwater recharge.

5.3.2 Modelling framework

We use a coupled modelling approach to simulate upstream water availability and downstream water supply and demand. To this end, two physically-based fully-distributed models are used: the cryospheric-hydrological Spatial Processes in HYdrology (SPHY) model (Terink et al., 2015) and an adjusted version of the (eco-)hydrological Lund-Potsdam-Jena managed Land (LPJmL) model (Biemans et al., 2013, 2016; Bondeau et al., 2007; Rost et al., 2008). SPHY and LPJmL are set up for a reference period (1981-2010) and a future period (2011-2100), and both run at a daily time step.

5.3.2.1 Upstream: SPHY

We use SPHY to simulate water availability from the upstream mountainous domains of the IGB. The SPHY model is developed specifically for the high mountain environment in Asia. The model runs at a spatial resolution of 5 km x 5 km and reports on a daily time step. SPHY has been used to assess climate change impacts for high mountain hydrology in Asia before (Lutz et al., 2014, 2016a; Wijngaard et al., 2017). The set up used was calibrated and validated using IceSat glacier mass

balance data (Kääb et al., 2012), MODIS snow cover data (Hall et al., 2002; Hall and Riggs, 2015), and observed discharge in a study on the impacts of climate change on hydrological extremes in the upstream domains of the IGB (Wijngaard et al., 2017). The model simulates daily discharge by calculating the amount of total runoff for each grid cell, and subsequently by routing the total runoff downstream by means of a simplified routing scheme that requires a digital elevation model (DEM) and a recession coefficient. Thereby, the total runoff is the sum of glacier runoff, snow runoff, surface runoff, lateral flow, and baseflow.

For the estimation of the contribution of glacier runoff, sub-grid variability (i.e. 1 km^2) is applied by determining the fractional ice cover in each cell, where fractional ice cover can range between 0 (no ice cover) and 1 (complete ice cover). Changes in fractional ice cover over time are modelled using an approach that considers mass conservation and ice redistribution (Terink et al., 2017). In addition to the determination of fractional ice cover, other information, such as initial ice thickness and the type of glacier (i.e. debris-free or debris-covered) is attributed to a unique identifier that is created for (a part of) each glacier within a model cell. The degree-day approach of Hock (2003) is used to simulate glacier melt, which is subsequently subdivided over the surface runoff and baseflow pathways by a calibrated glacier runoff fraction.

Those parts that are not covered by glaciers are covered by snow, bare soil, vegetation, or open water. For the snow-covered parts, the model of Kokkonen et al. (2006) is used to simulate snow storage dynamics. Snow accumulation and snowmelt is simulated by the degree-day approach of Hock (2003), whereas snow sublimation is estimated by a simple elevation-dependent potential sublimation function (Lutz et al., 2016a). Besides snow melt, accumulation, and sublimation, refreezing of snowmelt and rain are included as well. Rainfall runoff processes are simulated for those parts that are free of snow. Rain is subdivided over two pathways: i) a direct transport to the river network by surface runoff, or ii) an indirect transport to the river network via lateral flow or baseflow. For the simulation of soil water processes, processes as evapotranspiration, infiltration, and percolation are included. These processes are simulated for a topsoil and subsoil layer. For a more detailed description of SPHY we refer to Terink et al. (2015).

5.3.2.2 Downstream: LPJmL

The outflows of upstream domains that are simulated by SPHY are input to the hydrology and crop production model LPJmL, where water is withdrawn by users or continues its way downstream towards the Arabian Sea or the Bay of Bengal. LPJmL has an explicit representation of human interventions in the hydrological cycle that are relevant in the downstream domain, such as dynamic calculations of irrigation demand, withdrawal, and supply (Rost et al., 2008) as well as the operation of large reservoirs (Biemans et al., 2011). LPJmL has been applied to South Asia before (Biemans et al., 2013), but has recently been updated to represent the agricultural practice of multiple cropping with monsoon-dependent sowing dates (Biemans et al., 2016) and the distinction between different irrigation systems (Jägermeyr et al., 2015). The LPJmL model has been tested and validated for global applications, such as river discharge (Biemans et al., 2009), irrigation requirements (Rost et al., 2008), crop yields (Fader et al., 2010), and sowing dates (Waha et al., 2012). On a regional level, irrigation water withdrawals have been validated for India and Pakistan (Biemans et al., 2013, 2016). In this study, the model was further improved to represent groundwater withdrawal and depletion and the distribution of irrigation water through the extensive canal systems in the Indus and Ganges basins. Moreover, the resolution was increased to 5 arcmin x 5 arcmin.

LPJmL simulates daily discharge by 1) calculating the total amount of runoff generated for each grid cell as the sum of surface runoff, subsurface runoff, and baseflow, and 2) routing the total runoff downstream along a river network. Water enters a grid cell by precipitation and/or irrigation water and can be subdivided over two pathways: direct transport to the river network by surface runoff and indirect transport via infiltration and subsurface runoff or baseflow (Schaphoff et al., 2017). Groundwater reservoirs are recharged from the bottom soil layers. Water can be withdrawn from the groundwater reservoirs directly, or they contribute to baseflow through a delayed outflow parameterized by a linear reservoir model. Water can be removed from the grid cell by soil evaporation, plant transpiration, canopy interception, and percolation. Water can also be removed from the river network by lake or canal evaporation. For a more detailed description of LPJmL we refer to Rost et al. (2008) and Schaphoff et al. (2017).

In LPJmL, the daily irrigation water consumption is calculated for each grid cell as the minimum amount of additional water needed to fill the upper two soil layers to field capacity and the amount needed to fulfill the atmospheric evaporative demand (Rost et al., 2008). The gross irrigation demand (i.e. withdrawal) depends on the soil and the type of irrigation system that is installed. We assume that all irrigated areas in the IGB rely on flood irrigation (AQUASTAT; FAO, 2014), which is less efficient than sprinkler or drip irrigation systems (Jägermeyr et al., 2015). Daily water demand for other users (i.e. households and industry) is assumed to be constant throughout the year.

Water for irrigation and other uses can be withdrawn from surface water in a grid cell, surface water from a neighbouring grid cell or a canal system (i.e. if connected), an upstream reservoir build for water supply (i.e. if in place), and groundwater bodies. If long-term groundwater withdrawals exceed long-term groundwater recharge, the withdrawal is defined as unsustainable. In this study, we define the blue water gap as the mean annual groundwater depletion rate. Not all water that is withdrawn is consumed. Water can be lost during conveyance, by open water evaporation or as a return flow into the river network. After application to the field, again only part of the water will be used for evapotranspiration (blue water consumption), and the remaining part will recharge groundwater or discharge as return flow to the river.

5.3.3 Data

SPHY and LPJmL are forced with daily air temperature and precipitation fields from a dataset that is developed for the Indus, Ganges, and Brahmaputra river basins (Lutz and Immerzeel, 2015), which accounts for the underestimate of high altitude precipitation, which is common for gridded meteorological forcing datasets in the region (Immerzeel et al., 2015). The datasets are based on the Watch Forcing ERA-Interim (WFDEI) dataset (Weedon et al., 2014) and are bias-corrected and downscaled from a resolution of 0.5° x 0.5° to a resolution of 5 km x 5 km and 10 km x 10 km for the upstream and downstream domains, respectively. The LPJmL model is also forced with downward longwave and shortwave radiation, besides daily air temperature and precipitation fields. Downward shortwave radiation is not bias-corrected, since these datasets are corrected to observed cloud cover and by means of corrections for aerosol loadings (Weedon et al., 2010, 2011, 2014). For the application of the meteorological forcings in LPJmL the datasets were resampled to a resolution of 5 arcmin.

We use the 15 arcsec void-filled and hydrologically conditioned HydroSHEDS DEM (Lehner et al., 2008). For the use of the DEMs in SPHY the DEMs are resampled to 5 km x 5 km. LPJmL uses

the stream network from HydroSHEDS at 5 arcmin x 5 arcmin. Land use information in SPHY is extracted from the MERIS Globcover product (Defourny et al., 2007). In LPJmL, gridded crop fractions of 13 rainfed and irrigated crop classes for the two cropping seasons were derived from the MIRCA2000 dataset (Biemans et al., 2016; Portmann et al., 2010). For SPHY, soil information from the HiHydroSoil database (de Boer, 2016), which is a dataset of soil hydraulic properties derived from the Harmonized World Soil Database (FAO/IIASA/ISRIC/ISSCAS/JRC, 2012) using pedotransfer functions (Sarmadian and Keshavarzi, 2010). LPJmL soil classes were derived from the HWSD (Schaphoff et al., 2013).

Current 5 arcmin domestic and industrial water demand datasets are extracted from the PCR-GLOBWB model. In these datasets, water demands were estimated based on methods developed by Wada et al. (2011a, 2014). Domestic water withdrawals were derived by combining decadal and yearly population data (i.e. extracted from the HYDE v3.2. database (Klein Goldewijk et al., 2010) and the FAOSTAT database, respectively), country-specific per capita domestic withdrawal data (i.e. extracted from the FAO AQUASTAT database), and water use intensities. The water use intensities take country-specific economic and technological developments into account (Wada et al., 2011a). Hence, economic developments are based on changes in GDP, electricity production, energy and household consumption. Technological developments are derived as the energy consumption per unit of electricity production and accounts for domestic and industrial restructuring or improved water use efficiency (Wada et al., 2011a). Water use intensities are also used to derive industrial water withdrawal. Industrial water demands are assumed to remain constant throughout the year, whereas domestic water demands are assumed to vary throughout the year, depending on air temperature (Wada et al., 2010, 2011b). Not all the water that is withdrawn is consumed. A part of the water withdrawn for domestic and industrial purposes returns to the river network as return flows. The amount of return flow is calculated by means of recycling ratios that is depending on the country-specific GDP and level of economic development (Wada et al., 2011b).

5.3.4 Future climate and socio-economic development

To evaluate future changes in the water supply, demand, and gap due to climate change combined with socio-economic developments we use the RCP-SSP framework (van Vuuren et al., 2014). We force SPHY and LPJmL with an ensemble of downscaled GCM runs from the medium stabilization scenario RCP4.5 and the very high baseline emission scenario RCP8.5 (van Vuuren et al., 2011). From the CMIP5 multi-model ensemble (Taylor et al., 2012), we select four GCM runs for each RCP that represent the full CMIP5 ensemble in terms of projected ranges in the means and extremes of future air temperature and precipitation over the IGB region, and have sufficient skill to simulate historical climate conditions in the IGB (Lutz et al., 2016b). Subsequently, the selected models are downscaled using the reference climate data by applying a quantile mapping approach, which performs well in downscaling climate model data for floodplains as well as mountainous terrains (Themeßl et al., 2011). This method scales future GCMs down and bias-corrects them by means of empirical cumulative density functions that are calculated for the reference climate dataset and historical GCM runs (1981-2010).

For the representation of future socio-economic development, we select two SSP storylines (O'Neill et al., 2014, 2015; Riahi et al., 2017) that represent a "sustainability" scenario (SSP1) and a "fragmentation" scenario (SSP3). We choose to select SSP1 and SSP3, because these SSPs are most likely linked with RCP4.5 (i.e. RCP4.5-SSP1) and RCP8.5 (i.e. RCP8.5-SSP3) (van Vuuren

and Carter, 2014). Future 5 arcmin domestic and industrial water demand datasets are extracted from the IMAGE v3.0 model (Stehfest et al., 2014). Within the IMAGE model a sub-model (i.e. developed by Bijl et al., (2016)) is included, which calculates the future domestic and industrial water demands based on projections for population growth and economic development (based on GDP per capita) that are consistent with the selected SSPs. The projected population and GDP (PPP-purchasing power parity) changes for the IGB are summarized in Table 5.1 for SSP1 and SSP3.

Land use change scenarios that are consistent with the SSP storylines are calculated by integrated assessment models like IMAGE (Stehfest et al., 2014). IMAGE calculates land use change based on a set of SSP-specific assumptions regarding dietary changes and resulting per capita food demand, the level of intensification and potential yield increase on existing cropland, and changes in import and export of commodities. We use the SSP1 and SSP3 regional scale outcomes of IMAGE (Doelman et al., 2018) to derive changes in rainfed and irrigated cropland extents for Pakistan, India, Nepal, and Bangladesh between 2010 and 2100. Subsequently, we project those changes on our gridded datasets of current kharif and rabi cropped areas to construct transient datasets of land use change in the IGB. These gridded datasets are used in combination with the climate change datasets to estimate future water requirements for irrigation. We assume that both the crop distribution and crop types remain as they are. This implies that they are not adapted when crop growth conditions become unfavourable (e.g. due to changing climate conditions). It is beyond the scope of this study to investigate the impact of climate change adaptation of agricultural practices on irrigation water requirements and related impacts on the blue water gap.

5.3.5 Analysis of environmental flows

To assess the impacts of (blue) water consumption on environmental flow transgressions we estimate EFRs according to the variable monthly flow (VMF) method of Pastor et al. (2014). The VMF method is a valid method that considers intra-annual variability in streamflow and correlates well with locally calculated EFRs. The EFRs are calculated on a monthly basis by using the discharge at the river outlets of the Indus, Ganges, and Brahmaputra under naturalized conditions (i.e. without withdrawals for irrigation and other users). First, the mean annual flows (MAFs) and mean monthly flows (MMFs) are calculated for the reference (1981-2010) and far-future periods (2071-2100). The MAFs and MMFs are then used to determine low-flow (MMF≤0.4·MAF), high-flow (MMF>0.8·MAF), and intermediate flow seasons (MMF>0.4·MAF & MMF ≤ 0.8·MAF). Based on the seasonal classification, EFRs are subsequently calculated where the EFR is set equal to 60%,

Table 5.1. Projected basin-aggregated population counts and GDP (PPP = Purchasing Power Parity) for SSP1 and SSP3. The population counts are extracted from the HYDE v3.2 database (Klein Goldewijk et al., 2010). The GDP (PPP) is a product of the population counts and the country-specific GDP (PPP) per capita, which is derived from the IIASA SSP database (IIASA, 2017) as the ensemble mean of the IIASA GDP and OECD Environmental Growth models.

Basins	Countries	Population (x 10^6)			GDP (PPP) (x 10^9 US$2005)		
		2010	2050	2100	2010	2050	2100
Indus	AF, CN, IN, PK	245	346/469	289/725	631	5124/2894	14574/7191
Ganges	BD, CN, IN, NP	494	629/804	466/1073	1410	14276/8782	28796/15198
Brahmaputra	BD, BT, CN, IN	65	81/101	58/129	165	1601/952	3299/1689

45%, and 30% of the MMF during low, intermediate, and high-flow seasons, respectively. Finally, the discharge impacted by anthropogenic water withdrawals (i.e. with irrigation and full access to groundwater) is compared with the EFRs to assess whether environmental flows are met or not.

5.4 Results and discussion

5.4.1 Future climate change

In the IGB, both temperature and precipitation are projected to change towards the end of the 21st century. Figure 5.2 shows the projected annual and seasonal temperature and precipitation changes in the IGB for RCP4.5 and RCP8.5, at the end of the 21st century. On an annual basis, temperature is projected to increase by 1.5-2.9 °C for RCP4.5 and 2.8-5.2 °C for RCP8.5, with respect to the reference period (1981-2010). The largest increases are projected in the western and north-western parts of the Indus river basin (i.e. in the Hindu Kush and Karakoram mountain ranges) and on the Tibetan Plateau. The large temperature increases in these regions can most likely be attributed to elevation-dependent warming, which causes a stronger warming in the high-altitude upstream regions in comparison with the lower-lying downstream regions (Palazzi et al., 2016; Pepin et al., 2015). Precipitation is, in general, projected to increase by increases up to about 200% for RCP4.5 and up to about 100% for RCP8.5. Thereby, the largest increases are projected in the southernmost parts of the Indus river basin, which is a region where the amount of precipitation is relatively low (less than 300 mm yr^{-1}) and thus small absolute increases can result in large relative increases. In the same region, the range in model projections is also large. Besides precipitation increases, precipitation decreases are also projected. These decreases are mainly projected to occur in the westernmost part of the Indus river basin. On seasonal basis, the projected temperature changes do not show large seasonal differences. The main difference can be found between the projections made for RCP4.5 and RCP8.5 with temperature differences up to about 2 °C between RCP4.5 and RCP8.5. The projected precipitation changes show large seasonal differences. For RCP4.5, the largest and smallest increases are, in general, projected during post-monsoon and pre-monsoon/winter, respectively. During the pre-monsoon and winter seasons even a decrease in precipitation is projected in the UIB (~-1%) and UGB (~-5%), respectively. For RCP8.5, precipitation increases are, in general, largest during the post-monsoon period. During pre-monsoon, precipitation decreases are also projected in the UIB (~-4%). The range in model projections is especially large during the post-monsoon and winter seasons.

5.4.2 Blue water availability

In the IGB, the seasonal and spatial variability of surface water availability is quite large. Figure 5.3 shows the seasonal surface water availability (i.e. natural runoff) for the reference period (1981-2010) in the upstream and downstream domains of the IGB as simulated by SPHY and LPJmL. The surface water availability is generally largest during the monsoon season (Figure 5.3c), varying from less than 100 mm yr^{-1} in the floodplains of the Indus (LIB) to more than 3500 mm yr^{-1} in the mountainous upstream domains of the Ganges and Brahmaputra. In these domains, the large surface water availability can mainly be attributed to the combined contributions from ice and snowmelt, and monsoon precipitation that can reach amounts over 3000 mm yr^{-1} at the southern margins of the UGB and UBB (Wijngaard et al., 2017). During the winter season (Figure 5.3a) the surface water availability is generally lowest with rates less than 100 mm yr^{-1} in most regions of the IGB. Water availability is generally higher than 100 mm yr^{-1} in the LBB and directly south of the Himalayan arc. The higher surface water availability in these regions can likely be explained by the release of

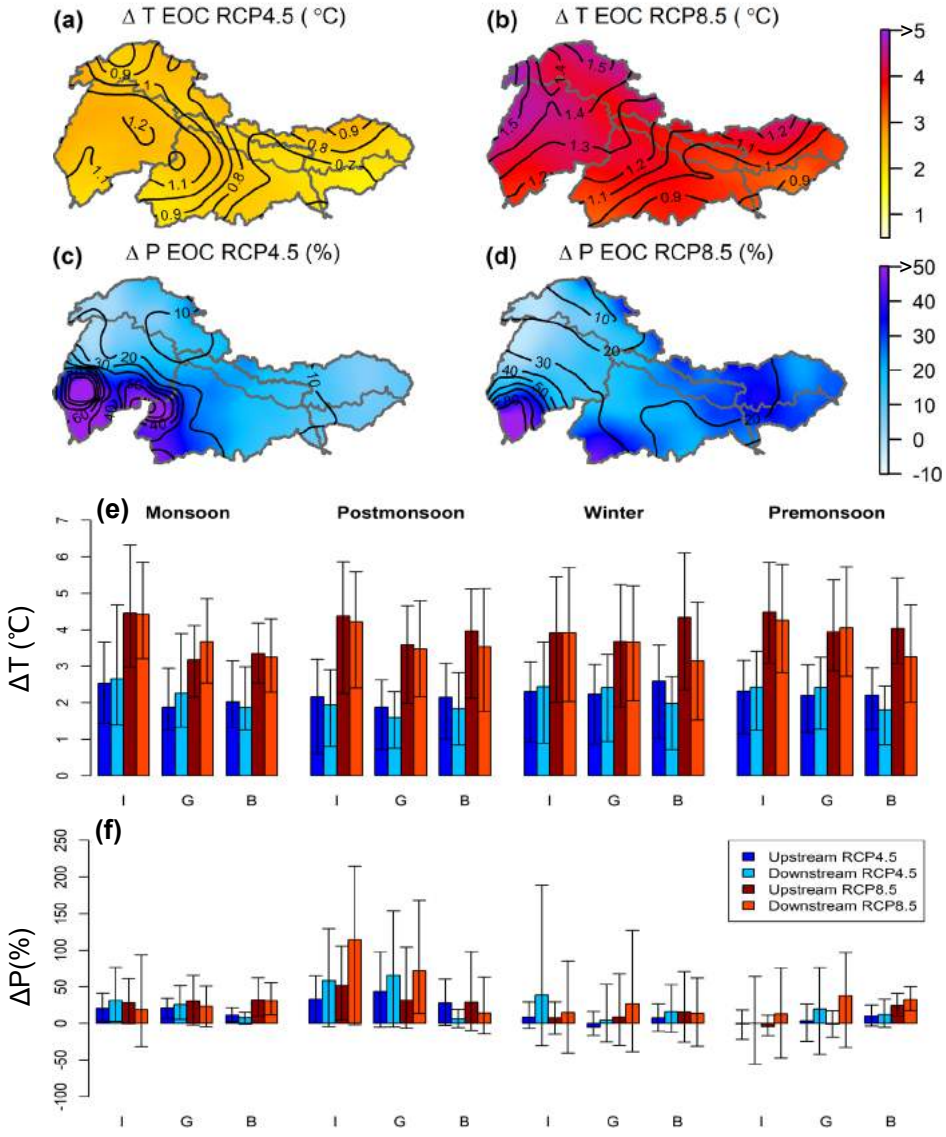

Figure 5.2. Maps showing the annual changes in temperature (a, b) and precipitation (c, d) between 2071-2100 and 1981-2010 for RCP4.5 and RCP8.5. The bar plots show seasonal changes in temperature (e) and precipitation (f) in the upstream and downstream domains of the IGB for RCP4.5 and RCP8.5. The contour lines within the maps and the error bars within the bar plots denote the ensemble range of the projections.

groundwater from aquifers that have been recharged during the monsoon season. A similar pattern can also be recognized for the same regions during the pre-monsoon (Figure 5.3b) and post-monsoon seasons (Figure 5.3d). During the pre-monsoon season surface water availability can reach up to about 1000-1500 mm yr^{-1} in the HKH mountain ranges, which can be attributed to snowmelt.

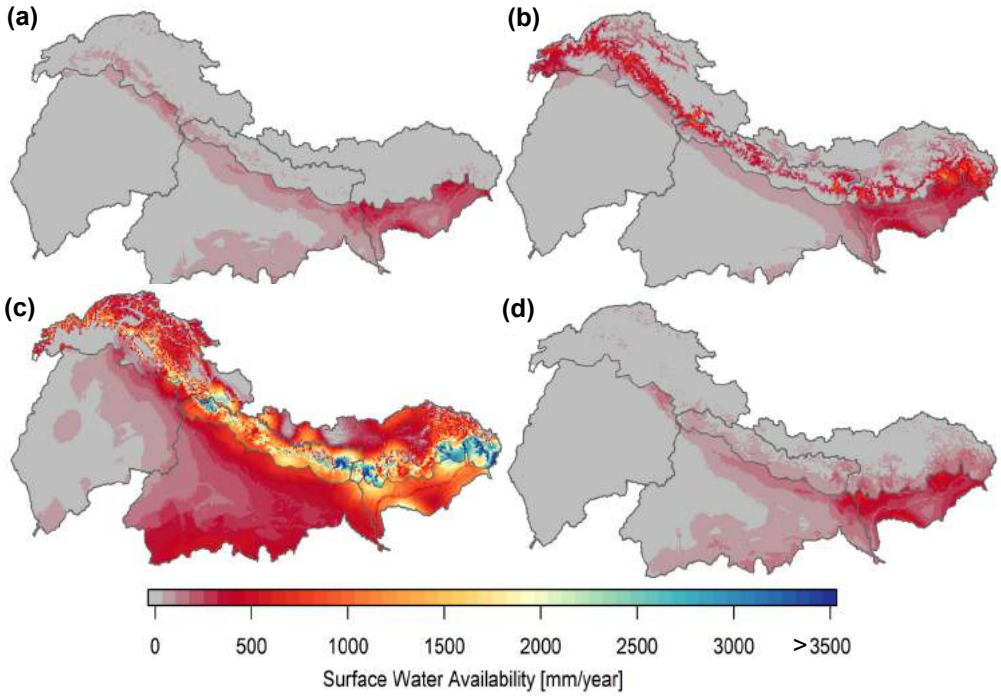

Figure 5.3. Maps showing the surface water availability in winter (a), pre-monsoon (b), monsoon (c), and post-monsoon (d) seasons.

Future water availability is expected to increase as a result of climate change. Figure 5.4 shows the current and future monthly surface water availability for the up- and downstream domains of the IGB under current (1981-2010), mid-future (2041-2070; MOC-mid 21st century), and far-future (2071-2100; EOC-end of the 21st century) climate conditions. Surface water availability is projected to increase for both RCP4.5 and RCP8.5 in the entire IGB. Similar trends have also been found in other studies conducted in (a part of) the IGB (Immerzeel et al., 2010; Lutz et al., 2014; Masood et al., 2015; Nepal, 2016). The increases in surface water availability are projected to be stronger during the monsoon season, which can likely be attributed to increases in monsoon precipitation (Figure 5.2) and increases in ice melt. The increases in melt (i.e. especially ice melt) are a likely reason that the natural runoff peaks in the upstream domains of the Ganges and Brahmaputra are projected to shift from July to August. Furthermore, increases are stronger for RCP8.5, with the exception of the Indus basin, where an opposite trend can be observed. The opposite trend can mainly be attributed to the reduction in snowmelt towards the end of the 21st century, which is most likely caused by the stronger temperature increases in the Indus basin (Figure 5.2), leading to a higher fraction of precipitation to fall as rain. The range among model runs is large, especially for RCP8.5, which indicates that uncertainty in future water availability projections is large, especially in the upstream mountainous domains. The graphs further show that, under current and future conditions, there is a clear upstream-downstream difference in the amount of water that is available in the Indus and Ganges, with significantly larger amounts of water available in the upstream domains. In the Brahmaputra basin, the upstream-downstream difference is smaller, which can be attributed to the East Asian monsoon systems that have a high intensity in the floodplains of the Brahmaputra. The

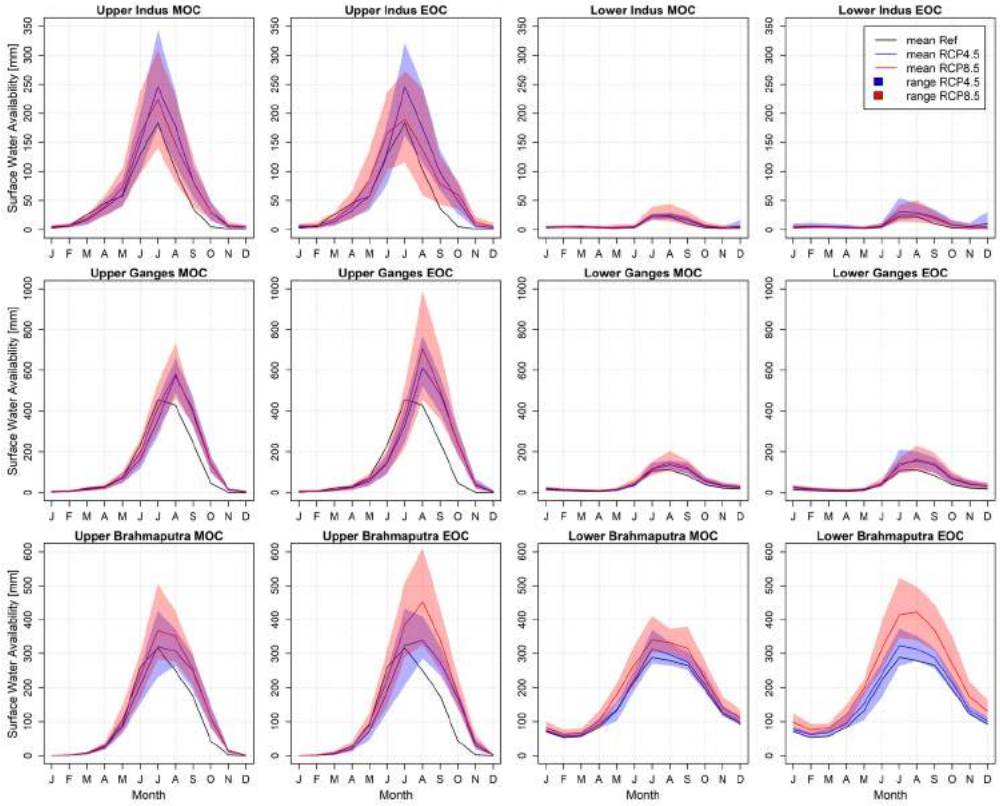

Figure 5.4. Plots showing the mean monthly blue water availability for the reference (1981-2010) and future periods (mid-century, MOC, 2041-2070; end of century, EOC, 2071-2100) under RCP4.5 (blue) and RCP8.5 (red). The coloured bands represent the range of ensemble projections that are resulting from forcing the SPHY and LPJmL models with the different climate models.

upstream-downstream differences in surface water availability indicate the significance of upstream water resources for the floodplains that are located downstream. In the future, it is projected that the upstream-downstream difference will be enhanced, implying that the dependency on upstream mountain water resources will increase.

5.4.3 Blue water consumption

Irrigation is by far the largest water consumer in the IGB. Figure 5.5 shows the annual and seasonal blue water consumption for irrigated croplands and the combined blue water consumption for domestic and industrial sectors. The maps indicate that the irrigation water consumption is largest in the Punjab and Haryana provinces (i.e. in northern part of the LIB and western part of the LGB), with consumption rates that reach over 600 mm yr^{-1} on an annual basis. In the Sindh province (i.e. located in the delta plains of the Indus) and along the Ganges river consumption rates are also high. The difference in water consumption between the rabi (winter) and kharif (monsoon) seasons is limited in the Indus river basin, whereas in the Ganges and Brahmaputra river basins the water consumption during the rabi season is significantly higher at most of the croplands than

during the kharif season. The seasonal differences are a result of rainfall patterns in the IGB. In the Ganges and Brahmaputra river basins, the Indian and East Asian monsoon systems prevail, which means that sufficient green water is available and thus (blue water) irrigation is less concentrated during the kharif season (Biemans et al., 2016). In the Indus river basin, the influence of monsoon systems is smaller, which means more irrigation is required to fulfill the crop demands. However, during the rabi seasons the amount of precipitation is limited, which also means (blue water) irrigation is required in the Ganges and Brahmaputra river basins. In comparison to irrigation, the water consumption in the domestic and industrial sectors is almost negligible. In most areas, the consumption rates are less than 100 mm yr^{-1}. Only in the larger urban areas, such as New Delhi, Islamabad, Lucknow, and Jaipur (location, Figure 5.1), the consumption rates can reach up to 380 mm yr^{-1}.

As a result of climate change and/or socio-economic developments, blue water consumption is projected to change into the future. Figure 5.6 shows the projected changes in the annual blue water consumption for irrigated croplands and other users (i.e. domestic and industrial sectors) for RCP4.5, RCP8.5, RCP4.5-SSP1, and RCP8.5-SSP3. Under current conditions (i.e. REF, 1981-2010), the total blue water consumption is largest in the Indus river basin, with a total rate of 145 km^3 yr^{-1}, of which 138 km^3 yr^{-1} (~95%) is consumed on irrigated croplands and 7 km^3 yr^{-1} (~5%) is consumed by domestic and industrial sectors. The total blue water consumption is smallest in the Brahmaputra river basin, with a total rate of 5 km^3 yr^{-1} of which 4 km^3 yr^{-1} (~80%) is consumed

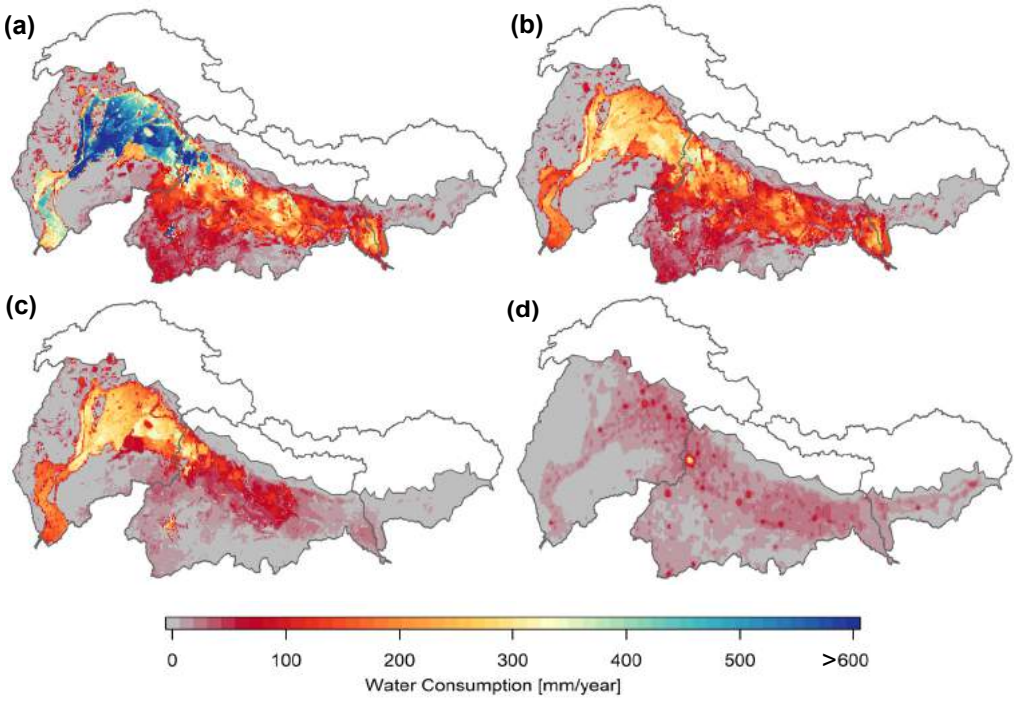

Figure 5.5. Maps showing the blue water consumption for irrigated croplands (a-c) and other users (i.e. domestic + industrial) (d). The irrigation water consumption is given on an annual basis (a), and for the rabi (b) and kharif seasons (c). The domestic + industrial water consumption is given on an annual basis.

on irrigated croplands and 1 km^3 yr^{-1} (~20%) is consumed by domestic and industrial sectors. The differences in total water consumption among the basins are due to the Indus river basin agriculture being dominated by irrigated croplands (Figure 5.1d), whereas in the Brahmaputra river basin agriculture is dominated by rainfed croplands. In addition, the LIB covers a larger area than the LBB, which eventually results in larger consumption rates when aggregating the grid values within a basin. Future total water consumption is projected to change. When only considering climate change, there will be no change in domestic and industrial water consumption. Irrigation water consumption is projected to decrease from 138, 91, and 4 km^3 yr^{-1} up to about 116, 69, and 3 km^3 yr^{-1} in the LIB, LGB, and LBB respectively for RCP8.5, at the end of the 21st century. This trend can be explained by growing seasons that become shorter for most crops due to temperature increases. The shorter growing seasons mean that less water is demanded and thus less water is consumed. In addition, precipitation is projected to increase (Figure 5.2), which means more green water will be available and less (blue water) irrigation is required. When considering future climate change and socio-economic developments, an increase in the total water consumption is projected with mean relative increases up to about 36% yr^{-1}, 60% yr^{-1}, and 147% yr^{-1} in the LIB, LGB, and LBB respectively for RCP8.5-SSP3, at the end of the 21st century. The increasing total water consumption can mainly be attributed to increasing domestic and industrial water consumption that emerge from population growth and economic development. Their increase ranges from 283% to 311% for RCP4.5-SSP1 and from 586% to 715% for RCP8.5-SSP3, at the end of the 21st century, indicating that domestic and industrial water consumption will be a significant component of the South Asian future water balance. Compared to the reference period there is, however, a slight decrease in irrigation water consumption projected, although the decreases are smaller than those for the runs considering climate change only, which is due to the expansion of irrigated croplands under the SSPs. Only for RCP8.5-SSP3 is a slight increase in the irrigation water consumption projected at the end of the 21st century.

Figure 5.7 shows the monthly projected changes in the total blue water consumption for RCP4.5, RCP8.5, RCP4.5-SSP1, and RCP8.5-SSP3. Under current climate conditions, two peaks in the total water consumption can be recognized in the Indus river basin, which coincide with the rabi and kharif crop seasons. In the Ganges and Brahmaputra river basins, the total water consumption is highest during the rabi season, but also smaller peaks can be recognized that coincide with the kharif season. Considering climate change only, the total water consumption is projected to decrease slightly throughout the entire year in the Indus river basin, with exception of the post-monsoon season, when a slight increase is projected. In the Ganges river basin, the total water consumption is projected to decrease during the second half of the rabi season, whereas during the first half of the rabi and kharif seasons the total water consumption is projected to increase slightly. These trends are also projected for the Brahmaputra river basin, with the exception of the second half of the kharif season, where a slight increase in total water consumption is also projected, though the projected increases are smaller than for the first half of the kharif season. The projected increases can most likely be explained by increasing temperatures (Figure 5.2) that enhance the atmospheric evaporative demand. The increasing atmospheric evaporative demand results in higher crop evapotranspiration and thus higher irrigation water consumption. Because growing seasons are projected to become shorter in the IGB and precipitation is projected to increase (Figure 5.2), total water consumption will eventually decrease in the second half of the rabi season, and also for RCP8.5 in the second half of the kharif season. The projected increases during the second half of the kharif season in the Brahmaputra river basin can likely be explained by increasing temperatures that

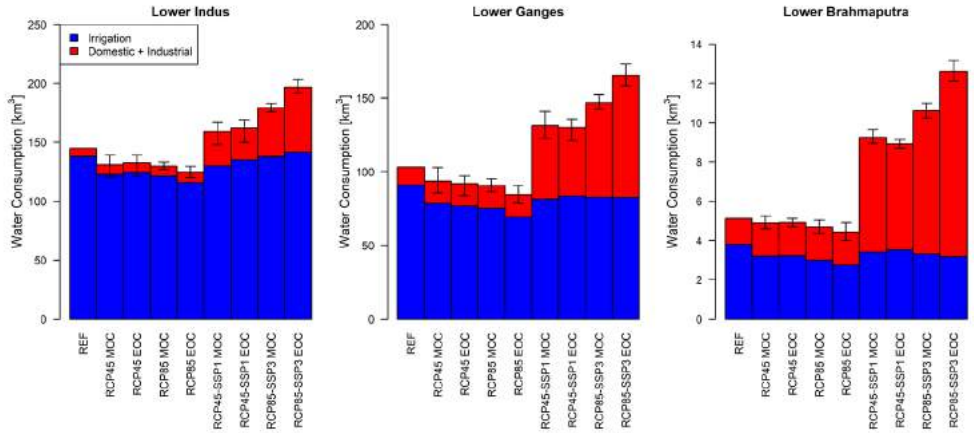

Figure 5.6. Projected changes in the annual blue water consumption for irrigated croplands and other users (i.e. domestic + industrial) for RCP4.5, RCP8.5, RCP4.5-SSP1, and RCP8.5-SSP3. The projected changes are given for the mid-21st century and end of the 21st century (MOC and EOC) and represent the ensemble mean. The error bars denote the range of the ensemble projections.

are smaller in the downstream domains of the Brahmaputra river basin than in other downstream domains (Figure 5.2). Due to the smaller temperature increases, the growing seasons show a smaller decline, and therefore the higher evapotranspiration rates emerging from temperature increases as well might outweigh the effect of shorter growing seasons, which eventually results in a slight increase in total water consumption. In the entire IGB, the water consumption for RCP8.5 is projected to be lower than for RCP4.5, which can most likely be attributed to the precipitation increases that are larger for RCP8.5 and thus cause blue water irrigation to be lower for RCP8.5 than for RCP4.5. When considering both climate change and socio-economic development, the total water consumption is projected to increase, where the largest increases are projected for RCP8.5-SSP3. Thereby, the difference in projected increases between the mid of the 21st century (MOC) and the end of the 21st century (EOC) are especially large for RCP8.5-SSP3, which can be explained by the extensive population growth that is projected at the end of the 21st century for SSP3 (Table 5.1). This eventually results in a larger increase in domestic water consumption. Further, the difference in projected increases between the RCP-SSP model runs and the reference model runs is especially large in the Brahmaputra river basin, which can be explained by the strong increases in domestic and industrial water consumption. For instance, for RCP8.5-SSP3 a relative increase of 619% is projected in domestic and industrial water consumption at the end of the 21st century. Although the difference between projected relative increases in the Indus and Ganges river basins (i.e. 715% and 586%, respectively) is not large, the impact is higher since the domestic and industrial sectors have a higher contribution in the total water consumption (i.e. ~20% for the reference period) in comparison with the Indus and Ganges river basins (i.e. ~5% and ~12%, respectively).

5.4.4 Blue water gap

Climate change is projected to have a mitigating effect on the future South Asian water gap, whereas socio-economic development is projected to have an enhancing effect on the water gap. Figure 5.8 shows the projected changes in the annual and seasonal blue water demand and supply for RCP4.5, RCP8.5, RCP4.5-SSP1, and RCP8.5-SSP3. In addition, Table 5.2 lists the ensemble mean, minimum,

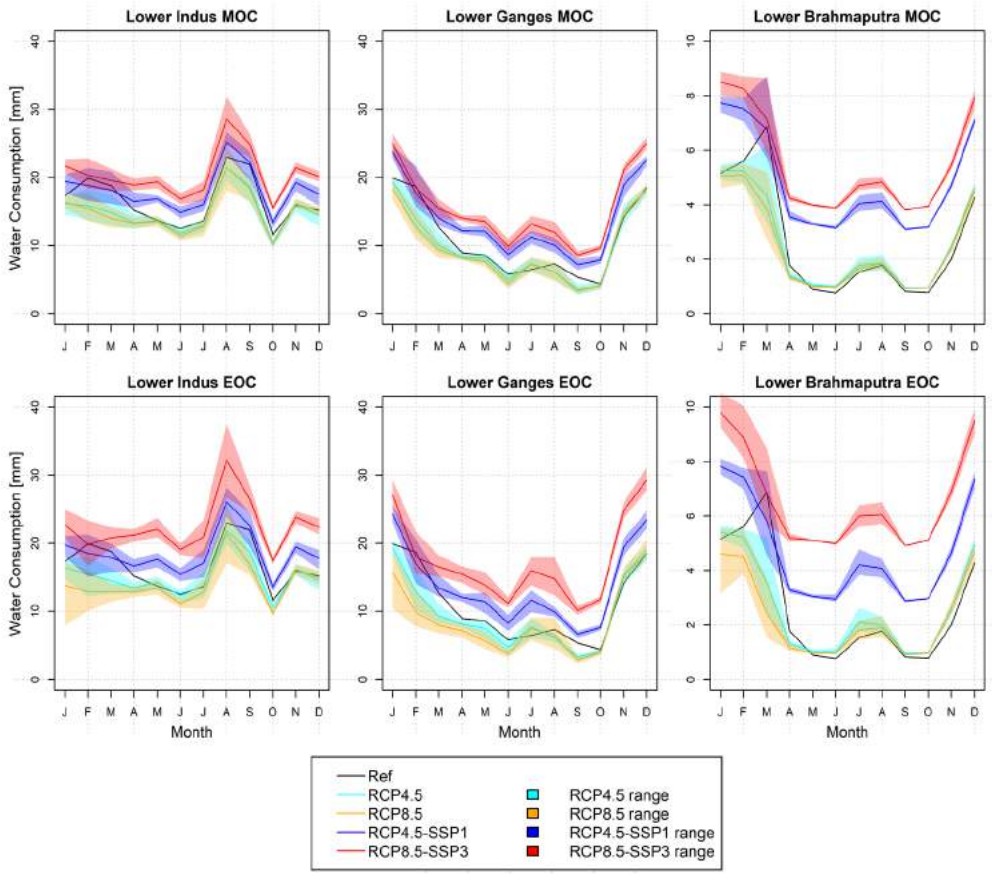

Figure 5.7. Monthly projected changes in the total water consumption for RCP4.5, RCP8.5, RCP4.5-SSP1, and RCP8.5-SSP3. The projected changes are given for the mid-21st century and end of the 21st century (MOC and EOC). The coloured bands represent the range of ensemble projections that are resulting from forcing the LPJmL model with the different climate models.

and maximum of the projected relative changes in the annual and seasonal blue water gap for the end of the 21st century (i.e. EOC). Under current climate conditions, the total demand is largest in the Indus river basin, with 767 km^3 yr^{-1}, and smallest in the Brahmaputra river basin, with 15 km^3 yr^{-1}. Most of the blue water supply consists of surface water (~67% in the Indus and ~93% in the Brahmaputra). The other part consists of sustainable and unsustainable groundwater. The latter is defined as the blue water gap or the unmet demand, assuming that any unmet demand is covered by additional groundwater abstractions. The unmet demand is largest in the Indus river basin with 83 km^3 yr^{-1} (~11% of total demand), followed by the Ganges river basin with an unmet demand of 35 km^3 yr^{-1} (~11% of total demand, Table 5.2). The simulated unmet demand in the Ganges river basin falls in range with reported historical values in other studies (Jacob et al., 2012; Richey et al., 2015; Rodell et al., 2009; Tiwari et al., 2009). The simulated unmet demand in the Indus river basin is more difficult to compare due to the limited amount of studies reporting groundwater depletion. Cheema et al., (2014) reports a groundwater depletion rate (i.e. unmet demand) of 31 km^3 yr^{-1},

which is lower than the simulated groundwater depletion rate in our study. The difference can mainly be explained by the fact that in our study the domestic and industrial sectors are also able to abstract groundwater, which consequently results in larger depletion rates. In the Brahmaputra river basin, no blue water gap is simulated, because all demands can be sustained by surface water and renewable groundwater. In the Indus river basin, the seasonal demand, supply, and gap are largest during the monsoon and melting season, which coincides with the prevailing growing season, the kharif. In the Ganges and Brahmaputra river basins, the seasonal demand, supply, and gap (i.e. only in the Ganges river basin) are largest during the winter, which coincides with the rabi season. Assuming climate change without socio-economic development, demand and supply are projected to decrease in all basins on an annual basis, and in general during the winter, pre-monsoon, and monsoon seasons for RCP4.5 and RCP8.5. During the monsoon (i.e. only in the Brahmaputra river basin) and post-monsoon seasons, demand and supply are projected to increase. The water gap is projected to decrease under all circumstances, with mean annual relative decreases of up to 37% and 55% (Table 5.2) in the Indus and Ganges river basins, respectively, for RCP8.5, at the end of the 21st century. On a seasonal basis, the largest mean relative decreases are projected during the winter season with relative decreases of up to 52% and 66% (Table 5.2) in the Indus and Ganges river basins, respectively, for RCP8.5, at the end of the 21st century. The decreasing demand (met and unmet) and supply can mainly be explained by shorter growing seasons that emerge from temperature increases, and increasing precipitation that result in a shift from blue water irrigation to green water or rainfed irrigation. The increases in monsoon and post-monsoon (i.e. first half of the kharif (monsoon) and rabi (post-monsoon) seasons) seasons can likely be explained by enhanced atmospheric evaporative demands and resulting increases in crop evapotranspiration that emerge from temperature increases. Despite the increases in demand, the water gap is projected to decrease, which can mainly be explained by the higher surface water availability (Figure 5.4) that eventually result in lower unsustainable groundwater withdrawals and thus a smaller water gap. Climate change and socio-economic developments combined result, on an annual basis, in increasing water supply and demand in the Brahmaputra and Ganges river basins for all RCP-SSP scenarios. In the Indus river basin, only increases are projected for RCP8.5-SSP3. For RCP4.5-SSP1, demand and supply slightly decrease. The reason for the decreasing trend is that the (relative) increase in domestic and industrial water consumption is limited in comparison with those projected under RCP8.5-SSP3 and other basins, which, in combination with declining irrigation water demand, eventually results in decreasing water demand and supply. The future water gap tends to increase for RCP8.5-SSP3 in the Indus and Ganges river basins with annual relative increases up to 7% and 14%, respectively, at the end of the 21st century (Table 5.2). On a seasonal basis, the relative increases are largest during the monsoon season with increases up to 30% and 55% in the Indus and Ganges river basin, respectively. For RCP4.5-SSP1 the gap decreases, since the declining irrigation water withdrawals are not outweighed by the increases in domestic and industrial water consumption.

This might also explain why the water gap for RCP8.5-SSP3 is projected to decline during the winter season. Finally, the changing water demands result in changing shares of the different sectors in the total water demand, which is especially striking during the pre-monsoon season in the Brahmaputra river basin. Due to a combination of increasing domestic and industrial water demand, and declining irrigation water demand (which is especially large during pre-monsoon in this basin) the domestic and industrial sectors are eventually projected to become the largest contributors to the total water demand. The projected mean relative changes in the blue water gap are accompanied by a large range in model outcomes that are generated for the different climate models, whether or not

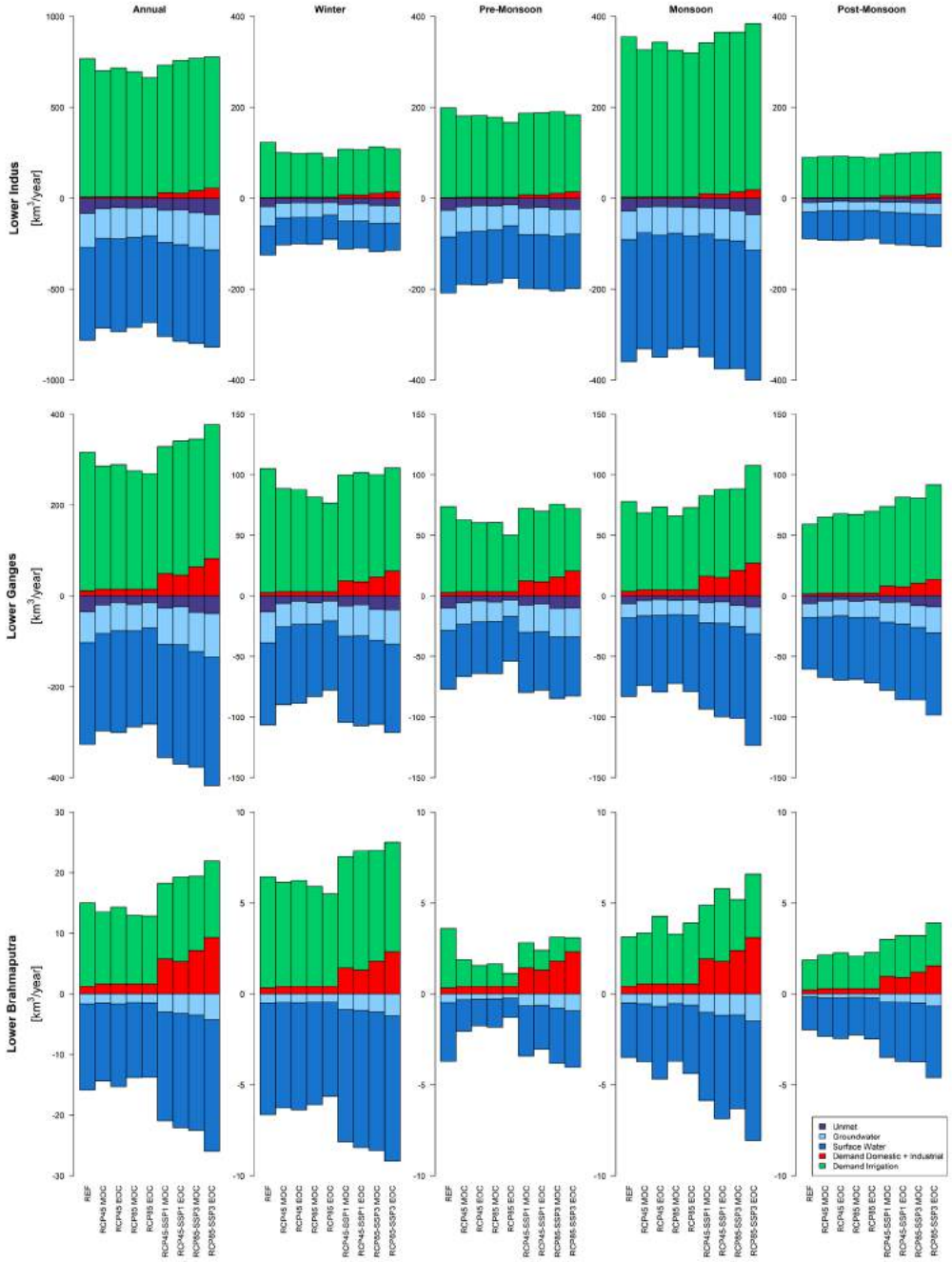

Figure 5.8. Projected changes in the annual and seasonal blue water demand and supply for RCP4.5, RCP8.5, RCP4.5-SSP1, and RCP8.5-SSP3. The projected changes are given for the mid-21st century and end of the 21st century (MOC and EOC).

Table 5.2. Projected changes in the annual and seasonal blue water gap of the Indus and Ganges river basins under present (1981-2010) and far-future (2071-2100; EOC) conditions for RCP4.5, RCP8.5, RCP4.5-SSP1, and RCP8.5-SSP3. The values between the parentheses represent the minimum and maximum projected changes in the blue water gap. The colours indicate the number of model runs (i.e. normal font: 3 or more runs; bold font: 2 runs; bold italic font: 1 run) that project the same sign of change as the projected mean change.

Basin	Scenario	Annual	Winter	Pre-monsoon	Monsoon	Post-monsoon
Indus	REF (km^3)	83	19	27	28	10
	RCP45 EOC (%)	-36 (-59/-19)	-47 (-70/-32)	-35 (-61/-18)	-32 (-53/-13)	-33 (-54/-13)
	RCP85 EOC (%)	-37 (-52/-15)	-52 (-59/-35)	-44 (-49/-35)	-23 (-58/14)	-29 (-44/-10)
	RCP45-SSP1 EOC (%)	-21 (-50/1)	-31 (-60/-11)	-21 (-53/0)	-16 (-42/7)	-15 (-42/9)
	RCP85-SSP3 EOC (%)	**7 (-18/42)**	-11 (-25/19)	-9 (-16/5)	**30 (-27/91)**	**18 (-8/48)**
Ganges	REF (km^3)	35	13	10	6	6
	RCP45 EOC (%)	-52 (-85/-26)	-61 (-89/-41)	-51 (-86/-23)	-44 (-82/-19)	-41 (-81/-8)
	RCP85 EOC (%)	-55 (-73/-23)	-66 (-78/-38)	-63 (-73/-45)	-39 (-72/14)	-34 (-64/10)
	RCP45-SSP1 EOC (%)	-23 (-74/16)	-37 (-79/-4)	-23 (-74/19)	**-9 (-66/28)**	**-8 (-67/41)**
	RCP85-SSP3 EOC (%)	**14 (-26/82)**	-11 (-40/49)	***1 (-23/44)***	**55 (-17/165)**	**50 (-11/131)**

they are generated in combination with SSP projections (Table 5.2). The large range in outcomes can mainly be attributed to the large spread in possible futures that are currently projected by climate models. For the RCP combinations and RCP4.5-SSP1, the decreasing trend is present. For RCP8.5-SSP3, however, the trend is less clear with projected increases for some GCM-SSP combinations and projected decreases for other combinations. The mean of the outcomes for RCP8.5-SSP3 indicate, however, that the blue water gap will increase and that climate change cannot compensate for the large projected changes in water demand anymore.

Figure 5.9 shows the spatial distribution of current groundwater depletion (i.e. indicator for the blue water gap) and future absolute changes in groundwater depletion for RCP4.5, RCP8.5, RCP4.5-SSP1, and RCP8.5-SSP3. Under current conditions, groundwater depletion is largest in the Punjab and Haryana provinces, with depletion rates of around 1000 mm yr^{-1} in the irrigated areas. In urban areas, such as New Delhi, depletion rates can even reach up to about 2000-2500 mm yr^{-1}. Also in the Sindh province, the water gap is large, with depletion rates in the range 300-350 mm yr^{-1}. The simulated depletion rates in the irrigated areas of the Indus river basin are similar with those that were found by Cheema et al. (2014). For RCP4.5 and RCP8.5, in general less groundwater depletion is projected, which is mainly caused by the declining irrigation blue water withdrawal and consumption. For both RCP-SSP combinations, depletion is expected to decrease in the irrigated croplands, whereas in the urban areas (e.g. New Delhi) depletion is projected to increase by more than 200 mm yr^{-1} (i.e. corresponding with a relative increase of more than 150%). For RCP8.5-SSP3, areas located in the Sindh province, and west of the Indus river are also expected to experience more depletion, due to population growth and economic development.

5.4.5 Environmental flows

The future socio-economic developments and associated increases in blue water consumption are expected to have a limited impact on environmental flow transgressions. Figure 5.10 shows the ensemble mean and range of the projected changes in EFRs and anthropogenically influenced discharge at the outlets of the Indus, Ganges and Brahmaputra under present and far-future (EOC)

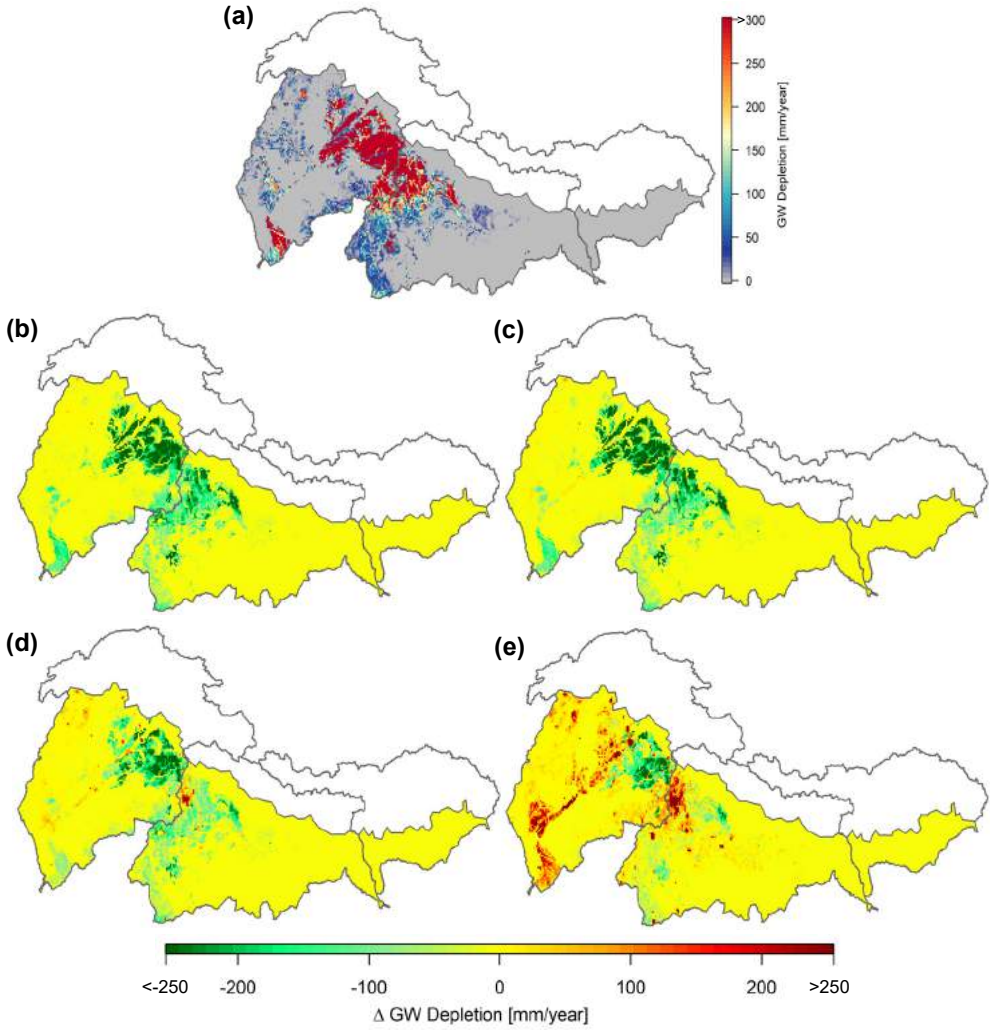

Figure 5.9. Maps showing the annual groundwater depletion for the reference period (a) and the projected changes in groundwater depletion for RCP4.5 (b), RCP8.5 (c), RCP4.5-SSP1 (d), and RCP8.5-SSP3 (e). The projected changes are given for the end of the 21st century. Green indicates less depletion and red indicates more depletion.

RCP-SSP conditions. Under current conditions, EFRs in the Indus, Ganges, and Brahmaputra are generally not met during the low-flow season (i.e. winter, pre-monsoon, and post-monsoon), whereas during the monsoon season EFRs are met. The combination of high unmet demands in the Indus river basin (Figure 5.8) on the one hand and sustained EFRs on the other can be explained by the absence of water shortages during the monsoon season due to the higher surface water availability. During the low-flow season, however, the surface water availability is low, which eventually results in EFRs and water demands not being met and high competition between different water users occurring. Future projections indicate that both EFRs and anthropogenically

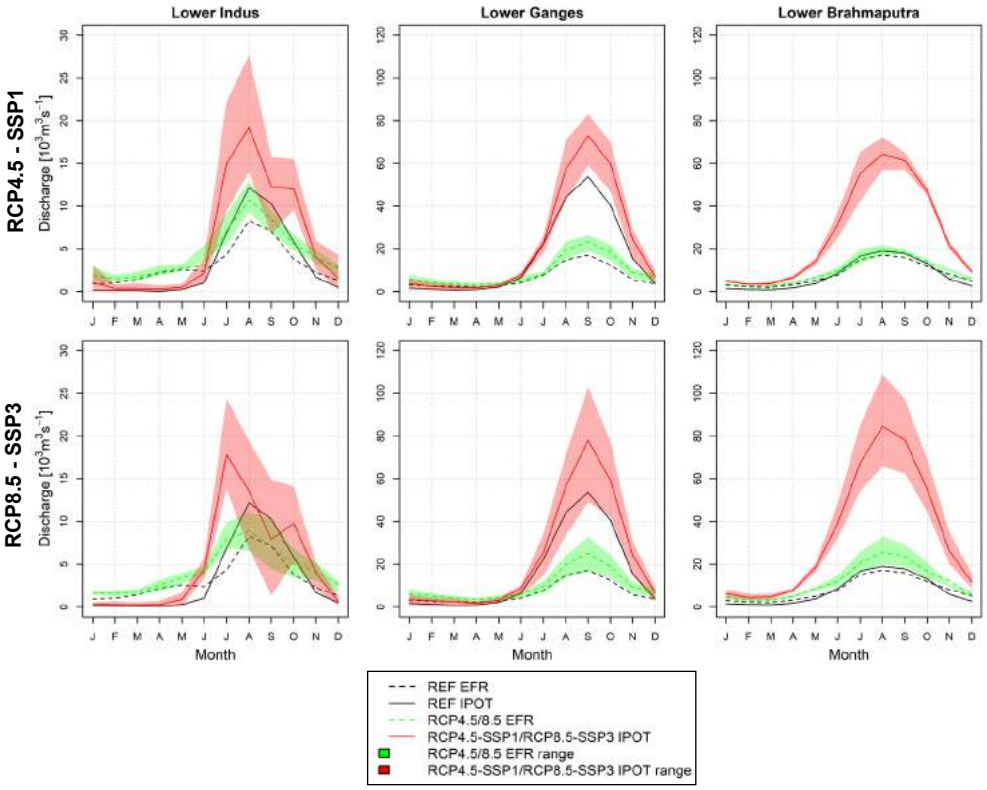

Figure 5.10. Monthly projected changes in the environmental flow requirements (EFRs) and anthropogenically influenced discharge (IPOT) at the outlets of the Indus, Ganges, and Brahmaputra rivers for RCP4.5-SSP1 (upper row) and RCP8.5-SSP3 (lower row). The projected changes are given for the end of the 21st century (EOC). The coloured bands represent the range of ensemble projections that are resulting from forcing the LPJmL model with the different climate models and SSP storylines.

influenced discharge will increase, which can most likely be attributed to the increase in surface water availability (Figure 5.4). Future EFRs are projected to be sustained during high-flow seasons, whereas during low-flow seasons EFRs remain unmet. However, due to low withdrawals in the Brahmaputra river basin it is projected that EFRs can be sustained all-year round. Further, the large uncertainty bands in the model projections of the Indus indicate that, especially for RCP8.5-SSP3, there is a probability that EFRs will not be met either during the second half of the monsoon season.

5.4.6 Comparison with other studies

The projected changes in the future water demand are, in general, in line with reported trends in other studies, although different processes can be responsible for the changes. In their global-scale study, Wada et al., (2013) also project, for instance, decreases in the irrigation water demand for RCP4.5 in the irrigated croplands of South Asia. Nevertheless, the authors project an increase in irrigation water demand for RCP8.5. According to the authors, increases in precipitation are responsible for the decrease in irrigation water demand for RCP4.5, and are outweighed by increases in temperature for RCP8.5, which cause atmospheric evaporative demand to be enhanced,

eventually resulting in increasing irrigation water demands. In our study, the seasonal increases in irrigation water demand (i.e. during the monsoon (partly) and post-monsoon seasons) can also be attributed to enhanced atmospheric evaporative demands emerging from temperature increases. Nevertheless, other processes are responsible for the decreases in irrigation water demand. Besides increases in precipitation, shorter growing seasons as a response to temperature increases, which are larger for RCP8.5, lead to decreasing irrigation water demands. Another study of Hanasaki et al., (2013) shows similar trends with decreasing irrigation water demands that are the result of increasing precipitation too.

5.4.7 Uncertainties and limitations

The projections of future water availability, demand, and supply are subject to several uncertainties and limitations that are mainly related to the climate change projections, the representation of (physical) processes and non-stationarity in the used hydrological models, and the land use change and socio-economic scenarios.

To assess the impacts of climate change on the future water gap, an ensemble of eight downscaled and bias-corrected GCMs were used that cover a wide range of climate conditions representative for RCP4.5 and RCP8.5. The GCMs have limited skill in simulating the regional climate in the complex (mountainous) terrains of Central and South Asia (Lutz et al., 2016b; Seneviratne et al., 2012). Despite the selection of GCMs based on their skill in simulating the regional climate by using an advanced envelope-based selection approach (Lutz et al., 2016b), uncertainties can still be introduced in assessments on future changes in water supply and demand. For instance, uncertainties can be introduced in the way in which GCM runs were selected. The models were selected in three consecutive steps that are based on changes in climatic means and extremes, and the skill in simulating the historical regional climate. Which method is chosen to select the climate models dictates which models are selected and therefore largely determine the outcomes of climate change impact studies like ours. In addition to the uncertainties, the variation in climate change projections between GCMs is large. Since the climate models we selected cover a wide range of possible future climate models, the large variation in climate change projections result in a large spread among the climate models, which subsequently propagates into the hydrological model outcomes. The upcoming CMIP6 model archive (Eyring et al., 2016) might improve the outcomes of the studies by reducing the variation in climate change projections between the different GCMs.

The LPJmL model version we used for our assessments has a limitation in simulating domestic and industrial water demand. In the current version, only annual values of domestic and industrial demand could be included. Since domestic water demand varies on a monthly basis with higher demands during the summer-monsoon season (i.e. higher temperatures during summer-monsoon result in higher demand) and lower demands during the winter season. This means that on a seasonal basis, the domestic water demand and consequently the water gap can be overestimated during the winter season, and underestimated during the summer-monsoon season. Further, the model has the limitation that the impact of water pollution on water availability cannot be simulated. This means that surface water and sustainable groundwater withdrawals can be overestimated and unsustainable groundwater withdrawals (i.e. the water gap) can be underestimated.

Whereas the LPJmL model includes human interventions, such as dam operations, and irrigation withdrawals and distribution through canals, the SPHY model that has been used for our upstream assessments does not include them. Since human interventions can influence the hydrological cycle, uncertainties might be introduced in the outflows of the upstream domains. Current impacts of dams and irrigation withdrawals are, however, assumed to be small due to the relative low number and total capacity of dams in the upstream domains compared to the number and total capacity of dams in the downstream domains. For instance, Tarbela Dam has a total capacity of 12 km^3, whereas the total capacity of dams in the upstream domains reach up to about 5.5 km^3 distributed over about 50 dams (FAO, 2016). Furthermore, most dams are designed as hydropower dams with limited storage or for run-off-the-river hydropower operations, which have a low degree of regulation in the upstream domains of the IGB (FAO, 2016; Lehner et al., 2011). The impact of agriculture is also assumed to be small due to the rather low irrigation water demands (and cropping intensity) in upstream domains (i.e. <100 mm yr^{-1}) compared to the irrigation water demands (and cropping intensity) in downstream domains (Biemans et al., 2016).

The parameterization of the SPHY and LPJmL models are based on present climatology, land use, and other physical catchment characteristics and is assumed to be stationary. Many hydrological parameters, such as parameters controlling snow processes, are, however, non-stationary and can change due to possible changes in climate, land use, or other characteristics (Brigode et al., 2013; Merz et al., 2011; Westra et al., 2014). According to several studies (e.g. Brigode et al., 2013; Vaze et al., 2010; Westra et al., 2014) the impact of non-stationarity is highly dependent on several factors, including the length and variability of the period of parameterization, which are decisive for the robustness of the models and thus the magnitude of uncertainty in the model outcomes. For instance, Vaze et al. (2010) indicated that models can be used for climate impact studies when parameterizations are based on data records of 20 years and longer, and for areas where future annual precipitation is not more than 15% dryer or 20% wetter than the mean annual precipitation that is derived from the data records. Other studies (e.g. Brigode et al., 2013) have indicated that shorter periods (e.g. 3 years) also can result in acceptable parameter sets. The disadvantage remains, however, that in the IGB long data records are scarce and future changes in climate and land use can be more extreme, especially in the southern part of the IGB, where precipitation increases over 100% are projected for the end of the 21st century (Figure 5.2). This indicates that the non-stationarity of hydrological parameters can result in uncertainties in the (future) model outcomes, such as hydrological flow predictions. To reduce the impact of non-stationarity other calibration strategies, such as the generalized split sample test procedure (Coron et al., 2012), are recommended, which aim to test several possible combinations of calibration-validation periods to test the model's performance under different climate conditions.

Land use change scenarios that are consistent with SSP1 and SSP3 were extracted from the IMAGE model (Doelman et al., 2018) and represent future changes in rainfed and irrigated cropland extents. One limitation is that only outcomes on future cropland extents were used as a representative for the land use change scenarios, whereas outcomes on future intensification of current croplands were not considered. Consequently, the projected yield increases and related increase in irrigation water consumption, though not linearly related, were not accounted for. This might eventually result in an underestimation of irrigation water demand. Further, future irrigation water demand can be overestimated since any future increases in irrigation efficiency were not included in our modelling approach. Another limitation that might influence the projections on irrigation water demand is

the way how irrigation practices are reflected within our modelling approach. In our approach, it is assumed that crop types are not adapted over time, which consequently results in decreasing irrigation water demands when growing seasons shorten. The reality, however, is that farmers may adapt to changing climate conditions (e.g. due to the higher risk for heat stress that is a consequence of increased temperature, i.e. extremes) by switching to different crop types that are more suitable for the changed climate. This might eventually influence projections on future irrigation water demand.

The SSP storylines that are used to project future changes in water demand do not account for potential feedbacks between climate change and socio-economic changes. For instance, the impacts of climate change on the land system are not included (Doelman et al., 2018). According to Nelson et al. (2014), climate change has an impact on agro-economic variables, such as agricultural area and production. The authors found, for example, that under climate change agricultural areas are projected to increase due to intensifying management practices that are induced by climate change. This means that without taking potential feedbacks between climate change and socio-economic changes into account, any future increases in cropland extents might be underestimated.

Finally, future changes in the water demand and gap that have been assessed are based on selected climate change scenarios and SSP storylines. The future changes that are assessed do not, however, reflect the impact of adaptation strategies. For instance, it is most likely that extra hydropower dams and reservoirs will be developed in the future (Mukherji et al., 2015). In the agricultural sector, it is most likely that irrigation efficiencies will be improved by changing irrigation systems or that crop types will be changed to ones that are more climate-tolerant (e.g. Biemans et al., (2013). Further, future developments, such as regional or transboundary cooperation that improves water and energy sharing and thus optimizes water resources use (Molden et al., 2017), and their impact on the water gap have not been assessed. Follow-up studies including the simulation of basin-scale effects of climate change adaptation measures are needed to investigate the impacts of future adaptation strategies and developments on the South Asian water gap and their potential in closing the water gap.

5.5 Conclusions

The objective of this study is to assess the impacts of climate change and socio-economic developments on the future blue water gap in the downstream domains of the Indus, Ganges, and Brahmaputra river basins. To this end, we use a coupled modelling system consisting of the cryospheric-hydrological SPHY model and the global dynamic hydrological and crop production model LPJmL. The models are forced with an ensemble of eight bias-corrected downscaled GCMs that represent a wide range of regional RCP4.5 and RCP8.5 climate conditions in combination with and without two socio-economic development scenarios (SSP1 and SSP3) that are likely linked with these RCPs. The model outcomes are analysed in terms of changes in the water availability, demand, and gap.

The outcomes indicate that surface water availability will increase towards the end of the 21st century with the largest projected increases for RCP8.5. Thereby, increases are projected to be stronger during the monsoon season, which can mainly be attributed to the increases in monsoon precipitation and glacier melt. The upstream-downstream difference in water availability is largest

in the Indus and Ganges river basins, whereas in the Brahmaputra river basin this difference is relatively small. This indicates that the dependency on upstream water resources is large, especially in the Indus and Ganges river basins. Future upstream-downstream differences in water availability are projected to be enhanced, implying that the dependency on upstream water resources will increase.

Annual and seasonal water consumption are projected to decrease when considering climate change only. This is mainly caused by the shortening of growing seasons that emerges from temperature increases, and precipitation increases that result in a shift from blue water irrigation to green water or rainfed irrigation and thus cause irrigation water consumption to decline. Only in the monsoon (partly) and post-monsoon seasons is water consumption expected to increase, which can mainly be attributed to enhanced atmospheric evaporative demand and resulting increases in crop evapotranspiration that emerge from temperature increases. The combination of climate change and socio-economic development result in increasing annual and seasonal water consumption for RCP4.5-SSP1 and RCP8.5-SSP3 due to population growth and economic developments.

Due to declining water demand under climate change only, the water gap is also expected to decrease by relative decreases up to 37% and 55% in the Indus and Ganges, respectively, for RCP8.5, at the end of the 21st century. The combination of climate change and socio-economic development is expected to result in increasing water gaps, with relative increases up to 7% and 14% in the Indus and Ganges, respectively, for RCP8.5-SSP3, at the end of the 21st century. Future EFRs are projected to be sustained during high-flow seasons, whereas during low-flow seasons EFRs cannot be met in the Indus and Ganges river basins. Based on the outcomes it can be concluded that socio-economic development is the key driver in the evolution of the South Asian water gap, whereas climate change plays a role as a decelerator. For the South Asian region, which is already facing water stress in a geopolitically complex situation, our findings provide valuable insights into the future evolution of the regional water gap, providing a scientific basis for the formulation of transboundary climate change adaptation policies.

Acknowledgements

I would like to thank Rens van Beek for the support in making the domestic and industrial water demands available, and Marc Bierkens for the helpful discussions.

6 Synthesis

Climate change is expected to impact the hydrology and cryosphere of mountainous river basins. Ice and snow reserves will most likely be affected by temperature increases. Also, precipitation amounts, patterns, and the intensity and frequency of extreme precipitation events will likely change under a changing climate. This will eventually have an impact on (seasonal) surface and groundwater availability and the frequency and intensity of natural hazards. It can therefore be expected that climate change will have a large impact on the society and the environment; impacts that will be amplified with the anticipated socio-economic developments and associated changes in water demand. To understand climate change impacts in mountainous river basins at different levels, i.e. varying from glaciers to the entire river basin, it is inevitable to examine these impacts at different spatial scales. For this reason, the following main objective of this Ph.D. research is formulated as:

Understanding the (cryospheric-)hydrological impacts and challenges of climate change across different spatial scales in mountainous river basins.

To address the main objective and the main challenges identified in the Introduction of this PhD research, I have formulated four specific research questions that have been addressed in the preceding chapters:

RQ1 What are the attributions of natural and anthropogenic climate change in the response of single glaciers to climate change?

RQ2 Is it possible to make reliable projections of climate change impacts on the hydrology of glacierized headwater catchments by using multiple conceptual hydrological models?

RQ3 What is the impact of climate change on hydrological extremes in regional mountainous domains?

RQ4 What are the key drivers in the potential development of a water gap in large mountainous river basins?

In this chapter I will synthesize the presented research, discuss the main findings and limitations, and provide an outlook on potential future research directions.

6.1 Simulating the response of glaciers under a changing climate

The ongoing global warming since the end of the Little Ice Age (LIA) has resulted in a widespread retreat of glaciers that have contributed to global sea level rise and hydrological shifts on land (Gregory et al., 2013; Huss and Hock, 2018). Throughout the 20th century and in particular after 1970, the anthropogenic influence on the climate-earth system has increased rapidly as a result of the industrial revolution (Myhre et al., 2013). These increases are reflected in glacier mass balance observations since the 1980s (Hirabayashi et al., 2016; Marzeion et al., 2014). Although the cited studies mainly have investigated the attribution of glacier mass changes to anthropogenic and

natural climate change, the effects of natural and anthropogenic climate change on changing glacier dynamics are little understood.

In chapter 2 the attribution of changing glacier mass balance and dynamics to anthropogenic and natural climate change was investigated by developing and applying a spatially-distributed coupled glacier mass balance and dynamical ice-flow model. The model is based on a spatially-distributed formulation of a shallow ice approximation and was applied from the end of the Little Ice Age (1850) to the present-day (2016). For the modelling the focus was on two glaciers with contrasting surface characteristics: the debris-covered Langtang Glacier in the Central Himalayas and the clean-ice Hintereisferner in the European Alps. The model was forced with four spatially distributed and bias-corrected GCM runs from the historical experiment of the CMIP5 archive. The selected GCM runs represent region-specific warm-dry, warm-wet, cold-dry, and cold-wet climate conditions. To separately assess the effects of human-induced climate change on glacier mass balance and dynamics separately, runs were used with and without further anthropogenic forcing from 1971 onwards until 2016.

The model outcomes showed that both glaciers experience the largest area and volume reductions under warm climate conditions, whereas for cold climate conditions the reduction in area and volume is smaller. Compared to the observed trends, the model forced by cold/dry and cold/wet climate conditions simulated glacier changes that are closest in agreement at Hintereisferner and Langtang Glacier, respectively. Under these climate conditions, the model simulated area (volume) reductions of 16% (42%) for Langtang Glacier and 40% (75%) at Hintereisferner between 1850 and 2016. Simultaneous with changes in glacier area and volume surface velocities generally decrease over time from up to 275 m a^{-1} to 66 m a^{-1} at Langtang Glacier and from up to 310 m a^{-1} to 25 m a^{-1} at Hintereisferner. Following a scenario without further anthropogenic forcing the outcomes showed a 3% (9%) smaller decline in glacier area (volume) for a debris-covered glacier and an 18% (39%) smaller decline in glacier area (volume) for a clean-ice glacier. The changes in area and volume were accompanied by surface velocities that either generally increase or do not show significant changes relative to a scenario with further anthropogenic forcing. The difference in magnitude of impact between a debris-covered and a clean-ice glacier can largely be attributed to differences in response time. The clean-ice Hintereisferner has a shorter response time, which causes the glacier to react faster to climatic changes and the thinning rates to be larger. The larger thinning rates do subsequently result in a larger decline in area, volume, cumulative mass balance, and velocity. The debris-covered Langtang Glacier has a longer response time, which leads to less pronounced changes over time. The longer response times can mainly be attributed to the debris cover that insulates the glacier surface and reduces melt. Based on the outcomes it can be concluded that the response of glaciers can mainly be attributed to anthropogenic climate change.

6.2 Hydrological projections at the catchment scale

In chapter 2 it is shown that glaciers are losing mass as a response to climate change. It is likely that glaciers will continue to lose mass in the future and that glaciers can even disappear in the long term (Huss and Hock, 2018; Kraaijenbrink et al., 2017). Additionally, snow cover and volumes will most likely reduce due to upward shifts of the snowline, a shorter duration of the snow season, and a higher fraction of liquid precipitation (Beniston et al., 2018; Marty et al., 2017b; Salzmann et al., 2014; Viste and Sorteberg, 2015). The diminishing ice and snow reserves will most likely affect

the hydrology of river basins. Especially in glacierized headwater catchments, where contributions of meltwater from ice and snow reserves can be large, the hydrological impacts can be significant. For this reason, reliable projections of the hydrological impacts of climate change in glacierized headwater catchments are needed to improve our understanding of these impacts.

In chapter 3 a study is presented that investigates the hydrological response of the Ötztal glacierized headwater catchments (Austria) to future climate change by applying two semi-distributed conceptual hydrological models with different degrees of complexity. The models, HBV (Light) (Seibert and Vis, 2012) and HQsim (Kleindienst, 1996), were forced with downscaled climate change projections following the SRES A1B scenario and outputs of an empirical glacier change model. The glacier change model simulates the future glacier geometry under changing climate conditions separately. The applied models showed very good model performances in the simulation of daily discharge in three (nested) catchments with varying degrees of glaciation. The models project that towards the end of the 21st century ice melt-dominated discharge regimes with discharge peaks in July/August will shift to (more) snowmelt dominated regimes with peaks in May/June. In the long term, summer discharge rates are projected to decrease, with relative changes up to 53%. Winter/spring discharge rates are projected to increase, with relative changes up to 249%. The seasonal changes are accompanied by an earlier appearance of flood peaks and a higher frequency of low flow conditions. Low flows are expected to occur more frequently in the downstream parts than in the upstream glacierized parts of the Ötztal. The summer discharge changes can mainly be attributed to glacier mass loss and retreat, an increase in evapotranspiration, and a decrease in precipitation. Winter/spring discharge changes can be attributed to a rising snowline, shorter snowpack durations, and a higher fraction of liquid precipitation.

The presented study showed that minor differences exist between the projected outcomes of the HBV and HQsim models. The differences were mainly found in the projected runoff variability, the seasonality of flood peaks, and to a smaller extent in the low flow projections. Since both models were forced under the same conditions (i.e. climate, glacier extents) it is likely that structural differences between these models can explain the variation in the outcomes between the HBV and HQsim. Despite the minor differences, both models were able to project trends (i.e. for the mean discharge and high flows) that agree well with projected trends found in other studies in the Ötztal and European Alps (Addor et al., 2014; Farinotti et al., 2012; Huss et al., 2014; Schneeberger et al., 2015; Tecklenburg et al., 2012; Weber et al., 2010). Also, a more recent study in the upstream glacierized parts of the Ötztal Alps (Hanzer et al., 2018) shows similar trends with decreasing annual/summer discharge rates and shifting discharge patterns in the long term. The minor differences between HBV and HQsim, and the performance of both models in simulating hydrological changes that agree well with observations and projected trends found in other studies indicate that, in general, the projected hydrological changes can be considered reliable. This means it is possible to make reliable projections of climate change impacts on the hydrology of glacierized headwater catchments by using multiple conceptual hydrological models.

6.3 Modelling hydrological extremes in mountainous river domains

As mentioned in chapter 2 and 3, climate change (will) affect the local hydrology and cryosphere of headwater catchments. The hydrological and cryospheric changes that occur in these catchments can most likely be related to climatic changes that occur on a regional scale. For example, large-scale

atmospheric systems, such as the South and East Asian monsoon systems, dominate the regional climate and are large suppliers of precipitation for the mountain ranges in the respective regions (Lau and Kim, 2018; Li et al., 2018). Changes in the intensity and patterns of these atmospheric systems might have implications for the regional hydrology and the occurrence of hydrological extremes in mountainous domains, which, in turn, will pose serious threats for the livelihoods of people. For this reason, there is a need to improve our understanding of the regional impact of climate change on hydrological extremes in mountainous domains. To this end, regional/basin scale modelling applications with sufficient representation of mountain-hydrological processes are required.

In chapter 4, a study is presented that investigates the impacts of climate change on future hydrological extremes in the upstream mountainous domains of the Indus, Ganges, and Brahmaputra (IGB) river basins. To this end, the physically-based fully distributed cryospheric-hydrological Spatial Processes in Hydrology (SPHY) model (Terink et al., 2015) was used to simulate current and future daily discharge. This high-resolution model has a strong representation of mountain-hydrological processes that explicitly simulates cryospheric changes (i.e. glaciers and snow cover). SPHY was forced with an ensemble of eight bias-corrected and downscaled GCM runs that represent different future climate conditions for RCP4.5 and RCP8.5, and were pre-selected by using an advanced envelope-based selection approach (Lutz et al., 2016b). The hydrological model and GCM outputs were used to analyse changes in future climatic and hydrological extremes.

The results showed that the magnitude of climatic means and extremes increase towards the end of the 21st century where climatic extremes tend to increase stronger than climatic means. The projected increase in precipitation is strongest in the upper Indus Basin (UIB). Temperature extremes tend to appear more frequently in the upper Brahmaputra Basin (UBB). The hydrological model outcomes showed that mean discharge and high flow conditions will very likely increase. For instance, the 50-year return level is expected to increase, with relative changes up to 305% relative to the current return levels. The largest changes are projected in the headwaters in the UBB, which can mostly be attributed to increased precipitation and to a smaller extent also to increased ice melt. In some regions decreases are also projected. In the westernmost part of the UIB relative decreases up to 25% are projected, which can mainly be attributed to decreases in precipitation and snow- and ice melt. In general, precipitation extremes will contribute most to the increases in hydrological extremes, although to some extent increasing temperature extremes will contribute as well. Low flows may occur less frequently but are partly accompanied by large uncertainties. These uncertainties can mainly be attributed to the large spread among the different climate models. In summary, climate-induced changes occurring in the regional mountainous domains of the IGB result in an increased magnitude and frequency of extreme discharge events and a decrease in the frequency of low flow conditions. The projected trends in hydrological extremes are not exceptional. Also in other mountain regions around the globe, such as the European Alps, it is likely that hydrological extremes as a result of climate change will occur more frequently (e.g. de Jong, 2015; see chapter 3).

6.4 Quantifying supply and demand changes in glacier and snowmelt dominated river basins

The recent and future developments as shown in the preceding chapters show a decline in ice and snow reserves and changes in the precipitation climatology. These changes affect the local and regional water availability and have implications for the occurrence of hydrological extremes. As mentioned in section 1.2.3 catchments are spatially connected with each other by downstream movement of water via surface or subsurface runoff (Sivapalan, 2018). This means that climate-induced changes in upstream water availability also affect the availability of water that can be provided for people living in (densely-populated) downstream domains. It is expected that rapid and continuous population growth accompanied by strong economic developments will result in a strong increase in water demand and withdrawals. These developments will most likely lead to increased pressure on water resources and the development of a potential water gap. The magnitude of the water gap depends highly on the effects of climate change and socio-economic developments on water supply and demand. To understand the role of these drivers in the potential development of a water gap it is therefore required to apply regional/basin-scale models that have sufficient representation of mountain-hydrological processes and the effects of human interventions on the hydrological cycle.

In chapter 5, a study is presented that assesses the combined impacts of climate change and socio-economic developments on the future "blue" water gap in the Indus, Ganges, and Brahmaputra river basins until the end of the 21st century. To this end, a novel coupled modelling approach was applied consisting of two physically-based fully-distributed models: the cryospheric-hydrological SPHY model (Terink et al., 2015) and an adjusted version of the (eco-)hydrological Lund-Potsdam-Jena managed Land (LPJmL) model (Biemans et al., 2013, 2016). The SPHY model was applied to simulate current and future water supply from the upstream mountainous domains (chapter 4). For the downstream domains, a LPJmL model with an explicit representation of human interventions in the hydrological cycle was applied to simulate current and future water supply and demand. The coupled models were forced with an ensemble of eight bias-corrected downscaled GCMs representing RCP4.5 and RCP8.5 in combination with and without a set of regional land use and socio-economic scenarios (consistent with SSP1 and SSP3) that are likely linked with these RCPs. The simulation outputs were analysed in terms of the blue water availability, demand, and gap, where the blue water gap is estimated as the amount of unsustainable groundwater that is withdrawn to fulfill the blue water demand.

The results showed that an increase in surface water availability towards the end of the 21st century, which can mainly be attributed to increases in monsoon precipitation. The climate-induced increases in temperature and precipitation will most likely lead to shorter growing seasons and a shift from blue water to green water/rainfed irrigation, respectively. As a result of these changes irrigation water consumption declines, which eventually results in declining annual and seasonal water consumption rates. However, during the monsoon (partly) and post-monsoon seasons enhanced atmospheric evaporative demands and resulting increases in crop evapotranspiration will most likely lead to increasing consumption rates. Declining water demands are expected to result in a declining water gap, with annual relative decreases up to 37% and 55% in the Indus and Ganges river basins, respectively, for RCP8.5, at the end of the 21st century. The combination of climate change and socio-economic developments is expected to result in increased annual and seasonal

water consumption rates, which can mainly be associated with population growth and economic developments. However, despite the increasing consumption rates and demands the blue water gap is projected to decrease for RCP4.5-SSP1. The declining water gap can mainly be explained by decreasing irrigation water demands and increasing surface water availability that outweighs the increasing domestic and industrial water demands. For RCP8.5-SSP3 climate-induced changes in water availability cannot compensate for the strong increases in water demand (by increasing evaporative demand and socio-economic developments) anymore. For this reason, it is very likely that the water gap will experience a substantial increase, with relative annual increases of 7% and 14% in the Indus and Ganges river basins, respectively, at the end of the 21st century. Based on the outcomes it can be concluded that socio-economic development is the key driver in the development of the regional water gap, whereas climate change plays a role as decelerator. Despite the increased water gap, the transgression of future environmental flows will likely be limited with sustained and unmet environmental flow requirements during the monsoon and low flow seasons, respectively, in the Indus and Ganges river basins.

6.5 Cryospheric-hydrological impacts of climate change in mountainous river basins

In the preceding chapters the cryospheric and hydrological impacts of climate change have been assessed at different spatial scales. As the model outcomes show in chapter 2, human-induced climate change have resulted in glacier mass losses over the past decades. A debris-covered glacier is found to respond differently to climate change than a clean-ice glacier. A debris-covered glacier shows a limited retreat and tends to lose less mass due to the insulation of the surface. A clean-ice glacier responds faster to climate change and shows a larger retreat. It is likely that glaciers will continue to lose mass in the future. For instance, the glacier areas in the Ötztal Alps are projected to decrease with 80-90% towards the end of the 21st century (chapter 3). Also snow cover and volumes are expected to decline. The combination of diminishing ice and snow reserves will result in changing discharge volumes and regimes in (glacierized) headwater catchments (chapter 3). These changes are accompanied by shifts in the seasonality of flood peaks and changes in the frequency of low flows (chapter 3). As a result, the local seasonal water availability will be affected and risks for local floods and droughts will increase. Besides diminishing ice and snow reserves, it is also expected that changes will occur in the precipitation climatology, especially in regions where the hydrology is dominated by large-scale atmospheric circulations, such as the Indian and East Asian monsoon circulations. An intensification of the monsoon circulation is accompanied by increasing precipitation amounts and extremes (chapter 4). In combination with increased snow- and ice melt that can be attributed to rising temperature means and extremes (chapter 2, 3, and 4), the increasing precipitation amounts and extremes will most likely contribute to higher discharge rates, more frequently occurring high flows, and less frequently occurring low flows (chapter 4). Consequently, surface water availability increases, which in combination with decreasing irrigation water demands can decelerate the effects of potentially increasing domestic and industrial water demand associated with future socio-economic developments in large mountainous river basins (chapter 5).

The research presented in the preceding chapters focused mainly on the mountainous catchments and river basins in the European Alps and High Mountain Asia. Other mountain regions, such as the Andes and the Rocky Mountains, will also be affected by climate change. For example, it is likely that climate change will have a large impact on a country such as Peru, which is located at

the leeward side of the Andes. The country is characterized by dry climate conditions and highly relies on Andean water resources that are dominated by contributions from glaciers and the páramos wetlands (e.g. Buytaert et al., 2011). Climate change projections indicate that precipitation will decrease in the region (IPCC, 2013; Kohler et al., 2014). Combined with the projected glacial retreat there is a high probability that water resources will be affected, which will have an enormous impact on the society and environment in the region. This means that there is a high priority in understanding climate change impacts in Peru and other countries that heavily rely on mountain water resources as well.

6.6 Research novelties

Throughout the thesis research is presented that has several novelties:

- A spatially-distributed glacier mass balance and ice-flow model is used that includes a spatially-distributed formulation of the Shallow Ice Approximation that does not provide a-priori knowledge about the flowline geometry of glaciers (chapter 2). The approach has been found to be a suitable alternative to the more complex higher order or Stokes approaches and has the potential to be used for future regional glacio-hydrological modelling. Further, new insights are provided on the (dynamical) response of a clean-ice glacier and a debris-covered glacier to natural and anthropogenic climate change (chapter 2).

- A catchment-scale assessment that is the first to use a combination of multiple conceptual hydrological models (HBV and HQsim), multiple downscaled climate models, and a glacier model to assess the hydrological response of the Ötztal glacierized catchments to future climate change is presented (chapter 3).

- A regional-scale assessment that is the first to investigate a full range of possible impacts of future climate change (i.e. in terms of climate extremes) on the occurrence of both high and low flows in the upstream mountainous domains of the Indus, Ganges, and Brahmaputra river basins is presented (chapter 4). New insights are provided on the intensity and frequency of future hydrological extremes in the upstream mountainous domains of these river basins.

- A novel coupled modelling approach that includes a high-resolution cryospheric-hydrological model (SPHY; 5 x 5 km) and a high-resolution hydrology and crop production model (LPJmL; 5 x 5 arcmin) is applied (chapter 5). The coupled model can simulate up- and downstream water availability and downstream water supply, demand, and gap in the Indus, Ganges, and Brahmaputra river basins, and takes upstream-downstream links and lateral transport into consideration. Further, the hydrology and crop production model applied for downstream domains, has been specially developed for this region in that it is able:

    - to simulate water distribution through extensive irrigation canal systems of the Indus and Ganges river basins,
    - to make improved simulations of the timing of water demand for agriculture due to an explicit representation of a multiple cropping system (Biemans et al., 2016), and
    - to simulate groundwater withdrawal and depletion rates.

The outcomes of the coupled modelling approach have provided new and valuable insights into the future evolution of the South Asian water gap.

6.7 Challenges, recommendations, and research outlook

The research presented in the preceding chapters provides new and valuable insights in the cryospheric and hydrological impacts of climate change in mountainous river basins. There are however several points that need to be resolved and requires further research. In this section, I will highlight these points, and provide recommendations and an outlook on potential future research directions

6.7.1 Improvements in modelling the essential components of the high-altitude water cycle

In this thesis, I assessed the effects of climate change by using modelling approaches varying from semi-distributed conceptual models (chapter 3) to fully-distributed physically-based models (chapter 2, 4, and 5). Although the models perform satisfactorily, further improvements are needed to model the essential components of the high-altitude water cycle. I will illustrate a few of these components.

6.7.1.1 Precipitation

Precipitation is a widely used input variable in cryospheric and hydrological models, and an important component in the glacier mass balance and the water balance of a catchment or river basin. Understanding the role of precipitation in high-mountain environments is, however, extremely challenging. The limited amount of precipitation measurements hamper the validation of precipitation, especially in the remote areas of HMA. For instance, only measurements of 40 meteorological stations were available for the upstream domains of the Indus, Ganges, and Brahmaputra (chapter 4). These stations are unequally distributed, which means there are large regions without any data available. In addition, the stations are valley-oriented, indicating there is a lack of data in the high-altitude areas. Similar difficulties can be found in the European Alps, although the data availability is significantly higher. The poor coverage of precipitation gauging stations, in particular at higher altitudes, introduces uncertainties in bias-corrected gridded precipitation products that are based on observations (e.g. APHRODITE; Yatagai et al., 2012), re-analysis (e.g. ERA-Interim; Dee et al., 2011), or satellite-derived imagery (TRMM; Huffman et al., 2007) (Immerzeel et al., 2015). The gridded products are not able to capture the spatial variation and magnitude of high-mountain precipitation, which often lead to significant precipitation underestimates (Immerzeel et al., 2015; Li et al., 2017, 2019; Palazzi et al., 2015). This means that more precipitation gauging stations need to be installed and precipitation correction methods are needed for reliable simulations of the glacier mass balance or the regional water balance. An example of a precipitation correction method is developed in Immerzeel et al. (2012a, 2015), which corrects precipitation based on observed glacier mass balance and river runoff. In chapter 4 a precipitation correction method is also used by applying correction factors based on observed river discharge. More improvements can potentially be achieved by using satellite-derived products such as measured by the Global Precipitation Measurement (GPM) Core Observatory (CO) spacecraft (Skofronick-Jackson et al., 2017). This spacecraft is able to measure light and intense rainfall, but also to detect moderate and heavy snowfall.

In addition to understanding the precipitation amounts, intensity, and distribution, another challenge is to understand the local and regional-scale atmospheric dynamics, which are often not well understood. Atmospheric modelling systems such as the Weather Research and Forecast (WRF) model might contribute to an improved understanding of the local and regional atmospheric dynamics. For instance, Collier and Immerzeel (2015) used the high-resolution WRF-CMB modelling system to assess the local atmospheric dynamics in a high-altitude catchment located in the Central Himalayas, and found a reversal of vertical and along-valley precipitation distributions between the monsoon and winter seasons. These valuable insights help us to understand how precipitation is distributed over catchments in mountainous terrain, especially since precipitation is often assumed to increase with altitude. The cited study also demonstrates the potential of high-resolution atmospheric models such as the WRF model in improving the quality and accuracy of local precipitation estimates and patterns. Similar findings were also reported by other studies conducted in other parts of HMA and other mountain regions (e.g. Norris et al., 2017; Yáñez-Morroni et al., 2018). Besides atmospheric models, Earth System Models such as the Community Earth System Model (CESM) of Hurrell et al. (2013) can help to improve our knowledge of regional and continental-scale atmospheric processes that influence the regional climate, particularly to improve our understanding of, for instance, large-scale teleconnections between the ENSO (El Niño and Southern Oscillation) and the Indian monsoon intensity (Kumar et al., 2006; Yeh et al., 2018) or relations between large-scale atmospheric circulations and the status of glaciers (e.g. Yao et al., 2012).

6.7.1.2 Sublimation and Evapotranspiration

One of the components of the high-altitude water cycle that requires an improved understanding is the role and quantification of snow and ice sublimation, which is not considered by the models applied in chapter 2 and 3. It is, however, found that sublimation can play a significant role in the snow hydrology and water balance of high mountain environments. For instance, in the Bavarian Alps (Germany) a study to snow sublimation indicated that between 10% and 90% of winter snowfall is lost due to sublimation, where the highest losses are modelled at very wind-exposed high mountain crests (Strasser et al., 2008). At Hintereisferner, sublimation losses of about 150 mm yr^{-1} have been reported (Kaser, 1983) and in the Langtang Valley it has been found that up to 21% of the total snowfall is lost by sublimation, which can even be higher at wind-exposed locations (Saloranta et al., 2019; Stigter et al., 2018). To quantify sublimation, energy-balance models (e.g. Strasser et al., 2008), coupled atmosphere-mass balance models (e.g. Collier et al., 2013, 2015), the combination of atmosphere models and snowdrift sublimation routines (Lenaerts et al., 2010) amongst others might be an alternative. The disadvantage however is that these type of models require more data, which are often not available, especially not in the remote areas of HMA. Furthermore, these type of models can be computationally expensive. For this reason, techniques that do not have high computational demand but still can give reasonable sublimation estimates are needed (Bowling et al., 2004; MacDonald et al., 2009). In the SPHY model (chapter 4 and 5) sublimation is included by a simplified linear function that assumes sublimation to be constant over time and to be highest at higher elevations where the air is driest and wind speeds are highest. The disadvantage of this approach is, however, that sublimation varies with time due to its dependency on wind speed and humidity. Further, the sublimation estimates are difficult to validate due to the limited amount of observed sublimation quantities, in particular in the remote areas of HMA. To validate sublimation estimates, more field measurements and research are required to quantify and understand the role of sublimation in the high-altitude water cycle.

At lower altitudes, evapotranspiration plays a more important role in the water balance. In the models applied throughout this thesis mainly temperature-based approaches, such as the Hamon method (Hamon, 1961) (chapter 3) and the modified Hargreaves method (Hargreaves and Samani, 1985) (chapter 4 and 5), were used to estimate potential evapotranspiration. Potential evapotranspiration is also dependent on relative humidity, wind speed, and long- and shortwave radiation, which would indicate that potential evapotranspiration is overestimated on cloudy and humid days and underestimated on windy days (Allen et al., 1998). For this reason, the energy-based Penman-Monteith method is often preferred due to the solid physics basis. The disadvantage, however, is that this method has a high data demand, which makes this method less suitable in data-scarce regions. Also, it can be quite sensitive to aridity and advection effects (Trigo et al., 2018). Therefore, other methods that have a low data demand and are able to give reliable estimates of potential evapotranspiration are needed. According to several studies (e.g. Li et al., 2016; Lu et al., 2005; Xu and Singh, 2002) radiation-based methods such as the Priestley-Taylor method (Priestley and Taylor, 1972) can be seen as more accurate methods and might be an alternative for future hydrological studies.

6.7.1.3 Ice and snowmelt

Ice and snowmelt are simulated using simple degree-day approaches that are based on empirical relations between air temperature and melt. The methods are easy to apply due to their low data demand. Only air temperature data is required to calculate ice and snowmelt. The degree-day approaches have been applied in several ways throughout the thesis. In chapter 2, the simple degree-day method is applied by distinguishing the effects of aspect and by including an elevation-dependent melt factor that accounts for the effects of debris thickness on melt rates. In chapter 3, methods are applied that mainly distinguish the effects of aspect and slope, and in the SPHY model (chapter 4 and 5) a fractional separation is made between debris-covered and clean-ice glaciers. Further a separate distinction is made between degree-day melt factors for snow, clean-ice and debris-covered ice. The disadvantage of simple degree-day approaches is, however, that the parameters of simple degree-day approaches are not robust in time and require re-calibration for different climate conditions (Gabbi et al., 2014). According to Gabbi et al. (2014), who compared five melt models (i.e. varying from simple degree-day methods to full energy-balance approaches), models including a separate term for shortwave radiation have the greatest potential in simulating ice and snowmelt. Similar findings were also found by Litt et al. (2019) who tested the performance of (enhanced) temperature-index approaches in the Central Himalayas. The authors indicated however that these approaches can be underperforming where sublimation or other wind-driven processes contribute to ablation. Nevertheless, models including a separate term for shortwave radiation can be seen as a suitable alternative for future cryospheric-hydrological studies.

Due to the dependency on air temperature, ice and snowmelt simulations are sensitive for temperature changes that emerge from small changes in temperature lapse rates, especially in the long-term. In chapter 2, 4, and 5 monthly temperature lapse rates are used that constant in space and vary from year-to-year. However, in reality, lapse rates are variable in space and time (Heynen et al., 2016; Kirchner et al., 2013; Nigrelli et al., 2018; Steiner and Pellicciotti, 2016), which means the interannual and spatial variability in lapse rates is lacking and uncertainties might be introduced in air temperature fields and subsequent simulations or projections in ice and snowmelt. More research will therefore be needed on the spatial and temporal distribution of lapse rates in mountain regions to improve air temperature fields.

6.7.1.4 Avalanching

Avalanching has been found to contribute significantly to glacier accumulation in steep mountain terrain (Laha et al., 2017; Ragettli et al., 2015; Scherler et al., 2011; Shea et al., 2015). Avalanching is only simulated in the coupled glacier mass balance and ice-flow model applied in chapter 2 and is not considered in other applied models such as SPHY. This might subsequently introduce uncertainties in glacier mass balance and the redistribution of ice within the model. In chapter 2, avalanching is simulated by the gravitational snow transport module SnowSlide (Bernhardt and Schulz, 2010), which has the disadvantage that it is solely restricted to snow avalanching. This means that the application of SnowSlide has limited suitability in areas that are classified as glaciers, and additional steps are required to avoid avalanching on steep slopes where glaciers are present. A future alternative to improve the simulation of avalanching in glacierized areas might be the combination of the SnowSlide module with existing modelling tools such as the mass-conserving algorithm MTD of Gruber (2007). This algorithm has the advantage that it can simulate the gravitational transport of other types of movements, such as ice avalanches and debris flows, as well. An additional advantage of this algorithm is that it is easy to be integrated into high-resolution cryospheric(-hydrological) models. Further, reliable observations of snowfall are often lacking, especially in remote areas, such as Langtang Glacier. This non-availability of snowfall observations hampers the verification of accumulation that is contributed by avalanching and also to improve our knowledge of the role of avalanching in the glacier mass balance and dynamics. For this reason, future research and model development and improvements are required to help us understand and quantify the role of avalanches.

6.7.1.5 Glaciers and ice flow

Since meltwater from glaciers can contribute significantly to the total runoff, (cryospheric-) hydrological models need to have a sufficiently accurate representation of glaciers and their evolution to reliably simulate meltwater. In this thesis, a variety of approaches was used to simulate the evolution of glaciers and meltwater through time.

In chapter 2, a coupled glacier mass balance and ice-flow model was used to simulate the response of glaciers under changing climate conditions. One of the largest challenges is to understand the response of debris-covered glaciers to climate change, which is extremely difficult due to many unknowns. A very good example is the so-called 'debris-cover anomaly', which is a phenomenon that debris-covered and clean-ice glaciers at the same elevation have similar thinning rates despite the melt-reducing effects of debris insulation on debris-covered glaciers (Brun, 2018; Salerno et al., 2017). Explanations of this anomaly vary from the presence of ice cliffs and supraglacial ponds that locally enhance melt to lower emergence velocities along the glacier (Banerjee, 2017; Brun et al., 2018; Nuimura et al., 2017; Ragettli et al., 2016a; Salerno et al., 2017; Steiner et al., 2015). To understand the responsible factors for the debris-cover anomaly and the dynamical response of debris-covered glaciers in general more research will be needed in the future. Another challenge is to capture the spatio-temporal variability of debris thickness and supraglacial features in the models. In the model applied in chapter 2 debris thickness is assumed to be constant over time and supraglacial feature such as ponds are not considered explicitly. This means the model might over- or underestimate melt rates locally, which subsequently result in an over- or underestimation of surface velocities. Further research will be needed on the spatio-temporal variability of supraglacial features, such as debris, ponds, and ice cliffs and their role in the amount of melt that can be generated on a glacier. Modelling tools that can simulate the spatio-temporal evolution of

supra-glacial debris (Jouvet et al., 2011; Naito et al., 2000; Rowan et al., 2015) might contribute to improved future melt simulations. Also, a challenge is to improve our understanding of processes and parameters that influence glacier dynamics. For instance, processes such as crevassing have not been considered in the model applied in chapter 2, whereas crevasses can play a crucial role in the mass balance and dynamics of glaciers by locally enhancing ablation and ice flow velocities (Colgan et al., 2016). For this reason, more research will be needed to quantify and understand the role of crevassing. Ice flow parameters, such as ice density and ice temperature, influence ice viscosity and subsequently ice dynamics, and vary in time and space (e.g. Zhang et al. (2013)). In the model applied in chapter 2, ice parameters, such as ice density and the temperature-dependent Glen's flow rate parameter, are, however, assumed to be constant, which subsequently might have introduced uncertainties in the simulated ice flow velocities. To improve the representation of feedbacks between ice temperature and flow velocities, coupled modelling approaches including models that simulate the thermodynamical behavior of glaciers might be an outcome in future studies.

In chapter 3, for example, a glacier change model was used to simulate future glacier geometries that do not consider the long-term effects of glacier dynamics. Several studies have outlined a relation between glacier dynamics and thinning rates and related ice thickness distributions (Banerjee, 2017; Berthier and Vincent, 2012; Dehecq et al., 2019). Approaches such as the glacier change model applied in chapter 3 are however largely empirical and may require local calibration. This means that, when they are used without location-specific parameters, large uncertainties are introduced in the projections of future glacier geometries and subsequently the amount of glacier melt and river discharge that is projected in conceptual models, such as HBV and HQsim. Also, many of these conceptual models lack the ability to simulate a change in glacier extent and assume glacier extent to be constant throughout a scenario period (i.e. 30 years in chapter 3). Especially under future climate conditions, that are characterized by strong glacier mass loss and retreat, the assumption of fixed glacier extents will introduce additional uncertainties in discharge projections. To reduce these uncertainties one might consider to use the updated version of the HBV Light model (Seibert et al., 2018), which includes a module that describes glacier areas changes by a single-valued relation between glacier mass and glacier area (i.e. the Δh parameterization; Huss et al., 2010). This model might then be used in combination with a coupled glacier mass balance and flow model, such as applied in chapter 2 to optimize future discharge projections or in combination with multi-model ensemble projections of future glacier changes that can be derived from model intercomparison projects, such as the Glacier Model Intercomparison Project (GlacierMIP; Giesen et al., 2016) or the Ice Sheet Model Intercomparison Project for CMIP6 (ISMIP6; Nowicki et al., 2016). Another alternative is to use fully-distributed physically-based models that have a better representation of cryospheric-hydrological processes, such as the SPHY model (chapter 4 and 5).

The SPHY model used in chapter 4 and 5 for the upstream mountainous domains projects future glacier changes by means of an ice redistribution module (Terink et al., 2017). The ice redistribution module is however limited in use due to the large spatial grid size it needs to provide meaningful results (i.e. 5 km x 5 km). The large spatial grid size prohibits the re-distribution of ice over small glaciers that fall within one pixel, which subsequently results in less accurate glacier change projections. Another limitation of this module is that it cannot simulate glacier surges. This introduces long-term uncertainties in the projected amount of glacier melt and river discharge. To overcome these uncertainties, it might be an option to apply hyper-resolution models (i.e. with a spatial resolution of 1 km or smaller) (Bierkens et al., 2015; Melsen et al., 2016) that can simulate

ice redistribution dynamically by means of simplified parameterizations of ice flow (chapter 2). A drawback of this approach are the computational requirements that can particularly be large when using it for regional/basin-scale model applications. To reduce the computational burden, one possible approach is to consider regional/basin-scale models that include nested higher resolution catchment-scale models that can be specifically applied to glaciers. Other improvements that are needed in the SPHY model are related to the differentiation of clean-ice and debris-covered glaciers. The differentiation between clean-ice and debris-covered glaciers is currently based on thresholds of elevation and slope without consideration of the local geology and geomorphology. This introduces additional uncertainties in the projected glacier melt, especially in the IGB where the fraction of debris-covered glaciers is relatively high (i.e. between 6.9% (Ganges) and 9.5% (Indus); Bajracharya and Shrestha, 2011). Debris classification techniques using spaceborne imagery (Kraaijenbrink et al., 2017) can be used to improve the differentiation of clean-ice and debris-covered glaciers and subsequently glacier melt projections.

6.7.1.6 Other components

There are several components of the high-altitude water cycle that have not been considered (explicitly) by the models applied in this thesis. One of these components is mountain permafrost. It is important to understand which implication climate change can have for mountain permafrost since natural hazards such as large rock avalanches can be triggered by thawing of mountain permafrost (Haeberli et al., 2017). These hazards can subsequently trigger other hazards such as large impact flood waves in glacial lakes that can have devastating consequences to thousands of people. An example of a natural hazard triggering other natural hazards occurred in Peru in 2002 when a rock avalanche fell into the moraine-dammed Laguna Safuna Alta and triggered an impact wave higher than 100 m that overtopped the moraine dam of the lake (Hubbard et al., 2005). Impact waves triggered by rockslides such as the one at Laguna Safuna Alta have resulted in the loss of over a thousand lives in the Peruvian Andes alone over the last 100 years (Hubbard et al., 2005). For this reason, implications of climate change for mountain permafrost need to be better understood, which can potentially be achieved by field measurement campaigns such as the long measurement campaigns at the Matterhorn, Switzerland (Weber et al., 2019) in combination with empirical-statistical or physically-based mountain permafrost distribution models (Harris et al., 2009; Riseborough et al., 2008). Subsurface and groundwater flow, have been simulated by the models applied in chapter 3, 4, and 5. Nevertheless, the role and contributions of groundwater and subsurface flow in the high-altitude water cycle were not considered, which can, however, be substantial (e.g. Andermann et al., 2012; Bookhagen, 2012). More research will therefore be needed to assess the role and contributions of groundwater and subsurface flow in the water balance of mountain regions.

6.7.1.7 Stationarity of model parameters

Modelling and parameterizing the different components of the high-altitude water cycle is challenging due to the non-stationarity of the environment. One of the main model limitations is therefore the assumed stationarity of model parameters in the models applied throughout this thesis. The parameterizations are based on the present climatology, land use and other physical catchment characteristics. The reality however is that many parameters, such as parameters controlling ice and snow melt, are non-stationary. These parameters can change due to possible changes in climate, land use, amongst others (Brigode et al., 2013; Merz et al., 2011; Westra et al., 2014). One of the factors that control the impact of non-stationarity is the length and variability

of the period of calibration (Brigode et al., 2013; Vaze et al., 2010; Westra et al., 2014), which are decisive for the reliability of model outcomes. According to Vaze et al. (2010) models can be used for climate change impact studies when parameterizations are based on data records of 20 years of longer and for areas where climatic-induced changes remain small relative to present-day climate conditions. Other studies (e.g. Brigode et al., 2013) have indicated that shorter periods (e.g. 3 years) also can result in acceptable parameter sets. The drawback however is that long records of measurements needed for model calibration and validation are scarce in the IGB and that changes in climate and land use can be rather extreme. To reduce the impact of non-stationarity, calibration approaches such as the generalized split sample test of Coron et al. (2012) might be an outcome. This method aims at testing several possible combinations of calibration-validation periods to test the performance of models under different (climate) conditions.

6.7.2 Assessing climate change impacts in mountain regions

6.7.2.1 Reliability of climate models

To assess the long-term effects of historical or future climate change in mountain regions General Circulation Models (GCMs) or Regional Climate Models (RCMs) are required. The reliability of historical or future projections from cryospheric or hydrological models that are forced with GCMs or RCMs depends to a large extent on the skill of climate models in simulating the local or regional climate. Several studies have outlined that the skill of climate models is poor over complex mountainous terrain, in particular in HMA (Kang et al., 2010; Mishra, 2015; Palazzi et al., 2015; Ramesh and Goswami, 2014; Seneviratne et al., 2012; Sperber et al., 2013; Su et al., 2013). Thereby, the discrepancies are in general larger for precipitation simulations or projections. Similar findings have also been found for climatic extremes by Sillmann et al. (2013b, 2013a). The authors evaluated the performance of climate models of the CMIP5 archive for the present and future climate. Their findings showed that climatic extremes and their trend patterns are generally simulated sufficiently by climate models for the present climate. For the future climate, climate models show a general agreement for the projected changes in temperature extremes, where discrepancies exist in the projected changes of several precipitation indices. Discrepancies are found for dry precipitation indices such as the consecutive dry-day (CDD) index in South Asia, whereas for wet precipitation indices such as the heavy precipitation days index (R10mm) discrepancies are larger in the European Alps (Sillmann et al., 2013b). The presence of discrepancies between climate models emphasizes therefore the importance of selecting climate models based on their skill in simulating climatic means and extremes in the regions of interest.

To select climate models for the research presented throughout this thesis (chapter 2, 4, and 5) an advanced envelope-based selection approach (Lutz et al., 2016b) was used. This approach follows a sequence of steps that selects models based on the projected ranges in climatic means and extremes, and the model's skill in simulating the present climate in the region of interest. The advantage of this approach is that a limited number of models is selected that still can represent a full range of possible conditions in terms of climate change. A disadvantage, however, is that the selection of models is dependent on the selection approach that is followed, and that the selection is based on GCMs that are not downscaled to the region of interest. This means the spatial variability in meteorological variables such as precipitation is not captured, which means the selected models might be less representative for the region of interest than what is indicated during the selection approach. For this reason, the selection approach might be improved by statistically downscaling

the GCMs prior to the selection. The drawback, however, is that such implementation is computationally very demanding, but it might be nonetheless an alternative option for future research, especially when considering the continuing development in computational power.

By the selection of climate models based on their skill in simulating the regional climate, the uncertainties related to the discrepancies in climate models are reduced. Nevertheless, the spread in possible futures that are currently projected by climate models remains large. This affects, in turn, the reliability of model outcomes, in particular for the research presented in chapter 4 and 5. The large spread propagates into the hydrological model outcomes, which causes the projected water gap trends in chapter 5 to be less clear for the RCP8.5-SSP3 scenario. The projections for this RCP-SSP combinations show increasing water gaps for some GCM-SSP combinations, whereas for other combinations a decreasing water gap is shown. For this reason, improvements in climate models are needed to reduce the variation in future climate change projections. To this end, the upcoming CMIP6 model archive (Eyring et al., 2016; Gidden et al., 2019) might be an outcome.

6.7.2.2 Downscaling

Downscaling is required to bridge the scale differences between GCMs and the cryospheric and hydrological models. In this thesis, two statistical downscaling techniques were used to downscale and/or to bias-correct climate change simulations and projections: the classical delta change approach of Bosshard et al. (2011) (chapter 3) and the Quantile Mapping (QM) approach (Themeßl et al., 2011) (chapter 2, 4 and 5). The classical delta change approach has the limitation that it retains the current climate variability in future climate change projections. This implies that, for instance, the future number of wet and dry days does not change (Graham et al., 2007) and uncertainties might be introduced in future precipitation projections and the representation of future hydrological extremes (i.e. the seasonality of annual flood peaks and low flow frequencies). Due to the low amount of studies focusing on low flows in the European or Austrian Alps, the simulated and projected low flows (chapter 3) are difficult to verify. For this reason, the conjecture is that low flows are deemed to be less reliable. To improve the representation of future hydrological extremes one might therefore consider to use alternative statistical downscaling approaches, such as the Advanced Delta Change (ADC) approach (Lutz et al., 2016a; van Pelt et al., 2012) or the QM approach. Where the classical delta change approach is based on precipitation means, the ADC approach is based on changes in the entire precipitation distribution, which means precipitation extremes are better represented. The QM approach applied in chapter 4 and 5 has been proven to perform well over mountainous regions (Devi et al., 2019; Immerzeel et al., 2013; Themeßl et al., 2011). In addition, the method proved to be useful in the presented research in chapter 4 for the assessment of future changes in climatic extremes. Besides statistical downscaling techniques, dynamical downscaling techniques using high-resolution weather models or regional climate models (RCMs) are also an option. Dynamical downscaling techniques can considerably improve the accuracy of climate fields in mountainous environments (e.g. Bonekamp et al., 2018) and are also able to result in realistic and improved simulations of climatic extremes in mountain regions and other regions as well (El-Samra et al., 2018; Frei et al., 2006; Park et al., 2016). The disadvantage is, however, that the computational requirements are large. Nevertheless, with the prospects of increasing computational power it is promising to use dynamical downscaling techniques to improve future projections on both climatic and hydrological extremes.

6.7.2.3 Compound events

In chapter 3 and 4 the effects of climate change on the future occurrence of climatic and hydrological extremes were assessed. The occurrence of these extremes were mainly related to either the occurrence of temperature extremes that induce rapid increases in ice and snowmelt or the occurrence of precipitation extremes that can trigger floods or droughts. In the presented research the potential role of compound climate events was however not considered, whereas many hazards, such as floods and droughts, often result from a combination of interacting physical processes across different scales (Zscheischler et al., 2018). For example, riverine floods in mountain regions and surrounding lowlands can be triggered by a coincidence of extensive rainfalls and rapid temperature-induced increases in ice and snowmelt. Another example are large-scale compound events such as the atmospheric teleconnections that have been found between the devastating Pakistan floods and the Russian heatwaves and droughts in 2010 (Lau and Kim, 2012). Compound events are not well understood, in particular in mountain regions such as HMA. For this reason, more research will be needed to compound events, which can potentially help us to answer questions on which drivers are responsible for natural hazards and how we can reduce the adverse impacts of these hazards.

6.7.3 Bridging the scale gap: from catchment-scale to regional/basin-scale

6.7.3.1 Bridging the scale gap

Throughout this thesis, climate change impacts have been assessed at different spatial scales. To this end, semi-distributed and fully-distributed models were used with different spatial resolutions varying from about 30 m in chapter 2 to 5 arcmin (~9 km at the equator) in chapter 5. One of the main challenges in assessing climate change impacts in mountain regions is how to capture the large spatial process variability sufficiently in models. For example, processes related to the dynamics of a glacier or the atmosphere are characterized by a large spatial variability over short horizontal and vertical distances. To simulate these processes more accurately, hyper-resolution models with a spatial resolution higher than 1 km would be more favorable and might improve the reliability of simulations (e.g. Bierkens et al., 2015; Bonekamp et al., 2018; Melsen et al., 2016). Hyper-resolution modelling is, however, challenging due to its large computational demand in terms of computation time and storage capacity, especially when modelling over very large areas. Increasing the model resolution with a factor of 10 would imply that the calculation time and storage capacity increases with a factor of 100 (Bierkens et al., 2015). To enable hyper-resolution modelling, powerful computing clusters such as the Dutch Cartesius supercomputer are needed.

Another challenge related to the spatial variability within mountain regions is the parameterization of models. For instance, the SPHY model applied in chapter 4 and 5 is forced with uniform parameter sets for each river basins specifically. The uniformity of the parameters might subsequently introduce uncertainties in the model outcomes since most parameters also vary spatially. For this reason attempts will be needed to reduce the uncertainties related to the spatial variability in parameter values. One of the option that can be considered is to apply regionalization methods by transposing parameter sets from gauged catchments to ungauged catchments with similar climatic or physiographic characteristics (e.g. topography, land use, soils, geology, etc.). According to Parajka et al. (2005), who evaluated several regionalization approaches in the Austrian Alps, the similarity and the kriging approaches belong to the best performing regionalization methods and are recommendable. The disadvantage of regionalization approaches is the difficulty

in implementing these in remote areas such as HMA. Many catchments are ungauged and a lot of detailed information (e.g. on geology) required for the implementation of these approaches is lacking. An alternative solution might therefore be to use standard parameterizations in combination with satellite-derived imagery, such as is done in state-of-the-art global hydrological models (e.g. PCR-GLOBWB2 (Sutanudjaja et al., 2018) or LPJmL4 (Schaphoff et al., 2018)).

6.7.3.2 Socio-economic development vs climate change

In chapter 5 the combined impacts of climate change and socio-economic development on the regional water gap of the Indus, Ganges, and Brahmaputra river basins were assessed. The main finding of this research is that socio-economic development can be considered as the key driver in the future evolution of the South Asian water gap, whereas climate change plays a role as a decelerator. The findings are, however, only representative for what might be expected for the Indus, Ganges, and Brahmaputra river basins. In other mountainous river basins the trade-off between socio-economic developments and climate changes might be different, which eventually also might result in a different evolution of the regional water gap. It is most likely that the water gap will become larger in regions where projected increases in the water demand coincide with projected decreases in water availability. Examples of such regions are Northern and Southern Africa, the Mediterranean region, the Middle East, Central Asia, Chile/Argentina, and USA/Mexico (Wada and Bierkens, 2014). In some of these regions that are already depending on mountain water resources, such as Central Asia and Chile/Argentina (see Figure 1.1), it is very likely that the dependency on mountain water resources will increase.

The future evolution of the South Asian water gap depends to a large extent on the selected climate scenarios and SSP storylines. There are several research gaps that need to be resolved in order to improve future water gap projections. One of the limitations is the limited interaction between climatic and socio-economic changes within SSP storylines. The storylines do, for instance, not consider the impacts of climate change on the land system or agro-economic variables, such as agricultural area and production (Doelman et al., 2018; Nelson et al., 2014). In this way, increases in the cropland extent as a response to climate change are not considered, which means future increases in cropland extent might be underestimated (Nelson et al., 2014). Further, the effects of several climate change adaptation strategies on the future evolution of the regional water gap are not considered. Future developments, such as the intensification of croplands were not considered, whereas irrigation efficiencies will most likely change due to changing irrigation systems that improve the efficiencies. Crop types were assumed to be constant, whereas it is likely that crops will be changed to types that are more climate-intolerant (Biemans et al., 2013). Also, the future potential development of hydropower dams and reservoirs is not considered, which can be expected to happen in the future (Mukherji et al., 2015). In addition, developments, such as regional and transboundary cooperation that can contribute to the optimization of water resources use (Molden et al., 2017), are not taken into account. For this reason, future research will need to focus on including interactions between climate change and socio-economic development, and the effects of future adaptation strategies on the regional water gap and its potentials in closing the water gap.

6.7.3.3 Understanding the human factor

Climate change impacts were assessed from different perspectives (cryospheric, hydrological, and anthropogenic). Although the gained knowledge contributes to an improved understanding of the cryospheric-hydrological impacts of climate change in mountainous river basins, still many

unknowns remain. For example, improvements are needed in understanding the role of human modifications on the environment and subsequent feedbacks that may occur between human-induced environmental changes and the regional climate. For example, a recent study by de Kok et al. (2018) found that a rapid intensification of irrigation in lowlands surrounding HMA can locally countereffect the effects of global warming on glaciers in parts of HMA (i.e. Kunlun Shan and parts of Pamir and northern Tibet). Another study of Lau and Kim (2018) found out that increased concentrations of light-absorbing aerosols from natural and anthropogenic sources can have a large impact on the regional climate in South and East Asia. During spring the deposition of aerosols in the Himalayas and on the Tibetan Plateau result in declining surface albedos, which can trigger enhanced melt and heating of the land surface and atmosphere over the Tibetan Plateau and the southern slopes of the Himalayas. The enhanced heating is subsequently followed by an amplification of low-level southwesterlies and associated increased transport of desert dust, an intensification of the Indian monsoon, and increased East Asian subtropical frontal rainfalls (Lau and Kim, 2018; Wang et al., 2008). To understand feedbacks between human modifications and other processes, such as atmospheric, cryospheric, and hydrological processes, a more integrated look is needed on how these processes operate and interact. This requires a perspective that enables the integration of multiple processes in one system, which can potentially be achieved by application and development of (hyper-resolution) Earth System Models. These models consider the co-evolution of earth system processes and might contribute to new insights on the role of human modifications. The knowledge that can be gained from these models can be a valuable addition to the insights that have already been gained on processes, feedback, and impacts in mountainous river basins over the last decades. Nonetheless, there is no doubt that many scientific challenges will be left to explore and mysteries to be unravelled in the future.

6.7.4 From understanding climate change impacts to adaptation

This thesis highlights a number of examples of potential climate change impacts. At the same time climate change will affect mountainous river basins in many other ways. For example, the retreat of glaciers can be accompanied by the development of moraine-dammed lakes, which itself can be advantageous since the lakes can contribute to increasing potential for hydropower generation (Frey et al., 2010). However, the lakes can also be a potential threat for the society since the risk for glacial lake outburst floods (GLOFs) increases. Other natural hazards that may appear more frequently are flash floods and debris flows triggered by extreme precipitation events. An example are the devastating rainfall events in Ladakh and Zanskar (i.e. located in north-western India) that occurred during the intense monsoonal rainstorms in August 2010. These rainstorms deposited more than half of the regional annual precipitation sum in a few hours and triggered destructive debris flows and floods resulting in more than 250 fatalities and severe damages in over 70 villages (Kohler et al., 2014). These rainstorms were a part in a chain of monsoonal rainstorms that also severely affected Pakistan with about 1950 fatalities and an overall loss of about 9.5 billion US dollars (Munich RE, 2011; Webster et al., 2011; World Bank, 2013). The devastating impacts of these natural hazards show that more research is needed on the relation between the frequency and magnitude of natural hazards and climate change in mountainous regions. These research outcomes will help to develop adaptation strategies that can reduce the adverse impacts of natural hazards. A potential way to develop adaptation strategies is to use the recently developed framework for upstream-linkages (UDL) of land and water management (Flügel et al., 2018). This framework is a multi-scale interdisciplinary approach that accounts for the natural and socio-economic processes within a river basin. The framework is applicable to micro, meso, and macro scale UDL applications

and consists of several components ranging from UDL system definition, assessment, and analysis to adaptation and decision information support. The adaptation component aims at developing and evaluating adaptation strategies with respect to Integrated Land and Water Resources Management (ILWRM) that mitigate changes in the UDL system.

Bibliography

Abbasi, S. S., Ahmad, B., Ali, M., Anwar, M. Z., Dahri, Z. H., Habib, N., et al. (2017). The Indus Basin: A glacier-fed lifeline for Pakistan. Kathmandu, Nepal: International Centre for Integrated Mountain Development (ICIMOD).

Abegg, B., Agrawala, S., Crick, F., and De Montfalcon, A. (2007). "Climate change impacts and adaptation in winter tourism," in Climate Change in the European Alps (Paris, France: OECD (Organisation for Economic Co-operation and Development)), 25–60. doi:10.1787/9789264031692-en.

Abermann, J., Lambrecht, A., Fischer, A., and Kuhn, M. (2009). Quantifying changes and trends in glacier area and volume in the Austrian Ötztal Alps (1969-1997-2006). Cryosph. 3, 205–215. doi:10.5194/tc-3-205-2009.

Abermann, J., Seiser, B., Meran, I., Stocker-Waldhuber, M., Goller, M., and Fischer, A. (2012). A new ALS glacier inventory of North Tyrol, Austria, for 2006. Zeitschrift für Gletscherkd. und Glazialgeol. 43, 109–119.

Achleitner, S., Schöber, J., Rinderer, M., Leonhardt, G., Schöberl, F., Kirnbauer, R., et al. (2012). Analyzing the operational performance of the hydrological models in an alpine flood forecasting system. J. Hydrol. 412–413, 90–100. doi:10.1016/j.jhydrol.2011.07.047.

Aðalgeirsdóttir, G., Guðmundsson, S., Björnsson, H., Palsson, F., Jóhannesson, T., Hannesdóttir, H., et al. (2011). Modelling the 20th and 21st century evolution of Hoffellsjökull glacier, SE-Vatnajökull, Iceland. Cryosph. 5, 1961–1975. doi:10.5194/tc-5-961-2011.

ADB (2018). Asian Development Outlook 2018: How Technology Affects Jobs. Mandaluyong City, Philippines doi:10.22617/FLS189310-3.

Addor, N., Rössler, O., Köplin, N., Huss, M., Weingartner, R., and Seibert, J. (2014). Robust changes and sources of uncertainty in the projected hydrological regimes of Swiss catchments. Water Resour. Res. 50, 7541–7562. doi:10.1002/2014WR015549.

Adhikari, S., and Huybrechts, P. (2009). Numerical modelling of historical front variations and the 21st-century evolution of glacier AX010, Nepal Himalaya. Ann. Glaciol. 50, 27–34. doi:10.3189/172756409789624346.

Adhikari, S., and Marshall, S. J. (2011). Improvements to shear-deformational models of glacier dynamics through a longitudinal stress factor. J. Glaciol. 57, 1003–1016. doi:10.3189/002214311798843449.

Adhikari, S., and Marshall, S. J. (2012a). Glacier volume-area relation for high-order mechanics and transient glacier states. Geophys. Res. Lett. 39, 6. doi:10.1029/2012GL052712.

Adhikari, S., and Marshall, S. J. (2012b). Parameterization of lateral drag in flowline models of glacier dynamics. J. Glaciol. 58, 1119–1132. doi:10.3189/2012JoG12J018.

Adhikari, S., and Marshall, S. J. (2013). Influence of high-order mechanics on simulation of glacier response to climate change: Insights from Haig Glacier, Canadian Rocky Mountains. Cryosph. 7, 1527–1541. doi:10.5194/tc-7-1527-2013.

Adhikari, S., Marshall, S. J., and Huybrechts, P. (2011). On Characteristic Timescales of Glacier AX010 in the Nepalese Himalaya. Bull. Glaciol. Res. 29, 19–29. doi:10.5331/bgr.29.19.

Akhtar, M., Ahmad, N., and Booij, M. J. (2008). The impact of climate change on the water resources of Hindukush–Karakorum–Himalaya region under different glacier coverage scenarios. J. Hydrol. 355, 148–163. doi:10.1016/j.jhydrol.2008.03.015.

Alcamo, J. M., Döll, P., Henrichs, T., Kaspar, F., Lehner, B., Rösch, T., et al. (2003). Development and testing of the WaterGAP 2 global model of water use and availability. Hydrol. Sci. 48, 317–337. doi:10.1623/hysj.48.3.317.45290.

Alcamo, J. M., Flörke, M., and Märker, M. (2007). Future long-term changes in global water resources driven by socio-economic and climatic changes. Hydrol. Sci. J. 52, 247–275. doi:10.1623/hysj.52.2.247.

Allen, R. G., Pereira, L. S., Raes, D., and Smith, M. (1998). Crop Evapotranspiration: Guidelines for Computing Crop Water Requirements. Irrig. Drain. Pap. No. 56, FAO, Rome, Italy. doi:10.4000/trema.1752.

<< The densely populated capital city of Nepal, Kathmandu (1350 m) seen from Swayambhu (R.R. Wijngaard)

Andermann, C., Longuevergne, L., Bonnet, S., Crave, A., Davy, P., and Gloaguen, R. (2012). Impact of transient groundwater storage on the discharge of Himalayan rivers. Nat. Geosci. 5, 127–132. doi:10.1038/ngeo1356.

Anderson, R. S. (2000). A model of ablation-dominated medial moraines and the generation of debris-mantled glacier snouts. J. Glaciol. 46, 459–469. doi:10.3189/172756500781833025.

Apel, H., Thieken, A. H., Merz, B., and Blöschl, G. (2004). Flood risk assessment and associated uncertainty. Nat. Hazards Earth Syst. Sci. 4, 295–308. doi:10.5194/nhess-4-295-2004.

Archer, D. R., and Fowler, H. J. (2004). Spatial and temporal variations in precipitation in the Upper Indus Basin, global teleconnections and hydrological implications. Hydrol. Earth Syst. Sci. 8, 47–61. doi:10.5194/hess-8-47-2004.

Arnell, N. W. (2004). Climate change and global water resources: SRES emissions and socio-economic scenarios. Glob. Environ. Chang. 14, 31–52. doi:10.1016/j.gloenvcha.2003.10.006.

Arnell, N. W., and Lloyd-Hughes, B. (2014). The global-scale impacts of climate change on water resources and flooding under new climate and socio-economic scenarios. Clim. Change 122, 127–140. doi:10.1007/s10584-013-0948-4.

Arora, V. K., Scinocca, J. F., Boer, G. J., Christian, J. R., Denman, K. L., Flato, G. M., et al. (2011). Carbon emission limits required to satisfy future representative concentration pathways of greenhouse gases. 38, 3–8. doi:10.1029/2010GL046270.

Asoka, A., Gleeson, T., Wada, Y., and Mishra, V. (2017). Relative contribution of monsoon precipitation and pumping to changes in groundwater storage in India. Nat. Geosci. 10, 109–117. doi:10.1038/ngeo2869.

Ayala, A., Pellicciotti, F., MacDonell, S., McPhee, J., Vivero, S., Campos, C., et al. (2016). Modelling the hydrological response of debris-free and debris-covered glaciers to present climatic conditions in the semiarid Andes of central Chile. Hydrol. Process. 30, 4036–4058. doi:10.1002/hyp.10971.

Bahr, D. B., Meier, M. F., and Peckham, S. D. (1997). The physical basis of glacier volume-area scaling. J. Geophys. Res. Solid Earth 102, 20355–20362. doi:10.1029/97JB01696.

Bahr, D. B., Pfeffer, W. T., and Kaser, G. (2015). A review of volume-area scaling of glaciers. Rev. Geophys. 53, 95–140. doi:10.1002/2014RG000470.

Bajracharya, S. R., and Shrestha, B. (2011). The status of glaciers in the Hindu Kush-Himalayan region. Kathmandu, Nepal.

Banerjee, A. (2017). Brief communication: Thinning of debris-covered and debris-free glaciers in a warming climate. Cryosph. 11, 133–138. doi:10.5194/tc-11-133-2017.

Banerjee, A., and Shankar, R. (2013). On the response of Himalayan glaciers to climate change. J. Glaciol. 59, 480–490. doi:10.3189/2013JoG12J130.

Barnett, T. P., Adam, J. C., and Lettenmaier, D. P. (2005). Potential impacts of a warming climate on water availability in snow-dominated regions. Nature 438, 303–309. doi:10.1038/nature04141.

Beniston, M. (2003). Climatic change in mountain regions: a review of possible impacts. Clim. Change 59, 5–31. doi:10.1023/A:1024458411589.

Beniston, M., Farinotti, D., Stoffel, M., Andreassen, L. M., Coppola, E., Eckert, N., et al. (2018). The European mountain cryosphere: a review of its current state, trends, and future challenges. Cryosph. 12, 759–794. doi:10.5194/tc-12-759-2018.

Bergström, S. (1992). The HBV model - its structure and applications. Swedish Meteorol. Hydrol. Inst. Reports Hydrol.

Bergström, S., Harlin, J., and Lindström, G. (1992). Spillway design floods in Sweden: I. New guidelines. Hydrol. Sci. J. 37, 505–519. doi:10.1080/02626669209492615.

Bernhardt, M., and Schulz, K. (2010). SnowSlide: A simple routine for calculating gravitational snow transport. Geophys. Res. Lett. 37. doi:10.1029/2010GL043086.

Berthier, E., and Vincent, C. (2012). Relative contribution of surface mass-balance and ice-flux changes to the accelerated thinning of Mer de Glace, French Alps, over 1979-2008. J. Glaciol. 58, 501–512. doi:10.3189/2012JoG11J083.

Biemans, H., Haddeland, I., Kabat, P., Ludwig, F., Hutjes, R. W. A., Heinke, J., et al. (2011). Impact of reservoirs on river discharge and irrigation water supply during the 20th century. Water Resour. Res. 47. doi:10.1029/2009WR008929.

Biemans, H., Hutjes, R. W. A., Kabat, P., Strengers, B. J., Gerten, D., and Rost, S. (2009). Effects of Precipitation Uncertainty on Discharge Calculations for Main River Basins. J. Hydrometeorol. 10, 1011–1025. doi:10.1175/2008JHM1067.1.

Biemans, H., Siderius, C., Lutz, A.F., Nepal, S., Ahmad, B., Hassan, S.M.T., von Bloh, W., Wijngaard, R.R., Wester, P., Shrestha, A.B. & Immerzeel, W.W. 2019. Importance of snow and glacier meltwater for agriculture on the Indo-Gangetic Plain. Nature Sustainability 2, 594-601. DOI: 10.1038/s41893-019-0305-3.

Biemans, H., Siderius, C., Mishra, A., and Ahmad, B. (2016). Crop-specific seasonal estimates of irrigation-water demand in South Asia. Hydrol. Earth Syst. Sci. 20, 1971–1982. doi:10.5194/hess-20-1971-2016.

Biemans, H., Speelman, L. H., Ludwig, F., Moors, E. J., Wiltshire, A. J., Kumar, P., et al. (2013). Future water resources for food production in five South Asian river basins and potential for adaptation — A modeling study. Sci. Total Environ. 468–469, 117–131. doi:10.1016/j.scitotenv.2013.05.092.

Bierkens, M. F. P. (2015). Global hydrology 2015: State, trends, and directions. Water Resour. Res. 51, 4923–4947. doi:10.1002/2015WR017173.

Bierkens, M. F. P., Bell, V. A., Burek, P., Chaney, N., Condon, L. E., David, C. H., et al. (2015). Hyper-resolution global hydrological modelling: what is next? Hydrol. Process. 29, 310–320. doi:10.1002/hyp.10391.

Bijl, D. L., Bogaart, P. W., Kram, T., de Vries, B. J. M., and van Vuuren, D. P. (2016). Long-term water demand for electricity, industry and households. Environ. Sci. Policy 55, 75–86. doi:10.1016/j.envsci.2015.09.005.

Blöschl, G., and Sivapalan, M. (1995). Scale issues in hydrological modelling: A review. Hydrol. Process. 9, 251–290. doi:10.1002/hyp.3360090305.

Blümcke, A., and Hess, H. (1895). Der Hochjochferner in Jahre 1893. Zeitschrift des Dtsch. und Österreichischen Alpenvereins 26, 340. Available at: https://www.e-rara.ch/zut/content/zoom/11639790.

BMLFUW (2007). Hydrological Atlas Austria. Vienna, Austria: BMLFUW (Federal Ministry of Agriculture, Forestry, Environment and Water Management), Division VII/3, Water Management.

Bolch, T., Kulkarni, A. V., Kaab, A., Huggel, C., Paul, F., Cogley, J. G., et al. (2012). The State and Fate of Himalayan Glaciers. Science (80-.). 336, 310–314. doi:10.1126/science.1215828.

Bondeau, A., Smith, P. C., Zaehle, S., Schaphoff, S., Lucht, W., Cramer, W., et al. (2007). Modelling the role of agriculture for the 20th century global terrestrial carbon balance. Glob. Chang. Biol. 13, 679–706. doi:10.1111/j.1365-2486.2006.01305.x.

Bonekamp, P. N. J., Collier, E., and Immerzeel, W. W. (2018). The Impact of Spatial Resolution, Land Use, and Spinup Time on Resolving Spatial Precipitation Patterns in the Himalayas. J. Hydrometeorol. 19, 1565–1581. doi:10.1175/JHM-D-17-0212.1.

Bookhagen, B. (2012). Himalayan groundwater. Nat. Geosci. 5, 97–98. doi:10.1038/ngeo1366.

Bookhagen, B., and Burbank, D. W. (2010). Toward a complete Himalayan hydrological budget: Spatiotemporal distribution of snowmelt and rainfall and their impact on river discharge. J. Geophys. Res. Earth Surf. 115. doi:10.1029/2009JF001426.

Bossard, M., Feranec, J., and Otahel, J. (2000). CORINE Land Cover. Technical Guide: Addendum 2000. Copenhagen, Denmark.

Bosshard, T., Kotlarski, S., Ewen, T., and Schär, C. (2011). Spectral representation of the annual cycle in the climate change signal. Hydrol. Earth Syst. Sci. 15, 2777–2788. doi:10.5194/hess-15-2777-2011.

Bowling, L. C., Pomeroy, J. W., and Lettenmaier, D. P. (2004). Parameterization of Blowing-Snow Sublimation in a Macroscale Hydrology Model. J. Hydrometeorol. 5, 745–762. doi:10.1175/1525-7541(2004)005<0745:POBSIA>2.0.CO;2.

Braithwaite, R. J., and Zhang, Y. (2000). Sensitivity of mass balance of five Swiss glaciers to temperature changes assessed by tuning a degree-day model. J. Glaciol. 46, 7–14. doi:10.3189/172756500781833511.

Brigode, P., Oudin, L., and Perrin, C. (2013). Hydrological model parameter instability: A source of additional uncertainty in estimating the hydrological impacts of climate change? J. Hydrol. 476, 410–425. doi:10.1016/j.jhydrol.2012.11.012.

Brun, F. (2018). Impact of the debris cover on High Mountain Asia glacier mass balances : a multi-scale approach.

Brun, F., Wagnon, P., Berthier, E., Shea, J. M., Immerzeel, W. W., Kraaijenbrink, P. D. A., et al. (2018). Ice cliff contribution to the tongue-wide ablation of Changri Nup Glacier, Nepal, central Himalaya. Cryosph. 12, 3439–3457. doi:10.5194/tc-12-3439-2018.

Buytaert, W., Cuesta-Camacho, F., and Tobón, C. (2011). Potential impacts of climate change on the environmental services of humid tropical alpine regions. Glob. Ecol. Biogeogr. 20, 19–33. doi:10.1111/j.1466-8238.2010.00585.x.

Casassa, G., López, P., Pouyaud, B., and Escobar, F. (2009). Detection of changes in glacial run-off in alpine basins: examples from North America, the Alps, central Asia and the Andes. Hydrol. Process. 23, 31–41. doi:10.1002/hyp.7194.

Charalampidis, C., Fischer, A., Kuhn, M., Lambrecht, A., Mayer, C., Thomaidis, K., et al. (2018). Mass-Budget Anomalies and Geometry Signals of Three Austrian Glaciers. Front. Earth Sci. 6. doi:10.3389/feart.2018.00218.

Cheema, M. J. M., and Bastiaanssen, W. G. M. (2010). Land use and land cover classification in the irrigated Indus Basin using growth phenology information from satellite data to support water management analysis. Agric. Water Manag. 97, 1541–1552. doi:10.1016/j.agwat.2010.05.009.

Cheema, M. J. M., Immerzeel, W. W., and Bastiaanssen, W. G. M. (2014). Spatial quantification of groundwater abstraction in the irrigated indus basin. Groundwater 52, 25–36. doi:10.1111/gwat.12027.

Christen, M., Kowalski, J., and Bartelt, P. (2010). RAMMS: Numerical simulation of dense snow avalanches in three-dimensional terrain. Cold Reg. Sci. Technol. 63, 1–14. doi:10.1016/j.coldregions.2010.04.005.

Clarke, G. K. C., Jarosch, A. H., Anslow, F. S., Radić, V., and Menounos, B. (2015). Projected deglaciation of western Canada in the twenty-first century. Nat. Geosci. 8, 372–377. doi:10.1038/ngeo2407.

Colgan, W., Rajaram, H., Abdalati, W., McCutchan, C., Mottram, R., Moussavi, M. S., et al. (2016). Glacier crevasses: Observations, models, and mass balance implications. Rev. Geophys. 54, 119–161. doi:10.1002/2015RG000504.

Collier, E., and Immerzeel, W. W. (2015). High-resolution modeling of atmospheric dynamics in the Nepalese Himalaya. J. Geophys. Res. 120, 9882–9896. doi:10.1002/2015JD023266.

Collier, E., Maussion, F., Nicholson, L., Mölg, T., Immerzeel, W. W., and Bush, A. B. G. (2015). Impact of debris cover on glacier ablation and atmosphere–glacier feedbacks in the Karakoram. Cryosph. 9, 1617–1632. doi:10.5194/tc-9-1617-2015.

Collier, E., Mölg, T., Maussion, F., Scherer, D., Mayer, C., and Bush, A. B. G. (2013). High-resolution interactive modelling of the mountain glacier–atmosphere interface: an application over the Karakoram. Cryosph. 7, 779–795. doi:10.5194/tc-7-779-2013.

Coron, L., Andréassian, V., Perrin, C., Lerat, J., Vaze, J., Bourqui, M., et al. (2012). Crash testing hydrological models in contrasted climate conditions: An experiment on 216 Australian catchments. Water Resour. Res. 48. doi:10.1029/2011WR011721.

Cuffey, K. M., and Paterson, W. S. B. (2010). Physics of Glaciers, Fourth Edition. 4th ed. Amsterdam, the Netherlands: Academic Press Inc.

de Boer, F. (2016). HiHydroSoil: A High Resolution Soil Map of Hydraulic Properties. Wageningen, the Netherlands.

de Graaf, I. E. M., van Beek, L. P. H., Gleeson, T., Moosdorf, N., Schmitz, O., Sutanudjaja, E. H., et al. (2017). A global-scale two-layer transient groundwater model: Development and application to groundwater depletion. Adv. Water Resour. doi:10.1016/j.advwatres.2017.01.011.

de Jong, C. (2015). Challenges for mountain hydrology in the third millennium. Front. Environ. Sci. 3, 38. doi:10.3389/fenvs.2015.00038.

de Kok, R. J., Tuinenburg, O. A., Bonekamp, P. N. J., and Immerzeel, W. W. (2018). Irrigation as a Potential Driver for Anomalous Glacier Behavior in High Mountain Asia. Geophys. Res. Lett. doi:10.1002/2017GL076158.

De Souza, K., Kituyi, E., Harvey, B., Leone, M., Murali, K. S., and Ford, J. D. (2015). Vulnerability to climate change in three hot spots in Africa and Asia: key issues for policy-relevant adaptation and resilience-building research. Reg. Environ. Chang. 15, 747–753. doi:10.1007/s10113-015-0755-8.

Dee, D. P., Uppala, S. M., Simmons, A. J., Berrisford, P., Poli, P., Kobayashi, S., et al. (2011). The ERA-Interim reanalysis: Configuration and performance of the data assimilation system. Q. J. R. Meteorol. Soc. 137, 553–597. doi:10.1002/qj.828.

Defourny, P., Vancutsem, C., Bicheron, C., Brockmann, C., Nino, F., Schouten, L., et al. (2007). GlobCover: A 300M Global Land Cover Product for 2005 Using ENVISAT MERIS Time Series. Proc. ISPRS Comm. VII Mid-Term Symp., 8–11.

Dehecq, A., Gourmelen, N., Gardner, A. S., Brun, F., Goldberg, D., Nienow, P. W., et al. (2019). Twenty-first century glacier slowdown driven by mass loss in High Mountain Asia. Nat. Geosci. 12, 22–27. doi:10.1038/s41561-018-0271-9.

Déqué, M. (2007). Frequency of precipitation and temperature extremes over France in an anthropogenic scenario: Model results and statistical correction according to observed values. Glob. Planet. Change 57, 16–26. doi:10.1016/j.gloplacha.2006.11.030.

Déqué, M., Dreveton, C., Braun, A., and Cariolle, D. (1994). The ARPEGE/IFS atmosphere model: a contribution to the French community climate modelling. Clim. Dyn. 10, 249–266. doi:10.1007/BF00208992.

Devi, U., Shekhar, M. S., Singh, G. P., Rao, N. N., and Bhatt, U. S. (2019). Methodological application of quantile mapping to generate precipitation data over Northwest Himalaya. Int. J. Climatol. 39, 3160–3170. doi:10.1002/joc.6008.

Dingman, S. L. (2008). Physical Hydrology. 2nd ed. Waveland Press, Inc.

Doelman, J. C., Stehfest, E., Tabeau, A., van Meijl, H., Lassaletta, L., Gernaat, D. E. H. J., et al. (2018). Exploring SSP land-use dynamics using the IMAGE model: Regional and gridded scenarios of land-use change and land-based climate change mitigation. Glob. Environ. Chang. 48, 119–135. doi:10.1016/j.gloenvcha.2017.11.014.

Doherty, J. (2018). PEST: Model-Independent Parameter Estimation, User Manual: 7th Edition. Brisbane, Queensland, Australia.

Döll, P., Fiedler, K., and Zhang, J. (2009). Global-scale analysis of river flow alterations due to water withdrawals and reservoirs. Hydrol. Earth Syst. Sci. 13, 2413–2432. doi:10.5194/hess-13-2413-2009.

Dooge, J. C. I. (1986). Looking for hydrologic laws. Water Resour. Res. 22, 46–58. doi:10.1029/WR022i09Sp0046S.

EEA (2009). Regional climate change and adaptation — The Alps facing the challenge of changing water resources. Copenhagen, Denmark.

EEA (2017). Digital Elevation Model over Europe (EU-DEM). Available at: https://www.eea.europa.eu/data-and-maps/data/eu-dem [Accessed September 26, 2017].

Egholm, D. L., Knudsen, M. F., Clark, C. D., and Lesemann, J. E. (2011). Modeling the flow of glaciers in steep terrains: The integrated second-order shallow ice approximation (iSOSIA). J. Geophys. Res. Earth Surf. 116. doi:10.1029/2010JF001900.

Einarsson, B., and Jónsson, S. (2010). The effect of climate change on runoff from two watersheds in Iceland. Reykjavik, Iceland.

El-Samra, R., Bou-Zeid, E., and El-Fadel, M. (2018). To what extent does high-resolution dynamical downscaling improve the representation of climatic extremes over an orographically complex terrain? Theor. Appl. Climatol. 134, 265–282. doi:10.1007/s00704-017-2273-8.

Eregno, F. E., Xu, C. Y., and Kitterød, N. O. (2013). Modeling hydrological impacts of climate change in different climatic zones. Int. J. Clim. Chang. Strateg. Manag. 5, 344–365. doi:10.1108/IJCCSM-04-2012-0024.

Eriksson, M., Jianchu, X., Shrestha, A. B., Vaidya, R. A., Nepal, S., and Sandström, K. (2009). The Changing Himalayas Impact of climate change on water resources and livelihoods in the greater Himalaya. Kathmandu, Nepal: International Centre for Integrated Mountain Development (ICIMOD). Kathmandu.

Eyring, V., Bony, S., Meehl, G. A., Senior, C. A., Stevens, B., Stouffer, R. J., et al. (2016). Overview of the Coupled Model Intercomparison Project Phase 6 (CMIP6) experimental design and organization. Geosci. Model Dev. 9, 1937–1958. doi:10.5194/gmd-9-1937-2016.

Fader, M., Rost, S., Müller, C., Bondeau, A., and Gerten, D. (2010). Virtual water content of temperate cereals and maize: Present and potential future patterns. J. Hydrol. 384, 218–231. doi:10.1016/j.jhydrol.2009.12.011.

Faillettaz, J., Funk, M., and Vincent, C. (2015). Avalanching glacier instabilities: Review on processes and early warning perspectives. Rev. Geophys. 53, 203–224. doi:10.1002/2014RG000466.

FAO/IIASA/ISRIC/ISSCAS/JRC (2012). Harmonized World Soil Database (version 1.2). Rome, Italy and Laxenburg, Austria.

FAO (2012). Irrigation in Southern and Eastern Asia in figures. Rome, Italy.

FAO (2016). AQUASTAT Database, Food and Agriculture Organization of the United Nations (FAO). Available at: http://www.fao.org/nr/water/aquastat/main/index.stm.

FAO (2017). FAOSTAT Database, Food and Agriculture Organization of the United Nations (FAO).

Farda, A., Déué, M., Somot, S., Horányi, A., Spiridonov, V., and Tóth, H. (2010). Model ALADIN as regional climate model for Central and Eastern Europe. Stud. Geophys. Geod. 54, 313–332. doi:10.1007/s11200-010-0017-7.

Farinotti, D., Huss, M., Bauder, A., Funk, M., and Truffer, M. (2009). A method to estimate the ice volume and ice-thickness distribution of alpine glaciers. J. Glaciol. 55, 422–430. doi:10.3189/002214309788816759.

Farinotti, D., Usselmann, S., Huss, M., Bauder, A., and Funk, M. (2012). Runoff evolution in the Swiss Alps: projections for selected high-alpine catchments based on ENSEMBLES scenarios. Hydrol. Process. 26, 1909–1924. doi:10.1002/hyp.8276.

Farr, T. G., Rosen, P. A., Caro, E., Crippen, R., Duren, R., Hensley, S., et al. (2007). The Shuttle Radar Topography Mission. Rev. Geophys. 45, RG2004. doi:10.1029/2005RG000183.

Federer, C. A., and Lash, D. (1978). Simulated streamflow response to possible differences in transpiration among species of hardwood trees. Water Resour. Res. 14, 1089–1097. doi:10.1029/WR014i006p01089.

Fischer, A. (2010). Glaciers and climate change: Interpretation of 50years of direct mass balance of Hintereisferner. Glob. Planet. Change 71, 13–26. doi:10.1016/j.gloplacha.2009.11.014.

Fischer, A., Seiser, B., Stocker-Waldhuber, M., Mitterer, C., and Abermann, J. (2015). Tracing glacier changes in Austria from the Little Ice Age to the present using a lidar-based high-resolution glacier inventory in Austria. Cryosph. 9, 753–766. doi:10.5194/tc-9-753-2015.

Flügel, W.-A., Nepal, S., and Shrestha, A. B. (2018). Framework for Upstream- Downstream Linkages of Land and Water Management in the Hindu Kush Himalaya (HKH) Region. Kathmandu, Nepal.

Flügel, W.-A., Pechstedt, J., Bongartz, K., Bartosch, A., Eriksson, M., and Clark, M. (2008). Analysis of climate change trend and possible impacts in the Upper Brahmaputra River Basin – the BRAHMATWINN Project. 13th IWRA World Water Congress 2008, Montpelier, France.

Formayer, H., and Haas, P. (2010). Correction of RegCM3 model output data using a rank matching approach applied on various meteorological parameters. Deliverable D3. 2 RCM output localization methods (BOKU-contribution of the FP 6 CECILIA project). Available at: www.cecilia-eu.org/restricted/%0Ddeliverables.php.

Forsythe, N., Fowler, H. J., Blenkinsop, S., Burton, A., Kilsby, C. G., Archer, D. R., et al. (2014). Application of a stochastic weather generator to assess climate change impacts in a semi-arid climate: The Upper Indus Basin. J. Hydrol. 517, 1019–1034. doi:10.1016/j.jhydrol.2014.06.031.

Fowler, H. J., and Archer, D. R. (2006). Conflicting signals of climatic change in the Upper Indus Basin. J. Clim. 19, 4276–4293. Available at: http://journals.ametsoc.org/doi/abs/10.1175/JCLI3860.1 [Accessed September 8, 2014].

Frei, C., and Schär, C. (1998). A precipitation climatology of the Alps from high-resolution rain-gauge observations. Int. J. Climatol. 18, 873–900. doi:10.1002/(SICI)1097-0088(19980630)18:8<873::AID-JOC255>3.0.CO;2-9.

Frei, C., Schöll, R., Fukutome, S., Schmidli, J., and Vidale, P. L. (2006). Future change of precipitation extremes in Europe: Intercomparison of scenarios from regional climate models. J. Geophys. Res. 111, D06105. doi:10.1029/2005JD005965.

Frei, P., Kotlarski, S., Liniger, M. A., and Schär, C. (2018). Future snowfall in the Alps: projections based on the EURO-CORDEX regional climate models. Cryosph. 12, 1–24. doi:10.5194/tc-12-1-2018.

Frey, H., Haeberli, W., Linsbauer, A., Huggel, C., and Paul, F. (2010). A multi-level strategy for anticipating future glacier lake formation and associated hazard potentials. Nat. Hazards Earth Syst. Sci. 10, 339–352. doi:10.5194/nhess-10-339-2010.

Frey, H., Machguth, H., Huss, M., Huggel, C., Bajracharya, S. R., Bolch, T., et al. (2014). Estimating the volume of glaciers in the Himalayan-Karakoram region using different methods. Cryosph. 8, 2313–2333. doi:10.5194/tc-8-2313-2014.

Gabbi, J., Carenzo, M., Pellicciotti, F., Bauder, A., and Funk, M. (2014). A comparison of empirical and physically based glacier surface melt models for long-term simulations of glacier response. J. Glaciol. 60, 1140–1154. doi:10.3189/2014JoG14J011.

Gain, A. K., Immerzeel, W. W., Sperna Weiland, F. C., and Bierkens, M. F. P. (2011). Impact of climate change on the stream flow of the lower Brahmaputra: Trends in high and low flows based on discharge-weighted ensemble modelling. Hydrol. Earth Syst. Sci. 15, 1537–1545. doi:10.5194/hess-15-1537-2011.

Gain, A. K., and Wada, Y. (2014). Assessment of Future Water Scarcity at Different Spatial and Temporal Scales of the Brahmaputra River Basin. Water Resour. Manag. 28, 999–1012. doi:10.1007/s11269-014-0530-5.

Galewsky, J. (2009). Rain shadow development during the growth of mountain ranges: An atmospheric dynamics perspective. J. Geophys. Res. Earth Surf. 114. doi:10.1029/2008JF001085.

Gernaat, D. E. H. J., Bogaart, P. W., Vuuren, D. P. van, Biemans, H., and Niessink, R. (2017). High-resolution assessment of global technical and economic hydropower potential. Nat. Energy 2, 821–828. doi:10.1038/s41560-017-0006-y.

Gibson, M. J., Glasser, N. F., Quincey, D. J., Mayer, C., Rowan, A. V., and Irvine-Fynn, T. D. L. (2017). Temporal variations in supraglacial debris distribution on Baltoro Glacier, Karakoram between 2001 and 2012. Geomorphology 295, 572–585. doi:10.1016/j.geomorph.2017.08.012.

Gidden, M. J., Riahi, K., Smith, S. J., Fujimori, S., Luderer, G., Kriegler, E., et al. (2019). Global emissions pathways under different socioeconomic scenarios for use in CMIP6: a dataset of harmonized emissions trajectories through the end of the century. Geosci. Model Dev. 12, 1443–1475. doi:10.5194/gmd-12-1443-2019.

Giesen, R., Hock, R., Marzeion, B., Bliss, A., Hirabayashi, Y., Huss, M., et al. (2016). GlacierMIP-A model intercomparison of global-scale glacier mass-balance models and projections. EGU Gen. Assem. Conf. Abstr. Available at: http://www.climate-cryosphere.org/activities/targeted/glaciermip [Accessed February 18, 2019].

Giorgi, F., Marinucci, M. R., and Bates, G. T. (1993). Development of a Second-Generation Regional Climate Model (RegCM2). Part I: Boundary-Layer and Radiative Transfer Processes. Mon. Weather Rev. 121, 2794–2813. doi:10.1175/1520-0493(1993)121<2794:DOASGR>2.0.CO;2.

Gleeson, T., and Paszkowski, D. (2014). Perceptions of scale in hydrology: what do you mean by regional scale? Hydrol. Sci. J. 59, 99–107. doi:10.1080/02626667.2013.797581.

Glen, J. W. (1955). The creep of polycrystalline ice. Proc. R. Soc. A 228, 519–538. doi:10.1098/rspa.1955.0066.

Gobiet, A., Kotlarski, S., Beniston, M., Heinrich, G., Rajczak, J., and Stoffel, M. (2014). 21st century climate change in the European Alps—A review. Sci. Total Environ. 493, 1138–1151. doi:10.1016/j.scitotenv.2013.07.050.

Graham, L. P., Andréasson, J., and Carlsson, B. (2007). Assessing climate change impacts on hydrology from an ensemble of regional climate models, model scales and linking methods – a case study on the Lule River basin. Clim. Change 81, 293–307. doi:10.1007/s10584-006-9215-2.

Graham, L. P., and Bergström, S. (2001). Water balance modelling in the Baltic Sea drainage basin - analysis of meteorological and hydrological approaches. Meteorol. Atmos. Phys. 77, 45–60. doi:10.1007/s007030170016.

Gregory, J. M., White, N. J., Church, J. A., Bierkens, M. F. P., Box, J. E., van den Broeke, M. R., et al. (2013). Twentieth-Century Global-Mean Sea Level Rise: Is the Whole Greater than the Sum of the Parts? J. Clim. 26, 4476–4499. doi:10.1175/JCLI-D-12-00319.1.

Greuell, W. (1992). Hintereisferner, Austria: mass-balance reconstruction and numerical modelling of the historical length variations. J. Glaciol. doi:10.1017/S0022143000003646.

Gruber, S. (2007). A mass-conserving fast algorithm to parameterize gravitational transport and deposition using digital elevation models. Water Resour. Res. doi:10.1029/2006WR004868.

Gu, H., Yu, Z., Wang, G., Wang, J., Ju, Q., Yang, C., et al. (2015). Impact of climate change on hydrological extremes in the Yangtze River Basin, China. Stoch. Environ. Res. Risk Assess. 29, 693–707. doi:10.1007/s00477-014-0957-5.

Gumbel, E. J. (1941). The Return Period of Flood Flows. Ann. Math. Stat. 12, 163–190. doi:10.1214/aoms/1177731747.

Gurung, A. B., Borsdorf, A., Füreder, L., Kienast, F., Matt, P., Scheidegger, C., et al. (2016). Rethinking Pumped Storage Hydropower in the European Alps. Mt. Res. Dev. 36, 222–232. doi:10.1659/MRD-JOURNAL-D-15-00069.1.

Haddeland, I., Heinke, J., Biemans, H., Eisner, S., Flörke, M., Hanasaki, N., et al. (2014). Global water resources affected by human interventions and climate change. Proc. Natl. Acad. Sci. 111, 3251–3256. doi:10.1073/pnas.1222475110.

Haeberli, W. (2011). Glacier mass balance. in Encyclopedia of Snow, Ice and Glaciers, eds. V. P. Singh, P. Singh, and U. K. Haritashya (Dordrecht, the Netherlands: Springer Netherlands), 399–408. doi:10.1007/978-90-481-2642-2_341.

Haeberli, W., Schaub, Y., and Huggel, C. (2017). Increasing risks related to landslides from degrading permafrost into new lakes in de-glaciating mountain ranges. Geomorphology 293, 405–417. doi:10.1016/j.geomorph.2016.02.009.

Hagg, W. (2003). Effects of glacier retreat on the water availability of high-alpine areas, a comparison between the Alps and Central Asia.

Hagg, W., Braun, L. N., Kuhn, M., and Nesgaard, T. I. (2007). Modelling of hydrological response to climate change in glacierized Central Asian catchments. J. Hydrol. 332, 40–53. doi:10.1016/j.jhydrol.2006.06.021.

Haiden, T., Kann, A., Wittmann, C., Pistotnik, G., Bica, B., and Gruber, C. (2011). The Integrated Nowcasting through Comprehensive Analysis (INCA) System and Its Validation over the Eastern Alpine Region. Weather Forecast. 26, 166–183. doi:10.1175/2010WAF2222451.1.

Hall, D. K., and Riggs, G. A. (2015). MODIS/Terra Snow Cover Monthly L3 Global 0.05Deg CMG, Version 6. Boulder, Colorado, USA.

Hall, D. K., Riggs, G. A., Digirolamo, N. E., and Bayr, K. J. (2002). MODIS Snow-Cover Products. Remote Sens. Environ. 83, 88–89.

Hambrey, M. J., Quincey, D. J., Glasser, N. F., Reynolds, J. M., Richardson, S. J., and Clemmens, S. (2009). Sedimentological, geomorphological and dynamic context of debris-mantled glaciers, Mount Everest (Sagarmatha) region, Nepal. Quat. Sci. Rev. 28, 1084. doi:10.1016/j.quascirev.2009.04.009.

Hamon, W. R. (1961). Estimating potential evapotranspiration. J. Hydraul. Div. Proc. Am. Soc. Civ. Eng. 87, 107–120.

Hanasaki, N., Fujimori, S., Yamamoto, T., Yoshikawa, S., Masaki, Y., Hijioka, Y., et al. (2013). A global water scarcity assessment under Shared Socio-economic Pathways - Part 2: Water availability and scarcity. Hydrol. Earth Syst. Sci. 17, 2393–2413. doi:10.5194/hess-17-2393-2013.

Hanasaki, N., Kanae, S., Oki, T., Masuda, K., Motoya, K., Shirakawa, N., et al. (2008a). An integrated model for the assessment of global water resources – Part 1: Model description and input meteorological forcing. Hydrol. Earth Syst. Sci. 12, 1007–1025. doi:10.5194/hess-12-1007-2008.

Hanasaki, N., Kanae, S., Oki, T., Masuda, K., Motoya, K., Shirakawa, N., et al. (2008b). An integrated model for the assessment of global water resources – Part 2: Applications and assessments. Hydrol. Earth Syst. Sci. 12, 1027–1037. doi:10.5194/hess-12-1027-2008.

Hanzer, F., Förster, K., Nemec, J., and Strasser, U. (2018). Projected cryospheric and hydrological impacts of 21st century climate change in the Ötztal Alps (Austria) simulated using a physically based approach. Hydrol. Earth Syst. Sci. 22, 1593–1614. doi:10.5194/hess-22-1593-2018.

Hargreaves, G. H., and Samani, Z. A. (1985). Reference crop evapotranspiration from temperature. Appl. Eng. Agric. 1, 96–99. doi:10.13031/2013.26773.

Harris, C., Arenson, L. U., Christiansen, H. H., Etzelmüller, B., Frauenfelder, R., Gruber, S., et al. (2009). Permafrost and climate in Europe: Monitoring and modelling thermal, geomorphological and geotechnical responses. Earth-Science Rev. 92, 117–171. doi:10.1016/j.earscirev.2008.12.002.

Hartmann, D. L., Klein Tank, A. M. G., Rusticucci, M., Alexander, L. V., Brönnimann, S., Charabi, Y. A. R., et al. (2013). "Observations: Atmosphere and Surface," in Climate Change 2013: The Physical Science Basis. Contribution of Working Group I to the Fifth Assessment Report of the Intergovernmental Panel on Climate Change (Cambridge, UK: Cambridge University Press.), 159–254. doi:10.1017/CBO9781107415324.008.

Haylock, M. R., Hofstra, N., Klein Tank, A. M. G., Klok, E. J., Jones, P. D., and New, M. (2008). A European daily high-resolution gridded data set of surface temperature and precipitation for 1950–2006. J. Geophys. Res. 113, 20119. doi:10.1029/2008JD010201.

Heynen, M., Miles, E., Ragettli, S., Buri, P., Immerzeel, W. W., and Pellicciotti, F. (2016). Air temperature variability in a high-elevation Himalayan catchment. Ann. Glaciol. 57, 212–222. doi:10.3189/2016AoG71A076.

Hirabayashi, Y., Kanae, S., Emori, S., Oki, T., and Kimoto, M. (2008). Global projections of changing risks of floods and droughts in a changing climate. Hydrol. Sci. J. 53, 754–772. doi:10.1623/hysj.53.4.754.

Hirabayashi, Y., Mahendran, R., Koirala, S., Konoshima, L., Yamazaki, D., Watanabe, S., et al. (2013). Global flood risk under climate change. Nat. Clim. Chang. 3, 816–821. doi:10.1038/nclimate1911.

Hirabayashi, Y., Nakano, K., Zhang, Y., Watanabe, S., Tanoue, M., and Kanae, S. (2016). Contributions of natural and anthropogenic radiative forcing to mass loss of Northern Hemisphere mountain glaciers and quantifying their uncertainties. Sci. Rep. 6, 29723. doi:10.1038/srep29723.

Hock, R. (1999). A distributed temperature-index ice- and snowmelt model including potential direct solar radiation. J. Glaciol. 45, 101–111. doi:10.1017/S0022143000003087.

Hock, R. (2003). Temperature index melt modelling in mountain areas. J. Hydrol. 282, 104–115. doi:10.1016/S0022-1694(03)00257-9.

Hock, R. (2005). Glacier melt: a review of processes and their modelling. Prog. Phys. Geogr. Earth Environ. 29, 362–391. doi:10.1191/0309133305pp453ra.

Hoekstra, A. Y., Mekonnen, M. M., Chapagain, A. K., Mathews, R. E., and Richter, B. D. (2012). Global monthly water scarcity: Blue water footprints versus blue water availability. PLoS One 7. doi:10.1371/journal.pone.0032688.

Houze, R. A., Rasmussen, K. L., Medina, S., Brodzik, S. R., and Romatschke, U. (2011). Anomalous atmospheric events leading to the summer 2010 floods in Pakistan. Bull. Am. Meteorol. Soc. 92, 291–298. doi:10.1175/2010BAMS3173.1.

Hrachowitz, M., and Clark, M. P. (2017). HESS Opinions: The complementary merits of competing modelling philosophies in hydrology. Hydrol. Earth Syst. Sci. 21, 3953–3973. doi:10.5194/hess-21-3953-2017.

Hubbard, B., Heald, A., Reynolds, J. M., Quincey, D., Richardson, S. D., Luyo, M. Z., et al. (2005). Impact of a rock avalanche on a moraine-dammed proglacial lake: Laguna Safuna Alta, Cordillera Blanca, Peru. Earth Surf. Process. Landforms 30, 1251–1264. doi:10.1002/esp.1198.

Huffman, G. J., Bolvin, D. T., Nelkin, E. J., Wolff, D. B., Adler, R. F., Gu, G., et al. (2007). The TRMM Multisatellite Precipitation Analysis (TMPA): Quasi-Global, Multiyear, Combined-Sensor Precipitation Estimates at Fine Scales. J. Hydrometeorol. 8, 38–55. doi:10.1175/JHM560.1.

Hurrell, J. W., Holland, M. M., Gent, P. R., Ghan, S., Kay, J. E., Kushner, P. J., et al. (2013). The Community Earth System Model: A Framework for Collaborative Research. Bull. Am. Meteorol. Soc. 94, 1339–1360. doi:10.1175/BAMS-D-12-00121.1.

Huss, M. (2012). Extrapolating glacier mass balance to the mountain-range scale: the European Alps 1900–2100. Cryosph. 6, 713–727. doi:10.5194/tc-6-713-2012.

Huss, M., Bookhagen, B., Huggel, C., Jacobsen, D., Bradley, R. S., Clague, J. J., et al. (2017). Toward mountains without permanent snow and ice. Earth's Futur. 5, 418–435. doi:10.1002/2016EF000514.

Huss, M., and Farinotti, D. (2012). Distributed ice thickness and volume of all glaciers around the globe. J. Geophys. Res. Earth Surf. 117. doi:10.1029/2012JF002523.

Huss, M., Farinotti, D., Bauder, A., and Funk, M. (2008). Modelling runoff from highly glacierized alpine drainage basins in a changing climate. Hydrol. Process. 22, 3888–3902. doi:10.1002/hyp.7055.

Huss, M., and Hock, R. (2018). Global-scale hydrological response to future glacier mass loss. Nat. Clim. Chang. 8, 135–140. doi:10.1038/s41558-017-0049-x.

Huss, M., Jouvet, G., Farinotti, D., and Bauder, A. (2010). Future high-mountain hydrology: a new parameterization of glacier retreat. Hydrol. Earth Syst. Sci. 14, 815–829. doi:10.5194/hess-14-815-2010.

Huss, M., Sugiyama, S., Bauder, A., and Funk, M. (2007). Retreat Scenarios of Unteraargletscher, Switzerland, Using a Combined Ice-Flow Mass-Balance Model. Arct. Antarct. Alp. Res. 39, 422–431. doi:10.1657/1523-0430(06-036).

Huss, M., Zemp, M., Joerg, P. C., and Salzmann, N. (2014). High uncertainty in 21st century runoff projections from glacierized basins. J. Hydrol. 510, 35–48. doi:10.1016/j.jhydrol.2013.12.017.

Hutter, K. (1983). Theoretical glaciology: material science of ice and the mechanics of glaciers and ice sheets. Dordrecht, the Netherlands: Reidel Publishing Company.

IIASA (2017). SSP Database. Available at: https://tntcat.iiasa.ac.at/SspDb/dsd?Action=htmlpage&page=about [Accessed January 10, 2018].

Immerzeel, W. W. (2008). Historical trends in future predictions of climate variability in the Brahmputra basin. Int. J. Climatol. 28, 243–254. doi:10.1002/joc.1528.

Immerzeel, W. W., Pellicciotti, F., and Bierkens, M. F. P. (2013). Rising river flows throughout the twenty-first century in two Himalayan glacierized watersheds. Nat. Geosci. 6, 742–745. doi:10.1038/ngeo1896.

Immerzeel, W. W., Pellicciotti, F., and Shrestha, A. B. (2012a). Glaciers as a Proxy to Quantify the Spatial Distribution of Precipitation in the Hunza Basin. Mt. Res. Dev. 32, 30–38. doi:10.1659/MRD-JOURNAL-D-11-00097.1.

Immerzeel, W. W., Petersen, L., Ragettli, S., and Pellicciotti, F. (2014). The importance of observed gradients of air temperature and precipitation for modeling runoff from a glacierized watershed in the Nepalese Himalayas. Water Resour. Res. 50, 2212–2226. doi:10.1002/2013WR014506.

Immerzeel, W. W., van Beek, L. P. H., and Bierkens, M. F. P. (2010). Climate change will affect the Asian water towers. Science (80-.). 328, 1382–5. doi:10.1126/science.1183188.

Immerzeel, W. W., van Beek, L. P. H., and Konz, M. (2012b). Hydrological response to climate change in a glacierized catchment in the Himalayas. Clim. Change 110, 721–736. doi:10.1007/s10584-011-0143-4.

Immerzeel, W. W., Wanders, N., Lutz, A. F., Shea, J. M., and Bierkens, M. F. P. (2015). Reconciling high altitude precipitation with glacier mass balances and runoff. Hydrol. Earth Syst. Sci. 12, 4755–4784. doi:10.5194/hessd-12-4755-2015.

International Monetary Fund (2016). World Economic Outlook 2016: Subdued Demand: Symptoms and Remedies. Available at: http://www.imf.org/external/pubs/ft/weo/2016/02/.

IPCC (2013). Climate Change 2013: The Physical Science Basis. Contribution of Working Group I to the Fifth Assessment Report of the Intergovernmental Panel on Climate Change. , eds. T. F. Stocker, D. Qin, G.-K. Plattner, M. Tignor, S. K. Allen, J. Boschung, et al. Cambridge, United Kingdom and New York, NY, USA doi:10.1017/CBO9781107415324.004.

IRENA (2018). International Renewable Energy Agency - Data and Statistics. Available at: http://resourceirena.irena.org/gateway/dashboard/ [Accessed January 10, 2019].

Ishaq, S., Ahmad, B., Kamran, A., Raza, N., Ahmed Khan, M., Tahir Virk, Z., et al. (2017). Classification of Adaptation Measures and Criteria for Evaluation: Case Studies in the Indus River-Basin. Kathmandu, Nepal.

Jacob, D., and Podzun, R. (1997). Sensitivity studies with the regional climate model REMO. Meteorol. Atmos. Phys. 63, 119–129. doi:10.1007/BF01025368.

Jacob, T., Wahr, J., Pfeffer, W. T., and Swenson, S. (2012). Recent contributions of glaciers and ice caps to sea level rise. Nature 482, 514–518. doi:10.1038/nature10847.

Jägermeyr, J., Gerten, D., Heinke, J., Schaphoff, S., Kummu, M., and Lucht, W. (2015). Water savings potentials of irrigation systems: Global simulation of processes and linkages. Hydrol. Earth Syst. Sci. 19, 3073–3091. doi:10.5194/hess-19-3073-2015.

Jägermeyr, J., Pastor, A., Biemans, H., and Gerten, D. (2017). Reconciling irrigated food production with environmental flows for Sustainable Development Goals implementation. Nat. Commun. 8, 15900. doi:10.1038/ncomms15900.

Jiang, T., Chen, Y. D., Xu, C., Chen, X., Chen, X., and Singh, V. P. (2007). Comparison of hydrological impacts of climate change simulated by six hydrological models in the Dongjiang Basin, South China. J. Hydrol. 336, 316–333. doi:10.1016/j.jhydrol.2007.01.010.

Jóhannesson, T., Raymond, C., and Waddington, E. (1989). Time–Scale for Adjustment of Glaciers to Changes in Mass Balance. J. Glaciol. 35, 355–369. doi:10.1017/S002214300000928X.

Jost, G., Dan Moore, R., Smith, R., and Gluns, D. R. (2012). Distributed temperature-index snowmelt modelling for forested catchments. J. Hydrol. 420–421, 87–101. doi:10.1016/j.jhydrol.2011.11.045.

Jouvet, G., and Funk, M. (2014). Modelling the trajectory of the corpses of mountaineers who disappeared in 1926 on Aletschgletscher, Switzerland. J. Glaciol. 60, 255–261. doi:10.3189/2014JoG13J156.

Jouvet, G., Huss, M., Funk, M., and Blatter, H. (2011). Modelling the retreat of Grosser Aletschgletscher, Switzerland, in a changing climate. J. Glaciol. 57, 1033–1045. doi:10.3189/002214311798843359.

Junghans, N., Cullmann, J., and Huss, M. (2011). Evaluating the effect of snow and ice melt in an Alpine headwater catchment and further downstream in the River Rhine. Hydrol. Sci. J. 56, 981–993. doi:10.1080/02626667.2011.595372.

Kääb, A., Berthier, E., Nuth, C., Gardelle, J., and Arnaud, Y. (2012). Contrasting patterns of early twenty-first-century glacier mass change in the Himalayas. Nature 488, 495–8. doi:10.1038/nature11324.

Kang, S., Xu, Y., You, Q., Flügel, W.-A., Pepin, N., and Yao, T. (2010). Review of climate and cryospheric change in the Tibetan Plateau. Environ. Res. Lett. 5, 015101. doi:10.1088/1748-9326/5/1/015101.

Kaser, G. (1983). Über die Verdunstung auf dem Hintereisferner. Zeitschrift für Gletscherkd. und Glazialgeol. 19, 149–162.

Kaser, G., Grosshauser, M., and Marzeion, B. (2010). Contribution potential of glaciers to water availability in different climate regimes. Proc. Natl. Acad. Sci. 107, 20223–20227. doi:10.1073/pnas.1008162107.

Khanal, S., Lutz, A. F., Immerzeel, W. W., Vries, H., Wanders, N., and van den Hurk, B. J. J. M. (2019). The Impact of Meteorological and Hydrological Memory on Compound Peak Flows in the Rhine River Basin. Atmosphere (Basel). 10, 171. doi:10.3390/atmos10040171.

Kirchner, M., Faus-Kessler, T., Jakobi, G., Leuchner, M., Ries, L., Scheel, H.-E., et al. (2013). Altitudinal temperature lapse rates in an Alpine valley: trends and the influence of season and weather patterns. Int. J. Climatol. 33, 539–555. doi:10.1002/joc.3444.

Kirkbride, M. P. (2011). "Debris-covered glaciers," in Encyclopedia of Snow, Ice and Glaciers, eds. V. P. Singh, P. Singh, and U. K. Haritashya (Dordrecht, the Netherlands: Springer Netherlands), 190–192. doi:10.1007/978-90-481-2642-2_622.

Klein Goldewijk, K., Beusen, A., and Janssen, P. (2010). Long-term dynamic modeling of global population and built-up area in a spatially explicit way: HYDE 3.1. The Holocene 20, 565–573. doi:10.1177/0959683609356587.

Kleindienst, H. (1996). Enhancement and testing of an application-oriented hydrological model to simulate hydrographs in torrent catchments.

Klemeš, V. (1986). Operational testing of hydrological simulation models. Hydrol. Sci. J. 31, 13–24. doi:10.1080/02626668609491024.

Klemeš, V. (1990). The modelling of mountain hydrology: the ultimate challenge. in Hydrology of Mountainous Areas (Proceedings of the Strbské Pleso Workshop, Czechoslovakia, June 1988). IAHS Publ. no. 190 (Wallingford, Oxfordshire, UK: IAHS Press).

Klug, C., Bollmann, E., Galos, S. P., Nicholson, L., Prinz, R., Rieg, L., et al. (2018). Geodetic reanalysis of annual glaciological mass balances (2001–2011) of Hintereisferner, Austria. Cryosph. 12, 833–849. doi:10.5194/tc-12-833-2018.

Kohler, T., and Maselli, D. (2009). Mountains and Climate Change - From Understanding to Action. Bern, Switzerland: Geographica Bernensia and SDC.

Kohler, T., Wehrli, A., and Jurek, M. (2014). Mountains and climate change: A global concern. Bern, Switzerland doi:10.1016/0360-8352(95)00014-R.

Kokkonen, T., Koivusalo, H., Jakeman, A., and Norton, J. (2006). Construction of a degree–day snow model in the light of the ten iterative steps in model development. Proc. iEMSs Third Bienn. Meet. "Summit Environ. Model. Software" (July 2006), 12. Available at: http://www.iemss.org/iemss2006/papers/w4/Kokkonen.pdf.

Konz, M., and Seibert, J. (2010). On the value of glacier mass balances for hydrological model calibration. J. Hydrol. 385, 238–246. doi:10.1016/j.jhydrol.2010.02.025.

Kormann, C., Bronstert, A., Francke, T., Recknagel, T., and Graeff, T. (2016). Model-Based Attribution of High-Resolution Streamflow Trends in Two Alpine Basins of Western Austria. Hydrology 3, 7. doi:10.3390/hydrology3010007.

Kotlarski, S., Bosshard, T., Lüthi, D., Pall, P., and Schär, C. (2012). Elevation gradients of European climate change in the regional climate model COSMO-CLM. Clim. Change 112, 189–215. doi:10.1007/s10584-011-0195-5.

Kraaijenbrink, P. D. A., Bierkens, M. F. P., Lutz, A. F., and Immerzeel, W. W. (2017). Impact of a global temperature rise of 1.5 degrees Celsius on Asia's glaciers. Nature 549, 257–260. doi:10.1038/nature23878.

Kuhn, M. (2008). A history of research on Hintereisferner. 40. Available at: https://www.projects.science.uu.nl/iceclimate/karthaus/archive/lecturenotes/2009/kuhn/MichaelKuhn.pdf.

Kuhn, M., and Batlogg, N. (1998). "Glacier runoff in Alpine headwaters in a changing climate," in Hydrology, Water resources and Ecology in Headwaters, IAHS Publication 248, eds. K. Kovar, U. Tappeiner, N. E. Peters, and R. G. Craig (Wallingford, Oxfordshire, UK), 79–88.

Kuhn, M., Markl, G., Kaser, G., Nickus, U., Obleitner, F., and Schneider, H. (1985). Fluctuations of climate and mass balance: different responses of two adjacent glaciers. Zeitschrift für Gletscherkd. und Glazialgeol. 21, 409–416.

Kuhn, M., Nickus, U., and Pellet, F. (1982). Precipitation Patterns in the Inner Ötztal. Offenbach, Germany Available at: http://epic.awi.de/32636/2/Kuhn_etal_1982.%0Dpdf.

Kumar, K. K., Patwardhan, S. K., Kulkarni, A. V., Kamala, K., Koteswara Rao, K., and Jones, R. (2011). Simulated projections for summer monsoon climate over India by a high-resolution regional climate model (PRECIS). Curr. Sci. 101, 312–326.

Kumar, K. K., Rajagopalan, B., Hoerling, M., Bates, G., and Cane, M. (2006). Unraveling the Mystery of Indian Monsoon Failure During El Nino. Science (80-.). 314, 115–119. doi:10.1126/science.1131152.

Laha, S., Kumari, R., Singh, S., Mishra, A., Sharma, T., Banerjee, A., et al. (2017). Evaluating the contribution of avalanching to the mass balance of Himalayan glaciers. Ann. Glaciol. 58, 110–118. doi:10.1017/aog.2017.27.

Lambrecht, A., and Kuhn, M. (2007). Glacier changes in the Austrian Alps during the last three decades, derived from the new Austrian glacier inventory. Ann. Glaciol. 46, 177–184. doi:10.3189/172756407782871341.

Lambrecht, A., Mayer, C., Hagg, W., Popovnin, V., Rezepkin, A., Lomidze, N., et al. (2011). A comparison of glacier melt on debris-covered glaciers in the northern and southern Caucasus. Cryosph. 5, 525–538. doi:10.5194/tc-5-525-2011.

Land Tirol (2006). Digital Terrain Model Tirol. Available at: https://www.tirol.gv.at/data/.

Lau, W. K. M., and Kim, K.-M. (2012). The 2010 Pakistan Flood and Russian Heat Wave: Teleconnection of Hydrometeorological Extremes. J. Hydrometeorol. 13, 392–403. doi:10.1175/JHM-D-11-016.1.

Lau, W. K. M., and Kim, K.-M. (2018). Impact of Snow Darkening by Deposition of Light-Absorbing Aerosols on Snow Cover in the Himalayas–Tibetan Plateau and Influence on the Asian Summer Monsoon: A Possible Mechanism for the Blanford Hypothesis. Atmosphere (Basel). 9, 438. doi:10.3390/atmos9110438.

Le Meur, E., Gagliardini, O., Zwinger, T., and Ruokolainen, J. (2004). Glacier flow modelling: A comparison of the Shallow Ice Approximation and the full-Stokes solution. Comptes Rendus Phys. 5, 709–722. doi:10.1016/j.crhy.2004.10.001.

Leclercq, P. W., and Oerlemans, J. (2012). Global and hemispheric temperature reconstruction from glacier length fluctuations. Clim. Dyn. 38, 1065–1079. doi:10.1007/s00382-011-1145-7.

Leclercq, P. W., Oerlemans, J., and Cogley, J. G. (2011). Estimating the Glacier Contribution to Sea-Level Rise for the Period 1800-2005. Surv. Geophys. 32, 519–535. doi:10.1007/s10712-011-9121-7.

Lehner, B., Liermann, C. R., Revenga, C., Vörösmarty, C. J., Fekete, B., Crouzet, P., et al. (2011). High-resolution mapping of the world's reservoirs and dams for sustainable river-flow management. Front. Ecol. Environ. 9, 494–502. doi:10.1890/100125.

Lehner, B., Verdin, K., and Jarvis, A. (2008). New global hydrography derived from spaceborne elevation data. Eos (Washington. DC). 89, 93–94. doi:10.1029/2008EO100001.

Lenaerts, J. T. M., van den Broeke, M. R., Déry, S. J., König-Langlo, G., Ettema, J., and Munneke, P. K. (2010). Modelling snowdrift sublimation on an Antarctic ice shelf. Cryosph. 4, 179–190. doi:10.5194/tc-4-179-2010.

Leprince, S., Barbot, S., Ayoub, F., and Avouac, J. P. (2007). Automatic and precise orthorectification, coregistration, and subpixel correlation of satellite images, application to ground deformation measurements. IEEE Trans. Geosci. Remote Sens. 45, 1529–1558. doi:10.1109/TGRS.2006.888937.

Leysinger Vieli, G. J.-M. C., and Gudmundsson, G. H. (2004). On estimating length fluctuations of glaciers caused by changes in climatic forcing. J. Geophys. Res. Earth Surf. 109. doi:10.1029/2003JF000027.

Li, H., Beldring, S., Xu, C. Y., Huss, M., Melvold, K., and Jain, S. K. (2015). Integrating a glacier retreat model into a hydrological model – Case studies of three glacierised catchments in Norway and Himalayan region. J. Hydrol. 527, 656–667. doi:10.1016/j.jhydrol.2015.05.017.

Li, L., Gochis, D. J., Sobolowski, S., and Mesquita, M. D. S. (2017). Evaluating the present annual water budget of a Himalayan headwater river basin using a high-resolution atmosphere-hydrology model. J. Geophys. Res. Atmos. 122, 4786–4807. doi:10.1002/2016JD026279.

Li, L., Shen, M., Hou, Y., Xu, C.-Y., Lutz, A. F., Chen, J., et al. (2019). Twenty-first-century glacio-hydrological changes in the Himalayan headwater Beas River basin. Hydrol. Earth Syst. Sci. 23, 1483–1503. doi:10.5194/hess-23-1483-2019.

Li, S., Kang, S., Zhang, L., Zhang, J., Du, T., Tong, L., et al. (2016). Evaluation of six potential evapotranspiration models for estimating crop potential and actual evapotranspiration in arid regions. J. Hydrol. 543, 450–461. doi:10.1016/j.jhydrol.2016.10.022.

Li, W., Guo, W., Qiu, B., Xue, Y., Hsu, P.-C., and Wei, J. (2018). Influence of Tibetan Plateau snow cover on East Asian atmospheric circulation at medium-range time scales. Nat. Commun. 9, 4243. doi:10.1038/s41467-018-06762-5.

Litt, M., Shea, J. M., Wagnon, P., Steiner, J. F., Koch, I., Stigter, E. E., et al. (2019). Glacier ablation and temperature indexed melt models in the Nepalese Himalaya. Sci. Rep. 9, 5264. doi:10.1038/s41598-019-41657-5.

Liu, J., Yang, H., Gosling, S. N., Kummu, M., Flörke, M., Pfister, S., et al. (2017). Water scarcity assessments in the past, present, and future. Earth's Futur. 5, 545–559. doi:10.1002/2016EF000518.

Liu, X., and Chen, B. (2000). Climatic warming in the Tibetan Plateau during recent decades. Int. J. Climatol. 20, 1729–1742. doi:10.1002/1097-0088(20001130)20:14<1729::AID-JOC556>3.0.CO;2-Y.

Liu, Y., Tian, F., Hu, H., and Sivapalan, M. (2014). Socio-hydrologic perspectives of the co-evolution of humans and water in the Tarim River basin, Western China: the Taiji–Tire model. Hydrol. Earth Syst. Sci. 18, 1289–1303. doi:10.5194/hess-18-1289-2014.

Lu, J., Sun, G., McNulty, S. G., and Amatya, D. M. (2005). A Comparison of Six Potential Evapotranspiration Methods for Regional Use in the Southeastern United States. J. Am. Water Resour. Assoc. 41, 621–633. doi:10.1111/j.1752-1688.2005.tb03759.x.

Lutz, A. F., and Immerzeel, W. W. (2015). HI-AWARE Reference Climate Dataset for the Indus , Ganges and Brahmaputra River Basins. FutureWater report 146. Wageningen, The Netherlands.

Lutz, A. F., Immerzeel, W. W., Gobiet, A., Pellicciotti, F., and Bierkens, M. F. P. (2013). Comparison of climate change signals in CMIP3 and CMIP5 multi-model ensembles and implications for Central Asian glaciers. Hydrol. Earth Syst. Sci. 17, 3661–3677. doi:10.5194/hess-17-3661-2013.

Lutz, A. F., Immerzeel, W. W., Kraaijenbrink, P. D. A., Shrestha, A. B., and Bierkens, M. F. P. (2016a). Climate Change Impacts on the Upper Indus Hydrology: Sources, Shifts and Extremes. PLoS One 11. doi:10.1371/journal.pone.0165630.

Lutz, A. F., Immerzeel, W. W., Shrestha, A. B., and Bierkens, M. F. P. (2014). Consistent increase in High Asia's runoff due to increasing glacier melt and precipitation. Nat. Clim. Chang. 4, 587–592. doi:10.1038/nclimate2237.

Lutz, A. F., ter Maat, H. W., Biemans, H., Shrestha, A. B., Wester, P., and Immerzeel, W. W. (2016b). Selecting representative climate models for climate change impact studies: an advanced envelope-based selection approach. Int. J. Climatol. 36, 3988–4005. doi:10.1002/joc.4608.

Lutz, A. F., ter Maat, H. W., Wijngaard, R. R., Biemans, H., Syed, A., Shrestha, A. B., et al. (2019). South Asian river basins in a 1.5 °C warmer world. Reg. Environ. Chang. 19, 833–847. doi:10.1007/s10113-018-1433-4.

MacDonald, M. K., Pomeroy, J. W., and Pietroniro, A. (2009). Parameterizing redistribution and sublimation of blowing snow for hydrological models: tests in a mountainous subarctic catchment. Hydrol. Process. 23, 2570–2583. doi:10.1002/hyp.7356.

Marshak, S. (2008). Earth: Portrait of a Planet. 3rd ed. W. W. Norton & Company, Inc.

Martinec, J., and Rango, A. (1986). Parameter values for snowmelt runoff modelling. J. Hydrol. 84, 197–219. doi:10.1016/0022-1694(86)90123-X.

Marty, C., Schlögl, S., Bavay, M., and Lehning, M. (2017a). How much can we save? Impact of different emission scenarios on future snow cover in the Alps. Cryosph. 11, 517–529. doi:10.5194/tc-11-517-2017.

Marty, C., Tilg, A.-M., and Jonas, T. (2017b). Recent Evidence of Large-Scale Receding Snow Water Equivalents in the European Alps. J. Hydrometeorol. 18, 1021–1031. doi:10.1175/JHM-D-16-0188.1.

Marzeion, B., Cogley, J. G., Richter, K., and Parkes, D. (2014). Attribution of global Glacier Mass Loss to Anthropogenic and Natural Climate Forcing. Science (80-.). 345, 919–921. doi:10.1126/science.1254702.

Marzeion, B., Jarosch, A. H., and Hofer, M. (2012). Past and future sea-level change from the surface mass balance of glaciers. Cryosph. 6, 1295–1322. doi:10.5194/tc-6-1295-2012.

Masood, M. J. F., Yeh, P., Hanasaki, N., and Takeuchi, K. (2015). Model study of the impacts of future climate change on the hydrology of Ganges-Brahmaputra-Meghna basin. Hydrol. Earth Syst. Sci. 19, 747–770. doi:10.5194/hess-19-747-2015.

Melsen, L. A., Teuling, A. J., Torfs, P. J. J. F., Uijlenhoet, R., Mizukami, N., and Clark, M. P. (2016). HESS Opinions: The need for process-based evaluation of large-domain hyper-resolution models. Hydrol. Earth Syst. Sci. 20, 1069–1079. doi:10.5194/hess-20-1069-2016.

Merz, R., Parajka, J., and Blöschl, G. (2011). Time stability of catchment model parameters: Implications for climate impact analyses. Water Resour. Res. 47. doi:10.1029/2010WR009505.

Miles, E. S., Willis, I., Buri, P., Steiner, J. F., Arnold, N. S., and Pellicciotti, F. (2018). Surface Pond Energy Absorption Across Four Himalayan Glaciers Accounts for 1/8 of Total Catchment Ice Loss. Geophys. Res. Lett. 45, 10,464-10,473. doi:10.1029/2018GL079678.

Miller, G. T., and Spoolman, S. E. (2012). Living in the Environment: Principles, Connections, and Solutions. 16th ed. Canada: Brooks/Cole Pub Co.

Mirza, M. M. Q. (2011). Climate change, flooding in South Asia and implications. Reg. Environ. Chang. 11, 95–107. doi:10.1007/s10113-010-0184-7.

Mirza, M. M. Q., Warrick, R. A., and Ericksen, N. J. (2003). The implications of climate change on floods of the Ganges, Brahmaputra and Meghna rivers in Bangladesh. Clim. Change 57, 287–318. doi:10.1023/A:1022825915791.

Mishra, V. (2015). Climatic uncertainty in Himalayan water towers. J. Geophys. Res. Atmos. 120, 2689–2705. doi:10.1002/2014JD022650.

Mittal, N., Mishra, A., Singh, R., and Kumar, P. (2014). Assessing future changes in seasonal climatic extremes in the Ganges river basin using an ensemble of regional climate models. Clim. Change 123, 273–286. doi:10.1007/s10584-014-1056-9.

Molden, D., Sharma, E., Shrestha, A. B., Chettri, N. ., Shrestha Pradhan, N., and Kotru, R. (2017). Advancing Regional and Transboundary Cooperation in the Conflict-Prone Hindu Kush–Himalaya. Mt. Res. Dev. 37, 502–508. doi:10.1659/MRD-JOURNAL-D-17-00108.1.

Mölg, T., Cullen, N. J., Hardy, D. R., Kaser, G., and Klok, L. (2008). Mass balance of a slope glacier on Kilimanjaro and its sensitivity to climate. Int. J. Climatol. 28, 881–892. doi:10.1002/joc.1589.

Mölg, T., Cullen, N. J., Hardy, D. R., Winkler, M., and Kaser, G. (2009). Quantifying Climate Change in the Tropical Midtroposphere over East Africa from Glacier Shrinkage on Kilimanjaro. J. Clim. 22, 4162–4181. doi:10.1175/2009JCLI2954.1.

Moors, E. J., Groot, A., Biemans, H., van Scheltinga, C. T., Siderius, C., Stoffel, M., et al. (2011). Adaptation to changing water resources in the Ganges basin, northern India. Environ. Sci. Policy 14, 758–769. doi:10.1016/j.envsci.2011.03.005.

Moriasi, D. N., Arnold, J. G., Van Liew, M. W., Binger, R. L., Harmel, R. D., and Veith, T. L. (2007). Model evaluation guidelines for systematic quantification of accuracy in watershed simulations. Trans. ASABE 50, 885–900. doi:10.13031/2013.23153.

MRI (2015). Elevation-dependent warming in mountain regions of the world. Nat. Clim. Chang. 5, 424–430. doi:10.1038/nclimate2563.

Mukherji, A., Molden, D., Nepal, S., Rasul, G., and Wagnon, P. (2015). Himalayan waters at the crossroads: issues and challenges. Int. J. Water Resour. Dev. 31, 151–160. doi:10.1080/07900627.2015.1040871.

Mukherji, A., Scott, C., and Molden, D. (2018). Assessing Global Water Megatrends. , eds. A. K. Biswas, C. Tortajada, and P. Rohner Singapore: Springer Singapore doi:10.1007/978-981-10-6695-5.

Munia, H., Guillaume, J. H. A., Mirumachi, N., Porkka, M., Wada, Y., and Kummu, M. (2016). Water stress in global transboundary river basins: significance of upstream water use on downstream stress. Environ. Res. Lett. 11, 014002. doi:10.1088/1748-9326/11/1/014002.

Munich RE (2011). Significant natural catastrophes worldwide 2010: 10 deadliest events. NatCatSERVICE. Available at: https://www.munichre.com/touch/naturalhazards/en/natcatservice/annual-statistics/index.html [Accessed February 8, 2017].

Myhre, G., Shindell, D., Bréon, F. M., Collins, W., Fuglestvedt, J., Huang, J., et al. (2013). "Anthropogenic and Natural Radiative Forcing," in Climate Change 2013: The Physical Science Basis. Contribution of Working Group I to the Fifth Assessment Report of the Intergovernmental Panel on Climate Change (Cambridge, UK: Cambridge University Press.), 659–740. doi:10.1017/ CBO9781107415324.018.

Naito, N., Nakawo, M., Kadota, T., and Raymond, C. F. (2000). "Numerical simulation of recent shrinkage of Khumbu Glacier, Nepal Himalayas," in Debris-covered glaciers, IAHS Publication 264, eds. M. Nakawo, C. F. Raymond, and A. Fountain (Seattle, Washington, USA), 245–254.

Nash, J. E., and Sutcliffe, J. V. (1970). River flow forecasting through conceptual models part I - A discussion of principles. J. Hydrol. 10, 282–290. doi:10.1016/0022-1694(70)90255-6.

Nearing, M. A., Deer-Ascough, L., and Chaves, H. M. L. (1989). "WEPP model sensitivity analysis," in Water Erosion Prediction Project: Hillslope Model Documentation, USDA-ARS NSERL Report 2, eds. L. J. Lane and M. A. Nearing (West Lafayette, Indiana, USA: USDA-ARS National Soil Erosion Research Laboratory), 14.1–14.33.

Nelson, G. C., Valin, H., Sands, R. D., Havlík, P., Ahammad, H., Deryng, D., et al. (2014). Climate change effects on agriculture: Economic responses to biophysical shocks. Proc. Natl. Acad. Sci. 111, 3274–3279. doi:10.1073/pnas.1222465110.

Nepal, S. (2016). Impacts of climate change on the hydrological regime of the Koshi river basin in the Himalayan region. J. Hydro-environment Res. 10, 76–89. doi:10.1016/j.jher.2015.12.001.

Nepal, S., Flügel, W.-A., Krause, P., Fink, M., and Fischer, C. (2017). Assessment of Spatial Transferability of Process-Based Hydrological Model Parameters in Two Neighboring Catchments in the Himalayan Region. Hydrol. Process. doi:10.1002/hyp.11199.

Nepal, S., Krause, P., Flügel, W.-A., Fink, M., and Fischer, C. (2014). Understanding the hydrological system dynamics of a glaciated alpine catchment in the Himalayan region using the J2000 hydrological model. Hydrol. Process. 28, 1329–1344. doi:10.1002/hyp.9627.

Nepal, S., Panday, A., Shrestha, A. B., and Mukherji, A. (2018). Revisiting Key Questions Regarding Upstream–Downstream Linkages of Land and Water Management in the Hindu Kush Himalaya (HKH) Region. Kathmandu, Nepal.

Nepal, S., and Shrestha, A. B. (2015). Impact of climate change on the hydrological regime of the Indus, Ganges and Brahmaputra river basins: a review of the literature. Int. J. Water Resour. Dev. 31, 201–218. doi:10.1080/07900627.2015.1030494.

Neuhold, C. (2010). Revised flood risk assessment: Quantifying epistemic uncertainty emerging from different sources and processes.

Nicholson, L., and Benn, D. I. (2006). Calculating ice melt beneath a debris layer using meteorological data. J. Glaciol. 52, 463–470. doi:10.3189/172756506781828584.

Nigrelli, G., Fratianni, S., Zampollo, A., Turconi, L., and Chiarle, M. (2018). The altitudinal temperature lapse rates applied to high elevation rockfalls studies in the Western European Alps. Theor. Appl. Climatol. 131, 1479–1491. doi:10.1007/s00704-017-2066-0.

Norris, J., Carvalho, L. M. V., Jones, C., Cannon, F., Bookhagen, B., Palazzi, E., et al. (2017). The spatiotemporal variability of precipitation over the Himalaya: evaluation of one-year WRF model simulation. Clim. Dyn. 49, 2179–2204. doi:10.1007/s00382-016-3414-y.

Nowicki, S. M. J., Payne, A., Larour, E., Seroussi, H., Goelzer, H., Lipscomb, W., et al. (2016). Ice Sheet Model Intercomparison Project (ISMIP6) contribution to CMIP6. Geosci. Model Dev. 9, 4521–4545. doi:10.5194/gmd-9-4521-2016.

NRC (2000). Risk Analysis and Uncertainty in Flood Damage Reduction Studies. Washington DC, USA.

Nuimura, T., Fujita, K., and Sakai, A. (2017). Downwasting of the debris-covered area of Lirung Glacier in Langtang Valley, Nepal Himalaya, from 1974 to 2010. Quat. Int. 455, 93–101. doi:10.1016/j.quaint.2017.06.066.

Nye, J. F. (1965). The flow of a glacier in a channel of rectangular, elliptic or parabolic cross-section. J. Glaciol. 5, 661–690. doi:10.3189/S0022143000018670.

O'Neill, B. C., Kriegler, E., Ebi, K. L., Kemp-Benedict, E., Riahi, K., Rothman, D. S., et al. (2015). The roads ahead: Narratives for shared socioeconomic pathways describing world futures in the 21st century. Glob. Environ. Chang. 42, 169–180. doi:10.1016/j.gloenvcha.2015.01.004.

O'Neill, B. C., Kriegler, E., Riahi, K., Ebi, K. L., Hallegatte, S., Carter, T. R., et al. (2014). A new scenario framework for climate change research: The concept of shared socioeconomic pathways. Clim. Change 122, 387–400. doi:10.1007/s10584-013-0905-2.

Oerlemans, J., Anderson, B., Hubbard, A., Huybrechts, P., Jóhannesson, T., Knap, W. H., et al. (1998). Modelling the response of glaciers to climate warming. Clim. Dyn. 14, 267–274. doi:10.1007/s003820050222.

Oerlemans, J., Haag, M., and Keller, F. (2017). Slowing down the retreat of the Morteratsch glacier, Switzerland, by artificially produced summer snow: a feasibility study. Clim. Change 145, 189–203. doi:10.1007/s10584-017-2102-1.

Østrem, G. (1959). Ice Melting under a Thin Layer of Moraine, and the Existence of Ice Cores in Moraine Ridges. Geogr. Ann. 41, 228–230. doi:10.1080/20014422.1959.11907953.

Palazzi, E., Filippi, L., and von Hardenberg, J. (2017). Insights into elevation-dependent warming in the Tibetan Plateau-Himalayas from CMIP5 model simulations. Clim. Dyn. 48, 3991–4008. doi:10.1007/s00382-016-3316-z.

Palazzi, E., Von Hardenberg, J., and Provenzale, A. (2013). Precipitation in the Hindu-Kush Karakoram Himalaya: Observations and future scenarios. J. Geophys. Res. Atmos. 118, 85–100. doi:10.1029/2012JD018697.

Palazzi, E., Von Hardenberg, J., Terzago, S., and Provenzale, A. (2015). Precipitation in the Karakoram-Himalaya: a CMIP5 view. Clim. Dyn. 45, 21–45. doi:10.1007/s00382-014-2341-z.

Parajka, J., Merz, R., and Blöschl, G. (2005). A comparison of regionalisation methods for catchment model parameters. Hydrol. Earth Syst. Sci. 9, 157–171. doi:10.5194/hess-9-157-2005.

Park, C., Min, S.-K., Lee, D., Cha, D.-H., Suh, M.-S., Kang, H.-S., et al. (2016). Evaluation of multiple regional climate models for summer climate extremes over East Asia. Clim. Dyn. 46, 2469–2486. doi:10.1007/s00382-015-2713-z.

Pastor, A. V., Ludwig, F., Biemans, H., Hoff, H., and Kabat, P. (2014). Accounting for environmental flow requirements in global water assessments. Hydrol. Earth Syst. Sci. 18, 5041–5059. doi:10.5194/hess-18-5041-2014.

Patzelt, G. (2013). Austrian glacier inventory 1969 (G I). doi:10.1594/PANGAEA.807098.

Paul, F. (2010). The influence of changes in glacier extent and surface elevation on modeled mass balance. Cryosph. 4, 569–581. doi:10.5194/tc-4-569-2010.

Paul, F., Huggel, C., and Kääb, A. (2004). Combining satellite multispectral image data and a digital elevation model for mapping debris-covered glaciers. Remote Sens. Environ. 89, 510–518. doi:10.1016/j.rse.2003.11.007.

Pecher, C., Tasser, E., and Tappeiner, U. (2011). Definition of the potential treeline in the European Alps and its benefit for sustainability monitoring. Ecol. Indic. 11, 438–447. doi:10.1016/j.ecolind.2010.06.015.

Pechlivanidis, I. G., Arheimer, B., Donnelly, C., Hundecha, Y., Huang, S., Aich, V., et al. (2016). Analysis of hydrological extremes at different hydro-climatic regimes under present and future conditions. Clim. Change 141, 467–481. doi:10.1007/s10584-016-1723-0.

Pellicciotti, F., Brock, B., Strasser, U., Burlando, P., Funk, M., and Corripio, J. (2005). An enhanced temperature-index glacier melt model including the shortwave radiation balance: development and testing for Haut Glacier d'Arolla, Switzerland. J. Glaciol. 51, 573–587. doi:10.3189/172756505781829124.

Pellicciotti, F., Buergi, C., Immerzeel, W. W., Konz, M., and Shrestha, A. B. (2012). Challenges and Uncertainties in Hydrological Modeling of Remote Hindu Kush–Karakoram–Himalayan (HKH) Basins: Suggestions for Calibration Strategies. Mt. Res. Dev. 32, 39–50. doi:10.1659/MRD-JOURNAL-D-11-00092.1.

Pellicciotti, F., Stephan, C., Miles, E. S., Herreid, S., Immerzeel, W. W., and Bolch, T. (2015). Mass-balance changes of the debris-covered glaciers in the Langtang Himal, Nepal, from 1974 to 1999. J. Glaciol. 61, 373–386. doi:10.3189/2015JoG13J237.

Pepin, N., Bradley, R. S., Diaz, H. F., Baraer, M., Caceres, E. B., Forsythe, N., et al. (2015). Elevation-dependent warming in mountain regions of the world. Nat. Clim. Chang. 5, 424–430. doi:10.1038/nclimate2563.

Pfeffer, W., Arendt, A. A., Bliss, A., Bolch, T., Cogley, J. G., Gardner, A. S., et al. (2014). The Randolph Glacier Inventory: a globally complete inventory of glaciers. J. Glaciol. 60, 537–552. doi:10.3189/2014JoG13J176.

Piani, C., Haerter, J. O., and Coppola, E. (2010). Statistical bias correction for daily precipitation in regional climate models over Europe. Theor. Appl. Climatol. 99, 187–192. doi:10.1007/s00704-009-0134-9.

Pianosi, F., Beven, K., Freer, J., Hall, J. W., Rougier, J., Stephenson, D. B., et al. (2016). Sensitivity analysis of environmental models: A systematic review with practical workflow. Environ. Model. Softw. 79, 214–232. doi:10.1016/j.envsoft.2016.02.008.

Porter, J. R., Xie, L., Challinor, A. J., Cochrane, K., Howden, S. M., Iqbal, M. M., et al. (2015). "Food security and food production systems," in Climate Change 2014 Impacts, Adaptation and Vulnerability: Part A: Global and Sectoral Aspects (Cambridge, UK: Cambridge University Press). doi:10.1017/CBO9781107415379.012.

Portmann, F. T., Siebert, S., and Döll, P. (2010). MIRCA2000-Global monthly irrigated and rainfed crop areas around the year 2000: A new high-resolution data set for agricultural and hydrological modeling. Global Biogeochem. Cycles 24. doi:10.1029/2008GB003435.

Pospichal, B., Formayer, H., Haas, P., and Nadeem, I. (2010). Bias correction and localization of regional climate scenarios over mountainous area on a 1 × 1 km grid. in 10th European Conference on Applications of Meteorology (ECAM) (Zürich, Switzerland).

Priestley, C. H. B., and Taylor, R. J. (1972). On the Assessment of Surface Heat Flux and Evaporation Using Large-Scale Parameters. Mon. Weather Rev. 100, 81–92. doi:10.1175/1520-0493(1972)100<0081:OTAOSH>2.3.CO;2.

Racoviteanu, A. E., Armstrong, R., and Williams, M. W. (2013). Evaluation of an ice ablation model to estimate the contribution of melting glacier ice to annual discharge in the Nepal Himalaya. Water Resour. Res. 49, 5117–5133. doi:10.1002/wrcr.20370.

Radić, V., Bliss, A., Beedlow, A. C., Hock, R., Miles, E. S., and Cogley, J. G. (2014). Regional and global projections of twenty-first century glacier mass changes in response to climate scenarios from global climate models. Clim. Dyn. 42, 37–58. doi:10.1007/s00382-013-1719-7.

Radić, V., and Hock, R. (2011). Regionally differentiated contribution of mountain glaciers and ice caps to future sea-level rise. Nat. Geosci. 4, 91–94. doi:10.1038/ngeo1052.

Raftery, A. E., Zimmer, A., Frierson, D. M. W., Startz, R., and Liu, P. (2017). Less than 2 °c warming by 2100 unlikely. Nat. Clim. Chang. 7, 637–641. doi:10.1038/nclimate3352.

Ragettli, S., Bolch, T., and Pellicciotti, F. (2016a). Heterogeneous glacier thinning patterns over the last 40 years in Langtang Himal, Nepal. Cryosph. 10, 2075–2097. doi:10.5194/tc-10-2075-2016.

Ragettli, S., Immerzeel, W. W., and Pellicciotti, F. (2016b). Contrasting climate change impact on river flows from high-altitude catchments in the Himalayan and Andes Mountains. Proc. Natl. Acad. Sci. 113, 9222–9227. doi:10.1073/pnas.1606526113.

Ragettli, S., and Pellicciotti, F. (2012). Calibration of a physically based, spatially distributed hydrological model in a glacierized basin: On the use of knowledge from glaciometeorological processes to constrain model parameters. Water Resour. Res. 48. doi:10.1029/2011WR010559.

Ragettli, S., Pellicciotti, F., Immerzeel, W. W., Miles, E. S., Petersen, L., Heynen, M., et al. (2015). Unraveling the hydrology of a Himalayan catchment through integration of high resolution in situ data and remote sensing with an advanced simulation model. Adv. Water Resour. 78, 94–111. doi:10.1016/j.advwatres.2015.01.013.

Rajbhandari, R., Shrestha, A. B., Kulkarni, A. V., Patwardhan, S. K., and Bajracharya, S. R. (2015). Projected changes in climate over the Indus river basin using a high resolution regional climate model (PRECIS). Clim. Dyn. 44, 339–357. doi:10.1007/s00382-014-2183-8.

Rajczak, J., Pall, P., and Schär, C. (2013). Projections of extreme precipitation events in regional climate simulations for Europe and the Alpine Region. J. Geophys. Res. Atmos. 118, 3610–3626. doi:10.1002/jgrd.50297.

Ramesh, K. V., and Goswami, P. (2015). Assessing reliability of regional climate projections: the case of Indian monsoon. Sci. Rep. 4, 4071. doi:10.1038/srep04071.

Rao, M. P., Cook, E. R., Cook, B. I., Palmer, J. G., Uriarte, M., Devineni, N., et al. (2018). Six Centuries of Upper Indus Basin Streamflow Variability and Its Climatic Drivers. Water Resour. Res. 54, 5687–5701. doi:10.1029/2018WR023080.

Rasul, G. (2014). Food, water, and energy security in South Asia: A nexus perspective from the Hindu Kush Himalayan region. Environ. Sci. Policy 39, 35–48. doi:10.1016/j.envsci.2014.01.010.

Rasul, G. (2016). Managing the food, water, and energy nexus for achieving the Sustainable Development Goals in South Asia. Environ. Dev. 18, 14–25. doi:10.1016/j.envdev.2015.12.001.

Rees, H. G., and Collins, D. N. (2006). Regional differences in response of flow in glacier-fed Himalayan rivers to climatic warming. Hydrol. Process. 20, 2157–2169. doi:10.1002/hyp.6209.

Reid, T. D., and Brock, B. W. (2010). An energy-balance model for debris-covered glaciers including heat conduction through the debris layer. J. Glaciol. 56, 903–916. doi:10.3189/002214310794457218.

Riahi, K., van Vuuren, D. P., Kriegler, E., Edmonds, J., O'Neill, B. C., Fujimori, S., et al. (2017). The Shared Socioeconomic Pathways and their energy, land use, and greenhouse gas emissions implications: An overview. Glob. Environ. Chang. 42, 153–168. doi:10.1016/j.gloenvcha.2016.05.009.

Richey, A. S., Thomas, B. F., Lo, M. H., Reager, J. T., Famiglietti, J. S., Voss, K., et al. (2015). Quantifying renewable groundwater stress with GRACE. Water Resour. Res. 51, 5217–5237. doi:10.1002/2015WR017349.

Rickenmann, D. (1996). Flow velocity in torrents and mountain rivers. Wasser-Energie-Luft 88, 298–303.

Ridder, N., de Vries, H., and Drijfhout, S. (2018). The role of atmospheric rivers in compound events consisting of heavy precipitation and high storm surges along the Dutch coast. Nat. Hazards Earth Syst. Sci. 18, 3311–3326. doi:10.5194/nhess-18-3311-2018.

Riseborough, D., Shiklomanov, N., Etzelmüller, B., Gruber, S., and Marchenko, S. (2008). Recent advances in permafrost modelling. Permafr. Periglac. Process. 19, 137–156. doi:10.1002/ppp.615.

Rodell, M., Velicogna, I., and Famiglietti, J. S. (2009). Satellite-based estimates of groundwater depletion in India. Nature 460, 999–1002. doi:10.1038/nature08238.

Roeckner, E., Bäuml, G., Bonaventura, L., Brokopf, R., Esch, M., Giorgetta, M., et al. (2003). The atmospheric general circulation model ECHAM5. Part I: Model description. Hamburg.

Rolland, C. (2003). Spatial and seasonal variations of air temperature lapse rates in alpine regions. J. Clim. 16, 1032–1046. doi:10.1175/1520-0442(2003)016<1032:SASVOA>2.0.CO;2.

Rosenberg, J., Davis, S. J., Narloch, U., and Hallegatte, S. (2015). Climate constraints on the carbon intensity of economic growth. Environ. Res. Lett. 10, 95006. doi:10.1088/1748-9326/10/9/095006.

Rost, S., Gerten, D., Bondeau, A., Lucht, W., Rohwer, J., and Schaphoff, S. (2008). Agricultural green and blue water consumption and its influence on the global water system. Water Resour. Res. 44. doi:10.1029/2007WR006331.

Rowan, A. V., Egholm, D. L., Quincey, D. J., and Glasser, N. F. (2015). Modelling the feedbacks between mass balance, ice flow and debris transport to predict the response to climate change of debris-covered glaciers in the Himalaya. Earth Planet. Sci. Lett. 430, 427–438. doi:10.1016/j.epsl.2015.09.004.

Roy, D. P., Wulder, M. A., Loveland, T. R., Woodcock, C. E., Allen, R. G., Anderson, M. C., et al. (2014). Landsat-8: Science and product vision for terrestrial global change research. Remote Sens. Environ. 145, 154–172. doi:10.1016/j.rse.2014.02.001.

Salerno, F., Thakuri, S., Tartari, G., Nuimura, T., Sunako, S., Sakai, A., et al. (2017). Debris-covered glacier anomaly? Morphological factors controlling changes in the mass balance, surface area, terminus position, and snow line altitude of Himalayan glaciers. Earth Planet. Sci. Lett. 471, 19–31. doi:10.1016/j.epsl.2017.04.039.

Saloranta, T., Thapa, A., Kirkham, J. D., Koch, I., Melvold, K., Stigter, E. E., et al. (2019). A Model Setup for Mapping Snow Conditions in High-Mountain Himalaya. Front. Earth Sci. 7. doi:10.3389/feart.2019.00129.

Salzmann, N., Huggel, C., Rohrer, M., and Stoffel, M. (2014). Data and knowledge gaps in glacier, snow and related runoff research – A climate change adaptation perspective. J. Hydrol. 518, 225–234. doi:10.1016/j.jhydrol.2014.05.058.

Sarmadian, F., and Keshavarzi, A. (2010). Developing Pedotransfer Functions for Estimating some Soil Properties using Artificial Neural Network and Multivariate Regression Approaches. Int. J. Environ. Earth Sci. 1, 31–37. doi:10.5281/zenodo.1060638.

Schaphoff, S., Heyder, U., Ostberg, S., Gerten, D., Heinke, J., and Lucht, W. (2013). Contribution of permafrost soils to the global carbon budget. Environ. Res. Lett. 8, 014026. doi:10.1088/1748-9326/8/1/014026.

Schaphoff, S., von Bloh, W., Rammig, A., Thonicke, K., Biemans, H., Forkel, M., et al. (2017). LPJmL4 – a dynamic global vegetation model with managed land – Part 1: Model description. Geosci. Model Dev. Discuss., 1–59. doi:10.5194/gmd-2017-145.

Schaphoff, S., von Bloh, W., Rammig, A., Thonicke, K., Biemans, H., Forkel, M., et al. (2018). LPJmL4 – a dynamic global vegetation model with managed land – Part 1: Model description. Geosci. Model Dev. 11, 1343–1375. doi:10.5194/gmd-11-1343-2018.

Scherler, D., Bookhagen, B., and Strecker, M. R. (2011). Hillslope-glacier coupling: The interplay of topography and glacial dynamics in High Asia. J. Geophys. Res. Earth Surf. 116. doi:10.1029/2010JF001751.

Schewe, J., Heinke, J., Gerten, D., Haddeland, I., Arnell, N. W., Clark, D. B., et al. (2014). Multimodel assessment of water scarcity under climate change. Proc. Natl. Acad. Sci. 111, 3245–50. doi:10.1073/pnas.1222460110.

Schlosser, E. (1997). Numerical simulation of fluctuations of Hintereisferner, Ötztal Alps, since AD 1850. Ann. Glaciol. 24, 199–202.

Schneeberger, K., Dobler, C., Huttenlau, M., and Stötter, J. (2015). Assessing potential climate change impacts on the seasonality of runoff in an Alpine watershed. J. Water Clim. Chang. 6, 263–277. doi:10.2166/wcc.2014.106.

Schulla, J. (2017). Model Description WaSiM. Zürich, Switzerland.

Seibert, J. (1997). Estimation of Parameter Uncertainty in the HBV Model. Nord. Hydrol. 28, 247–262. doi:10.2166/nh.1997.015.

Seibert, J., and Vis, M. J. P. (2012). Teaching hydrological modeling with a user-friendly catchment-runoff-model software package. Hydrol. Earth Syst. Sci. 16, 3315–3325. doi:10.5194/hess-16-3315-2012.

Seibert, J., Vis, M. J. P., Kohn, I., Weiler, M., and Stahl, K. (2018). Technical note: Representing glacier geometry changes in a semi-distributed hydrological model. Hydrol. Earth Syst. Sci. 22, 2211–2224. doi:10.5194/hess-22-2211-2018.

Seneviratne, S. I., Nicholls, N., Easterling, D., Goodess, C. M., Kanae, S., Kossin, J., et al. (2012). "Changes in Climate Extremes and their Impacts on the Natural Physical Environment," in Managing the Risks of Extreme Events and Disasters to Advance Climate Change Adaptation, eds. C. B. Field, V. Barros, T. F. Stocker, Q. Dahe, D. I. Dokken, K. L. Ebi, et al. (Cambridge, UK, and New York, USA: Cambridge University Press), 109–230. doi:10.1017/CBO9781139177245.006.

Seroussi, H., Morlighem, M., Rignot, E., Larour, E., Aubry, D., Ben Dhia, H., et al. (2011). Ice flux divergence anomalies on 79north Glacier, Greenland. Geophys. Res. Lett. 38, n/a-n/a. doi:10.1029/2011GL047338.

Sharmila, S., Joseph, S., Sahai, A. K., Abhilash, S., and Chattopadhyay, R. (2015). Future projection of Indian summer monsoon variability under climate change scenario: An assessment from CMIP5 climate models. Glob. Planet. Change 124, 62–78. doi:10.1016/j.gloplacha.2014.11.004.

Shea, J. M., Immerzeel, W. W., Wagnon, P., Vincent, C., and Bajracharya, S. R. (2015). Modelling glacier change in the Everest region, Nepal Himalaya. Cryosph. 9, 1105–1128. doi:10.5194/tc-9-1105-2015.

Shrestha, A. B., Agrawal, N. K., Alfthan, B., Bajracharya, S. R., Maréchal, J., and van Oort, B. (2015). The Himalayan Climate and Water Atlas: Impact of climate change on water resources in five of Asia's major river basins. ICIMOD, GRID-Arendal and CICERO.

Shrestha, A. B., Wahid, S. M., Vaidya, R. A., Shrestha, M. S., and Molden, D. J. (2013). "Regional Water Cooperation in the Hindu Kush Himalayan Region," in Free Flow - Reaching Water Security Through Water Cooperation, eds. J. Griffiths and R. Lambert (Paris, France: United Nations Educational, Scientific and Cultural Organization), 65–69.

Shrestha, A. B., Wake, C. P., Dibb, J. E., and Mayewski, P. A. (2000). Precipitation fluctuations in the Nepal Himalaya and its vicinity and relationship with some large scale climatological parameters. Int. J. Climatol. 20, 317–327. doi:10.1002/(SICI)1097-0088(20000315)20:3<317::AID-JOC476>3.0.CO;2-G.

Siebert, S., Burke, J., Faures, J. M., Frenken, K., Hoogeveen, J., Döll, P., et al. (2010). Groundwater use for irrigation - A global inventory. Hydrol. Earth Syst. Sci. 14, 1863–1880. doi:10.5194/hess-14-1863-2010.

Sigdel, S. R., Wang, Y., Camarero, J. J., Zhu, H., Liang, E., and Peñuelas, J. (2018). Moisture-mediated responsiveness of treeline shifts to global warming in the Himalayas. Glob. Chang. Biol. 24, 5549–5559. doi:10.1111/gcb.14428.

Sillmann, J., Kharin, V. V., Zhang, X., Zwiers, F. W., and Bronaugh, D. (2013a). Climate extremes indices in the CMIP5 multimodel ensemble: Part 1. Model evaluation in the present climate. J. Geophys. Res. Atmos. 118, 1716–1733. doi:10.1002/jgrd.50203.

Sillmann, J., Kharin, V. V., Zwiers, F. W., Zhang, X., and Bronaugh, D. (2013b). Climate extremes indices in the CMIP5 multimodel ensemble: Part 2. Future climate projections. J. Geophys. Res. Atmos. 118, 2473–2493. doi:10.1002/jgrd.50188.

Singh, P., Kumar, N., and Arora, M. (2000). Degree–day factors for snow and ice for Dokriani Glacier, Garhwal Himalayas. J. Hydrol. 235, 1–11. doi:10.1016/S0022-1694(00)00249-3.

Sivapalan, M. (2018). From engineering hydrology to Earth system science: milestones in the transformation of hydrologic science. Hydrol. Earth Syst. Sci. 22, 1665–1693. doi:10.5194/hess-22-1665-2018.

Skamarock, W. C., and Klemp, J. B. (2008). A time-split nonhydrostatic atmospheric model for weather research and forecasting applications. J. Comput. Phys. 227, 3465–3485. doi:10.1016/j.jcp.2007.01.037.

Skofronick-Jackson, G., Petersen, W. A., Berg, W., Kidd, C., Stocker, E. F., Kirschbaum, D. B., et al. (2017). The Global Precipitation Measurement (GPM) Mission for Science and Society. Bull. Am. Meteorol. Soc. 98, 1679–1695. doi:10.1175/BAMS-D-15-00306.1.

Span, N., Kuhn, M., and Schneider, H. (1997). 100 years of ice dynamics of Hintereisferner, Central Alps, Austria, 1894–1994. Ann. Glaciol. 24, 297–302. doi:10.1017/S0260305500012349.

Sperber, K. R., Annamalai, H., Kang, I.-S., Kitoh, A., Moise, A., Turner, A., et al. (2013). The Asian summer monsoon: an intercomparison of CMIP5 vs. CMIP3 simulations of the late 20th century. Clim. Dyn. 41, 2711–2744. doi:10.1007/s00382-012-1607-6.

Stahl, K., Moore, R. D., Shea, J. M., Hutchinson, D., and Cannon, A. J. (2008). Coupled modelling of glacier and streamflow response to future climate scenarios. Water Resour. Res. 44. doi:10.1029/2007WR005956.

Stehfest, E., van Vuuren, D. P., Kram, T., Bouwman, L., Alkemade, R., Bakkenes, M., et al. (2014). Integrated assessment of global environmental change with IMAGE 3.0: Model description and policy applications. the Hague, the Netherlands.

Steiner, J. F., Buri, P., Miles, E. S., Ragettli, S., and Pellicciotti, F. (2019). Supraglacial ice cliffs and ponds on debris-covered glaciers: spatio-temporal distribution and characteristics. J. Glaciol., 1–16. doi:10.1017/jog.2019.40.

Steiner, J. F., and Pellicciotti, F. (2016). Variability of air temperature over a debris-covered glacier in the Nepalese Himalaya. Ann. Glaciol. 57, 295–307. doi:10.3189/2016AoG71A066.

Steiner, J. F., Pellicciotti, F., Buri, P., Miles, E. S., Immerzeel, W. W., and Reid, T. D. (2015). Modelling ice-cliff backwasting on a debris-covered glacier in the Nepalese Himalaya. J. Glaciol. 61, 889–907. doi:10.3189/2015JoG14J194.

Stigter, E. E., Litt, M., Steiner, J. F., Bonekamp, P. N. J., Shea, J. M., Bierkens, M. F. P., et al. (2018). The Importance of Snow Sublimation on a Himalayan Glacier. Front. Earth Sci. 6. doi:10.3389/feart.2018.00108.

Stigter, E. E., Wanders, N., Saloranta, T. M., Shea, J. M., Bierkens, M. F. P., and Immerzeel, W. W. (2017). Assimilation of snow cover and snow depth into a snow model to estimate snow water equivalent and snowmelt runoff in a Himalayan catchment. Cryosph. 11, 1647–1664. doi:10.5194/tc-11-1647-2017.

Stocker-Waldhuber, M., Fischer, A., Helfricht, K., and Kuhn, M. (2019). Long-term records of glacier surface velocities in the Ötztal Alps (Austria). Earth Syst. Sci. Data 11, 705–715. doi:10.5194/essd-11-705-2019.

Strasser, U., Bernhardt, M., Weber, M., Liston, G. E., and Mauser, W. (2008). Is snow sublimation important in the alpine water balance? Cryosph. 2, 53–66. doi:10.5194/tc-2-53-2008.

Strasser, U., Marke, T., Braun, L., Escher-Vetter, H., Juen, I., Kuhn, M., et al. (2018). The Rofental: A high Alpine research basin (1890-3770ma.s.l.) in the Ötztal Alps (Austria) with over 150 years of hydrometeorological and glaciological observations. Earth Syst. Sci. Data 10, 151–171. doi:10.5194/essd-10-151-2018.

Su, F., Duan, X., Chen, D., Hao, Z., and Cuo, L. (2013). Evaluation of the Global Climate Models in the CMIP5 over the Tibetan Plateau. J. Clim. 26, 3187–3208. doi:10.1175/JCLI-D-12-00321.1.

Sutanudjaja, E. H., van Beek, R., Wanders, N., Wada, Y., Bosmans, J. H. C., Drost, N., et al. (2018). PCR-GLOBWB 2: a 5 arcmin global hydrological and water resources model. Geosci. Model Dev. 11, 2429–2453. doi:10.5194/gmd-11-2429-2018.

Taylor, K. E., Stouffer, R. J., and Meehl, G. A. (2012). An Overview of CMIP5 and the Experiment Design. Bull. Am. Meteorol. Soc. 93, 485–498. doi:10.1175/BAMS-D-11-00094.1.

Taylor, R. (2009). Rethinking water scarcity: The role of storage. Eos (Washington. DC). 90, 237–238. doi:10.1029/2009EO280001.

Tecklenburg, C., Francke, T., Kormann, C., and Bronstert, A. (2012). Modeling of water balance response to an extreme future scenario in the Ötztal catchment, Austria. Adv. Geosci. 32, 63–68. doi:10.5194/adgeo-32-63-2012.

Terink, W., Immerzeel, W. W., Lutz, A. F., Droogers, P., Khanal, S., Nepal, S., et al. (2017). Hydrological and Climate Change Assessment for Hydropower development in the Tamakoshi River Basin, Nepal. Wageningen, the Netherlands.

Terink, W., Lutz, A. F., Immerzeel, W. W., Nepal, S., Khanal, S., and Shrestha, A. B. (2016). Improvement of the SPHY Model Glacier Module and its Application in the Tamakoshi River Basin, Nepal. in AGU Fall Meeting Abstracts.

Terink, W., Lutz, A. F., Simons, G. W. H., Immerzeel, W. W., and Droogers, P. (2015). SPHY v2.0: Spatial Processes in HYdrology. Geosci. Model Dev. 8, 2009–2034. doi:10.5194/gmd-8-2009-2015.

Themeßl, M. J., Gobiet, A., and Heinrich, G. (2011). Empirical-statistical downscaling and error correction of regional climate models and its impact on the climate change signal. Clim. Change 112, 449–468. doi:10.1007/s10584-011-0224-4.

Tiwari, V. M., Wahr, J., and Swenson, S. (2009). Dwindling groundwater resources in northern India, from satellite gravity observations. Geophys. Res. Lett. 36, L18401. doi:10.1029/2009GL039401.

Trigo, I. F., de Bruin, H., Beyrich, F., Bosveld, F. C., Gavilán, P., Groh, J., et al. (2018). Validation of reference evapotranspiration from Meteosat Second Generation (MSG) observations. Agric. For. Meteorol. 259, 271–285. doi:10.1016/j.agrformet.2018.05.008.

Turner, A. G., and Annamalai, H. (2012). Climate change and the South Asian summer monsoon. Nat. Clim. Chang. 2, 587–595. doi:10.1038/nclimate1495.

UN-DESA (2018). World Urbanization Prospects 2018. Available at: https://esa.un.org/unpd/wup/ [Accessed June 6, 2018].

Vaidya, R. (2013). Water and Hydropower in the Green Economy and Sustainable Development of the Hindu Kush-Himalayan Region. Hydro Nepal J. Water, Energy Environ. 10, 11–19. doi:10.3126/hn.v10i0.7097.

van Beek, L. P. H., Wada, Y., and Bierkens, M. F. P. (2011). Global monthly water stress: 1. Water balance and water availability. Water Resour. Res. 47. doi:10.1029/2010WR009791.

van de Wal, R. S. W., and Oerlemans, J. (1995). Response of valley glaciers to climate change and kinematic waves: a study with a numerical ice-flow model. J. Glaciol. 41, 142–152. doi:10.1017/S0022143000017834.

van der Esch, S., ten Brink, B., Stehfest, E., Bakkenes, M., Sewell, A., Bouwman, A., et al. (2017). Exploring future changes in land use and land condition and the impacts on food, water, climate change and biodiversity: Scenarios for the Global Land Outlook. the Hague, the Netherlands.

van der Veen, C. J. (1999). Fundamentals of Glacier Dynamics. 1st ed. Rotterdam: A.A. Balkema.

van Engelen, A., Klein Tank, A. M. G., van de Schier, G., and Klok, L. (2008). Climate Assessment & Dataset (ECA&D): Towards an operational system for assessing observed changes in climate extremes. Available at: http://eca.knmi.nl/documents/ECAD_report_2008.pdf [Accessed April 24, 2017].

van Genuchten, M. (1980). A Closed-form Equation for Predicting the Hydraulic Conductivity of Unsaturated Soils1. Soil Sci. Soc. Am. J. 44, 892. doi:10.2136/sssaj1980.03615995004400050002x.

van Pelt, S. C., Beersma, J. J., Buishand, T. A., van den Hurk, B. J. J. M., and Kabat, P. (2012). Future changes in extreme precipitation in the Rhine basin based on global and regional climate model simulations. Hydrol. Earth Syst. Sci. 16, 4517–4530. doi:10.5194/hess-16-4517-2012.

van Vuuren, D. P., and Carter, T. R. (2014). Climate and socio-economic scenarios for climate change research and assessment: Reconciling the new with the ol. Clim. Change 122, 415–429. doi:10.1007/s10584-013-0974-2.

van Vuuren, D. P., Edmonds, J., Kainuma, M., Riahi, K., Thomson, A., Hibbard, K., et al. (2011). The representative concentration pathways: An overview. Clim. Change 109, 5–31. doi:10.1007/s10584-011-0148-z.

van Vuuren, D. P., Kriegler, E., O'Neill, B. C., Ebi, K. L., Riahi, K., Carter, T. R., et al. (2014). A new scenario framework for Climate Change Research: Scenario matrix architecture. Clim. Change 122, 373–386. doi:10.1007/s10584-013-0906-1.

van Woerkom, T., Steiner, J. F., Kraaijenbrink, P. D. A., Miles, E. S., and Immerzeel, W. W. (2019). Sediment supply from lateral moraines to a debris-covered glacier in the Himalaya. Earth Surf. Dyn. 7, 411–427. doi:10.5194/esurf-7-411-2019.

Vaze, J., Post, D. A., Chiew, F. H. S., Perraud, J. M., Viney, N. R., and Teng, J. (2010). Climate non-stationarity – Validity of calibrated rainfall–runoff models for use in climate change studies. J. Hydrol. 394, 447–457. doi:http://dx.doi.org/10.1016/j.jhydrol.2010.09.018.

Veldkamp, T. I. E., Wada, Y., Aerts, J. C. J. H., Döll, P., Gosling, S. N., Liu, J., et al. (2017). Water scarcity hotspots travel downstream due to human interventions in the 20th and 21st century. Nat. Commun. 8, 15697. doi:10.1038/ncomms15697.

Viste, E., and Sorteberg, A. (2015). Snowfall in the Himalayas: an uncertain future from a little-known past. Cryosph. 9, 1147–1167. doi:10.5194/tc-9-1147-2015.

Viviroli, D., Archer, D. R., Buytaert, W., Fowler, H. J., Greenwood, G. B., Hamlet, A. F., et al. (2011). Climate change and mountain water resources: Overview and recommendations for research, management and policy. Hydrol. Earth Syst. Sci. 15, 471–504. doi:10.5194/hess-15-471-2011.

Viviroli, D., Dürr, H. H., Messerli, B., Meybeck, M., and Weingartner, R. (2007). Mountains of the world, water towers for humanity: Typology, mapping, and global significance. Water Resour. Res. 43, 1–13. doi:10.1029/2006WR005653.

Viviroli, D., and Weingartner, R. (2004). The hydrological significance of mountains: from regional to global scale. Hydrol. Earth Syst. Sci. 8, 1017–1030. doi:10.5194/hess-8-1017-2004.

Vörösmarty, C. J., Green, P., Salisbury, J., and Lammers, R. B. (2000). Global Water Resources: Vulnerability from Climate Change and Population Growth. Science (80-.). 289, 284–288. doi:10.1126/science.289.5477.284.

Wada, Y. (2016). Modeling Groundwater Depletion at Regional and Global Scales: Present State and Future Prospects. Surv. Geophys. 37, 419–451. doi:10.1007/s10712-015-9347-x.

Wada, Y., and Bierkens, M. F. P. (2014). Sustainability of global water use: past reconstruction and future projections. Environ. Res. Lett. 9, 104003. doi:10.1088/1748-9326/9/10/104003.

Wada, Y., de Graaf, I. E. M., and van Beek, L. P. H. (2016a). High-resolution modeling of human and climate impacts on global water resources. J. Adv. Model. Earth Syst. 8, 735–763. doi:10.1002/2015MS000618.

Wada, Y., Flörke, M., Hanasaki, N., Eisner, S., Fischer, G., Tramberend, S., et al. (2016b). Modeling global water use for the 21st century: The Water Futures and Solutions (WFaS) initiative and its approaches. Geosci. Model Dev. 9, 175–222. doi:10.5194/gmd-9-175-2016.

Wada, Y., van Beek, L. P. H., and Bierkens, M. F. P. (2011a). Modelling global water stress of the recent past: On the relative importance of trends in water demand and climate variability. Hydrol. Earth Syst. Sci. 15, 3785–3808. doi:10.5194/hess-15-3785-2011.

Wada, Y., van Beek, L. P. H., van Kempen, C. M., Reckman, J. W. T. M., Vasak, S., and Bierkens, M. F. P. (2010). Global depletion of groundwater resources. Geophys. Res. Lett. 37. doi:10.1029/2010GL044571.

Wada, Y., van Beek, L. P. H., Viviroli, D., Dürr, H. H., Weingartner, R., and Bierkens, M. F. P. (2011b). Global monthly water stress: 2. Water demand and severity of water stress. Water Resour. Res. 47. doi:10.1029/2010WR009792.

Wada, Y., Wisser, D., and Bierkens, M. F. P. (2014). Global modeling of withdrawal, allocation and consumptive use of surface water and groundwater resources. Earth Syst. Dyn. 5, 15–40. doi:10.5194/esd-5-15-2014.

Wada, Y., Wisser, D., Eisner, S., Flörke, M., Gerten, D., Haddeland, I., et al. (2013). Multimodel projections and uncertainties of irrigation water demand under climate change. Geophys. Res. Lett. 40, 4626–4632. doi:10.1002/grl.50686.

Waha, K., van Bussel, L. G. J., Müller, C., and Bondeau, A. (2012). Climate-driven simulation of global crop sowing dates. Glob. Ecol. Biogeogr. 21, 247–259. doi:10.1111/j.1466-8238.2011.00678.x.

Wang, B., Bao, Q., Hoskins, B., Wu, G., and Liu, Y. (2008). Tibetan Plateau warming and precipitation changes in East Asia. Geophys. Res. Lett. 35, L14702. doi:10.1029/2008GL034330.

Weber, M., Braun, L., Mauser, W., and Prasch, M. (2010). Contribution of rain, snow- and icemelt in the Upper Danube discharge today and in the future. Geogr. Fis. e Din. Quat. 33, 221–230.

Weber, S., Beutel, J., Da Forno, R., Geiger, A., Gruber, S., Gsell, T., et al. (2019). A decade of detailed observations (2008 - 2018) in steep bedrock permafrost at Matterhorn Hörnligrat (Zermatt, CH). Earth Syst. Sci. Data Discuss., 1–48. doi:10.5194/essd-2019-14.

Webster, P. J., Toma, V. E., and Kim, H. M. (2011). Were the 2010 Pakistan floods predictable? Geophys. Res. Lett. 38. doi:10.1029/2010GL046346.

Weedon, G. P., Balsamo, G., Bellouin, N., Gomes, S., Best, M. J., and Viterbo, P. (2014). The WFDEI meteorological forcing data set: WATCH Forcing data methodology applied to ERA-Interim reanalysis data. Water Resour. Res. 50, 7505–7514. doi:10.1002/2014WR015638.

Weedon, G. P., Gomes, S., Adam, J. C., Bellouin, N., Viterbo, P., Bellouin, N., et al. (2010). The Watch Forcing Data 1958-2001: a Meteorological Forcing Dataset for Land Surface-and Hydrological-Models. Watch Tech. Rep. 22, 41p.

Weedon, G. P., Gomes, S., Viterbo, P., Shuttleworth, W. J., Blyth, E., Österle, H., et al. (2011). Creation of the WATCH Forcing Data and Its Use to Assess Global and Regional Reference Crop Evaporation over Land during the Twentieth Century. J. Hydrometeorol. 12, 823–848. doi:10.1175/2011JHM1369.1.

Weertman, J. (1957). On the Sliding of Glaciers. J. Glaciol. 3, 33–38. doi:10.3189/S0022143000024709.

Weingartner, R., Viviroli, D., and Greenwood, G. (2009). "Mountain waters in a changing world," in Global Change and Sustainable Development in Mountain Regions, eds. R. Jandl, A. Borsdorf, H. van Miegroet, R. Lackner, and R. Psenner (Innsbruck: Innsbruck University Press), 11–24.

Westra, S., Thyer, M., Leonard, M., Kavetski, D., and Lambert, M. (2014). A strategy for diagnosing and interpreting hydrological model nonstationarity. Water Resour. Res. 50, 5090–5113. doi:10.1002/2013WR014719.

WGMS (2018). Reference glaciers for mass balance. Available at: https://wgms.ch/products_ref_glaciers/ [Accessed November 30, 2018].

Wijngaard, R. R., Biemans, H., Lutz, A. F., Shrestha, A. B., Wester, P., and Immerzeel, W. W. (2018). Climate change vs. socio-economic development: understanding the future South Asian water gap. Hydrol. Earth Syst. Sci. 22, 6297–6321. doi:10.5194/hess-22-6297-2018.

Wijngaard, R. R., Helfricht, K., Schneeberger, K., Huttenlau, M., Schneider, K., and Bierkens, M. F. P. (2016). Hydrological response of the Ötztal glacierized catchments to climate change. Hydrol. Res. 47, 979–995. doi:10.2166/nh.2015.093.

Wijngaard, R. R., Lutz, A. F., Nepal, S., Khanal, S., Pradhananga, S., Shrestha, A. B., et al. (2017). Future changes in hydro-climatic extremes in the Upper Indus, Ganges, and Brahmaputra River basins. PLoS One 12, 26. doi:10.1371/journal.pone.0190224.

Winsemius, H. C., Aerts, J. C. J. H., van Beek, L. P. H., Bierkens, M. F. P., Bouwman, A., Jongman, B., et al. (2015). Global drivers of future river flood risk. Nat. Clim. Chang. 6, 381–385. doi:10.1038/nclimate2893.

WMO (2008). Manual on Low-flow Estimation and Prediction. Koblenz, Germany.

World Bank (2013). Turn Down the Heat: Climate Extremes, Regional Impacts, and the Case for Resilience. Washington DC, USA: World Bank Available at: http://documents.worldbank.org/curated/en/975911468163736818/Turn-down-the-heat-climate-extremes-regional-impacts-and-the-case-for-resilience-full-report.

Xu, C. Y., and Singh, V. P. (2002). Cross comparison of empirical equations for calculating potential evapotranspiration with data from Switzerland. Water Resour. Manag. 16, 197–219. doi:10.1023/A:1020282515975.

Yáñez-Morroni, G., Gironás, J., Caneo, M., Delgado, R., and Garreaud, R. (2018). Using the Weather Research and Forecasting (WRF) Model for Precipitation Forecasting in an Andean Region with Complex Topography. Atmosphere (Basel). 9, 304. doi:10.3390/atmos9080304.

Yao, T., Thompson, L., Yang, W., Yu, W., Gao, Y., Guo, X., et al. (2012). Different glacier status with atmospheric circulations in Tibetan Plateau and surroundings. Nat. Clim. Chang. 2, 663–667. doi:10.1038/nclimate1580.

Yatagai, A., Kamiguchi, K., Arakawa, O., Hamada, A., Yasutomi, N., and Kitoh, A. (2012). APHRODITE constructing a long-term daily gridded precipitation dataset for Asia based on a dense network of rain gauges. Bull. Am. Meteorol. Soc. 93, 1401–1415. doi:10.1175/BAMS-D-11-00122.1.

Yeh, S.-W., Cai, W., Min, S.-K., McPhaden, M. J., Dommenget, D., Dewitte, B., et al. (2018). ENSO Atmospheric Teleconnections and Their Response to Greenhouse Gas Forcing. Rev. Geophys. 56, 185–206. doi:10.1002/2017RG000568.

ZAMG (2013). Climate Data of Austria 1971–2000. Available at: http://www.zamg.ac.at/fix/klima/oe71-00/klima2000/klimadaten_oesterreich_1971_frame1.htm [Accessed January 10, 2019].

Zekollari, H., Fürst, J. J., and Huybrechts, P. (2014). Modelling the evolution of Vadret da Morteratsch, Switzerland, since the Little Ice Age and into the future. J. Glaciol. 60, 1208–1220. doi:10.3189/2014JoG14J053.

Zhang, T., Xiao, C., Colgan, W., Qin, X., Du, W., Sun, W., et al. (2013). Observed and modelled ice temperature and velocity along the main flowline of East Rongbuk Glacier, Qomolangma (Mount Everest), Himalaya. J. Glaciol. 59, 438–448. doi:10.3189/2013JoG12J202.

Zhang, Y., Liu, S., and Ding, Y. (2006). Observed degree-day factors and their spatial variation on glaciers in western China. Ann. Glaciol. 43, 301–306. doi:10.3189/172756406781811952.

Zscheischler, J., Westra, S., van den Hurk, B. J. J. M., Seneviratne, S. I., Ward, P. J., Pitman, A., et al. (2018). Future climate risk from compound events. Nat. Clim. Chang. 8, 469–477. doi:10.1038/s41558-018-0156-3.

Appendix A

Supplement to Chapter 3

Table A.1. Mean absolute runoff changes (mm/day) on monthly and annual basis. The absolute changes formatted in bold represent the maximum absolute increases and the absolute changes formatted in bold/italic represent the maximum absolute decreases. Abbreviations: P1 = 2010-2039, P2 = 2040-2069, and P3 = 2070-2099.

	Jan	Feb	Mar	Apr	May	Jun	Jul	Aug	Sep	Oct	Nov	Dec	Annual
HBV													
Brunau_P1	0.03	0.02	0.02	0.23	**0.73**	0.02	0.11	0.05	0.27	0.19	0.08	0.05	0.15
Brunau_P2	0.04	0.03	0.06	0.39	**0.40**	-1.32	-2.06	***-2.06***	-0.71	-0.01	0.09	0.07	-0.43
Brunau_P3	0.07	0.05	0.14	**0.77**	0.10	-2.57	***-3.75***	-3.55	-1.42	-0.18	0.07	0.08	-0.86
Obergurgl_P1	0.02	0.01	0.03	0.48	**1.25**	0.60	0.87	0.73	0.86	0.50	0.10	0.05	0.46
Obergurgl_P2	0.07	0.04	0.08	**0.53**	0.22	-1.94	-2.94	***-2.96***	-0.91	0.21	0.23	0.13	-0.61
Obergurgl_P3	0.12	0.07	0.20	**0.93**	-0.33	-3.94	***-5.79***	-5.69	-2.31	-0.12	0.29	0.20	-1.38
Vent P1	0.03	0.02	0.02	0.19	**0.87**	0.24	0.28	0.15	0.44	0.27	0.09	0.07	0.22
Vent P2	0.07	0.04	0.04	**0.22**	0.15	-1.58	-3.60	***-3.75***	-1.00	0.13	0.17	0.11	-0.76
Vent P3	0.06	0.04	0.06	**0.45**	0.27	-2.92	-6.43	***-6.50***	-2.25	-0.13	0.12	0.09	-1.44
HQsim													
Brunau_P1	0.01	-0.03	***-0.06***	0.15	**0.93**	0.44	0.60	0.44	0.42	0.23	0.13	0.08	0.21
Brunau_P2	0.06	0.03	0.01	0.42	**1.00**	-0.50	-1.27	***-1.63***	-0.59	0.02	0.22	0.16	-0.19
Brunau_P3	0.14	0.08	0.11	0.62	**0.77**	-1.57	-2.97	***-3.10***	-1.23	-0.18	0.28	0.24	-0.57
Obergurgl_P1	-0.05	***-0.06***	-0.04	0.46	**2.24**	1.66	1.63	1.16	0.90	0.29	0.06	0.01	0.67
Obergurgl_P2	0.06	0.02	0.05	0.82	**2.43**	0.60	-1.22	***-2.30***	-0.55	0.25	0.37	0.18	0.25
Obergurgl_P3	0.18	0.11	0.18	1.03	**2.39**	-0.80	-4.27	***-5.42***	-2.00	-0.16	0.54	0.33	-0.46
Vent P1	0.04	-	***-0.02***	0.13	**1.35**	0.92	0.83	0.07	0.12	-0.01	0.13	0.11	0.38
Vent P2	0.15	0.09	0.06	0.36	**1.64**	-0.04	-2.77	***-4.48***	-1.78	-0.21	0.39	0.28	-0.41
Vent P3	0.25	0.16	0.16	0.54	**1.94**	-1.19	-5.86	***-7.43***	-3.01	-0.51	0.52	0.40	-1.06

Table A.2. Mean relative runoff changes (%) on monthly and annual basis. The relative changes formatted in bold represent the maximum relative increases and the relative changes formatted in bold/italic represent the maximum relative decreases. Abbreviations: P1 = 2010-2039, P2 = 2040-2069, and P3 = 2070-2099.

	Jan	Feb	Mar	Apr	May	Jun	Jul	Aug	Sep	Oct	Nov	Dec	Annual
HBV													
Brunau_P1	6	6	8	**27**	*22*	1	2	1	8	9	6	6	5
Brunau_P2	8	9	19	**57**	18	-17	-26	***-29***	-14	1	6	7	-14
Brunau_P3	11	14	44	**132**	16	-35	-48	***-51***	-31	-7	4	8	-29
Obergurgl_P1	9	9	15	**44**	23	6	7	7	17	19	9	9	10
Obergurgl_P2	24	26	55	**99**	13	-14	-21	***-23***	-6	18	22	23	-13
Obergurgl_P3	47	55	149	**238**	10	-31	-43	***-46***	-28	8	30	39	-29
Vent P1	7	7	8	35	**36**	5	3	3	11	13	8	8	5
Vent P2	16	16	20	**67**	34	-8	-25	***-29***	-9	11	16	17	-18
Vent P3	14	14	31	**157**	53	-19	-47	***-53***	-30	-	11	14	-34
HQsim													
Brunau_P1	2	-5	***-11***	20	**63**	22	15	12	17	16	15	12	8
Brunau_P2	12	6	1	58	**76**	7	-14	***-21***	-9	9	22	23	-7
Brunau_P3	27	17	19	**88**	77	-10	-40	***-45***	-26	1	28	34	-21
Obergurgl_P1	-10	***-17***	-14	96	**164**	54	20	16	25	17	10	2	16
Obergurgl_P2	13	5	14	190	**196**	46	-1	***-10***	7	24	41	31	6
Obergurgl_P3	42	29	49	**249**	219	36	-26	***-36***	-12	19	64	60	-10
Vent P1	11	1	***-7***	23	**106**	48	15	9	14	13	22	23	10
Vent P2	37	27	19	85	**148**	48	-13	***-26***	-9	16	53	54	-10
Vent P3	63	47	47	138	**186**	45	-38	***-50***	-26	12	73	79	-25

Acknowledgements

Over the past few years I undertook a journey that ended up in this Ph.D. thesis. For me it is possible to have some debate about the starting point of the journey. Is it the first publication, which was written about 5 years ago in Austria, or did it start with an idea based on memories from the past? For instance, the full bag of stones that I dragged from the mountains into the valley during the numerous holidays in Austria with my parents, brother and sister, or the trekking in the Khumbu region, Nepal, which I undertook with my dad in 2010. Whatever the exact starting point of the journey might be, it was a beautiful journey that gave me the possibility to learn a lot, especially in the last few years. Not only as a researcher, but also as a person. Although the journey was beautiful, there were times when it was not easy. However, the support of numerous people helped me to go on and keep track. I can only say that this thesis would never be there without the support of these people and that I am really thankful for their support.

First of all, I want to thank Arthur, my former colleague at FutureWater and co-promotor at Utrecht University (UU). Dear Arthur, thank you very much for your support during my time at FutureWater and afterwards. It was a real pleasure to work with you and I learned a lot from you in all kind of prospects. I am thankful you were there to help me with problems or questions, to give a boost when it was needed, and to give me valuable advices and feedback. Finally, I am thankful you gave me the chance to join several projects and to make two beautiful trips to Nepal. I hope that in the future more possibilities will appear that we can work together. Next, I would like to thank my promotors, Walter and Marc. Dear Walter, it is a real honor to have you as my promotor. I can still remember you were one of the evaluators of my Master thesis and that I spend a few words on you in the acknowledgements of that thesis. My feelings about these words haven't changed since. Somehow I have the feeling that even while working on the contaminant hydrology in 2015/2016 the mountains were still calling via your work. Probably this lead to the start of the ice flow model project at that time. Your work, advices, and feedback helped me to become a better researcher, to keep an critical eye on the work I was doing, and to get a better understanding of the complexity of the mountain environment. I want to thank you for introducing me at FutureWater, to give me a chance to work on our ice flow model project, and of course for the nice talks about (trail)running, etc. I hope that in the future more opportunities will rise to work together. Dear Marc, you have been there since the beginning when you were my MSc thesis supervisor and contributed to my first publication (and several publications afterwards). I am really grateful for your good advices and smart solutions that improved my work significantly, also during my time at FutureWater. I want to thank you for the chances you gave me to work at the UU and also for your effort and time in reviewing the papers I wrote.

Much of the work that ended up in this thesis would have not been possible without the support of alpS and FutureWater. Firstly, I want to thank the former director of alpS, Eric Veuilliet, and my MSc thesis supervisors Matthias Huttenlau and Katrin Schneider. Dear Eric, Matthias, and Katrin, thank you very much for the opportunity to work at alpS and your support I received while writing my first publication. I am very grateful for my time and experiences at alpS. I also would like to thank my other former alpS colleagues Klaus, Kay, Benjamin, Paul, Johannes, Kristian, Florian, and Christian for the fun and scientific support. Secondly, I want to thank the (former) directors of FutureWater Peter Droogers, Gijs Simons, and Johannes Hunink. Dear Peter, Gijs,

and Johannes, thank you very much for the opportunity to join and work at FutureWater, and to contribute in several nice projects, which resulted in three nice publications. I learned a lot from you at FutureWater, especially in keeping the work flow efficient. I would like to thank the other former FutureWater colleagues as well. Dear Martijn, Wilco, Sergio, Alberto, Froukje, Maurits, Femke, Remo, and Sonu, I would like to thank you for your pleasant collaboration, the support, and especially for the fun during breaks or after work. I still think a lot about our dart contests and other team activities. I hope that in the future more dart arrows will fly and will end up in the dartboard (and not the wall).

Furthermore I would like to thank for the fun and support I experienced with my (former) colleagues of the UU and the mountain hydrology group. Jakob, Philip, and Max, thank you very much for the valuable contributions and feedback that helped to improve the ice flow paper. I also would like to thank you, Pleun, Emmy, and Remco for being part of the mountain hydrology group. Besides work it was also important to have some distraction from time to time and to have company at work. The Gutenberg cappuccino's have definitely contributed to that, but also the walks, talks and other activities. For these moments I am very grateful and want to thank Sebastian, Joost, Eelco, Daniel, Sepehr, Joeri, Daan, Klaas, Anouk, Jantien, Tim, Pam, Geert, Gerben, Marcel, Edwin, Oliver, Meng, and Jiong in particular. I also want to express my gratitude for Rens. Dear Rens, you have always been there since the beginning. For talks, for feedback, for help, and other valuable support or contributions. Thank you very much for everything.

I also would like to thank people from the International Centre for Integrated Mountain Development (ICIMOD), Nepal. A large part of the work in this thesis is based on the HI-AWARE assignments, which made it possible to write two publications. I want to thank Arun Shrestha, Santosh Nepal, and Saurav Pradhananga in particular. Dear Arun, Santosh, and Saurav, thank you very much for your support in all kind of ways, the pleasant collaboration, the fun, and the opportunities to visit ICIMOD. I also want to thank other people at ICIMOD who made it possible to have a good stay in Kathmandu and facilitated all the meetings and activities I attended.

All the publications that ended up in this thesis would not have been there without the support of the numerous co-authors. For the contribution to these publications I also want to thank the people I did not mention so far: Hester, Flip, Surendra, Argha, Francesca, and Christoph. Also, my work would have not been possible without the financial support of several agencies and organizations. For the financial support I want to acknowledge the organizations and agencies that have not been mentioned before: the Leonardo da Vinci programme, the United Kingdom Government's Department for International Development, the International Development Research Centre, the Netherlands Organization for Scientific Research, and the European Research Council.

I would never been able to do my work without the support of my friends and family. Friends and family who were there for me when I needed them most, provided moments of distraction and relaxation, or who were just there to support me, to listen, and to show interest in what I was doing. I learned a lot from them on a personal level.

I would like to start with the groups I joined occasionally. Groeigroepers, OTR-ers, BoBo's en Taizé-groepers, ik wil jullie ontzettend bedanken voor de vele leuke en goede momenten, weekendjes, reisjes, en gesprekken in de afgelopen jaren. Taizé-groepers, jullie wil ik ook bedanken voor de

bijzondere reis naar Taizé. Ik heb toen in ieder geval geleerd dat Fransen een bijzondere associatie hebben met jeu de boule sticks en dat cappuccino ook gebruikt kan worden om een brandje te blussen.

I would like to thank my friends from Austria, whom I met when I lived there for a year. In particular, I want to thank Raphael, Iris, and Sandro. Liebe Raphael, Iris, und Sandro, vielen Dank für eure Freundschaft. Wir haben uns getroffen in Innsbruck und haben viel geteilt zusammen wann ich dort war und später wann ich zurückgekehrt war in die Niederlande. Liebe Sandro, vielen Dank für die besondere Couchsurfing Momenten und das du mich gehost hat in Innsbruck.

Over the last year I made several beautiful trips, where I made a lot of new friends. I want to thank my friends I met on the Camino de Santiago. Anne, Lisa & Sebastiaan, Li, Kseniya, Trevor, Letitia, and Sarah, I would like to thank you in particular for the numerous special moments and conversations we shared, which gave me a boost in finishing this work, helped me to move forward, and gave me more self-confidence. I also want to thank my Korean friends. 함께한 매 순간과 대화에 감사합니다 ^−^. Dear Lydia, I want to say that I am very grateful for your support and our conversations during the last stage of my PhD!

At home I spent a lot of time with a few very good friends I see (more than) regularly. In particular I want to mention: Vincent & Jasmijn, Steven, Alexandros & Veerle, Jef & Dennis, Babs, Arrom & Lisa, Karina, Melita, Sonu, and Meng. Ontzettend bedankt voor jullie support in de afgelopen jaren. Bedankt voor de vele bijzondere en gezellige momenten, gesprekken, en wijsheden/adviezen. Ik vond het fijn dat ik bij jullie altijd terecht kon voor een biertje, een babbeltje, of om even mijn verhaal kwijt te kunnen. Dear Sonu, we started at FutureWater and we have become very good friends since then. I enjoy the moments and conversations we share a lot. I want to thank you for showing me the Newari kitchen when we visited Nepal together and I am very grateful that you can be one of my paranymps. Dear Meng, we met each other about a year ago and we have become very good friends since then. Thank you very much for the special moments and conversations we share(d). The moments and conversations with you learn(ed) me to become a more open person and gave me more self-confidence. I am very grateful for that. I also want to say that I really appreciate our music practices (and your piano music) and that I am very grateful you would like to be one of my paranymphs as well.

In this penultimate paragraph I want to spend a few words to express my gratitude towards my dad, mom, brother & girlfriend, and sister. Pap en mam, ontzettend bedankt dat jullie er altijd waren voor mij. Jullie hebben van het begin af aan altijd in mij geloofd en mij gebracht en begeleid naar de plek waar ik mij nu bevind. Ik dank jullie voor de vele vakanties naar Oostenrijk en de trip naar Nepal die naar mijn mening de basis hebben gevormd voor dit werk en voor jullie luisterend oor wanneer dan ook. Rick & Colette, en Pauline, ook jullie wil ik bedanken voor jullie support en de gezellige momenten die we delen met elkaar.

In the last sentence I want to thank everyone I did not mention here, but still have accompanied me during this interesting journey.

René Wijngaard
Bennekom, 4 August 2019

About the author

René Wijngaard was born on March 6th, 1990 in Heemskerk and grew up in Bennekom, the Netherlands. René attended his secondary school at the Pantarijn, Wageningen, where he obtained his certificate in 2008. His large fascination for the mountain environment, and other natural environments on Planet Earth as well, lead him to Utrecht University where he started his Bachelor in Earth Sciences in the same year. He gained his BSc degree in 2012 and continued with a Master in Water Science and Management, where he received his MSc degree in 2014. During his Master he developed a large interest for catchment hydrology where several disciplines, such as hydrology, climatology, and glaciology come together. He completed a graduation internship at the alpS Centre for Climate Change Adaptation in Innsbruck, Austria, a research and consultancy firm that focusses on climate change impacts and adaptation in mountain regions. There, he investigated the effects of future climate change on the hydrological response of glacierized catchments, and followed a trainee internship as well. After his internship, René started working as research employee at Utrecht University where he investigated the impacts of climate change on metal and pathogen transport in lowland catchments. Between 2016 and 2018 he worked as a hydrologist at FutureWater, Wageningen, the Netherlands, which is a research and consultancy company that works throughout the world to combine scientific research with practical solutions for water management. There, he worked mainly on research projects with a focus on climate change impacts in the Indus, Ganges, and Brahmaputra river basins, and worked on other projects in the Netherlands, Angola, and Indonesia, as well. The combination of research projects conducted at alpS and FutureWater lead to the start of a Ph.D. track in 2017/2018. In 2018 and 2019 he worked for several months as a research employee at Utrecht University, where he continued his Ph.D. research by investigating the response of glaciers to historical climate change. René has a strong background in hydrological and cryospheric sciences, and developed strong skills in cryospheric/hydrological modelling, programming, and GIS.

List of publications

First authored publications

Wijngaard, R.R., Steiner, J.F., Kraaijenbrink, P.D.A., Klug, C., Adhikari, S., Banerjee, A., Pellicciotti, F., van Beek, L.P.H., Bierkens, M.F.P., Lutz, A.F., and Immerzeel, W.W. Modelling the response of the Langtang Glacier and the Hintereisferner to a changing climate since the Little Ice Age. Frontiers in Earth Science 7 (143). DOI: 10.3389/feart.2019.00143.

Wijngaard, R.R., Biemans, H., Lutz, A.F., Shrestha, A.B., Wester, P., and Immerzeel, W.W. 2018. Climate change vs. socio-economic development: understanding the future South Asian water gap. Hydrology and Earth System Sciences 22, 6297-6321. DOI: 10.5194/hess-22-6297-2018.

Wijngaard, R.R., Lutz, A.F., Nepal, S., Khanal, S., Pradhananga, S., Shrestha, A.B., and Immerzeel, W.W. 2017. Future changes in hydro-climatic extremes in the Upper Indus, Ganges, and Brahmaputra River basins. PLoS ONE 12(12). DOI: 10.1371/journal.pone.0190224.

Wijngaard, R.R., van der Perk, M., van der Grift, B., de Nijs, T.C.M. & Bierkens, M.F.P. 2017. The impacts of climate change on metal transport in a lowland catchment. Water, Air, and Soil Pollution, 228(107). DOI: 10.1007/s11270-017-3261-4.

Wijngaard, R.R., Helfricht, K., Schneeberger, K., Huttenlau, M., Schneider, K., and Bierkens, M.F.P. 2016. Hydrological response of the Ötztal glacierized catchments to climate change. Hydrology Research 47(5), 979-995. DOI: 10.2166/nh.2015.093.

Co-authored publications

Biemans, H., Siderius, C., Lutz, A.F., Nepal, S., Ahmad, B., Hassan, S.M.T., von Bloh, W., Wijngaard, R.R., Wester, P., Shrestha, A.B. & Immerzeel, W.W. 2019. Importance of snow and glacier meltwater for agriculture on the Indo-Gangetic Plain. Nature Sustainability 2, 594-601. DOI: 10.1038/s41893-019-0305-3.

Lutz, A.F., ter Maat, H.W., Wijngaard, R.R., Biemans, H., Syed. A., Shrestha, A.B., Wester. P. & Immerzeel, W.W. 2018. South Asian river basins in a 1.5 °C warmer world. Regional Environmental Change. DOI: 10.1007/s10113-018-1433-4.

Confererence Abstracts and Proceedings

Immerzeel, W.W., Wijngaard, R.R., Biemans, H., Lutz, A.F., and Kraaijenbrink, P.D.A., 2017, Understanding the drivers of the future water gap in the Indus-Ganges-Brahmaputra basins. AGU Fall Meeting 2017, December, 2017, New Orleans, USA.

Helfricht, K., Wijngaard, R.R., Huttenlau, M., and Schneider, K., 2015, The separated effects of atmospheric forcing and changes in ice cover on runoff in the Ötztal catchment. In: Proceedings of the 26th IUGG General Assembly 2015, June/July 2015, Prag, Czech Republic.

Wijngaard, R.R., Helfricht, K., Schneeberger, K., Huttenlau, M., Schneider, K., & Bierkens, M.F.P., 2015, Climate change effects on runoff in the Ötztal glacierized catchments, Geophysical Research Abstracts, Vol. 17, EGU2015-11014.

Wijngaard, R.R., Helfricht, K., Huttenlau, M., Schneider, K. & Bierkens, M.F.P., 2014, Hydrological Response of Glacierized Catchments to Future Climate Change. In: Book of Abstracts Tri-National Workshop Obergurgl - "Hydrological processes in high mountain regions over the course of time", September/ October 2014, Obergurgl, Austria.

Financial support

A number of organisations and funding agencies have supported the research presented in this thesis financially by means of several research projects and programmes. These organisations and funding agencies are listed below:

alpS GmbH, Innsbruck, Austria

FutureWater, Wageningen, the Netherlands

University of Natural Resources and Life Sciences (BOKU), Vienna, through the project StartClim2013.C (StartClim2013, AustroClim)

Leonardo da Vinci programme (EU Lifelong Learning Programme), through the fellowship at alpS Centre for Climate Change Adaptation.

United Kingdom Government's Department for International Development (DFID) and the International Development Research Centre (IDRC), Ottawa, Canada, through the Himalayan Adaptation, Water and Resilience (HIAWARE) consortium under the Collaborative Adaptation Research Initiative in Africa and Asia (CARIAA).

ICIMOD core funds contributed by the governments of Afghanistan, Australia, Austria, Bangladesh, Bhutan, China, India, Myanmar, Nepal, Norway, Pakistan, Switzerland, and the United Kingdom.

Netherlands Organization for Scientific Research (NWO), through the VIDI grant of W.W. Immerzeel (project number 016.161.208).

European Research Council (ERC) under the European Union's Horizon 2020 research and innovation programme (grant agreement 676819 W.W. Immerzeel)